Dissertation
submitted to the
Combined Faculties for the Natural Sciences and for Mathematics
of the Ruperto-Carola University of Heidelberg, Germany
for the degree of
Doctor of Natural Sciences

presented by
Alina Steinbach, M.Sc. Molecular Biosciences
born in: Dieburg, Germany
Oral examination: 17th of January 2017

Identification and functional analysis of the antigen processing machinery component ERAP1 as a possible novel immune evasion mechanism of HPV-induced malignancies

Referees: Prof. Dr. Lutz Gissmann

PD. Dr. Dr. Angelika Riemer

The work described in this thesis was performed from January 2013 to August 2016 under supervision of PD Dr. Dr. Angelika Riemer in the group Immunotherapy and -prevention at the German Cancer Research Center (DKFZ) in Heidelberg, Germany.

Conference and workshop presentations based on this study

Steinbach A., Winter J., Grabowska A. K., Riemer A. B. *Systematic analysis of changes in the antigen processing machinery in HPV transformed cells.* (05/2014) Poster presentation at the 12th Cancer Immunotherapy Meeting (CIMT), Mainz, Germany.

Steinbach A., Winter J., Grabowska A. K., Riemer A. B. *Systematic analysis of changes in the antigen processing machinery in HPV transformed cells.* (07/2014) Poster presentation at the DKFZ PhD Retreat, Weil der Stadt, Germany.

Steinbach A., Winter J., Grabowska A. K., Blatnik R., Hoppe S., Khallouf H., Riemer A. B. *Systematic analysis of the antigen processing machinery in HPV transformed cells.* (09/2014) Poster presentation at the 44th Annual Meeting of the German Society for Immunology (DGfI), Bonn, Germany.

Steinbach A., Winter J., Grabowska A. K., Blatnik R., Hoppe S., Khallouf H., Riemer A. B. *Systematic analysis of the antigen processing machinery in HPV transformed cells.* (12/2014) Poster presentation at the DKFZ PhD Poster Presentation, Heidelberg, Germany.

Steinbach A., Winter J., Grabowska A. K., Reuschenbach M., Hoppe S., Klevenz A., Blatnik R., Khallouf H., von Knebel Döberitz M., Riemer A. B. *Altered expression of the ER aminopeptidase ERAP1 in HPV-induced malignancies.* (09/2015) Poster presentation at the 4th European Congress of Immunology (ECI), Vienna, Austria.

I Abstract

The development of a therapeutic human papillomavirus (HPV) vaccine is important to cure people that are already infected with HPV. However, multiple immune evasion mechanisms have been described for HPV-induced malignancies, including altered expression of antigen processing machinery (APM) components. These changes are able to directly influence epitope presentation and thus hamper CD8 T cell responses and are therefore regarded as considerable challenges in the development of a therapeutic vaccine.

Until now, no systematic analysis of the APM had been performed in a large array of different HPV-positive tumor samples. Therefore, a systematic analysis of APM component expression on the mRNA level was performed in a comprehensive collection of HPV16-positive tumor cell lines in this study. The experiments revealed an upregulation of several APM components, which were subsequently investigated on the protein level. This analysis showed that the only component that was consistently upregulated in HPV16-positive tumor cells was the endoplasmic reticulum aminopeptidase 1 (ERAP1). Immunohistochemistry revealed that ERAP1 was more highly expressed in cervical intraepithelial lesions and cervical cancer than in nonmalignant cervical epithelium. Mechanisms that could account for ERAP1 overexpression were investigated. Single nucleotide polymorphisms (SNPs) of *ERAP1* were analyzed in selected HPV-negative and HPV16-positive cell lines. Further, knockdown of HPV16 *E6* and *E7* was performed to investigate whether HPV oncogenes may influence ERAP1 expression levels. However, no influence of SNPs or the HPV oncogenes could be observed.

ERAP1 plays a key role in editing the human leukocyte antigen (HLA) class I epitope repertoire. Therefore, we further focused on the question whether ERAP1 overexpression influences HPV16 E6 and E7 epitope presentation. To do so, an *ERAP1* siRNA-mediated knockdown approach was established. HPV16-positive cells lines with attenuated ERAP1 expression or normal (over)expression were compared. To assess epitope presentation, a panel of HPV16-derived epitopes was analyzed using mass spectrometry. Additionally, T cell lines were generated from healthy donors, who showed memory responses against HPV16 epitopes. T cell lines were used to investigate the influence of ERAP1 expression levels in target cells on HPV16-specific CD8 T cell-mediated cytotoxicity. Mass spectrometry revealed that ERAP1 attenuation had no influence on presentation of the selected epitopes. Conversely, T cell assays showed that cytotoxicity against some HPV16-derived epitopes is influenced by ERAP1 expression levels, including one T cell line that showed enhanced killing towards HPV16-positive cells upon ERAP1 attenuation.

Taken together, ERAP1 was observed to be highly expressed in HPV-induced malignancies. It was shown that ERAP1 influences the presentation of some, but not all, HPV16 E6 and E7-derived epitopes in an epitope-specific and tumor-specific way. In conclusion, ERAP1 overexpression can inhibit some HPV16-specific CD8 T cell responses and thus possibly represents a novel immune evasion mechanism of HPV-induced malignancies.

ABSTRACT

II Zusammenfassung

Die Entwicklung eines therapeutischen Impfstoffes gegen das humane Papillomvirus (HPV) ist wichtig um Menschen zu heilen, die bereits mit HPV infiziert sind. Für HPV-induzierte bösartige Tumore wurden jedoch mehrere Mechanismen der Umgehung einer Immunantwort beschrieben. Dazu zählt die veränderte Expression von Komponenten der Antigenprozessierung. Diese Veränderungen können die Präsentation von Epitopen und daher CD8 T-Zell-Antworten direkt hemmen und werden als erhebliche Herausforderung in der Entwicklung eines therapeutischen Impfstoffes betrachtet.

Bis heute wurde keine systematische Analyse von Komponenten der Antigenprozessierung in einer großen Anzahl von verschiedenen HPV-positiven Tumorproben durchgeführt. Daher wurde in dieser Arbeit eine systematische Analyse der Expression von Komponenten der Antigenprozessierung auf Ebene der mRNA in einer umfassenden Sammlung von HPV16-positiven Tumorzelllinien ausgeführt. Generell zeigen die Experimente eine Hochregulierung von mehreren Komponenten, die darauffolgend auf Proteinebene untersucht wurden. Diese Analyse zeigte, dass die einzige Komponente, die in HPV16-positiven Tumorzellen konsistent hochreguliert war, die Endoplasmatische Retikulum Aminopeptidase 1 (ERAP1) ist. In immunhistochemischen Färbungen von prämalignen Zervix-Läsionen und Zervixkarzinomen war ERAP1 höher exprimiert als im nicht veränderten Zervixepithel. Es wurden Mechanismen untersucht, die für eine Überexpression von ERAP1 verantwortlich sein könnten. Einzelnukleotid-Polymorphismen von *ERAP1* wurden in ausgewählten HPV-negativen und HPV16-positiven Zellen analysiert. Außerdem wurde ein Knockdown von HPV16 *E6* und *E7* durchgeführt, um zu untersuchen, ob HPV-Onkogene einen Einfluss auf die Expressionsstärke von ERAP1 haben. Es wurde jedoch kein Einfluss von Einzelnukleotid-Polymorphismen oder HPV-Onkogenen beobachtet.

ERAP1 spielt eine Schlüsselrolle im Editieren des Epitop-Repertoires, das auf humanen Leukozytenantigen (HLA) Klasse I-Molekülen präsentiert wird. Aus diesem Grund haben wir uns auf die Frage konzentriert, ob die Überexpression von ERAP1 die Präsentation von HPV16 E6- und E7-Epitopen beeinflusst. Um diese Frage zu beantworten, wurde ein siRNA-vermittelter Knockdown von *ERAP1* etabliert. HPV16-positive Zelllinien mit abgeschwächter ERAP1-Expression wurden mit Zellen mit für sie normaler Überexpression verglichen. Um die Epitop-Präsentation zu untersuchen, wurde eine Gruppe von HPV16 E6- und E7-Epitopen durch Massenspektrometrie analysiert. Zudem wurden T-Zelllinien von gesunden Spendern generiert, die immunologische Gedächtnisantworten gegen HPV16-Epitope zeigten. T Zelllinien wurden verwendet, um den Einfluss der Expressionsstärke von ERAP1 in Zielzellen auf HPV16-spezifische CD8 T-Zell vermittelte Zytotoxizität zu untersuchen. Die Massenspektrometrie ergab, dass eine geringere ERAP1-Expression keinen Einfluss auf die Präsentation der ausgewählten Peptide hatte. Im Gegensatz dazu war die Zytotoxität gegen HPV16-Epitope von der Expressionsstärke von ERAP1 beeinflusst. Eine T Zelllinie wies verstärkte Zytotoxizität gegen HPV16-positive Zielzellen mit verringerter ERAP1 Expression auf.

Zusammenfassend wurde beobachtet, dass ERAP1 stark in HPV-induzierten Tumoren

exprimiert wird. Es wurde gezeigt, dass ERAP1 die Präsentation von manchen, aber nicht allen, HPV16 E6- und E7-Epitopen in einer epitopspezifischen und tumorspezifischen Art beeinflusst. Die Überexpression von ERAP1 kann manche HPV16-spezifische CD8 T Zell-Antworten hemmen und stellt daher einen möglichen neuen Mechanismus von HPV-induzierten Tumoren zur Umgehung der Immunantwort dar.

III Acknowledgments

An dieser Stelle möchte ich mich bei allen Personen bedanken, die mich bei dem Erstellen dieser Doktorarbeit auf verschiedene Weise unterstützt haben.

Zuerst möchte ich PD Dr. Dr. **Angelika Riemer** danken, weil sie mir die Möglichkeit gegeben hat meine Doktorarbeit in ihrer Arbeitsgruppe anzufertigen. Sie hat von Anfang an immer an dieses Projekt geglaubt und sich durch Unterstützung und Vertrauen in diese Arbeit eingebracht.

Bei Prof. Dr. **Lutz Gissmann** möchte ich mich dafür bedanken, dass er die Rolle als Erstgutachter übernommen hat. Vielen Dank auch für die vielen hilfreichen Ideen während meiner TAC Meetings. Außerdem danke ich PD. Dr. **Suat Özbek** und Dr. **Steeve Boulant** dafür, dass Sie als Prüfer an meiner Disputation teilgenommen haben. Vielen Dank auch an Prof. Dr. **Alexander Dalpke**, der ein Mitglied meiner TAC Meetings war und mir während dieser unterstützend und mit Ratschlägen zur Seite stand.

Ein ganz besonderer Dank gilt allen ehemaligen und aktuellen Labormitgliedern: **Stephanie Hoppe**, **Renata Blatnik**, **Alexandra Klevenz**, **Jan Winter**, **Agnieszka Grabowska**, **Miriam Bertrand**, **Sebastian Utz**, **Florian Müller**, **Maria Bonsack**, **Sebastian Kruse, Hadeel Khallouf** und **Martin Wühl**. Vielen Dank an euch für euer Interesse an meinem Projekt und die damit verbundenen Ideen, Ratschläge und Diskussionen. Außerdem danke ich euch dafür, dass wir neben der fachlichen Zusammenarbeit auch außerhalb des Labors viel Spaß zusammen hatten. Das hat maßgeblich zu einer positiven Arbeitsatmosphäre beigetragen.

Ein ganz großes Dankeschön gilt **Alex**. Du bist eine große Bereicherung für unser Labor und hast mir von allen am meisten bei den Experimenten geholfen. Darüber hinaus bist du eine tolle Freundin und das braucht keine weiteren Worte. **Stephanie**, vielen Dank dafür, dass du immer ein offenes Ohr hattest und mir mit Rat und Tat zur Seite standest. Dankeschön für unzähliges Korrekturlesen. Außerdem danke ich dir für deinen Sarkasmus, der mich in der richtigen Zeit immer zum Lachen brachte. Danke auch für die wundervollen Backkreationen und natürlich für diverse Freizeitaktivitäten außerhalb des Labors. Vielen Dank möchte ich auch dir sagen, **Renata**, denn du hast mir zur Seite gestanden als ich fachlich das Neuland Immunopräzipitationen betreten habe und du hast mit deinem enormen Fleiß die Massenspektrometrie durchgeführt. Ich danke dir besonders auch dafür, dass du eine gute Zuhörerin bist und für die großartige slowenische Putizza. **Jan** auch dir spreche ich ein großes Dankeschön aus, dafür dass du dieses Projekt mit so viel Fleiß und Eifer begonnen hast. Auch ein großes Dankeschön an **Agi**, die mich so freundlich und unterstützend in das Labor aufgenommen hat und mit vielen Meetings ebenso wie praktischer Unterstützung den Anfang meiner Arbeit maßgeblich bestimmt hat. Vielen Dank an **Miriam Betrand**, die mich als Praktikantin ein halbes Jahr begleitet hat und mit sehr viel Fleiß und Herzblut zu meiner Arbeit beigetragen hat. Dankeschön auch an **Sebastian Utz**, denn auch du hast ein halbes Jahr mit mir zusammengearbeitet, um deine Masterarbeit anzufertigen. Du warst unglaublich hilfreich und zusammen waren wir einfach ein super

Team. Darüber hinaus danke ich dir auch für deine Freundschaft und unglaublich lustige Partys. Lieben Dank an dich **Florian** für deine tatkräftige Unterstützung bei zahlreichen Experimenten vor allem in der Experiment/Schreib-Übergangsphase.

Danke auch an die anderen Praktikanten und Studenten: **Kinga Grabowska**, **Marius Küpper**, **Jasmin Mangei**, **Julia Schessner**, **Lisa Dreßler**, **Kathrin Josef**, **Marleen Büchler** und **Sina Knapp**.

Ein großes Dankeschön gilt den Kollegen aus der Pathologie: Dr. **Miriam Reuschenbach**, **Jonathan Dörre** und Prof. Dr. **Magnus von Knebel Döberitz**. Durch ihre Fachkompetenz in der Immunhistologie haben sie einen großen Teil zu dieser Arbeit beigetragen. Vielen Dank **Miriam** für die vielen Tipps und praktische Unterstützung bei der Mikroskopie, denn ich habe viel von dir gelernt.

Desweiterem möchte ich Prof. Dr. **Karin Hoppe-Seyler** und Prof. Dr. **Felix Hoppe-Seyler** danken, dass sie mit ihrer Erfahrung im Knockdown von HPV16 Onkogenen einen Teil zu dieser Arbeit beigetragen haben. Außerdem seid ihr immer sehr hilfsbereit gewesen, wann immer ich andere fachliche Fragen hatte.

Für die große Unterstützung in allen bürokratischen Dingen möchte ich **Monika Bock** danken.

Danke natürlich auch an die unzähligen **Blutspender**, ohne die diese Arbeit in diesem Maß nicht existieren würde.

Über das Labor hinaus möchte ich unbedingt meinen Freunden danken, die mein Leben lebenswert machen. Danke an meinen Freund **Marcus** dafür, dass du der tollste Partner bist, den man sich vorstellen kann. Du nimmst mich einfach so wie ich bin und bist immer für mich da. Vielen Dank für unser harmonisches Zusammenleben, deine Kochkünste und die vielen wunderschönen Urlaube. Vielen Dank an **Nikola** für unsere langjährige Freundschaft, die auch über die Distanz niemals an Glanz verloren hat. Ich danke dir dafür, dass ich weiß, wenn meine Welt zusammenfällt, kommst du und rettest mich. Ein großes Dankeschön geht an **Lisa**. Wir kennen uns schon unser ganzes Leben und trotz langjähriger Distanz haben wir immer den Kontakt zueinander gepflegt. Dankeschön **Kristin** für deine liebevolle Art, Disneyabende und für die Begleitung in den Kölner Karneval. Auch **Sandra** möchte ich danken für deine bodenständige und stets direkte Art. Du bist für mich ein wertvoller Mensch geworden auf den ich mich immer verlassen kann. Außerdem vielen Dank an **Denise**, **Julia**, **Astrid** und **Raphaela.**

Zuletzt, aber dafür keineswegs weniger, möchte ich meiner Familie danken, **Fabian**, **Cornelia** und **Reinhold Steinbach**. Ihr habt mich in allen Lebenslagen unterstützt. Danke für Liebe, Verständnis, Geduld und selbstlose Unterstützung in allen Lebenslagen.

IV Table of Contents

TABLE OF CONTENTS

V List of Figures

VI List of Tables

1 Introduction

1.1 The immune system

Every day, we are surrounded by viruses, bacteria, parasites and fungi and many of these have the potential to cause disease. The immune system has evolved from simplicity in invertebrates to complexity in vertebrates as the body's defense against infection. Vaccinology has its roots in the 18th century when Edward Jenner investigated the disease smallpox. He observed that inoculation of individuals with a moderate disease, cowpox, conferred protection to infection with smallpox and he called this procedure "vaccination" for the first time in history (1).

The immune system is composed of primary and secondary lymphoid organs. In the primary lymphoid organs, the thymus and the bone marrow, leukocytes are generated. In secondary lymphoid organs, the lymph nodes, the spleen and the mucosal lymphoid tissue in the nasal, respiratory and urogenital tract, the gut and other mucosae, leukocytes are maintained and immune responses are initiated. Protection of our body by immunological recognition is carried out by the two branches of the immune system: the innate immune system and the adaptive. Usually, the innate immune system is the first barrier that provides a fast response. Cells of the innate immune system express several pattern recognition receptors (PRR) and each receptor recognizes a feature shared by many pathogens. The adaptive immune system has a delayed response during infection, but it is very specific and able to establish long term protection, which is called immunological memory (1). Both the innate and the adaptive branch of the immune system have cellular and humoral effector systems.

1.1.1 The adaptive immune system

The adaptive immune response takes longer to form, because for its induction antigen uptake by antigen presenting cells (APCs) in secondary lymphoid organs is needed. Mostly, these APCs are dendritic cells (DCs) (see 1.1.2). APCs take up antigens, degrade them intracellularly and present protein fragments, i.e. peptides, derived from for instance a pathogen, on their surface. Antigen recognition is conducted by T cells which express antigen receptors that have been rearranged during their maturation in the thymus. The adaptive immune system has another powerful subset of antigen recognizing cells, B cells. These cells mature in the bone marrow and also undergo receptor gene rearrangements. The receptor gene rearrangements are called V(D)J recombination. In each human individual, there are lymphocytes of at least 10^8 different specificities highlighting the huge repertoire that, in theory, can recognize virtually any antigen (1).

When a B or a T cell recognizes its antigen it undergoes clonal expansion in order to produce many identical cells to fight the infection. These activated and proliferating cells are called effector cells. T and B cells operate in a different way. B cells differentiate into plasma cells and produce antibodies, which are the secreted form of their antigen receptor, known as adaptive humoral

immunity. On the contrary, T cells develop into different subsets and produce specific cytokines and cytotoxic effector functions, known as adaptive cell-mediated immunity. Depending on their cell surface proteins, T cells are classified into CD4 and CD8 T cells. In general, CD4 T cells are destined to become T helper cells (Th) which recognize antigens derived from extracellular pathogens that have been taken up by APCs and presented on the major histocompatibility complex class II (MHC II). Additionally, Th cells help B cells to produce antibodies and cytotoxic T cells (CTLs) to mature. The majority of CD8 T cells become CTLs and respond to an MHC I presented antigen which is derived from cytosolic proteins (1).

1.1.2 Antigen presenting cells

APCs are crucial to induce cell-mediated immunity by T cells. There are three professional antigen presenting cell types: DCs, macrophages and B cells. Of these cell types, DCs are most important in vertebrates in orchestrating an effective immune response (2). However, macrophages and B cells are also able to present antigens and activate T cells, but they do not have the potential to guide the direction of an immune response. Thus, this section will focus on the description of DCs.

DCs as highly phagocytic sentinel cells have the unique ability among APCs to not only sense pathogens and to process them into peptides for T cell recognition, but also to direct the specificity, magnitude and polarity of immune responses. These specialized cells can be found in the blood, epithelia and lymphoid tissues (2). Ralph Steinmann discovered and named this unique cell type in the 1970s (3). Importantly, DCs form the interface between innate and adaptive immunity and they confer peripheral tolerance to self-peptides, which can be derived from engulfed dead cells (4). DCs can differentiate between self and non-self antigens depending on the context of uptake. Quiescent DCs take up soluble proteins or apoptotic bodies from cellular turnover and since these uptakes do not activate DCs, they do not express co-stimulatory molecules and induce either deletion or anergy of autoreactive T cells (5). However, DCs express PRRs such as toll-like receptors (TLRs) to sense non-self antigens. PRRs recognize, for instance, lipopolysaccharides (LPS) found in the outer membrane of gram-negative bacteria or double stranded RNA (dsRNA) of viruses. When these receptors get triggered, DCs undergo maturation, upregulate MHC molecules and co-stimulatory molecules and secrete pro-inflammatory cytokines such as interleukin (IL)-1α, IL-1β, IL-6 and interferon (IFN)α (1).

DCs are also specialized in antigen processing because they are capable of presenting endogenous and exogenous antigens on both MHC I and MHC II molecules, respectively. Furthermore, they can cross-present antigens, which means that an exogenously derived antigen is presented on MHC I (6). Cross-presentation is crucial in immune responses directed against extracellular pathogens. It is important to note that cross-presentation also works the other way around with endogenous antigens that are presented on MHC II (7). Both types of cross-presentation are under intensive investigation (8). Recently, Alloatti and colleagues observed that efficient cross-presentation

only takes place when the activating TLR ligand and sufficient antigen were engulfed simultaneously (9). This reflects the natural situation in which DCs only become activated and induce immune responses when pathogens are present.

The activation of a naïve T cell only happens if three signals, coming from the same DC, are delivered to a T cell (Figure 1.1 A) (1). The first signal is antigen specific and results from the binding of the cognate peptide:MHC complex to the T cell receptor (TCR) with help of the co-receptor CD4 or CD8. Signal 2 is delivered by molecules belonging to the B7 family on the APC and CD28 on the T cell. This second signal is also called the co-stimulatory signal and is crucial for clonal expansion (Figure 1.1 B). It also triggers the production of the T cell growth factor, IL-2. T cells secrete this cytokine themselves and it drives their proliferation and differentiation. Finally, the third signal is a cocktail of instructing cytokines that together influence the fate of the activated T cell, in particular differentiation into the various CD4 T cell types. It is important to point out that this crosstalk between a T cell and a DC is bidirectional, because T cells expressing CD40L support DC maturation, thus boosting the immune response (10).

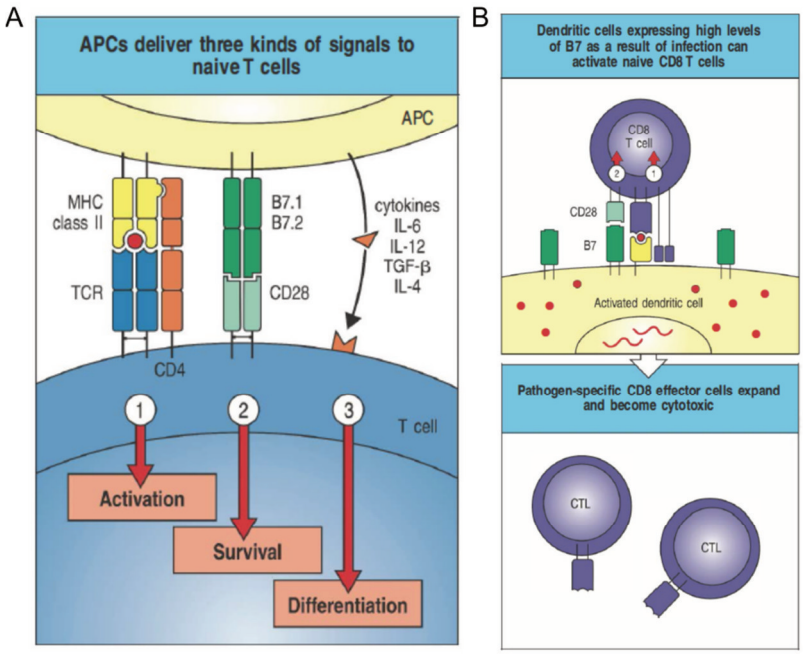

Figure 1.1: Antigen presenting cells deliver three signals to naïve T cells, thereby activating them. A. The induction of T cell-mediated immunity needs three kinds of signals provided by APCs. The first signal is the encounter of the cognate peptide:MHC with the T cell receptor (TCR), which causes G_1 phase entry of the T cell. Signal 2, called co-stimulatory signal, is conducted by molecules of the B7 family. The third signal is secretion of a specific cytokine cocktail which determines the direction of T cell differentiation, particularly different subsets of effector CD4 T cells. **B.** Mature dendritic cells express high levels of co-stimulatory B7 molecules. Upon binding, naïve CD8 T cells are activated and undergo clonal expansion and differentiation into cytotoxic T cells. Taken from (1).

1.1.3 T lymphocytes

Immunity mediated by T lymphocytes involves three steps: priming/activation of naïve T cells, activated T cells performing effector functions and establishment of long-term T cell memory. There are two major T cell subsets having different TCRs (11). The majority is known as the αβ T cell

subset, while a minority of T cells expresses γδ TCRs. Those γδ T cells are less heterogenic and reside in the skin and mucosal surfaces. This section will focus on the αβ T cell subset bearing a diverse repertoire of antigen receptors. T cells mature in the thymus, but only a small number of them leaves it again. The major part of T cells is eliminated because either they are not able to properly bind to MHC molecules (positive selection) or they are self-reactive (negative selection). Hence, the thymus represents the first layer of T cell tolerance, called central tolerance (1). Each individual T cell has a unique TCR, which can recognize a peptide only in the context of a MHC complex. This phenomenon is called MHC restriction.

Mature T cells that leave the thymus are called naïve, because they have not yet seen their cognate antigen and have not been activated. They circulate in the blood, the lymphatic system and secondary lymphoid organs, always on the mission to encounter their cognate peptide bound to MHC on an APC (12). Naïve T cells express L-selectin (CD62L), the CC chemokine receptor 7 (CCR7) and leukocyte function antigen (LFA)-1 (12, 13). These surface molecules, also known as "homing molecules", enable the T cells to travel through high endothelial venules localized in lymphoid tissues. In lymphoid tissues, they bind to APCs, mostly DCs. Upon high-affinity interaction of the TCR with the cognate peptide:MHC complex, the immunological synapse between the APC and the T cell is formed and the T cell becomes primed (see 1.1.2). The immunological synapse is composed of the TCR:peptide:MHC interaction, co-receptors (CD4 and CD8), accessory molecules (e.g. LFA-1 and CD2) that stabilize the cellular contact, and co-stimulatory molecules (e.g. CD28), all of which have corresponding ligands on the APC (14). During T cell activation, the T cell undergoes phenotypical changes such as the expression of CD69, CD25 (the α-chain of the IL-2 receptor) and CD40 (1). In addition, CD28-related proteins such as the inducible T cell co-stimulator (ICOS) and cytotoxic T lymphocyte associated antigen (CTLA)-4 are found on activated T cells. ICOS is especially important for proper CD4 T cell function and does not trigger IL-2 production like CD28, but rather stimulates the production of IL-4 and IFNγ (15, 16). On the contrary, CTLA-4 inhibits T cell activation and IL-2 production (17). Thus, this molecule is seen as an "immunological break" since it limits the proliferative T cell response which is a crucial negative feedback loop. Moreover, tumor necrosis factor (TNF) family members like CD27, 4-1BB and OX40 (and their matching ligands on the APC) transmit further co-stimulatory signals. With regard to adhesion molecules, activated T cells lose CD62L and express an integrin, very late antigen (VLA)-4, which allows them to enter inflammation sites through vascular epithelium (1). Eventually, activated T cells differentiate into effector T cells that do no longer need a co-stimulatory signal, leading to their capability of immediate action.

After activation, the CD4 T cell subset differentiates into six functional classes: Th1, Th2, Th9, Th17, T follicular helper cells (T_{FH}) and regulatory T cells (Treg). While Th1 cells mainly drive a pro-inflammatory response by secreting IFNγ, IL-2 and TNFα, Th2 cells promote non-inflammatory responses and secrete IL-4 and IL-5. Th1 and Th2 mediated immune responses are mutually antagonistic. A Th1-driven immune response involves cell-mediated immunity by macrophages and

CTLs, whereas Th2-driven immune responses control parasites by eosinophils and IgE production by B cells. In addition, Th2 cells are involved in allergic immune reactions (1). Recently, a new T cell subset - Th9 cells - specifically secreting IL-9 was identified. Th9 cells are implicated in the immunopathology of allergy and autoimmunity. Furthermore, they were shown to support immunity against worms in the intestine and against melanoma (18). The Th17 subset is characterized by the secretion of IL-17 and IL-22. This subset plays a pivotal role in combating infections with extracellular bacteria and fungi, together with the participation of neutrophils (1). T_{FH} cells are distinguished by the expression of CXCR5 and their localization in lymphoid follicles where they promote B cell mediated immunity (19, 20). The last CD4 T cell subset, the Tregs, has immunosuppressive functions by secreting tumor growth factor (TGF)β, IL-10 and IL-35 as well as by expressing CTLA-4 on the surface (21). Their pivotal role is the prevention of autoimmunity and they serve to control the amplitude of immune responses. About 10% of CD4 T cells are natural Tregs (nTreg) which express CD25 and the transcription factor forkhead box p3 (Foxp3). They develop in the thymus as a part of central tolerance. There is also a small proportion known as induced Treg (iTreg), which develops in the periphery as a result of a particular immunosuppressive environment or in the absence of co-stimulation. This type of Tregs belongs to peripheral tolerance and complements central tolerance (21). Of note, there are also experimental models demonstrating an important role of CD8 Tregs (22, 23), but so far more is known about the CD4 Treg population.

In general, naïve CD8 T cells differentiate into CTLs, which can directly kill target cells infected with an intracellular pathogen, such as a virus, or malignant cells. CD8 T cells need more co-stimulatory signals than CD4 T cells. In many cases, co-stimulation provided by mature DCs is not enough and additional support by CD4 effector T cells is needed. CD4 effector T cells bind to their cognate peptide:MHC II complex on the APC and induce them to increase levels of co-stimulatory molecules. Additionally, CD4 effector T cells produce IL-2. Together, this activates the naïve CD8 T cell recognizing its cognate peptide:MHC I complex. The additional need for CD4 T cell help may be due to the extremely damaging effects of CTLs (1). Cytotoxicity mediated by CTLs happens by two pathways. On the one hand, lytic granules consisting of granzymes and perforins are released. Perforin supports the transport of granzymes through the plasma membrane of the target cell. Granzymes are serine proteases that can induce apoptosis (24) via the caspase-dependent and -independent pathway. On the other hand, CTLs express CD95L (FasL), a member of the TNF receptor family, that induces Fas-mediated apoptosis (25). The binding of FasL to Fas on the target cell triggers the intracellular "death" domain leading to caspase-mediated apoptosis.

The end of an immune response is characterized by apoptosis of the majority of effector T cells (26). Only a small population survives and forms the immunological memory. When the body is challenged again with the same pathogen, memory T cells can act immediately with a reduced need for co-stimulation. T cell memory is composed mainly of central memory T cells (T_{CM}) and effector memory T cells (T_{EM}). T_{CM} cells are found in the blood and lymphoid tissues. Upon recognition of

their cognate antigen they rapidly proliferate and gain effector functions. On the contrary, T_{EM} cells circulate in non-lymphoid tissues and can directly execute effector functions (27).

1.1.4 Antigen processing and presentation on MHC I

Antigen processing and presentation on MHC I is a fundamental process needed for all CTL-mediated immune responses. The processing of antigens into peptides and their presentation on the cellular surface is a multistep pathway involving the following steps: 1) peptide generation/trimming; 2) peptide transport into the ER; 3) MHC I assembly/peptide loading and 4) peptide:MHC I presentation (28). Whereas MHC II is mainly expressed by APCs, MHC I is expressed on all nucleated cells, thus enabling the immune system to detect viral infections and malignant cells (characterized e.g. by mutated proteins) (29). The structure and peptide-binding preferences of the two MHC types (Figure 1.2) are different. MHC I is composed of an α-chain and a non-covalently associated β2-microglobulin chain. The binding cleft is closed and binds peptides in their elongated form with a length of 8-11 amino acids. On the contrary, MHC II molecules are heterodimers composed of an α- and β-chain with an open peptide-binding cleft. Thus, peptides of up to 25 amino acids are able to bind (30).

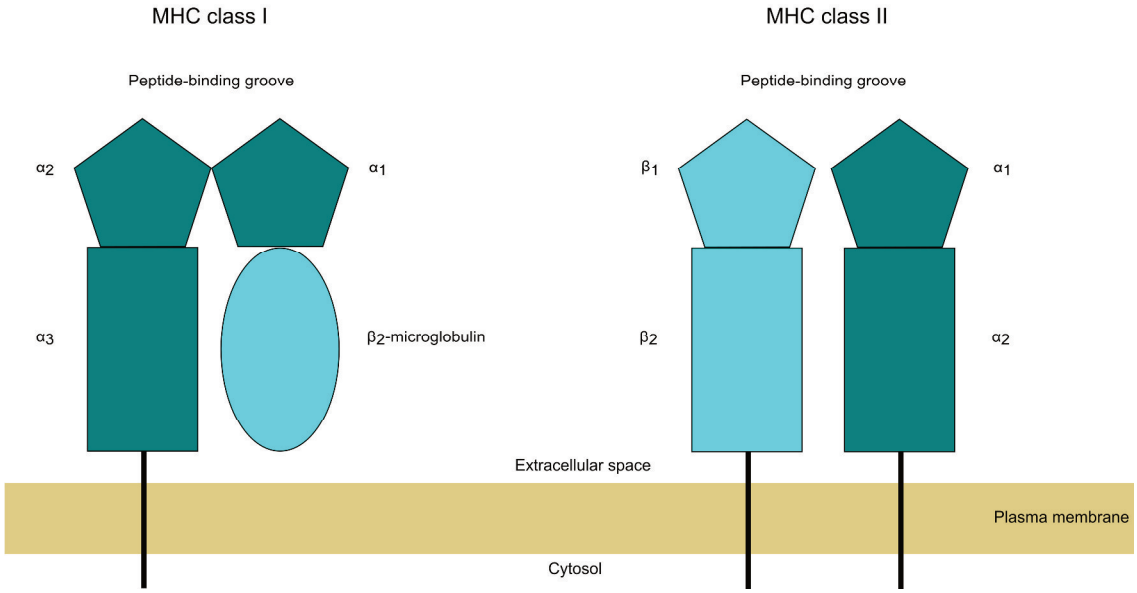

Figure 1.2: Schematic illustration of the MHC I and II molecules. MHC I consists of an α-chain that is anchored in the plasma membrane and has three immunoglobulin domains ($\alpha_{1\text{-}3}$). The β_2-microglobulin chain is non-covalently bound. The peptide-binding groove is closed which limits the length of binding peptides to 8-11 residues. MHC II consists of two transmembrane chains (α and β) each composed of two immunoglobulin domains. The peptide-binding groove is open at both ends, enabling binding of peptides of differing lengths up to 25 residues.

MHC I presents self- and non-self peptides. The presentation of self-peptides contributes to tolerance, whereas non-self peptides derived from viruses or mutated proteins in malignant cells induce an immune response. Antigen generation starts in the cytosol (Figure 1.3). Here, proteins are degraded by the ubiquitin-proteasome pathway, which controls normal physiological protein turnover. Other proteins that get degraded by the proteasome are either short-lived regulatory proteins, damaged or misfolded proteins (31) including defective ribosomal products (DRiPs), which are degraded within minutes after their synthesis (32, 33). In the ubiquitin-proteasome pathway, proteins are tagged by covalent linkage of a polyubiquitin chain (34, 35). These proteins are destined for degradation by the proteasome, which is constitutively expressed in all cells. The proteasome is a barrel-shaped, multimeric protein complex composed of a catalytic core, the 20S proteasome, and two regulatory particles, the 19S proteasomes, functioning as proteasome activators (28, 35). The 20S proteasome is a stack of four heptameric rings with a central opening. The two outer rings consist of seven α-subunits (PSMA1-7) and the two adjacent inner rings consist of seven β-subunits (PSMB1-7). All α- and β-subunits are structurally similar but have different functions. Three β-subunits, PSMB5, 6 and 7, have threonine-protease catalytic activities and hydrolyze peptide bonds at the C-terminus. PSMB5 is associated with a chymotrypsin-like activity (hydrolysis after hydrophobic residues), PSMB6 with a caspase-like activity (hydrolysis after acidic residues) and PSMB7 with a trypsin-like activity (hydrolysis after basic residues) (36, 37). The catalytic core is usually capped on one or both sites by the 19S activator, which identifies an ubiquitin-tagged protein, removes polyubiquitin chains, unfolds the protein and transfers it into the catalytic core by opening the α-ring (38). Of note, six subunits of the activator are ATPases, since these processes are dependent on energy.

Upon exposure of the cell to IFNγ, the three catalytic subunits of the 20S core are replaced by functionally different subunits (PSMB8, 9 and 10). Also another activator, composed of PSME1 and 2, is expressed in this context, forming a proteasome which is called immunoproteasome. This name has been chosen because in comparison to the constitutive proteasome, immunoproteasomes assemble in a type I IFN (α and β) and type II IFN (γ) containing milieu (39, 40). Interestingly, they are constitutively expressed in lymphoid organs. Immature DCs express equivalent amounts of proteasomes and immunoproteasomes, but only immunoproteasomes when they are mature (41, 42). The exact role of immunoproteasomes in immunity is still under extensive investigation, but it is known that they change the MHC I epitope repertoire. It is generally thought that immunoproteasomes have a positive effect on MHC I antigen presentation by producing CD8 T cell epitopes more efficiently (43). A major breakthrough in analyzing the mechanism of the immunoproteasome activator has been achieved by Raule and colleagues. They showed that the immunoproteasome activator does not increase the rate of substrate turnover but reduces size and increases hydrophilicity of peptide products (44).

Peptides released from the proteasome have a length between 2 and 25 amino acids (28) with variation in terms of sequence and quantity depending on the presence of proteasomes or

immunoproteasomes. In the cytosol, peptides can be further cleaved by peptidases such as nardilysin, thimet oligopeptidase (TOP), tripeptidyl peptidase II (TPPII) and insulin-degrading enzyme. There is experimental evidence that a minority of epitopes depends on cleavage by one or two of these peptidases (45, 46). However, these peptidases are mainly associated with destruction rather than generation of MHC ligands (47-49) rendering the cytosol an unfavorable environment for MHC I ligands. To continue antigen processing, peptides have to be transported into the endoplasmic reticulum (ER) by the transporter associated with antigen processing (TAP). TAP is a transmembrane pore composed of two parts, TAP1 and TAP2, which can switch between an open and a closed state in an ATP dependent way (50) and mainly transports peptides with a length of 8-12 residues and hydrophobic or basic C-termini. Thus, TAP preferentially transports peptides that bind to MHC I (51). Inside the ER, peptides are trimmed by ER aminopeptidases (ERAP1 and ERAP2) (49). ERAPs contribute fundamentally to the generation of MHC I ligands (see 1.1.4.1). Notably, DCs also bear the insulin-regulated aminopeptidase (IRAP), an endosomal protease, which has been demonstrated to play an important role in cross-presentation (52). Optimal MHC I ligands are loaded onto MHC molecules by the help of the chaperones calnexin, calreticulin and tapasin. The thiol oxidoreductase protein disulfate isomerase A3 (PDIA3 or ERp57) is also assisting this process (28). Together these proteins form the peptide loading complex (PLC). Together, calnexin and PDIA3 ensure the correct folding and oxidative state of the nascent MHC I molecule until β2-microglobulin can bind. Further, calreticulin supports the “open” form of the MHC I molecule which is now prepared to be loaded with a peptide (53). Tapasin functions as a bridge between TAP and MHC I, thus ensuring that imported peptides can bind (54). Once an optimal peptide binds to MHC I, the complex becomes stabilized, released from the PLC and is transported via the Golgi apparatus to be presented on the cellular surface.

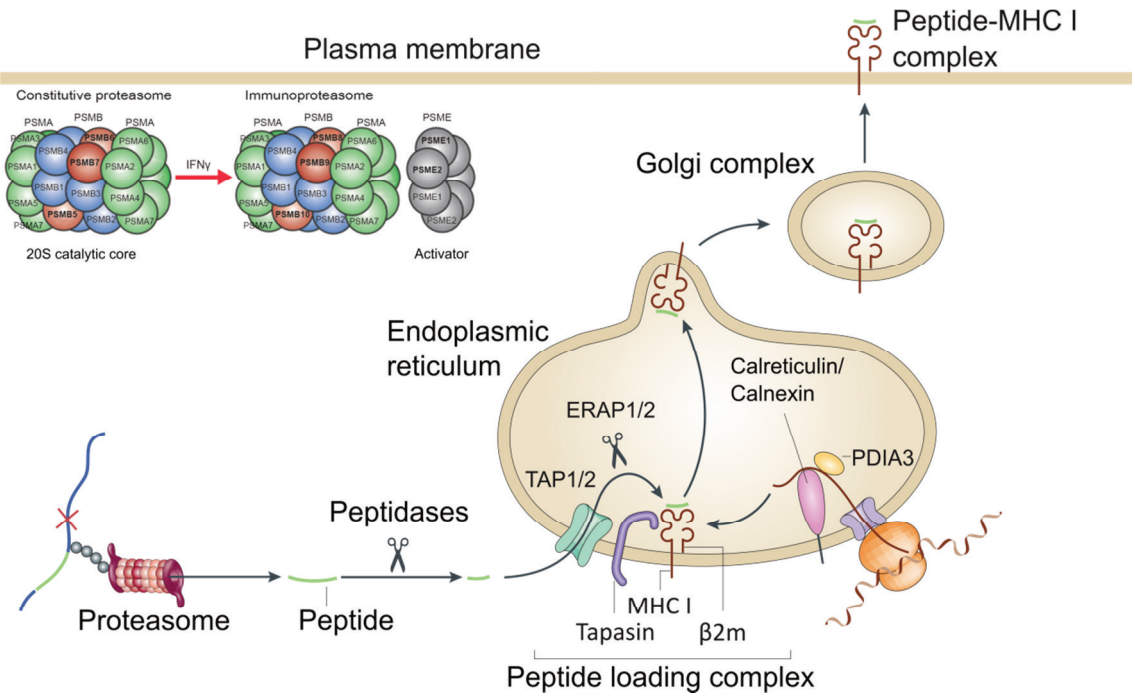

Figure 1.3: Antigen processing and presentation via the classical MHC class I pathway. Antigen processing starts with the destruction of ubiquitinated proteins by the constitutive proteasome or the immunoproteasome, which is inducible by IFNγ, but also by type I interferons. The peptides that leave the proteasome can be further cleaved by peptidases in the cytosol and are actively transported into the ER by the TAP transporter. In the ER, peptides are cleaved by aminopeptidases so that they perfectly fit into the MHC I peptide-binding groove. The peptide loading complex, a complex of three chaperones (calreticulin, calnexin and tapasin) and the thiol oxidoreductase PDIA3, ensures correct folding and stabilization of the nascent MHC I molecules. Upon binding of a high-affinity peptide, the MHC complex is stabilized and transported via the Golgi apparatus to the plasma membrane of the cell. Modified from (29) and (43).

The antigen processing machinery is tightly regulated, as productive antigen processing is crucial to elicit specific and robust CTL responses against viruses and also cancer. Thus, it is not surprising that there is considerable experimental evidence for alterations in the APM in viral infections and tumors (28, 55, 56).

1.1.4.1 Endoplasmic reticulum aminopeptidase 1

The first time *ERAP1* has been cloned and characterized was in 1999 (57). The gene is located on chromosome 5 in humans and chromosome 13 in mice, where it is frequently called *ERAAP* (ER aminopeptidase associated with antigen processing). ERAP1 is an ER resident zinc metalloaminopeptidase and belongs to the M1 protease family. Together with ERAP2, which is absent in mice, and IRAP these three enzymes have been classified into the oxytocinase subfamily of M1 proteases (58). *ERAP1* and *ERAP2* are highly homologous and have a sequence identity of 50%. The current opinion is that *ERAP2* has evolved by an evolutionary recent gene duplication event of *ERAP1* (59) explaining why there are no analogues in rodents. Notably, a minor allele of *ERAP2* has a single nucleotide polymorphism (SNP) that results in alternative splicing and degradation by nonsense mediated decay. Hence, approximately 25% of the population do not express ERAP2 at all, highlighting the pivotal role of ERAP1. Nevertheless, it has been proposed that ERAP1 and ERAP2 form heterodimers because both enzymes can be co-immunoprecipitated from cells (60). However,

direct experimental evidence for a heterodimer from crystallization studies is still missing.

Multiple functions have been attributed to ERAP1, including antigen processing, post-natal angiogenesis, shedding of several cytokine receptors (e.g. TNFR1), and blood pressure regulation. The latter effect is mediated by a secreted form of ERAP1 (61). This and the following section focus on the role of ERAP1 in antigen processing. The structure of ERAP1 has been solved and has essentially facilitated the understanding of the mode of action of this enzyme (62). ERAP1 is composed of four domains. The catalytic site with the zinc atom is located within domain II, which is capped by domain I. Domain III has the role of a hinge between domain II and IV and is thought to enable conformational changes between an "open" and a "closed" state (Figure 1.4). Domain IV has a concave shape and its orientation relative to domain I and II is changing during conformational changes. During the "open" state of ERAP1, the protein exposes a cavity, because domain IV is orientated away from domain II. In this state, elongated peptides can enter the cavity of ERAP1. The peptide is then trapped inside of the enzyme since domain IV is placed alongside of domain I and II. Next, the active site is activated and can trim peptides at their N-terminus. ERAP1 controls antigenic peptide generation by both generating and destroying MHC I ligands (63), thereby editing the antigenic peptide repertoire and immunodominance hierarchy of peptides (64, 65). The unique biological role of ERAP1 is attributed to its ability to spare shorter peptides (8-9 residues) and to prefer longer peptides (9-16 amino acids) (66). This length dependence of ERAP1 is called "the molecular ruler" property and is essential for its role in trimming MHC I ligands. Additionally, ERAP1 prefers substrates with several positively charged amino acids, hydrophobic C-termini and it preferentially removes hydrophobic residues (e.g. leucine, methionine, and phenylalanine) (66). The strong association of ERAP1 with immune responses is stressed by the fact that it is inducible by IFNγ (67).

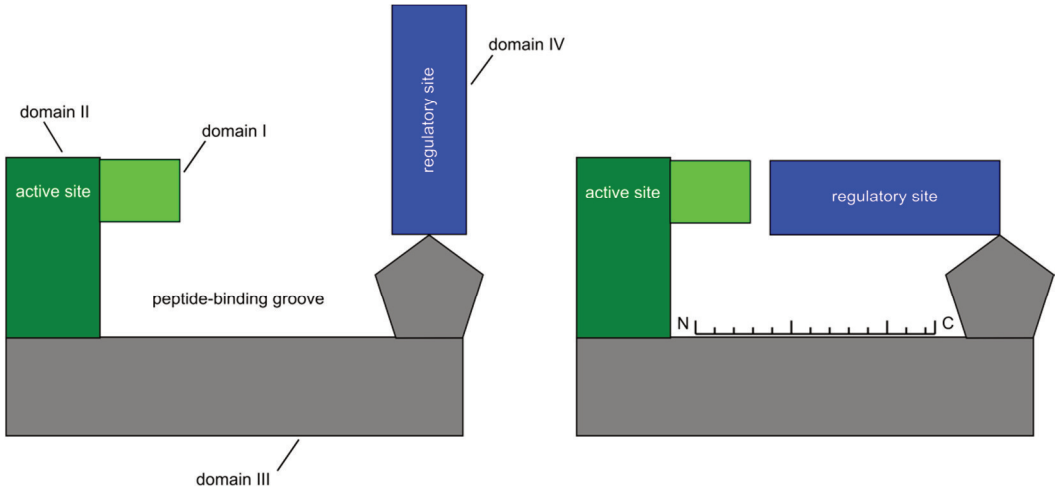

Figure 1.4: The molecular ruler mechanism of ERAP1. ERAP1 has two conformations, an "open" (left) and a "closed" (right) conformation. In the closed state, the active site of the enzyme is active and the interface is structured like a molecular ruler. The elongated peptide binds with its N-terminus facing the active site. Adapted from (49).

After the identification of ERAP1, its biological function in the immune system has been studied in *ERAAP* knockout mice by several groups independent of each other (reviewed in (61)). It has been observed that the loss of *ERAAP* moderately reduced MHC I molecules on the surface, ranging from 20-40% for the mouse MHC I molecules K^b and D^b. Moreover, it was reported that transfer of splenocytes from wild type mice into *ERAAP* knockout mice led to CTL responses, confirming that ERAP1 has a quantitative and qualitative effect on epitope generation as the wild type splenocytes were recognized as foreign. Experiments exploiting peptide-specific CD8 T cell hybridomas demonstrated that *ERAAP* loss had a neutral effect on some epitopes. However, other epitopes were either lacking or were upregulated, reflecting the chemical preferences of the peptidase.

1.1.4.2 ERAP1 in health and disease

There is abundant experimental evidence that ERAP1 is associated with different diseases, namely infection, autoimmune diseases and cancer. In an infection model of LCMV (lymphocytic choriomeningitis virus), the investigators observed that in mice lacking *ERAP1* CD8 T cell responses to LCMV peptides were altered in regard to magnitude, confirming that ERAP1 is a key player in the immunodominance hierarchy of epitopes (64). Further, escape mutations of the human immunodeficiency virus (HIV) alter HIV epitope processing dependent on ERAP1 (68). One such mutation was a change from alanine to proline at residue 146 in the HIV Gag protein immediately before the N-terminus, inhibiting trimming by ERAP1 and reducing CTL responses. In 2011, the first evidence of *ERAP1* as a direct target of a human cytomegalovirus (HCMV)-encoded microRNA (miR-US4-1) was reported (69). This microRNA downregulated the expression of *ERAP1*, which rendered HCMV infected cells less susceptible to CTLs, representing a novel immune evasion mechanism.

ERAP1 is a polymorphic gene and naturally occurring SNPs have been shown to be associated with susceptibility for several autoimmune diseases (70). In recent years, it has become clear that HLA-B27 and the ERAP1 variant K528R predispose to develop ankylosing spondylitis (AS) (71-73). Interestingly, AS-associated ERAP1 allotypes have altered trimming activities *in vitro*, which has a negative impact on peptide presentation by HLA-B27. In general, a pathogenesis mechanism for AS was characterized by very active or hypoactive ERAP1 variants that overtrimmed or undertrimmed their substrates (73). A recent study demonstrated that ERAP1 variants profoundly shape the HLA-A29:02 peptidome, suggesting that *ERAP1* SNPs influence the susceptibility to Birdshot Chorioretinopathy (74). In addition, SNPs of *ERAP1* in combination with certain HLA class I alleles are also associated with psoriasis (75) and Behçets disease (76).

The expression of ERAP1 has been studied in a panel of different cancers compared to normal counterparts. These studies revealed that ERAP1 was expressed at highly varying levels in all examined samples, including melanoma, leukemia-lymphomas, carcinoma of breast, colon, lung, skin, chorion, cervix, prostate, kidney and bladder (61, 77-79). In 12 cervical cancer samples, ERAP1 was found to be expressed at normal (7 out of 12), high (3 out of 12) and low (2 out of 12) levels compared to normal tissue, which was shown by the Human Protein Atlas project available from

www.proteinatlas.org (80). Another study of cervical cancer tissue observed a downregulation of ERAP1 in 15% of more than 100 investigated samples (81). ERAP1 variants were correlated with increased metastases and decreased survival in this disease (81, 82). Interestingly, SNPs in the polymorphic *ERAP1-127* locus, which is coding for the M1 peptidase domain, were associated with a bad prognosis. So far, only a few studies could directly show that ERAP1 expression affects the presentation of a specific epitope. The attenuation of ERAP1 expression in tumor entities where ERAP1 overexpression was reported showed increased anti-tumor immune responses against a colorectal carcinoma epitope and a melanoma epitope (83, 84). Taken together, all these studies show that ERAP1 is a key determinant of the MHC I epitope repertoire. For this reason, several groups are working on the identification of a specific chemical inhibitor for ERAP1. However, due to the similarity of ERAP1 to ERAP2 and IRAP, the inhibitors still exhibit cross-reactivity (85, 86). Whether ERAP1 drives destruction or generation of a peptide is dependent on the ERAP1 variant, the presenting MHC I allele and the specific peptide and has to be tested in each individual setup.

1.2 Human Papillomavirus

Papillomaviruses (PVs) have evolved successfully over millions of years to propagate in most mammals and birds. The papillomavirus group has two distinctive characteristics, which are the strict genotype-specific host-restriction and the epithelial tropism. Today, more than 300 PVs have been identified and sequenced, including over 200 human papillomaviruses (HPVs) (87). HPV is the most common sexually transmitted agent in the world. Harald zur Hausen postulated the connection between cervical cancer and HPV for the first time in the 1970s (88, 89). From the 80s on, when HPV16 and HPV18 were first isolated (90-92), the viruses have been investigated intensively.

HPVs are grouped into different genera, species and types (Figure 1.5). HPVs from the alpha genus are classified into low-risk and high-risk types (Figure 1.5) depending on the oncogenic potential. Notably, most high-risk types belong to the alpha9 species. While low-risk types cause benign ano-genital and skin warts, a persistent infection with a high-risk type can cause ano-genital cancer, such as cervical, vaginal, penile and anal cancer as well as a certain subset of head and neck cancer, namely oropharyngeal cancer (93-97). Of note, the low-risk types can also cause problematic diseases such as recurrent respiratory papillomatosis (RRP), which is associated with HPV11 (98). Every HPV type has a different pathology. For instance, HPV6 shows a preference for genital sites whereas HPV11 is the most prominent type at oral sites (99). Additionally, HPV16 is associated with cervical cancer ten times stronger than HPV31 and HPV35, and of these three types HPV16 is the only one that has been found in oropharyngeal tumors (99). To date, these subtle tropism differences cannot be explained, but they may be controlled at the level of viral gene expression by regulatory elements (100). The two high-risk types HPV16 and HPV18 mediate approximately 70% of all cervical cancers.

In virtually all other cervical cancers, DNA derived from other high-risk types can be found (101). To stress the importance of HPV research one should note that almost every sexually active individual will acquire at least one high-risk type infection during their lifetime (102). Usually, HPV infections are cleared by the immune system within 6 to 18 months (103, 104). In the minority of cases, less than 5%, a persistent infection establishes which is necessary for subsequent malignant transformation. Interestingly, a latent papillomavirus infection remains to be convincingly validated in humans, but experiments in animal models suggest that also this is likely (99).

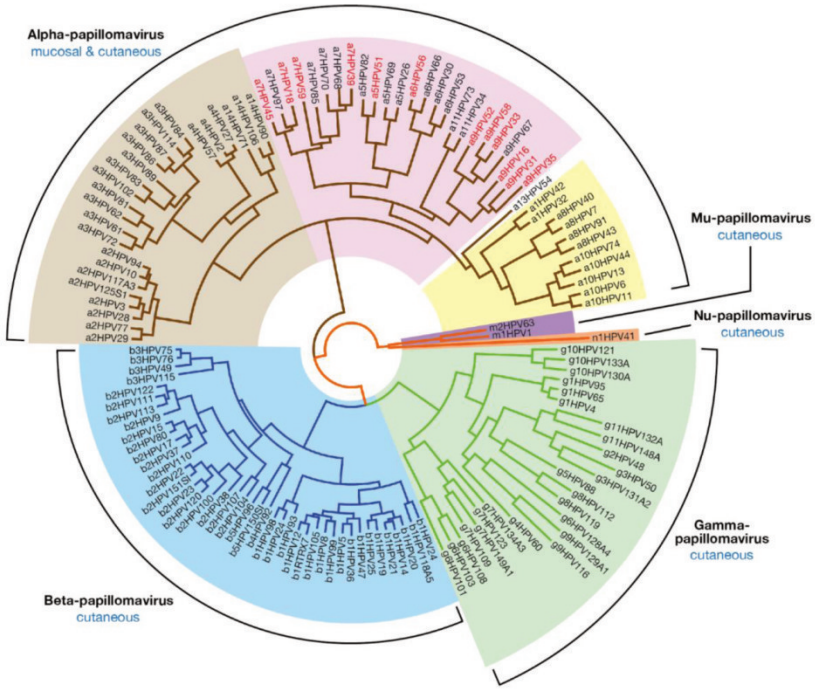

Figure 1.5: Human papillomavirus types fall into five genera. Types from the alpha genus are classified into low-risk cutaneous (brown), low-risk mucosal (yellow) or high-risk (pink). High-risk types highlighted in red are reported to be carcinogenic and the other high-risk types are possible carcinogens. The phylogenetic tree was prepared according to alignments of the E1, E2, L1 and L2 genes. Taken from (99).

1.2.1 HPV genome, viral life cycle and viral proteins

PVs are small (50-60nm diameter), non-enveloped and double-stranded DNA viruses with an icosahedral capsid illustrated in Figure 1.6 A. The circular DNA genome of HPVs comprises approximately 8,000 base pairs containing 8 or 9 open reading frames (ORFs) (105). Since the HPV genome is so small, the virus employs an elegant mechanism to make maximal use of its genome. The number of encoded proteins is increased, because gene expression involves the usage of many promoters and alternative splicing (106-108). The HPV genome encodes for early (E) and late (L) genes depending on their expression during the viral life cycle (Figure 1.6 B).

In general, the viral genome contains an upstream regulatory region (URR), comprising transcription factor binding sites and the replication origin, as well as the two ORFs encoding early and late genes. The early proteins (E1, E2, E4, E5, E6 and E7) are important for viral maintenance, replication and oncogenesis; whereas the late proteins (L1 and L2) are the capsid forming units. The

genes involved in replication (E1 and E2) and capsid formation (L1 and L2) are highly conserved among PVs, whereas the other genes (E4, E5, E6 and E7) have a greater diversity (109). The lack of an E3 ORF is attributed to an initial sequencing error in the bovine papillomavirus (BPV)1 genome (105).

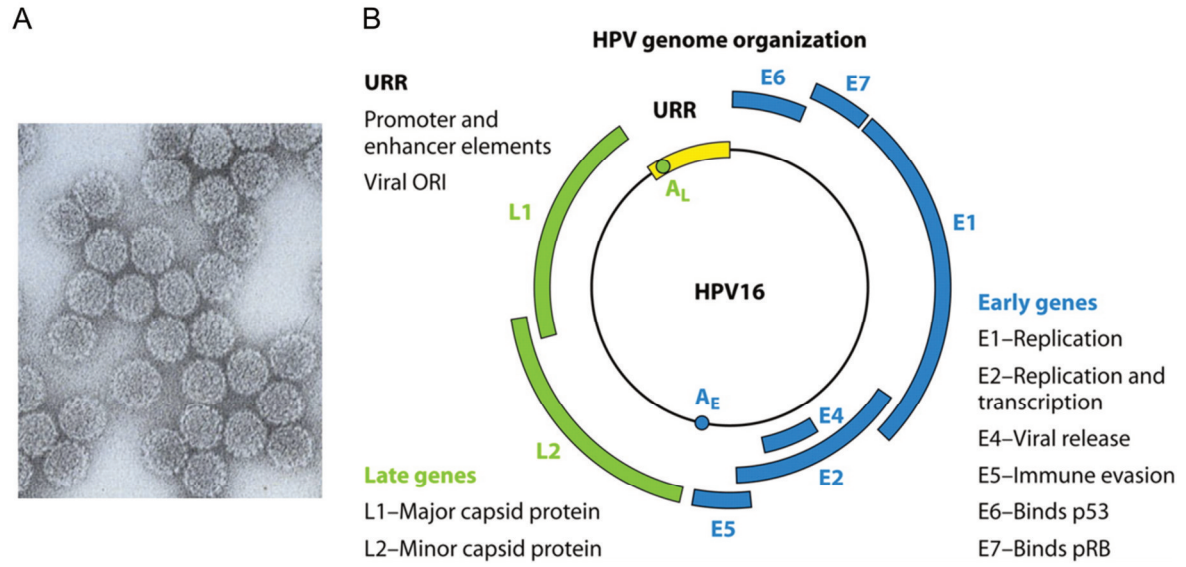

Figure 1.6: Viral particles and genome organization of HPV16. A. Negatively stained HPV16 particles photographed by electron microscopy. The particles are approximately 55nm in diameter and non-enveloped. The individual capsomeres of the capsid structure are clearly visible. Taken from (105). **B.** The HPV16 genome is circular and encodes for 6 early (blue) and 2 late (green) proteins. Whereas the early proteins are important for viral replication, maintenance and oncogenesis, the late proteins form the viral capsid. The upstream regulatory region (URR) controls early gene expression and replication since it contains promoter and enhancer elements and the viral origin of replication (ORI). Taken from (108). A_L = late polyadenylation signal, A_E = early polyadenylation signal

The viral life cycle of PVs is perfectly adapted to their host cells. PVs enter squamous epithelia of mucosa and skin through microabrasions, where they exclusively infect undifferentiated basal keratinocytes (Figure 1.7). Upon wound healing, cell proliferation is occurring, which is crucial for episomal maintenance of the viral genome and its entry into the nucleus (110). The cervical transformation zone is particularly susceptible for infections with high-risk HPV types. In this zone, squamous metaplasia occurs, which is the process of replacing the everted columnar epithelium on the ectocervix with a newly formed squamous epithelium from the sub-columnar reserve cells. The presence of cuboidal stem-like cells was suggested at the squamo-columnar junction, rendering this area prone to infection by high-risk types and susceptible to cancer progression (111). In addition, the incidence of infection is elevated during puberty since then metaplastic cells are present at this site (112). Of note, primary infections leading to malignant transformation have been observed mostly in the late teens or early twenties. The development from infection to persistent infection to late cervical intraepithelial lesion (CIN III) was estimated to be 7 to 15 years with a faster development following HPV16 and HPV18 infections (113).

Initially, virions bind to glycosaminoglycan (GAG) chains of heparan sulfate proteoglycan (HSPG) of the exposed basement membrane. This binding leads to a conformational change of the virion, exposing furin/proprotein convertase cleavage sites at the amino terminus of the virion coat protein L2 (105). Only after this conformational change basal keratinocytes can be infected. After infection, it is generally thought that an initial phase of genome amplification takes place before the viral episome is maintained at a low copy number within the basal cell. Here, E1, a DNA helicase, and E2, which binds to the non-coding region within the viral genome, initiate viral DNA replication. Laser capture methods (114) revealed that the episomal copy number in the infected cell is 50-100. For the initial genome amplification, E1 and E2 are essential, but E1 is dispensable for episomal maintenance when the copy number becomes constant. E2 is important for genome partitioning, replication and viral gene expression (105). Furthermore, E2 is repressing the expression of the oncogenes E6 and E7.

After cell division, one daughter cell moves to upper epithelial layers and starts differentiating, eventually leading to terminal differentiation (107). In an infected cell, terminal differentiation is prevented since the cell would enter cell cycle arrest, which would end viral replication. The transmembrane protein E5 has an important role in modulating cellular signaling by stabilizing the epidermal growth factor (EGF) receptor and enhancing mitogen-activated protein (MAP) kinase activity. This keeps the cell in a replicative state (115). Further, proliferation is mediated by E6 and E7, which allow expansion in lesion size. The role of E6 and E7 as key regulators of cell cycle progression is clearly defined for the high-risk types, whereas it is uncertain for the low-risk types that do not generally cause neoplasia. E7 promotes S-phase-entry by binding to the retinoblastoma protein (pRB), thereby activating the transcription factor E2F, which causes induction of S-phase genes such as cyclins (116, 117). Additionally, the binding of E7 to pRB leads to the upregulation of $p16^{INK4A}$, a surrogate biomarker for HPV oncogene expression and regulator of active cyclin kinases. The expression of p16 is found in 86% of cervical intraepithelial lesions grade I (CIN I), 100% of CIN II and CIN III and in 97% of cervical carcinomas (118). Eventually, cell cycle progression mediated by E7 would result in apoptosis, as p53 increases. The virus uses the E6 protein to counteract apoptosis. E6 interacts with an E3-ubiquitin E6-associated protein (E6-AP), which results in polyubiquitination of p53 leading to its degradation by the proteasome. Until now, 14 additional possible binding partners carrying a PDZ domain (that is bound by E6), have been identified. The majority of those is implicated in cell polarity, cell adhesion and cell differentiation (105, 119). Moreover, E6 is required for episomal maintenance of HPV16 and HPV31 genomes in primary human keratinocytes. With regard to its mechanism it is believed that E6 is controlled by phosphorylation, and binding to its substrates reveals an alternative binding site for the ubiquitin ligase (105). Taken together, E6 and E7 have a very large number of targets within the cell. The targets vary between HPV high-risk and low-risk groups and even between different high-risk types.

The HPV life cycle is completed by the expression of minor coat protein (L2), major coat protein (L1) and cell cycle exit to allow genome packaging. 72 capsomers form the HPV virion with approximately 80% L1 and 20% L2, which is mainly located on the inside (120, 121). Virus maturation takes place in the terminally differentiated cell and virions are released by the natural process of epithelial shedding. It is supposed but not exactly defined that E4 amyloid fibers are supporting virion release.

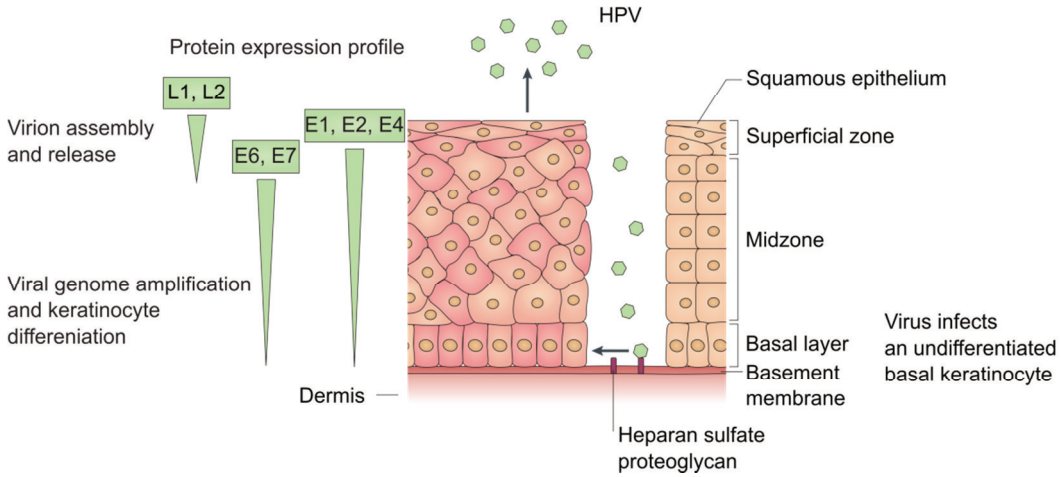

Figure 1.7: Viral life cycle of HPV16. The viral life cycle starts with the infection of a basal keratinocyte which is exposed by epithelial trauma. As the infected cell starts to differentiate and moves to upper layers of the epithelium, viral replication is triggered by the viral proteins E1 and E2. E6, E7 and E5 keep the cell in a proliferative state, but rising levels of E2 limit the expression of E6 and E7, allowing the cell to differentiate. The viral capsid proteins L1 and L2 are produced in the uppermost layer of the epithelium. Here, high levels of E4 enable virion release. Eventually, the virions are released during the normal process of epithelial cell shedding after the keratinocyte has undergone terminal differentiation. Modified from (107).

In HPV-associated neoplasia, protein expression leading to virus maturation and release is disrupted. An important step towards cancer progression is the integration of high-risk HPV DNA into the host genome. This happens in premalignant lesions, CIN II or CIN III. The integration of the high-risk type HPV genome happens in many cases via opening of the episome within the ORF of E2, which leads to the upregulation of the two oncoproteins E6 and E7. This scenario is often observed in late CIN II stages and the thus caused elevated proliferative phenotype of the cell favors the accumulation of genetic errors that contribute to cancer progression (122). Of note, E6 activates the human telomerase reverse transcriptase (*hTERT*) gene. A higher expression of hTERT results in telomerase activity, which adds hexamer repeats to the telomeric ends of chromosomes thereby immortalizing the cells (115).

1.2.2 Immune responses to HPV and immune evasion by HPV

The majority of HPV infections is cleared by the host immune system within 1-2 years after infection and only a minority of infected individuals develop HPV-mediated cancer (103). The natural immune

control of an HPV infection is achieved by innate and adaptive immune responses including specific antibodies and effector T cells (104). DCs within the dermis and Langerhans' cells, which are immature DCs resident in the epidermis and superficial epithelial layers of the mucosa, induce the adaptive immune response by detecting viral structures by pattern recognition through their TLRs. A protective immunity against local reinfection is accomplished by neutralizing antibodies against HPV capsid proteins, though these antibodies do not help against infected cells and a subsequent infection with other HPV types and do not form in every individual (123). Thus, it has become clear that the induction of a T cell mediated immune response and T cell memory is essential for the effective clearance of HPV (108). However, many naturally exposed individuals have a poor anti-HPV humoral immunity and patients with high grade CIN have an impaired T cell immunity against the HPV proteins E2, E6 and E7, when compared to patients with regressed lesions (124). This is the result of a broad and very effective spectrum of immune evasion strategies of HPV. Immune evasion strategies can be classified into immunosuppressive mechanisms during infection and in HPV-driven tumors (125).

During HPV infection, the virus follows the principle of "staying invisible" which also leads to a slower clearance compared to other viruses. The viral life cycle by itself is already an immune evasion strategy, because the virus stays outside the basement membrane, has no secreted proteins, keeps protein expression at a low level and does neither induce host cell death nor inflammation. HPV only infects basal keratinocytes and does not cross the basement membrane or enter the blood stream (104, 125). Access of the immune system to these regions of the skin is limited and furthermore HPV can impair the attraction of APCs such as LCs and macrophages. It is thought that this is due to an E6-mediated reduced E-cadherin expression on HPV-infected keratinocytes (105, 126) and a downregulation of macrophage inflammatory protein (MIP)-3α (127) in HPV16 E6 and E7 expressing keratinocytes. During normal physiologic conditions, LC trafficking is regulated by attaching to E-cadherin expressed on keratinocytes, and macrophages are attracted to the site of infection by MIP-3α. Furthermore, viral early gene expression is kept at low levels controlled by E2 (see 1.2.1) in the basal and lower layers of the epithelium, and HPV proteins are non-secreted. These low levels of viral protein expression can hinder the activation of local APCs and thus the induction of a potent adaptive immune response against HPV infected cells. The highly immunogenic virions and a higher expression of viral proteins happen only in the upper epithelial layers. At this time point, infected keratinocytes have entered the terminal differentiation phase and virions will only be released by the natural process of cell shedding from the surface of the epithelium, away from circulating immune cells (108, 124).

In addition, HPV has evolved multiple strategies to reduce the sensitivity of infected cells to anti-viral responses. It has been reported that TLR9 signaling is impaired, which has been attributed to HPV16 E6 and E7 (125, 128), thereby hindering the recognition of unmethylated CpG sequences in viral DNA. Moreover, the production and signaling of type I IFNs (IFN-α, IFN-β and IFN-κ), which

act as a first line of immune response against viruses, can be directly modified by HPV16. The E6 protein interferes with IFNα transcription by binding to the transcription activator interferon regulatory factor (IRF)3 and impairs IFNα signaling by inhibiting tyrosine kinase 2 (TYK2). Normally, TYK2 binds to the intracellular site of the IFN receptor. IFNβ can also be targeted by E6 via the inhibition of IRF3 transactivation. Lately, there has been experimental evidence for an implication of E6 in the transcription of IFNκ, a type I IFN only expressed in keratinocytes and DCs. The study showed that E6 contributed to *de novo* methylation near the transcriptional site of IFNκ. Besides high-risk E6, high-risk E7 blocks IFNβ transcription by an interaction with IRF1, and IFNα by binding to IRF9 (125, 129). In addition to the modulation of the IFN response, other cytokines are affected by HPV as well. IL-6, which is constitutively expressed by keratinocytes, and IL-1β have been found to be downregulated in a genome wide expression profiling array (130). Recently, the mechanism of IL-1β downregulation has been unraveled. IL-1β has been demonstrated to be degraded by the proteasome in HPV16 E6 expressing cells, which is caused by the ubiquitin-ligase E6-AP and p53 (131).

Most of the mechanisms explained above primarily affect inflammation and APC activation, the crucial link between the innate and the adaptive immune system. However, HPV has also evolved strategies to stay invisible for T cells. Inside the keratinocyte, HPV can perturb antigen processing and presentation (see 1.1.4) at multiple steps, thereby directly interfering with the effective generation of CTL epitopes. In the cytoplasm, the proteasome subunits PSMB8 and PSMB9 have a decreased expression in HPV16 infected cells (132). PSMB9 expression has been found to be repressed by HPV16 and HPV18 E7 (133), whereas the promoter of the *PSMB8* gene has been observed to be highly methylated in HPV16-positive cervical cancer (134). At the membrane of the ER, the TAP transporter can also be affected by HPV. Both, TAP1 and TAP2 are expressed at lower levels in cervical cancer. *TAP1* transcription can be inhibited by HPV16 E7 and additionally its promoter is highly methylated in HPV16-positive cervical cancer (132, 134). Furthermore, a loss or a partial loss of protein expression of MHC I, calreticulin, calnexin, ERAP1, PDIA3 and tapasin was described in cervical cancer (134). The expression of MHC I is impaired on the transcriptional level and during its presentation to the surface. E7 has been shown to directly block the MHC I heavy chain promoter (133). HLA-A and -B, but not HLA-C and -E, can be retained by an HPV16 E5-mediated mechanism within the cell (135). The E5 protein can interact with leucine pairs in the first transmembrane domain of the MHC I heavy chain. Alternatively, E5 keeps MHC I in the Golgi apparatus by vesicle alkalinization (136).

The combination of direct immune evasion, the lack of inflammation and a low level presentation of viral antigens rather favors immune tolerance than a potent T cell response that is able to quickly clear virus infected cells. For the effective clearance of HPV, a robust Th1 and CTL response is needed (125). Interestingly, it has been unraveled that HPV is also able to interfere with Th1/Th2 polarization of the immune response. In early HPV induced lesions, cytokines associated with a Th2-like immune response such as IL-6 and IL-10 are detected and only low or no IFNγ

mediated Th1 responses. On the contrary, high-grade epithelial lesions have upregulated TNFα and elevated levels of both Th1 and Th2 associated cytokines, reflecting an uncoordinated immune response in advanced disease. The shift from Th1 to Th2 during the early lesions may perturb proper virus immune recognition and thus promote disease persistence and progression (137, 138).

Besides the immune evasion strategies during infection, HPV-driven tumors employ additional strategies to hide from the host immune system. Almost all immune evasion strategies are present during infection as well as in HPV-driven tumors. In cancer, it is important to note that the expression of E6 and E7 is no longer attenuated, because E2 is lost when the HPV genome is integrated into the host genome (see 1.2.1). In order to evade immune recognition, HPV-driven tumors create an immunosuppressive environment similar to many other tumor types. Immunosuppressive cell types such as tumor-associated macrophages (TAMs), myeloid-derived suppressor cells (MDSCs) and Tregs are recruited to infiltrate the tumor (125). TAMs are a heterogeneous population of macrophages mostly with an M2-like phenotype that are known to inhibit antitumor T cell responses, attract Tregs and secrete the immunosuppressive cytokines IL-10 and TGFβ (139). MDSCs produce reactive oxygen species (ROS). Although the role of MDSCs in HPV-driven tumors has not been fully elucidated, it is believed that ROS cause inhibition of T cell activation by downregulating the CD3ζ-chain of the TCR complex (140). In addition, Tregs, important players of peripheral tolerance, secrete immunosuppressive cytokines such as IL-10 and TGFβ and can directly inactivate T cells for example by surface-expressed CTLA-4 (see 1.1.3).

In summary, HPV is a very successful virus because it is able to stay invisible to the immune system by employing different immune evasion mechanisms already during early infection. This enables HPV to persist for a long time and increases the risk of lesion persistence and the onset of malignant transformation. Fortunately, most HPV infections and lesions are cleared by the host immune system eventually, with HPV-specific CD4 and CD8 T cells as the crucial driving force to fight the infection. For this reason, therapeutic vaccines that trigger T cell responses are under intensive investigation and further insights of the molecular mechanisms of HPV immune escape can contribute to render these vaccines more successful.

1.3 Immunotherapy approaches against HPV

HPV is the most frequent viral infectious agent of the reproductive tract and HPV-induced diseases are regarded as a significant global health burden. Although most infections do not cause symptoms and are cleared by the host immune system, there is a risk that an infection becomes persistent and causes a pre-cancer lesion which can progress to cancer (see 1.2.2). In developing countries, cervical cancer is the second most common cancer in women. The impact of HPV is even higher because the virus also causes other ano-genital and also oropharyngeal cancers (93-97). Hence, vaccination against HPV is

one of the major breakthroughs in medical research.

There are two different vaccination concepts, prophylactic and therapeutic vaccination, which are used against HPV-induced malignancies. Prophylactic vaccines are administered to individuals that have not yet been exposed to the virus in order to prevent infection. On the contrary, therapeutic vaccination concepts intend to cure patients that already suffer from an HPV infection by mounting specific cellular immune responses against HPV antigens.

1.3.1 Prophylactic vaccines

In the 1980s, zur Hausen and colleagues were able to prove that HPV causes cervical cancer (90-92) and this was honored with the Nobel Prize for Physiology and Medicine in 2008. After this discovery, it was shown that HPV-specific immunoglobulins protect animals against a subsequent challenge with the virus (141). Several years later, it was reported that HPV virus-like particles (VLPs) consisting of the capsid protein L1 are highly immunogenic and stimulate the induction of neutralizing antibodies, which confer protection against infection with the HPV type of which the L1 protein was used (142, 143). L1 is produced recombinantly and the proteins self-assemble spontaneously into VLPs, resulting in conformationally correct capsids containing no viral DNA. Thus, VLPs harbor major epitopes of the HPV virion and have a good safety profile, which render this technology a clear candidate for a prophylactic vaccine. Indeed, the first two HPV VLP-based prophylactic vaccines were approved in 2006.

Today, two prophylactic vaccines are approved by the FDA in the US and the European Medicines Agency (EMA) of the European Union (144). One of the first two vaccines, Cervarix™ (GlaxoSmithKline), is bivalent and effective against the most common HPV high-risk types, HPV16 and HPV18. The included VLPs are produced recombinantly in *Trichoplusia ni* Hi-5 insect cells by baculovirus expression vectors and as an adjuvant, a mixture of aluminum hydroxide and monophosphoryl lipid A (MPLA), known as AS04, is included (145). The other vaccine, Gardasil™ (Merck) is quadrivalent and protects against infections with HPV16/18 and the low-risk types HPV6 and 11 that cause genital warts and respiratory papillomatosis. In contrast to Ceravix™, the VLPs are produced in *Saccharomyces cerevisiae* and the adjuvant is aluminum hydroxyphosphate sulphate (146). In 2014, the FDA approved Gardasil™9, which is a nonavalent vaccine containing VLPs from HPV6, 11, 16, 18, 31, 33, 45, 52 and 58. Currently, the EMA is evaluating the new vaccine for approval in Europe. Joura and colleagues have performed a clinical study on 14,215 women and showed that Gardasil™9 has the potential to protect against more HPV types, thereby increasing the overall prevention of cervical cancer from 70% to 90% (147). However, the exact impact of the prophylactic vaccines cannot be determined yet, because the time span from initial infection to development of cancer is 10-20 years. A long-term follow up study (9.4 years), which assessed the efficacy of Cervarix™, showed that antibody titers were much higher compared to natural infection

and remained high during the whole study period. Furthermore, vaccinated individuals were 100% protected from incident infection, persistent infection and cancer precursor lesions (CIN I and CIN II) (148). The final report of the PATRICIA (Papilloma Trial against Cancer In Young Adults) trial strengthened that vaccination of teenagers was effective against high-grade cervical lesions (149). FUTURE and FUTURE II (Females United to Unilaterally Reduce Endo/Ectocervical Disease), the follow-up studies of Gardasil™, evaluated the efficacy of the vaccine against infection, malignant disease and *condylomata acuminate* and found similar positive results (150).

1.3.2 Therapeutic vaccines

Although the prophylactic vaccines against HPV are highly effective, vaccination coverage is not optimal everywhere (151-153). Australia is a good example of effective vaccination introduction because a national HPV immunization program was introduced in 2007, which already resulted in coverage of over 70% of eligible persons. In developing countries, vaccination coverage is poor caused by financial and social issues. But even in the US and Europe, HPV vaccination coverage is lower when compared to other vaccines. Additionally, prophylactic vaccines are HPV type specific (see above) resulting only in protection against the strains included in the vaccine. Thus, there are still many people prone to HPV infection. Moreover, prophylactic vaccination has no therapeutic effect and cannot cure individuals that already have an infection (154). The current treatments for HPV lesions are surgical, but these treatments entail disfigurations, functional impairment and also high recurrence rates. For all these reasons, the development of a non-invasive therapeutic vaccine represents an attractive option to fight HPV-mediated cancer.

HPV-associated malignancies represent a perfect target for immunotherapeutic anti-cancer approaches, because in this case the malignant cells permanently express the viral proteins E6 and E7, which are non-self antigens. Various therapeutic anti-HPV vaccination approaches are being investigated, including DNA-based, viral/bacterial vector-based, cell-based, protein-based and peptide-based approaches (155, 156).

DNA vaccines offer many advantages in regard to safety, production and stable antigen production. Furthermore, the DNA itself may have adjuvant functions since DNA plasmids contain unmethylated CpG motifs that are detected by TLR9. Clinical trials have been performed for a DNA plasmid called ZYC101. ZYC101 encodes $E7_{83-95}$ derived from HPV16, which contains several HLA-A2-restricted CTL epitopes, and achieved immune responses in 11 out of 15 CIN2/3 patients, with 5 patients even showing complete histological regression (157). The enhanced vaccine ZYC101a contains E6 and E7 fragments derived from HPV16 and HPV18, but the phase 2 clinical trials did not result in an overall significant difference between treatment and placebo groups (158). Nevertheless, in women younger than 25 the resolution of CIN2/3 was promoted and reached statistical significance. Recently, another DNA vaccine named VGX-3100 (Inovio Pharmaceuticals), consisting of plasmids

encoding mutated HPV16 and HPV18 E6 and E7 proteins that are delivered by electroporation, was proved to be effective against CIN2/3 in a phase 2b trial (159). This vaccine was selected as the "Best Therapeutic Vaccine" by the World Vaccine Congress (March, 2016 in Washington, D.C.) and honored with a Vaccine Industry Excellence Award.

Viral vectors have also been used as a basis for therapeutic HPV vaccines. The viral vector itself represents a strong immunogenic stimulant resulting in a wide range of immune responses. However, one has to keep in mind that individuals may already have existing immunity against the viral vector or that they produce neutralizing antibodies upon vaccination, which renders a subsequent treatment non effective. This problem is primarily addressed by the use of viruses that normally infect other species. For therapeutic vaccination, Vaccinia virus, modified vaccinia virus ankara (MVA), recombinant adenoviral vectors, alphaviruses and lentiviruses are currently exploited for vaccine design. However, not all viral vectors have been introduced into a clinical trial due to different reasons. Viral vectors based on recombinant adenovirus have the major disadvantage that there is a high prevalence of already existing humoral responses in humans and so far no therapeutic effect of these vectors was reported (155). The main limitations of lentiviruses are safety concerns, since they harbor the risk of malignant transformation due to insertion of the viral vector to the host's genome. Alphaviruses are under extensive study because as RNA viruses they do not integrate into the host's genome and the recombinant gene is expressed transiently at a high level within the cytoplasm. Vaccinia virus based vaccines (TA-HPV) encoding a HPV16 and HPV18 E6/E7 fusion protein have been used in several clinical trials (160-163). E7 is mutated and the fusion construct has no transforming capacity. It was reported that this vaccine elicited HPV-specific CTL responses, antibody responses and partial regression of vulvar intraepithelial neoplasia (VIN). Clinical trials using a MVA vector were more successful and even achieved complete regressions in some patients (164).

Only one **bacterial-based vaccine** was employed for several clinical studies. The vaccine is based on *Listeria monocytogenes* (ADXC11-001), which is live attenuated and produces a fusion protein consisting of HPV16 E7 and a truncated form of listeriolysin O (LLO) serving as an adjuvant (155). The fusion protein has no transforming activity. During the phase 1 trial, 4 high-grade cervical cancer patients showed tumor regression (165). One phase 2 trial has been terminated in April 2016 due to lack of enrollment (NCT01116245). The second phase 2 trial has suspended patient recruitment because of a pending safety amendment (NCT01266460) and is estimated to be completed in 2018. For both phase 2 trials no preliminary results are available yet.

Clinical trials based on **cell-based vaccines** using autologous DCs also have been conducted. To this end, DCs from a patient were loaded with HPV specific peptides or proteins or they were transduced with HPV-protein-encoding DNA or viral vectors and reinjected into the patient. Although T cell responses against HPV antigens were observed, there were no clinical responses (155).

The use of **complete E6 and E7 proteins** in vaccine design was not promising for a long time. Recently, van Damme and colleagues reported the outcome from a phase I clinical trial with

their vaccine called GTL001, used to treat women infected with HPV16 or HPV18 and normal cytology (166). GTL001 contains recombinant versions from HPV16 and HPV18 E7. To prevent binding of E7 to pRB, parts of E7 were separately fused to inactive *Bordetella pertussis* CyaA. Immunogenicity and safety of this vaccine could be confirmed in this first clinical study.

The disadvantage of whole protein vaccines is that E6 and E7 need to be mutated for their use in a vaccine to ensure loss of their oncogenic properties, but possibly leading to destruction of immunodominant epitopes. This issue is circumvented by **peptide vaccines**, which only present part of the oncoproteins to the immune system. The most important advantage of peptide vaccines is that antigen presentation is facilitated by using peptides because they are quickly translocated from endolysosomes to the cytoplasm after DC uptake. Thus, antigens can be efficiently cross-presented leading to both CD4 and CD8 T cell responses (167). Peptides can be categorized into short minimal peptides and ***synthetic long peptides*** (SLP). Whereas short peptides consist of a specific CTL epitope of 8-11 amino acids in length, SLPs are between 15 to 35 amino acids long and therefore contain potential CD4 and CD8 T cell epitopes. At the Leiden University Medical Center, SLP-based vaccines have reached the clinical trial phase, representing a milestone in cancer vaccination research. The vaccine, HPV16-SLP, consists of 9 E6 and 4 E7 SLPs derived from HPV16 and was injected subcutaneously together with the adjuvant Montanide ISA 51 in patients suffering from VIN lesions, resulting in complete regression in 47% of VIN3 patients (168). Follow-up studies in CIN, however, showed CTL responses but they were not accompanied by clinical responses (155, 169). The authors suggest that subsequent trials should be based on combination therapies including for instance checkpoint inhibitors and immunmodulators to improve the efficacy of the vaccine. The VIN study was recently repeated with the addition of the immunmodulator imiquimod at the injection site. However, the success of the vaccination was not enhanced by imiquimod (170). The latest study from the group in Leiden combined standard chemotherapy, carboplatin and paclitaxel, with HPV16-SLP vaccination (171). Chemotherapy promoted tumor-specific T cell responses when the patients were vaccinated after carboplatin/paclitaxel therapy. The time point after chemotherapy was optimal when abnormal elevated frequencies of circulating myeloid cells, observed during tumor progression and induced by chemotherapy, had reached normal levels.

Vaccines based on SLPs contain several potential epitopes for CD4 and CD8 T cells, which entails the problem that it is not exactly known in which direction the immune response is triggered and the risk of unwanted immune responses cannot be excluded. Therefore, vaccines based on ***short peptides***, which contain defined CTL epitopes, is an approach to circumvent these problems. With short peptides, however, it is indispensable to design the vaccine for the different HLA types present within the population, since CTL epitopes are HLA-restricted (see 1.1.3). This issue is addressed using epitope prediction servers and employing HLA supertypes, which share peptide-binding specificities, allowing narrowing down the number of potential epitopes. In HLA binding assays, the binding specificity of a given peptide can be analyzed experimentally. In addition, mass spectrometry is an

important tool to investigate whether an epitope is truly presented on the target cell (172). For HPV16, the HLA-A2-restricted epitope $E7_{11-19}$ has been found on the long-standing HPV16-positive tumor cell line CaSki and two other cell lines transfected with the whole HPV16 genome (C66-3 and C66-7). Importantly, $E7_{11-19}$ elicited CTL immune responses *in vitro* (173). Nevertheless, the immunogenicity of a peptide has to be tested *in vitro* and *in vivo*. It also becomes clear that T helper cell epitopes should be included in a successful vaccine because they support the optimal activation and prolong the period of robust CTL responses (174, 175). In clinical trials, the HPV16 epitopes $E7_{11-20}$, $E7_{12-20}$ and $E7_{86-93}$ have been employed. One of the major challenges in short peptide vaccination is the right choice of adjuvants. The best clinical responses (complete regression in 3 of 18 patients) of a vaccine formulation with these peptides linked to a lipid tail (lipopeptides) included the CD4 T cell epitope PADRE and incomplete Freud's adjuvant (176). Recently, a phase 1 clinical trial with 24 enrolled patients suffering from CIN2/3 finished successfully (177). The vaccine called PepCan was composed of 4 HPV16 E6 epitopes and *Candida albicans* extract as a new adjuvant. The vaccine reached an overall regression rate of 52%. In order to improve clinical success of vaccines there are other novel adjuvant and delivery systems in preclinical studies such as liposomes (VacciMax®) and nanoparticles (155). Nanoparticles are polymers that gain increasing interest because the antigen can be delivered along with the adjuvant to the same APC (see 1.1.1).

In summary, there are various approaches for therapeutic HPV vaccination. Unfortunately, overall clinical success is so far limited. However, preclinical and clinical data are promising and demonstrate that the development of a therapeutic HPV vaccine is feasible. Besides vaccine formulation including antigens and adjuvants, it is absolutely necessary to further unravel mechanisms of immune evasion in HPV-induced malignancies in order to make vaccines more powerful.

1.4 Aims of this study

Nowadays, prophylactic HPV vaccines can prevent initial infection with up to nine HPV types, whereas experimental therapeutic vaccines can cure patients with already established infections. However, the overall clinical success of anti-HPV therapeutic approaches is limited so far. To increase the success of vaccines, it is important to thoroughly study molecular mechanisms that may hinder the optimal efficacy of a vaccine.

Manipulation of APM component expression is observed in various tumor entities. For some clinically relevant and dominant tumor-associated antigens it has been demonstrated that altered APM component expression decreases the presentation of these antigens. Inhibition of antigen presentation has been shown to be directly associated with reduced anti-tumor CTL responses. In HPV-induced malignancies, multiple strategies of immune evasion were described, including changes of APM component expression. However, potent T cell responses are necessary to clear HPV infections and lesions. Until now, a systematic analysis of the whole APM has not been performed in a large array of HPV-positive tumor samples. Moreover, experimental evidence describing the immunological consequences of APM changes is limited.

The first aim of this thesis was a systematic analysis of the APM on the mRNA level in a comprehensive collection of HPV16-positive tumor cell lines compared to HPV-negative cell lines. According to this screen, selected APM components were analyzed on the protein level in selected cell lines. This analysis revealed that the only APM component that was consistently overexpressed in HPV16-positive cell lines was ERAP1. This could be confirmed in immunohistochemistry of cervical tissue including all three grades of CIN and established cervical cancer. The second aim of this thesis was to analyze whether the elevated ERAP1 expression impacts on the HPV16 E6 and E7 epitope presentation. This question was addressed first by analyzing HLA-A2-restricted peptides using a highly sensitive mass spectrometry approach and second by peptide-specific CTLs in cytotoxicity assays.

2 Materials and Methods

2.1 Materials

2.1.1 Laboratory equipment

Equipment	Name	Company
Analytical balance		Ohaus, Nänikon, Switzerland
Cell counter	Countess® Automated Cell Counter	Invitrogen, Carlsbad, CA, USA
Cell freezing device	Cryo-Safe cryogenic vial cooler	Bel-Art Products, Wayne, NJ, USA
Centrifuge	Biofuge Pico, Fresco Centrifuge 5417R, 5418 Labofuge 400R Minicentrifuge SU1550 Multifuge® 16R Refrigerated Ultracentrifuge Sorvall RC5C	Heraeus, Hanau Eppendorf, Hamburg Heraeus, Hanau Sunlab, Aschaffenburg Heraeus, Hanau DuPont Instruments
Centrifuge rotor	75008179 A-8-11 FA-45-18-11 FA-45-30-11 TX-400 M-20	Heraeus, Hanau Eppendorf, Hamburg Eppendorf, Hamburg Eppendorf, Hamburg Heraeus, Hanau Heraeus, Hanau
Cytology processor	Cytyc ThinPrep® 2000 system	Hologic, Wiesbaden
Documentation agarose gels	Gel Jet Imager 2006 Printer P39D	Intas, Göttingen Mitsubishi, Electric, Tokio
	Gel Doc ™ EZ Imager	Biorad, Hercules, CA, USA
Documentation polyacrylamide gels	Fusion-SL chemiluminescence camera	Vilber Lourmat, Eberhardzell
Electrophoresis chamber for agarose gels	Owl Easycast B2	Owl Seperation Systems, Portsmouth, NH, USA
Electrophoresis chamber for SDS-PAGE	Mini-PROTEAN® Tetra Cell	Biorad, Hercules, CA, USA
ELISpot plate reader	CTL-Immunospot® S6 Ultra-UV	CTL, Bonn
Flow cytometer	FACS Canto II™	BD Biosciences, Franklin Lakes, NJ, USA
Freezer (-20°C)	Mediline	Liebherr, Biberach an der Riss Bosch, Stuttgart
Freezer (-80°C)	U725 Innova	New Brunswick, Nürtingen
Glasware	Duran Fisherbrand	Schott, Mainz Thermo Fisher Scientific, Waltham, MA, USA
Ice machine	Hoshizaki Cube Star	Hoshizaki, Tokio, Japan
Incubator (37°C, 5% CO_2, cell culture)	Heracell 150i C200	Thermo Fisher Scientific, Waltham, MA, USA Labotec Göttingen

Incubator (37°C)		WTB Binder, Tüttlingen
Irradiator	Gammacell 1000	Atomic Energy of Canada Limited, Ottawa, Canada
Laminar flow hood	SterilGard® Class II TypA B3	The Baker Company, Sanford, ME, USA
Light microscope	Wilovert Standard 30 microscope Olympus BX43, Olympus Colorview Camera	Hund Wetzlar, Wetzlar Olympus, Hamburg
Liquid nitrogen tank	Locator 8 plus	Barnstead/Thermolyne, Dubuque, IA, USA
Magnet for MACS	Quadro MACS	Miltenyi Biotec, Bergisch Gladbach
Magnetic stirrer	Combimag RCO	IKA-Werke GmbH, Staufen Heidolph Instruments, Schwabach
Mass spectrometer	Qtrap6500	Ab Sciex, Foster City, CA, USA
Microwave		Sharp, Osaka, Japan
Multilable plate reader	Multiskan™ FC microplate photometer	Thermo Scientific, Rockford, IL, USA
	Victor3	Perkin Elmer, Waltham, MA, USA
Nano Drop	ND-1000	PeqLab Biotechnologies, Erlangen
Neubauer cell counting chamber	Profondeur	Brand, Wertheim
PCR cycler	C1000 Touch™ Thermal Cycler PTC-200	Biorad, Hercules, CA, USA MJ Research, Canada
pH Meter	766 MP220 InLab Microelectrode	Knick, Berlin Mettler Toledo, Glostrup, Denmark
Pipette-Boy	Pipetboy acu	Integra Biosciences, Biebertal
Pipettes (single-channel)	Pipetman® Gilson FinnPipette F2 ErgoOne Eppendorf Reference®	Gilson, Bad Camberg Thermo Scientific, Rockford, IL, USA Starlab, Hamburg Eppendorf, Hamburg
Pipette (multi-channel)	Transferpette® S-12, 20-200µl, yellow	Brand, Wertheim
Pipettes glass		Hirschmann Labortechnik, Eberstadt
Platform shaker	STR6 Rotamax120 3013	Stuart Bibby Scientific, Staffordshire, UK Heidolph Instruments, Schwabach GFL, Burgwedel
Power supply	EPS500-400, EPS3500 MP 250V PowerPac300	Pharmacia, Uppsala, Sweden MS Major Science, Saratoga, CA, USA BioRad, Hercules, CA, USA

Pump	N86KT.18	KNF Neuberger, Freiburg
Quantitative PCR	MX300P qPCR System	Agilent Technologies, Waldbronn
Refrigerator (4°C)	Mediline	Liebherr, Biberach an der Riss Bosch, Stuttgart
Rolling shaker	CAT RM5	Zipperer, Staufen
Rotator		NeoLab, Heidelberg
Scale	Kern EG 4200-2NM	Kern & Sohn, Balingen
Surgical tweezer and scissors		Dimeda, Tuttlingen
Thermomixer	Thermomixer compact	Eppendorf, Hamburg
Trans-blot Semidry Transfer Cell		Biorad, Hercules, CA, USA
Ultrasonic water bath	VWR Ultrasonic cleaner USC300TH	VWR International, Leuven, Belgium
UPLC	nanoAcquity UPLC system	Waters, Milford, MA, USA
Vacuum centrifuge	Speedvac concentrator	Bachofer, Laboratoriumsgeräte, Reutlingen
Vortexer	Vortex-Genie 2	Scientific Industries, Bohemia, NY, USA
Water bath		GFL, Burgwedel
Water purification system	TKA™ X-CAD	Thermo Scientific, Braunschweig
WB transfer chamber (tank blot)	Mini Trans-Blot® Cell	Biorad, Hercules, CA, USA
WB transfer chamber (semidry)		Cti, Idstein/Taunus

2.1.2 Consumables

Name	**Company**
96-well qPCR plate semi-skirted, transparent	Applied Biosystems at Thermo Fisher Scientific, Waltham, MA, USA
Aluminium foil	CeDo GmbH, Mönchengladbach
Blood collection tubes (Sodium Heparin, 170 I.U.)	BD, Plymouth, UK
Blood collection set (Safety-lok™)	BD, Franklin Lakes, NJ, USA
Cell culture dish (60mm D x 16mm H; 6cm ø)	TPP, Trasadingen, Switzerland
Cell culture dish (100mm D x 20mm H; 10cm ø)	TPP, Trasadingen, Switzerland
Cell culture flask (25cm^2)	TPP, Trasadingen, Switzerland
Cell culture flask (75cm^2)	TPP, Trasadingen, Switzerland
Cell culture flask (150cm^2)	TPP, Trasadingen, Switzerland
Cell culture plate “CytoOne” (6-well)	Starlab, Hamburg
Cell culture plate (12-well)	Corning, Corning, NY, USA
Cell culture plate (24-well)	Corning, Corning, NY, USA
Cell culture plate (48-well)	Corning, Corning, NY, USA
Cell culture plate (96-well) - Flat bottom - U bottom	 BD, Franklin Lakes, NJ, USA TPP, Trasadingen, Switzerland
Cell scraper	Sarstedt, Newton, NC, USA
Cell strainer (40µM, 70µM)	BD, Corning, NY, USA

Cling film	CeDo GmbH, Mönchengladbach
Countess® cell counting chamber slides	Invitrogen, Carlsbad, CA, USA
Cryogenic vials (Nalgene)	Thermo Fisher Scientific, Rochester, NY, USA
ESI emitters	New objective, Woburn, USA
FACS tubes (5ml Polystrene round-bottom tube)	BD, Franklin Lakes, NJ, USA
Falcon tubes (15ml and 50ml)	Nerbe Plus, Winsen
Leucosep™	Greiner Bio-One, Frieckenhausen
Filter (Millex®-GS, pore size 0.22µm)	Merck Milipore, Cork, Ireland
GammaBind™ Plus Sepharose™	GE Healthcare, München
Gel-loading tips	Starlab, Hamburg
Gloves	Microflex, Reno, NV, USA
Immobilon®-P PVDF Transfer Membrane	Millipore, Bedford, MA, USA
Kimwipes delicate task wipers	Kimberly-Clark, Irving, TX, USA
Kimtech precision wipes tissue wipers	Kimberly-Clark, Irving, TX, USA
MACS Seperation Column LS	Miltenyi Biotec, Bergisch Gladbach
MultiScreen®-HA, 96-well filtration plate	Merck Milipore, Cork, Ireland
Mini-PROTEAN®TGX™ gels, Any kD™, various combs	Biorad, Hercules, CA, USA
nanoAcquity UPLC column, 75µm ID, length 25cm, 1.7µm CSH130 C18 material	Waters, Milford, MA, USA
NuPAGE Novex 4–12% Bis-Tris Mini Gels	Life Technologies, Brown Deer, WI, USA
Optical adhesive covers	Applied Biosystems
Pap Pen	Dako Agilent Pathology Solutions, Hamburg
Parafilm	Bemis, Neeah, WI, USA
PVDF Transfer Membrane	Thermo Scientific, Rockford, IL, USA
Pipette tips, with and without filter	Starlab, Hamburg
Reaction tubes (0.2ml, 0.5ml, 1.5ml and 2ml)	Starlab, Hamburg
Reaction tubes, black, flip cap (1.5ml)	NeoLab, Heidelberg
Reaction tubes, protein low binding (1.5ml)	Eppendorf, Hamburg
Scalpel	Feather, Osaka, Japan
Syringe (2ml Injekt®)	Braun, Melsungen
Syringe (10ml BD Plastipak Luer-Lok™)	BD, Drogheda, Ireland
Syringe (20ml BD Plastipak Luer-Lok™)	BD, Drogheda, Ireland
Syringe (50ml BD Plastipak Luer-Lok™)	BD, Drogheda, Ireland
Syringe for MS injection (500µl and 1ml)	Hamilton, Reno, USA
UPLC vials	MZ-Analysentechnik, Mainz, Germany
Vacuum filter (bottle top, 500ml, pore size 0.22µM)	TPP, Trasadingen, Switzerland
Western Blotting Filter Paper	Thermo Scientific, Rockford, IL, USA

2.1.3 Chemicals and biological reagents

Product	**Company**
6x Orange DNA Loading Dye	Thermo Fisher Scientific Ldt., Loughborogh, UK
Acetic acid (100%)	Merck Millipore, Billerica, MA, USA
Acetone	Sigma-Aldrich, Taufkirchen

Acteonitrile (I), HPLC/MS grade	Biosolve BV, CE Valkenswaard, The Netherlands
Agarose NEEO Ultra-Qualität Roti®garose	Roth, Karlsruhe
Albumin, from bovine serum albumin (BSA)	Sigma-Aldrich, Taufkirchen
Ammonium chloride (NH_4Cl)	Roth, Karlsruhe
Ammonium hydroxide (NH_4OH)	Sigma-Aldrich, Steinheim
Aquatex® aqueous mounting agent	Merck Millipore, Darmstadt
β-mercaptoethanol	Roth, Karlsruhe
BCIP/NBT-Plus substrate for ELISpot	Mabtech, Nacka Strand, Sweden
Bromophenol blue sodium salt	Roth, Karlsruhe
BSA standard	Biorad, Hercules, CA, USA
Calcium chloride ($CaCl_2$)	Sigma-Aldrich, Taufkirchen
Carboxyfluorescein (CFSE)	Invitrogen, Carlsbad, CA, USA
CEF Control Peptide Pool HLA Class I	PANATecs, Heilbronn
CE Peptide Pool HLA-A24	PANATecs, Heilbronn
Citric acid	AppliChem, Darmstadt
Complete mini protease inhibitor cocktail	Roche, Basel, Switzerland
Concanavalin A (ConA) from *Canavalia ensiformis*	Sigma-Aldrich, Steinheim
Deoxynucleoside Triphosphate	Roche, Mannheim
Dimethyl sulfoxide (DMSO)	Sigma-Aldrich, Taufkirchen
Disodium hydrogen phosphate (Na_2HPO_4 2 H_2O)	Sigma-Aldrich, Taufkirchen
Distilled DNase/RNase free water	MP Biomedicals, Illkirch, France
ECL Prime Western Blotting Detection Reagent	GE Healthcare, Buckinghamshire, UK
Empore Octyl C8 extraction material	3M company, St. Paul, MN, USA
Ethanol (absolute)	Sigma-Aldrich, Taufkirchen
Ethylenediaminetetraacetic acid (EDTA)	Sigma-Aldrich, Taufkirchen
FarRed (dimethyldodecylamine oxide-succinimidyl ester)	Invitrogen, Carlsbad, CA, USA
Formic acid (FA), LC/MS grade	ProteoChem, Inc., Denver, USA Biosolve BV, CE Valkenswaard, The Netherlands
GelRed™ 10,000x in water	Biotium, CA, USA
Glow Writer Phosphorescent Marking Pen	Diversified Biotech, MA, USA
Glycerole	Sigma-Aldrich, Taufkirchen
Glycine	Sigma-Aldrich, Taufkirchen
Hydrogen chloride (HCl)	VWR International, Fontenay-sous-Bois, France
Hydrogen peroxide (H_2O_2)	Sigma-Aldrich, Taufkirchen
IGE-PAL-630	Sigma-Aldrich, Taufkirchen
Isopropanol	Sigma-Aldrich, Taufkirchen
Magnesium chloride ($MgCl_2$)	Roche, Branchburg, NJ, USA
Mayer's Hematoxylin	Dako Agilent Pathology Solutions, Hamburg
Methanol	Sigma-Aldrich, Taufkirchen
Milk powder, low-fat	Roth, Karlsruhe
Nonyl phenoxypolyethoxylethanol (NP-40)	Sigma-Aldrich, Taufkirchen
OneComp eBeads	eBioscience, San Diego, CA, USA
Pefabloc	Merck, Whitehouse Station, NJ, USA
Phenylmethylsulfonylfluorid (PMSF)	Roth, Karlsruhe
Pierce ECL Western Blotting Substrate	Thermo Fisher Scientific, Waltham, MA, USA

Ponceau red solution	Serva, Heidelberg
Potassium bicarbonate ($KHCO_3$)	Roth, Karlsruhe
Potassium chloride (KCl)	Roth, Karlsruhe
Potassium dihydrogen phosphate (KH_2PO_4)	Roth, Karlsruhe
PreservCyt solution	Hologic, Wiesbaden
Protease Inhibitor Cocktail	Sigma-Aldrich, Steinheim
Proteinase K	Qiagen, Hilden
Seppak extraction cartridge C18	Waters, Milford, MA, USA
Sodium acetate ($C_2H_3NaO_2$)	Roth, Karlsruhe
Sodium azide (NaN_3)	AppliChem, Darmstadt
Sodium bicarbonate ($NaHCO_3$)	Sigma-Aldrich, Taufkirchen
Sodium chloride (NaCl)	Sigma-Aldrich, Taufkirchen
Sodium dihydrogen phosphate (NaH_2PO_4 2 H_2O)	Sigma-Aldrich, Taufkirchen
Sodium dodecyl sulfate (SDS), ultrapure	Roth, Karlsruhe
Sodium deoxycholate (Na-DOC)	AppliChem, Darmstadt
Sodium hydroxide (NaOH)	Sigma-Aldrich, Taufkirchen
Streptavidin-Alkaline Phosphatase	Mabtech, Nacka Strand, Sweden
ThinPrep®, cytology slides	Hologic, Wiesbaden
Trifluoroacetic acid (TFA), > 99% pure, protein sequencing grade	Sigma-Aldrich, Steinheim
Trizmabase	Sigma-Aldrich, Taufkirchen
Trypan blue stain (0.4%)	Invitrogen, Carlsbad, CA, USA
Tween20 (= Polysorbat 20)	MP Biomedicals, Illkirch, France
LC/MS grade water	Biosolve BV, CE Valkenswaard, The Netherlands
Xylol	VWR Chemicals, Darmstadt
Zorbax C18 chromatographic material, 5µm	Agilent Technologies, Santa Clara, CA, USA

2.1.4 Cell culture basal media and supplements

Basal media	
Product	**Company**
DermaLife K serum free keratinocyte culture medium	Cell Systems, Troisdorf
Dulbecco's Modified Eagle Medium (DMEM)	Sigma-Aldrich, Taufkirchen
DMEM with GlutaMAX™	Invitrogen, Carlsbad, CA, USA
Eagle's minimum essential medium (EMEM)	Sigma-Aldrich, Taufkirchen
Iscove's Modified Dulbecco's Medium (IMDM)	Life Technologies, Brown Deer, WI, USA
Ham's F12 Nutrient Mix	Invitrogen, Carlsbad, CA, USA
Keratinocyte serum-free medium (K-SFM)	Invitrogen, Carlsbad, CA, USA
Opti-MEM®	Invitrogen, Darmstadt
RPMI 1640 with L-glutamine	Sigma-Aldrich, Taufkirchen

Supplements	
Product	**Company**
Adenine	PAA Laboratories, Cölbe
β-mercaptoethanol, 50mM, sterile	Life Technologies, Grand Island, NY, USA

Bovine pituitary extract (BPE)	Invitrogen, Carlsbad, CA, USA
Calcium chloride ($CaCl_2$)	Sigma-Aldrich, Steinheim
Cholera toxin	Sigma-Aldrich, Taufkirchen
Cyclosporin A	Sigma, St. Louis, MO, USA
Epidermal growth factor (EGF)	Invitrogen, Carlsbad, CA, USA
Fetal Calf Serum (FCS)	Biowest, Nuaillé, France Sigma-Aldrich, Taufkirchen
Ficoll-Paque™ Plus	GE Healthcare Bio-Sciences, Uppsala, Sweden
G-418 Sulfate	Cayman Chemical, Ann Arbor, MI, USA
Gentamycin	BioConcept, Allschwil, Switzerland
GM-CSF, recombinant human	R & D Systems, Minneapolis, MN, USA
HEPES	Life Technologies, Grand Island, NY, USA
Human serum, type AB	Sigma-Aldrich, Taufkirchen
Hydrocortizone	Sigma-Aldrich, Taufkirchen
IL-1β, recombinant, human	R & D Systems, Minneapolis, MN, USA
IL-2, recombinant, human	PeproTech, Rocky Hill, NJ, USA
IL-4, recombinant, human	R & D Systems, Minneapolis, MN, USA
IL-6, recombinant, human	R & D Systems, Minneapolis, MN, USA
IL-7, recombinant, human	R & D Systems, Minneapolis, MN, USA
IFNγ, recombinant, human	BASF, Ludwigshafen
Insulin, recombinant, human	Sigma-Aldrich, Taufkirchen
L-glutamine	Sigma-Aldrich, Taufkirchen
Lipopolysaccharide (LPS)	Invivogen, Toulouse, France
MEM non-essential amino acid solution (MEM NEAA)	Invitrogen, Carlsbad, CA, USA
Paraformaldehyde (PFA)	Sigma-Aldrich, Taufkirchen
Penicillin/Streptomycin-Solution (P/S)	Sigma-Aldrich, Taufkirchen
Prostaglandin E_2 (PGE_2)	Cayman Chemical, Ann Arbor, MI, USA
Sodium bicarbonate ($NaHCO_3$)	Sigma-Aldrich, Taufkirchen
Sodium pyruvate ($C_3H_3NaO_3$)	PAA Laboratories, Cölbe
TNFα, recombinant human	R & D Systems, Minneapolis, MN, USA
Transferrin, recombinant human	Sigma-Aldrich, Taufkirchen
Tri-iodo-thyronine	Sigma-Aldrich, Taufkirchen
Trypsin-EDTA solution	Sigma-Aldrich, Taufkirchen

2.1.5 Kits

Name	**Company**
AccuScript High Fidelity 1st Strand cDNA Synthesis Kit	Agilent Technologies, Waldbronn
CD8 T Cell untouched Isolation Kit, human	Miltenyi Biotec, Bergisch Gladbach
CD14 microbeads, human	Miltenyi Biotec, Bergisch Gladbach
DC™ Protein Assay	Biorad, Hercules, CA, USA
DharmaFECT I	Thermo Fisher Scientific, Carlsbad, CA, USA
Lipofectamine® RNAiMAX	Invitrogen, Carlsbad, CA, USA
peqGOLD Gel Extraction Kit	PEQLAB Biotechnologie, Erlangen

QIAamp DNA Mini Kit	Qiagen, Hilden
QIAquick PCR Purification Kit	Qiagen, Hilden
QuantiTect Reverse Transcription Kit	Qiagen, Hilden
QIAshredder Homogenization Kit	Qiagen, Hilden
RNeasy Mini Kit	Qiagen, Hilden
TaqMan® Gene Expression Assay Kits	Applied Biosystems at Thermo Fisher Scientific, Waltham, MA, USA
TaqMan® Gene Expression Master Mix	Applied Biosystems at Thermo Fisher Scientific, Waltham, MA, USA
VECTASTAIN Elite ABC Kit	Vector Laboratories, Burlingame, CA, USA

2.1.6 Enzymes

Enzyme	Company
AmpliTaq Gold®	Roche, Branchburg, NJ, USA
KOD Hot Start Master Mix	Merck Millipore, Billerica, MA, USA

2.1.7 Antibodies

Name	Clone	Species	Company
Western blot			
anti-HPV16 E7	NM2	mouse	Kindly provided by Martin Müller, Tumorvirus-specific Vaccination Strategies, DKFZ, Heidelberg
anti-human α-tubulin	B-5-1-2	mouse	Sigma-Aldrich, Steinheim
anti-human β-actin	AC-74	mouse	Sigma-Aldrich, Steinheim
anti-human calreticulin	EPR3924	rabbit	Merck Millipore, Billerica, MA, USA
anti-human ERAP1	EPR6069	rabbit	OriGene, Rockville, MD, USA
anti-human ERAP2	3F5	rabbit	R&D Systems, MN, USA
anti-human MHC class I	EP1395Y	rabbit	Abgent, San Diego, CA, USA
anti-human PSMB8	polyclonal	rabbit	Enzo Life Sciences, Lörrach
anti-human PSMB9	polyclonal	rabbit	Enzo Life Sciences, Lörrach
anti-human PSMB10	polyclonal	rabbit	Enzo Life Sciences, Lörrach
anti-human PSME1	polyclonal	rabbit	Enzo Life Sciences, Lörrach
anti-human PSME1	polyclonal	rabbit	Enzo Life Sciences, Lörrach
anti-human tapasin	polyclonal	rabbit	LifeSpan BioSciences, WA, USA
Immunohistochemistry			
anti-human ERAP1	EPR6069	rabbit	OriGene, Rockville, MD, USA
anti-human $p16^{INK4a}$ (CINtec® Histology)	E6H4	mouse	Roche mtm Laboratories, Mannheim
ELISpot			
anti-human IFNγ	1-D1K	mouse	Mabtech, Nacka Strand, Sweden
anti-human IFNγ biotin	7-B6-1	mouse	Mabtech, Nacka Strand, Sweden

Immunoprecipitation			
anti-human HLA-A2	BB7.2	mouse	BD Biosciences, San Diego, CA, USA and a kind gift from Hans-Georg Rammensee (University of Tübingen, Germany)

Flow cytometry			
anti-human CD3-Pacific Blue™	UCHT1	mouse	BioLegend, San Diego, CA, USA
anti-human CD4-PE	RPA-T4	mouse	BD Biosciences, San Diego, CA, USA
anti-human CD8-APC	SK1	mouse	BioLegend, San Diego, CA, USA
anti-human CD8-FITC	RPA-T8	mouse	BD Biosciences, San Diego, CA, USA
anti-human CD14-FITC	M5E2	mouse	BD Biosciences, San Diego, CA, USA
anti-human CD19-Pacific Blue™	HIB19	mouse	BioLegend, San Diego, CA, USA
anti-human CD40-APC	HB14	mouse	BioLegend, San Diego, CA, USA
anti-human CD80-PE/Cy7	2D10	mouse	BioLegend, San Diego, CA, USA
anti-human CD83-PE/Cy7	HB15e	mouse	BD Biosciences, San Diego, CA, USA
anti-human CD86-APC	2331	mouse	BD Biosciences, San Diego, CA, USA
anti-human CD154-PE	24-31	mouse	BioLegend, San Diego, CA, USA
anti-human HLA-A2-FITC	BB7.2	mouse	BioLegend, San Diego, CA, USA
anti-human HLA-A24	17A10	mouse	MBL, Nagano, Japan
anti-human HLA-A,-B,-C-FITC	W6/32	mouse	BioLegend, San Diego, CA, USA
Mouse IgG1 κ isotype control-Pacific Blue™	MOPC-21	mouse	BioLegend, San Diego, CA, USA

Conjugated secondary antibodies			
anti-mouse IgG (H&L) horseradish peroxidase (HRP)	anti-mouse IgG (H&L) horseradish peroxidase (HRP)	goat	Dianova, Hamburg
anti-mouse IgG (H&L) HRP	anti-mouse IgG (H&L) HRP	goat	Promega, Madison, WI, USA
anti-rabbit IgG (H&L) HRP	anti-rabbit IgG (H&L) HRP	goat	Rockland Immunochemicals, Limerick, PA, USA
anti-mouse FITC	anti-mouse FITC	goat	BD Biosciences, San Diego, CA, USA

2.1.8 Cell lines

Cell line	Description	HPV status	Source	Medium	Reference
866	human, cervical, adherent	HPV16 positive	kindly provided by Peter L. Stern, University of Manchester, Manchester, UK	F-medium	(178)

915	human, cervical, adherent	HPV16 positive	kindly provided by Peter L. Stern, University of Manchester, Manchester, UK	F-medium	(178)
C66-3	human, cervical, HPV-transfected, adherent	HPV16 positive	kindly provided by John H. Lee, Sanford Health Center, Sioux Falls, SD, USA	E-medium	(179)
C66-7	human, cervical, HPV-transfected, adherent	HPV16 positive	kindly provided by John H. Lee, Sanford Health Center, Sioux Falls, SD, USA	E-medium	(179)
CaSki	human, cervical, adherent	HPV16 positive	kindly provided by Felix Hoppe-Seyler, Molecular Therapy of Virus-Associated Cancers, DKFZ, Heidelberg; purchased from ATCC	complete DMEM CaSki medium	(180)
FK16A	human, foreskin keratinocytes, HPV-transfected, adherent	HPV16 positive	kindly provided by Renske Steenbergen, University Medical Center Amsterdam, Netherlands	complete K-SFM	(181)
Goe	human, cervical, adherent	HPV16 positive	kindly provided by Andreas Kaufmann, Charité, Berlin	M10 medium	
HPK1A	human, foreskin keratinocytes, HPV-transfected, adherent	HPV16 positive	Kindly provided by Elisabeth Schwarz, Molecular Diagnostics of Oncogenic Infections, DKFZ, Heidelberg	complete DMEM	(182)
Mar	human, keratinocytes, adherent	HPV16 positive	kindly provided by Andreas Kaufmann, Charité, Berlin	complete DMEM	
MRIH196	human, cervical, adherent	HPV16 positive	kindly provided by Elisabeth Schwarz, DKFZ, Heidelberg	complete DMEM	(183)
SiHa	human, cervical, adherent	HPV16 positive	kindly provided by Felix Hoppe-Seyler, Molecular Therapy of Virus-Associated Cancers, DKFZ, Heidelberg	complete DMEM	(184)
SNU1000	human, cervical, adherent	HPV16 positive	Korean Cell Line Bank, Seoul, South Korea	complete RPMI-H	(185)
SNU1005	human, cervical, adherent	HPV16 positive	Korean Cell Line Bank, Seoul, South Korea	complete RPMI-H	(185)

SNU1299	human, cervical, adherent	HPV16 positive	Korean Cell Line Bank, Seoul, South Korea	complete RPMI-H	(185)
SNU17	human, cervical, adherent	HPV16 positive	Korean Cell Line Bank, Seoul, South Korea	complete RPMI-H	(185)
SNU703	human, cervical, adherent	HPV16 positive	Korean Cell Line Bank, Seoul, South Korea	complete RPMI-H	(185)
2A3	human, HNSCC, HPV-transfected, adherent	HPV16 positive	kindly provided by Ekaterina Dadachova, Albert Einstein College of Medicine, Bonx, NY, USA	2A3 medium	(186)
93VU147T	human, HNSCC, adherent	HPV16 positive	kindly provided by Renske Steenbergen, University Medical Center Amsterdam, Netherlands	complete DMEM	(187)
SCC090	human, HNSCC, adherent	HPV16 positive	kindly provided by Susanne Gollins, University of Pittsburgh, Pittsburgh, PA, USA	M10 medium	(188)
SCC152	human, HNSCC, metastasis of SCC90, adherent	HPV16 positive	kindly provided by Susanne Gollins, University of Pittsburgh, Pittsburgh, PA, USA	M10 medium	(188)
SCC154	human, HNSCC,	HPV16 positive	kindly provided by Susanne Gollins, University of Pittsburgh, Pittsburgh, PA, USA	M10 medium	(189)
UDSCC2	human, HNSCC, adherent	HPV16 positive	kindly provided by Thomas Hoffmann, Uniklinikum Essen, Essen	complete RPMI-P + 1% (v/v) P/S	(190)
UMSCC47	human, HNSCC, adherent	HPV16 positive	kindly provided by Tom Carey, University of Michigan, Ann Arbor, MI, USA	complete DMEM	(191)
SNU1160	human, cervical, adherent	HPV18 positive	Korean Cell Line Bank, Seoul, South Korea	complete RPMI-H	(185)
C33A	human, cervical, adherent	HPV negative	kindly provided by Felix Hoppe-Seyler, Molecular Therapy of Virus-Associated Cancers, DKFZ, Heidelberg	complete DMEM	

HaCat	human, keratinocytes, adherent	HPV negative	kindly provided by Petra Boukamp, Genetics of Skin Carcinogenesis, DKFZ, Heidelberg	complete DMEM	(192)
NOK	human, oral keratinocytes (hTERT immortalized)	HPV negative	kindly provided by Karl Münger, Brigham and Women's Hospital, Boston, MA, USA	complete K-SFM	(193)
RiSh	human, B-LCL, EBV-immortalized, suspension	HPV negative	generated from a healthy blood donor by Stephanie Hoppe, Immunotherapy and -prevention, DKFZ, Heidelberg	B-LCL medium	(194)
tCD40L NIH3T3	mouse, fibroblasts, transduced with human tCD40L	HPV negative	kindly provided by Derin Keskin, Harvard Medical School, Boston, MA, USA	NIH 3T3 tCD40L, NIH 3T3 WT	(195)

2.1.9 Primary cells

Cell line	Description	Source	Medium
primary human keratinocytes (pHK)	human, keratinocytes, adherent	kindly provided by Petra Boukamp, Genetics of Skin Carcinogenesis, DKFZ, Heidelberg	Complete DermaLife K
primary human foreskin keratinocytes (pHFK)	human, keratinocytes, adherent	purchased from Life Technologies, CA, USA	Complete DermaLife K

2.1.10 Primers

All primers used in this study were synthesized by Sigma-Aldrich (Taufkirchen). The primers in the Table below are listed in the direction 5'→3'.

Primers for *ERAP1* amplification and sequencing	
ERAP1 F	ATGGTGTTTCTGCCCCTCAAATGG
ERAP1 F 955	CAGCATACCGTATCCCCTACCC
ERAP1 F 1773	CACCAGCAAATCCGACATGGTCC
ERAP1 F seq6	AAGTGGAAGGAATCCAATGG
ERAP1 F seq7	AATACGACTTCCTGAGTACG
ERAP1 R	TTACATACGTTCAAGCTTTTCACTTT
ERAP1 R 1031	CAGTCCCCAGTTTTCCATAGCACC
ERAP1 R 1881	GTAATAGCCATTCATGCCCACATTA
ERAP1 seq1	GATTTTGAGTCTGTCAGCAAGAT
ERAP1 seq2	GGGGAGGAATGTACACATGA

ERAP1 seq3	CCCTAGATATCTGCAGGTGG
Other primers	
HPRT1.FOR	TATGGACAGGACTGAACGTCTT
HPRT1.REV	TCCCCTGTTGACTGGTCATT
Myco1.F	GGGAGCAAACAGGATTAGATACCCT
Myco2.R	TGCACCATCTGTCACTCTGTTAACCTC

2.1.11 TaqMan® Gene Expression Assays

Gene	Assay ID	NCBI ID	Amplicon length
β2m	Hs00984230 m1	NM 004048.2	81
calreticulin	Hs00189032 m1	NM 004343.3	95
calnexin	Hs01558409 m1	NM 001024649.1, NM 001746.3	129
ERAP1	Hs00429970 m1	NM 001040458.1, NM 001198541.1, NM 016442.3	66
ERAP2	Hs01073631 m1	NM 001130140.1, NM 022350.3	116
GAPDH	Hs02758991 g1	NM 001256799.1, NM 002046.4	93
HLA-A	Hs01058806 g1	NM 001242758.1, NM 002116.7	70
HLA-B	Hs00818803 g1	NM 005514.6	189
HLA-E	Hs03045171 m1	NM 005516.5	130
IPO8	Hs00183533 m1	NM 001190995.1, NM 006390.3	71
PDIA3	Hs00607126 m1	NM 005313.4	129
PGK1	Hs00943178 g1	NM 000291.3	73
PPIA	Hs04194521 s1	NM 021130.3	97
PSMB10	Hs00988194 g1	NM 002801.3	60
PSMB5	Hs00605652 m1	NM 001144932.1, NM 002797.3	149
PSMB6	Hs00382586 m1	NM 002798.1	93
PSMB7	Hs00160607 m1	NM 002799.2	120
PSMB8	Hs00544757 g1	NM 148919.3, NM 004159.4	72
PSMB9	Hs00160610 m1	NM 002800.4	80
PSME1	Hs00389210 g1	NM 176783.1, NM 006263.2	115
PSME2	Hs01923165 u1	NM 002818.2	95
TAP1	Hs00388675 m1	NM 000593.5	74
TAP2	Hs00241060 m1	NM 000544.3, NM 018833.2	66
tapasin	Hs00917451 g1	NM 172208.2, NM 172209.2, NM 003190.4	73

2.1.12 Small interference RNAs (siRNAs)

The siRNA sequences in the Table below are listed in the direction 5'→3'.

Name	Target/Sequence	Features	Company
siERAP1	*ERAP1* (NCBI ID: 51752)	pool of 30 specific siRNAs	siTOOLs Biotech, Martinsried
sicontrol		pool of 30 non-specific siRNAs	siTOOLs Biotech, Martinsried

siHPV16E6/E7	CCGGACAGAGCCCAUUACA CACCUACAUUGCAUGAAUA CAACUGAUCUCUACUGUUA	pool targets all 3 HPV16 *E6/E7* transcript classes	Ambion, Life Technologies, Carlsbad, CA, USA
control siRNA	CAGUCGCGUUUGCGACUGG	contains at least 4 mismatches to all known human genes	Ambion, Life Technologies, Carlsbad, CA, USA

2.1.13 Protein Marker

Name	Company
Precision Plus Protein™ Standards Kaleidoscope™, 10-250kDa	Biorad, Hercules, CA, USA

2.1.14 DNA Ladder

Name	Company
GeneRuler™ Ladder Mix, 100-10,000bp	Thermo Fisher Scientific Ldt., Loughborogh, UK

2.1.15 Buffers, solutions and media

Molecular Biology	
50x TAE	484g Tris 41g $C_2H_3NaO_2$ 37g EDTA pH 7.8 adjusted with acetic acid ad. 2l ddH_2O
dNTP mix	10mM each dATP, dCTP, dGTP, dTTP
Proteinase K buffer	50mM Tris 20mM NaCl 1mM EDTA 1% (w/v) SDS pH 8.0

Protein analysis	
0.5% IGE-PAL-630 buffer	1xPBS 0.5% (v/v) IGE-PAL-630
10x SDS-PAGE running buffer	30.3g Tris 144g Glycine 10g SDS ad. 1l ddH_2O
Complete mini protease inhibitor cocktail stock (14x)	2 tablets dissolved in 1.5ml ddH_2O
GammaBind™ Plus Sepharose™ beads washing buffer	ddH_2O 10% (v/v) acetic acid pH 3.0
GammaBind™ Plus Sepharose™ beads storage buffer	1x PBS 0.02% (v/v) sodium azide

IP lysis buffer	1xPBS 1% (v/v) IGE-PAL-630 2x complete mini protease inhibitor cocktail 1mM PMSF
PMSF stock (100mM)	PMSF dissolved in 100% ethanol
Protein sample buffer (4x)	222.24mM Tris (pH 6.8) 3.52% (w/v) SDS 35.2% (v/v) glycerol 0.016% (w/v) bromophenol blue 10% (v/v) β-mercaptoethanol
RIPA buffer	1% (w/v) Na-DOC (Sodium Deoxycholate) 0.1% (w/v) SDS 0.15M NaCl 0.01M Na-phosphate, pH 7 2mM EDTA 1% (v/v) NP-40 1mM PMSF 2x complete mini protease inhibitor cocktail
RIPA buffer II	0.5% (w/v) Na-DOC (sodium deoxycholate) 0.1% (w/v) SDS 150mM NaCl 10mM Tris, pH 7.5 1mM EDTA 1% (v/v) NP-40 25µl/ml Pefabloc 10µl/ml Protease Inhibitor Cocktail
Western blot blocking buffer	1xPBS 5% (w/v) milk powder
Western blot semidry transfer buffer	48mM Tris 39mM glycine 1.3mM SDS 20% (v/v) methanol pH 9-9.4
Western blot tank transfer buffer	9g Tris 43.2g glycine 20% (v/v) methanol ad. 3l ddH_2O
Western blot washing buffer	1xPBS 0.1% (v/v) Tween20

LC mobile phases and MS solutions prepared with LC/MS grade water	
Mobile phase A	0.1% (v/v) FA 0.01% (v/v) TFA in LC/MS grade water
Mobile phase B	0.1% (v/v) FA 0.01% (v/v) TFA in ACN
Solvent for manual injection of peptides	50% (v/v) ACN 0.1% (v/v) FA in LC/MS grade water

Other solutions used for detergent removal from IP samples and LC-MS are indicated within the method section 2.2.2.7.

Other buffers	
10x Phosphate buffered saline (1xPBS)	1.37M NaCl 27mM KCl 100mM Na_2HPO_4 20mM KH_2PO_4 pH 7.2 adjusted with NaOH or HCl
Ammonium-chloride-potassium (ACK) lysis buffer	0.829g NH_4Cl 0.1g $KHCO_3$ 0.38mg EDTA pH 7.2-7.4 adjusted with NaOH or HCl ad. 100ml ddH_2O
Antigen retrieval buffer	ddH_2O 10mM citric acid pH 6.0
Blocking buffer (FACS)	1xPBS 10% (v/v) FCS
Blocking buffer (immunohistochemistry)	1xPBS 10% (v/v) horse serum
FACS buffer	1x PBS 1% (v/v) FCS 0.1% (v/v) NaN_3
Fixation buffer	1x PBS 1% (w/v) PFA
MACS buffer	1xPBS 0.5% (w/v) BSA 2mM EDTA
ELISpot washing buffer	1xPBS 0.05% (v/v) Tween20
Permeabilization and washing buffer (immunohistochemistry)	1x PBS 0.1% (v/v) Tween20

Cell culture media	
2A3 medium	DMEM 10% (v/v) FBS, 1% P/S, 0.2mg/ml G418
B cell medium	IMDM 10% (v/v) human serum, AB, 2mM L-glutamine, 50µg/ml human transferrin, 5µg/ml human insulin, 15µg/ml gentamycin
B-LCL medium	RPMI-1640 10%-20% (v/v) FCS
CaSki medium	RPMI-1640 1% (v/v) P/S, 10% (v/v) FCS, 2mM L-glutamine
Cell freezing medium	Heat-inactivated FCS or human serum with 20% DMSO
Complete DermaLife K	DermaLife K 1% (v/v) P/S, 10% (v/v) FCS
Complete DMEM	DMEM 1% (v/v) P/S, 10% (v/v) FCS, 2mM L-glutamine
Complete K-SFM	K-SFM 1% (v/v) P/S, 10% (v/v) FCS, 5ng/ml EGF, 50µg/ml bovine pituitary extract (BPE)
Complete RPMI-P	RPMI-1640 15% (v/v) FCS, 1% 100mM sodium pyruvate

Complete RPMI-H	RPMI-1640 1% (v/v) P/S, 10% (v/v) FCS, 25mM HEPES, 25mM $NaHCO_3$
DC medium	DMEM with GlutaMAX™ 1% (v/v) P/S, 10% (v/v) human serum, AB, 10mM HEPES
E-medium	DMEM 22.5% (v/v) Ham's F12. 10% (v/v) FCS 1% (v/v) P/S, 0.5µg/ml hydrocortisone, 8.4ng/ml cholera toxin, 5µg/ml transferrin, 5µg/µL insulin, 1.36ng/ml tri-iodo-thyronine, 5µg/ml EGF
F-medium	Ham's F12 DMEM 25% (v/v), 5% (v/v) FCS, 1% (v/v) P/S, 0.4mg/ml hydrocortisone, 0.5µg/ml cholera toxin, 5µg/ml insulin, 24.2µg/ml adenine, 0.1µg/ml EGF
M10 medium	EMEM 10% (v/v) FCS, 1% (v/v) P/S, 2mM L-glutamine, 1% (v/v) MEM NEAA
T cell medium	RPMI 1% (v/v) P/S, 10% (v/v) human serum, AB, 2mM L-glutamine, 12.5mM HEPES, 0.05mM β-mercaptoethanol
T cell ELISpot medium	RPMI 1% (v/v) P/S, 5% (v/v) FCS, 2mM L-glutamine, 12.5mM HEPES, 0.05mM β-mercaptoethanol
NIH3T3 tCD40L	Ham's F12/DMEM 10% (v/v) FCS, 2mM L-glutamine, 10mM HEPES, 15µg/ml gentamycin, 500µg/ml G418
NIH3T3 WT	Ham's F12/DMEM 10% (v/v) FCS, 2mM L-glutamine, 10mM HEPES, 15µg/ml gentamycin

2.1.16 Peptides

Peptides were synthesized with a purity of > 95% from the in-house Peptide Production Unit (Prof. Stefan Eichmüller, GMP & T Cell Therapy Unit, DKFZ, Heidelberg). For the solid phase synthesis, the Fmoc-strategy (196, 197) in a fully automated multiple synthesizer Syro II (MultiSyn Tech, Germany) was employed. The synthesis was carried out on preloaded Wang-Resins. 2-(1H-benzotriazole-1-yl)-1, 1, 3, 3-tetramethyluronium hexafluorophosphate (HBTU) was used as a coupling agent. The material was purified by preparative HPLC on a Kromasil 100-10C 10µm 120A reverse phase column (20 x 150mm) using an eluent of 0.1% TFA in water (A) and 80% I in water (B). The peptide was eluted within 30min with a successive linear gradient of 25% B up to 80% B at a flow rate of 10ml/min. The fractions corresponding to the purified protein were lyophilized. The purified material was characterized with analytical HPLC and MS (Thermo Finnigan LCQ). Lyophilized peptides were dissolved in DMSO at a concentration of 10mg/ml and stocked in small aliquots at -80°C.

2.1.16.1 Control peptides

Corresponding HLA alleles for peptide binding are indicated.

Name	Source	Region	Amino acid sequence	HLA allele	Reference
Negative control peptides for ELISpot					
HIV-A2	HIV-1 Nef	137-145	LTFGWCFKL	HLA-A2	(198)
HIV-A24	HIV-1 Env gp41	583-591	RYLKDQQLL	HLA-A24	(199)
Positive control peptides for MS					
PC1	p68 RNA helicase	96-104	YLLPAIVHI	HLA-A2	
PC2	coatomer subunit gamma-1	147-155	AIVDKVPSV	HLA-A2	

2.1.16.2 HP16 E6 and E7 peptides

Corresponding HLA alleles for peptide binding are indicated. **Bold** letters are highlighting amino acid changes in peptides from HPV variants.

E6				
Name	**Origin**	**Region**	**Amino acid sequence**	**HLA allele**
$E6_{18\text{-}26variant}$	HPV16 E6	18-26	KLP**D**LCTEL	HLA-A2
$E6_{18\text{-}28}$	HPV16 E6	18-28	KLPQLCTELQT	HLA-A2
$E6_{18\text{-}28variant}$	HPV16 E6	18-28	KLP**D**LCTELQT	HLA-A2
$E6_{25\text{-}33}$	HPV16 E6	25-33	ELQTTIHDI	HLA-A2
$E6_{25\text{-}33variant}$	HPV16 E6	25-33	ELQTTIH**E**I	HLA-A2
$E6_{28\text{-}38}$	HPV16 E6	28-38	TTIHDIILECV	HLA-A2
$E6_{28\text{-}38variant1}$	HPV16 E6	28-38	TTIH**E**IILECV	HLA-A2
$E6_{28\text{-}38variant2}$	HPV16 E6	28-38	TTIH**E**I**R**LECV	HLA-A2
$E6_{29\text{-}38}$	HPV16 E6	29-38	TIHDIILECV	HLA-A2
$E6_{29\text{-}38variant}$	HPV16 E6	29-38	TIH**E**IILECV	HLA-A2
$E6_{34\text{-}44}$	HPV16 E6	34-44	ILECVYCKQQL	HLA-A2
$E6_{52\text{-}60}$	HPV16 E6	52-60	FAFRDLCIV	HLA-A2
$E6_{26\text{-}34}$	HPV16 E6	26-34	LQTTIHDII	HLA-A24
$E6_{26\text{-}34variant}$	HPV16 E6	26-34	LQTTIH**E**II	HLA-A24
$E6_{38\text{-}45}$	HPV16 E6	38-45	VYCKQQLL	HLA-A24
$E6_{38\text{-}46}$	HPV16 E6	38-46	VYCKQQLLR	HLA-A24
$E6_{38\text{-}47}$	HPV16 E6	38-47	VYCKQQLLRR	HLA-A24
$E6_{44\text{-}54}$	HPV16 E6	44-54	LLRREVYDFAF	HLA-A24
$E6_{47\text{-}54}$	HPV16 E6	47-45	REVYDFAF	HLA-A24
$E6_{49\text{-}57}$	HPV16 E6	49-57	RAHYNIVTF	HLA-A24
$E6_{49\text{-}58}$	HPV16 E6	49-58	VYDFAFRDLC	HLA-A24
$E6_{49\text{-}59}$	HPV16 E6	49-59	VYDFAFRDLCI	HLA-A24
$E6_{51\text{-}59}$	HPV16 E6	51-59	DFAFRDLCI	HLA-A24
$E6_{60\text{-}69}$	HPV16 E6	60-69	VYRDGNPYAV	HLA-A24
$E6_{66\text{-}74}$	HPV16 E6	66-74	PYAVCDKCL	HLA-A24
$E6_{66\text{-}75}$	HPV16 E6	66-75	PYAVCDKCLK	HLA-A24

$E6_{66-76}$	HPV16 E6	66-76	PYAVCDKCLKF	HLA-A24
$E6_{72-80}$	HPV16 E6	72-80	KCLKFYSKI	HLA-A24
$E6_{75-83}$	HPV16 E6	75-83	KFYSKISEY	HLA-A24
$E6_{76-83}$	HPV16 E6	76-83	FYSKISEY	HLA-A24
$E6_{76-85}$	HPV16 E6	76-85	FYSKISEYRH	HLA-A24
$E6_{76-86}$	HPV16 E6	76-86	FYSKISEYRHY	HLA-A24
$E6_{81-90}$	HPV16 E6	81-90	SEYRHYCYSL	HLA-A24
$E6_{81-90variant}$	HPV16 E6	81-90	SEYRHYCYS**V**	HLA-A24
$E6_{82-90}$	HPV16 E6	82-90	EYRHYCYSL	HLA-A24
$E6_{82-91}$	HPV16 E6	82-91	EYRHYCYSLY	HLA-A24
$E6_{82-91variant}$	HPV16 E6	82-91	EYRHYCYS**V**Y	HLA-A24
$E6_{85-95}$	HPV16 E6	85-95	HYCYSLYGTTL	HLA-A24
$E6_{87-96}$	HPV16 E6	87-96	CYSLYGTTLE	HLA-A24
$E6_{88-95}$	HPV16 E6	88-95	YSLYGTTL	HLA-A24
$E6_{88-95variant}$	HPV16 E6	88-95	YS**V**YGTTL	HLA-A24
$E6_{90-99}$	HPV16 E6	90-99	LYGTTLEQQY	HLA-A24
$E6_{90-99variant}$	HPV16 E6	90-99	**V**YGTTLEQQY	HLA-A24
$E6_{98-106}$	HPV16 E6	98-106	QYNKPLCDL	HLA-A24
$E6_{98-108}$	HPV16 E6	98-108	QYNKPLCDLLI	HLA-A24
$E6_{128-135}$	HPV16 E6	128-135	KKQRFHNI	HLA-A24
$E6_{131-139}$	HPV16 E6	131-139	RFHNIRGRW	HLA-A24

E7				
Name	**Origin**	**Region**	**Amino acid sequence**	**HLA allele**
$E7_{7-15}$	HPV16 E7	7-15	TLHEYMLDL	HLA-A2
$E7_{7-17}$	HPV16 E7	7-17	TLHEYMLDLQP	HLA-A2
$E7_{10-19}$	HPV16 E7	10-19	EYMLDLQPET	HLA-A2
$E7_{11-18}$	HPV16 E7	11-18	YMLDLQPE	HLA-A2
$E7_{11-19}$	HPV16 E7	11-19	YMLDLQPET	HLA-A2
$E7_{11-20}$	HPV16 E7	11-20	YMLDLQPETT	HLA-A2
$E7_{11-21}$	HPV16 E7	11-21	YMLDLQPETTD	HLA-A2
$E7_{12-19}$	HPV16 E7	12-19	MLDLQPET	HLA-A2
$E7_{12-20}$	HPV16 E7	12-20	MLDLQPETT	HLA-A2
$E7_{66-74}$	HPV16 E7	66-74	RLCVQSTHV	HLA-A2
$E7_{76-86}$	HPV16 E7	76-86	IRTLEDLLMGT	HLA-A2
$E7_{77-86}$	HPV16 E7	77-86	RTLEDLLMGT	HLA-A2
$E7_{77-87}$	HPV16 E7	77-87	RTLEDLLMGTL	HLA-A2
$E7_{78-86}$	HPV16 E7	78-86	TLEDLLMGT	HLA-A2
$E7_{80-90}$	HPV16 E7	80-90	EDLLMGTLGIV	HLA-A2
$E7_{81-90}$	HPV16 E7	81-90	DLLMGTLGIV	HLA-A2
$E7_{81-91}$	HPV16 E7	81-91	DLLMGTLGIVC	HLA-A2
$E7_{82-90}$	HPV16 E7	82-90	LLMGTLGIV	HLA-A2
$E7_{82-91}$	HPV16 E7	82-91	LLMGTLGIVC	HLA-A2
$E7_{82-92}$	HPV16 E7	82-92	LLMGTLGIVCP	HLA-A2
$E7_{83-93}$	HPV16 E7	83-93	LMGTLGIVCPI	HLA-A2
$E7_{84-93}$	HPV16 E7	84-93	MGTLGIVCPI	HLA-A2

$E7_{85-93}$	HPV16 E7	85-93	GTLGIVCPI	HLA-A2
$E7_{86-93}$	HPV16 E7	86-93	TLGIVCPI	HLA-A2
$E7_{48-57}$	HPV16 E7	48-57	DRAHYNIVTF	HLA-A24
$E7_{50-57}$	HPV16 E7	50-57	AHYNIVTF	HLA-A24
$E7_{51-58}$	HPV16 E7	51-58	HYNIVTFC	HLA-A24
$E7_{51-59}$	HPV16 E7	51-59	HYNIVTFCC	HLA-A24
$E7_{56-65}$	HPV16 E7	56-65	TFCCKCDSTL	HLA-A24
$E7_{67-76}$	HPV16 E7	67-76	LCVQSTHVDI	HLA-A24
$E7_{69-76}$	HPV16 E7	69-76	VQSTHVDI	HLA-A24

2.1.17 Blood samples

In this study, blood samples were taken from healthy donors after written informed consent (ethical approval S-393/2011). HLA typing of volunteers was performed by a diagnostic lab (Bernhard Thiele, Institut für Immunologie und Genetik, Kaiserslautern).

2.1.18 Software

Name	**Company**
Adobe Illustrator CS4	Adobe, San José, CA, USA
Analyst 1.6.2	Ab Sciex, Foster City, CA, USA
BD FACS Diva Software	BD Biosciences, San José, CA, USA
Cell^{D} Imaging Software 5	Olympus Soft Imaging Solutions, Hamburg
Chromas 2.1.1	Technelysium Pty Ltd
CTL ImmunoSpot 5.1.36 Professional DC	CTL, Bonn
EndNote X7.5	Thomas Reuters, Philadelphia, PA, USA
FlowJo 6.5 FlowJo 10.1	TreeStar, Ashland, OR, USA
Fusion	Vilber Lourmat, Eberhardzell
GENtle	Magnus Manske, University of Cologne, Cologne
GIMP 2.8.14	Spencer Kimball, Peter Mattis and the GIMP development team, *www.gimp.org*
ImageJ 1.45b	Rasband, W.S., ImageJ, U. S. National Institutes of Health, Bethesda, Maryland, USA, *http://imagej.nih.gov/ij/, 1997-2015*
Inkscape 0.48	The Inkscape Team, *www.inkscape.org*
LinRegPCR 2012.3	Heart Failure Research Center, Amsterdam
MS Office 2010	Microsoft Corporation, Redmond, WA, USA
MxPRO 4.10 build 389	Agilent Technologies, Santa Clara, CA, USA
PRISM® 5	GraphPad, La Jolla, CA, USA
Notepad 6.1 build 7601	Microsoft Corporation, Redmond, WA, USA
Notepad ++ 6.6.9	Notepad++ Team, *www.notepad-plus-plus.org*
qBase Plus 2.4	Biogazelle, Zwijnaarde, Belgium
R 2.15.2	R Project, *www.r-project.org*
SnapGene® 3.1	GSL Biotech LLC, Chicago, IL, USA

2.2 Methods

2.2.1 Molecular biological methods

2.2.1.1 Isolation of genomic DNA

DNA extraction using proteinase K

Cells were harvested (approximately $1x10^6$ cells) and washed once with 1xPBS and transferred to a 1.5ml reaction tube. The cell pellet was digested in 49µl proteinase K buffer supplemented with 1µl of proteinase K and incubated at 56°C overnight or for 3-4h. After the digest, samples were spun down, 300µl of distilled DNase/RNase free water were added and the enzyme was inactivated at 95°C for 1min. The samples were stored at 4°C or at -20°C until analysis.

DNA isolation using the QiaAmp DNA Kit

This kit is based on DNA-binding columns. Genomic DNA was purified using $1x10^6$ cells in 200µl 1xPBS per column. 20µl of Proteinase K was pipetted to a 1.5ml tube and the cells were added. 200µl of AL buffer was added and the sample was quickly vortexed and incubated for 10min at 56°C. Then, 200µl of 100% ethanol was added, mixed and the sample was transferred to a spin column and spun (1min, 6,000xg). The filtrate was removed and 500µl AW1 buffer was added and centrifuged (1min, 6,000xg). Afterwards, the sample was washed by centrifugation (1min, full speed) using 500µl of AW2 buffer. To remove residual washing buffer the column was centrifuged (1min, full speed). For eluting the DNA, the column was placed in a new 1.5ml reaction tube, 200µl of distilled DNase/RNase free water was added to the column, incubated for 1min and eluted by centrifugation (1min, 6,000xg,). DNA samples were stored at 4°C or at -20°C for further analysis.

2.2.1.2 RNA isolation

RNA isolation was done using the RNeasy Kit. RNA purification is based on RNA-binding columns. First, cells were harvested (see 2.2.3). A maximum of $8x10^6$ cells was taken for a single RNA isolation preparation. Cells were washed twice with sterile 1xPBS and the supernatant was removed carefully. Cells from a T75 cell culture bottle ($2\text{-}8x10^6$ cells) were resuspended in 600µl of RLT buffer, and 350µl of this buffer was taken for the cells from one well of a 12-well plate ($1x10^5\text{-}5x10^5$). The mix was vortexed and kept for 2min on ice to disrupt the cell membrane. 700µl of the whole cell lysate was transferred to the QIAshredder spin column and centrifuged (1min, full speed) for homogenization of cell lysates. Then, the flow through was mixed 1:1 with 70% ethanol and slowly pipetted up and down to precipitate the DNA. 700µl of this mixture was transferred to the spin column and centrifuged (1min, > 8,000xg). If the sample volume exceeded 700µl the step was repeated within the same spin column. The flow through was discarded after each centrifugation. 700µl of RW1 buffer was added to the spin column and centrifuged (1min, > 8,000xg). Then, the spin column was washed with 500µl of

RPE buffer by centrifugation (1min, > 8,000xg). This step was repeated, but centrifugation was done for 2min at 8,000xg. A dry spin was performed by centrifugation (1min, > 8,000xg) to remove residual buffer from the column. The column was inserted into a new collection tube and 35µl (cell amount from a T75 cell culture bottle) or 15-25µl (cell amount from one well of a 12-well plate) of distilled DNase/RNase free water was added to the column and incubated for 1min. Only then, the cap of the tube was closed gently and the RNA was eluted (1min, > 8,000xg). The flow through containing the RNA was kept at -20°C and for long-time storage samples were stored at -80°C. The concentration was measured via Nano Drop (see 2.2.1.3).

2.2.1.3 Determination of DNA and RNA concentration

1µl of DNA or RNA sample was applied to the Nano Drop spectrophotometer. This device can measure the concentration and the purity of a sample. Nucleic acids absorb light at different wavelengths. The absorbance can be related to the concentration of a sample by using the Lambert-Beer law.

$$A = \varepsilon \, x \, c \, x \, d$$

(A: absorbance, ε: extinction coefficient; c: concentration; d: distance)

At a wavelength of 260nm, the extinction coefficient for dsDNA is $0.02(\mu g/ml)^{-1}cm^{-1}$ and for RNA $0.025(\mu g/ml)^{-1}cm^{-1}$. In contrast, proteins show a maximum light absorption at 280nm. Thus, the purity of nucleic acids can be determined by measuring the ratio of 260nm to 280nm with an optimal value between 1.8 and 1.95.

2.2.1.4 Agarose gel electrophoresis

Nucleic acids are negatively charged because of their covalently bound phosphate groups. Therefore, they can easily be separated by agarose gel electrophoresis using an electric field (200). 1-2% agarose gels were prepared by boiling agarose powder in TAE buffer. The agarose was chilled to approximately 50°C and supplemented with GelRed™ (1:10,000). The agarose gel tray was placed in the electrophoresis chamber and the comb was inserted. Then, the agarose was poured on the agarose gel tray for solidification. Later, the comb was removed and the electrophoresis chamber was filled with TAE buffer. Before loading, the DNA was mixed with 6x Orange loading buffer. Additionally, 4µl of the DNA marker GeneRuler™ 100-10,000bp was used as a reference for DNA fragment size. The gel was run at 80-120V depending on the gel volume until the DNA fragments were sufficiently separated. For visualization of the separated DNA, UV light excitation was used employing the Gel Doc™ EZ Imager.

2.2.1.5 Agarose gel extraction

After agarose gel electrophoresis, specific bands were cut out and the DNA was extracted with the peqGOLD™ Gel Extraction Kit. In this thesis, bands of *ERAP1* amplified by the KOD enzyme (see 2.2.1.6) were cut out, purified and send for sequencing to GATC Biotech, Konstanz.

The DNA band was cut out from the agarose gel with a scalpel on the UV table of the Gel Doc™ EZ Imager. The agarose gel slice was cut as small as possible and the duration while cutting on the UV table was kept short in order to reduce UV-induced DNA damage. The agarose slice containing the DNA of interest was transferred into a 1.5ml reaction tube and was weighed. Binding buffer was added 1:1 to the agarose gel slice (e.g. 0.2g of agarose + 0.2ml binding buffer). The agarose gel slice was dissolved on a thermoblock at 60°C for approximately 7min. In between, the mix was shortly vortexed or shaken once in a while. After an agarose gel slice is dissolved, the color of the solution should be bright yellow. In the case of a color shift towards orange or red 5µl of 3M sodium acetate (pH 5.2) was added. 750µl of the solution was added to the spin column, centrifuged (1min, 10,000xg) and the flow through was discarded. This step was repeated if the volume was more than 750µl. Later, 300µl of binding buffer was added, centrifuged (1min, 10,000xg) and the flow through was discarded. Then, 750µl of CE washing buffer was added to the column and centrifuged (1min 10,000xg). This washing step was repeated and the flow through discarded. The column was centrifuged once again to get rid of all residual buffer (1min, 10,000xg). For DNA elution, the column was put into a new 1.5ml reaction tube, 30-50µl of distilled DNase/RNase free water was added on the silica membrane of the column and centrifuged (1min, 10,000xg). The flow through containing the DNA was kept for further analysis and stored at -20°C. DNA concentration was measured via Nano Drop (see 2.2.1.3).

2.2.1.6 Polymerase chain reaction (PCR)

The polymerase chain reaction is a molecular biological method used to amplify a particular DNA fragment (201, 202). Short synthetic oligonucleotides, called primers, are used as starter molecules that specifically flank the DNA fragment which is going to be amplified. A heat stable polymerase is used for the synthesis of the strand occurring in 5' to 3' direction.

An initial heating step is conducted before the first denaturation step to activate the polymerase (hot start polymerase). Then, the PCR reaction starts by heating up the DNA template to 95°C, which denatures the double strands into single strands. The sample is cooled to a specific temperature which is primer specific and allows the primers to anneal to the ssDNA templates. Primers were designed to have an annealing temperature of 60°C and the GC content was 40-60%.

The sample is subsequently heated up again to the polymerase-specific extension temperature. Then, the polymerase utilizes the primers as starting points to synthesize a complementary DNA strand to the DNA template. This cycle is repeated multiple times as indicated in the temperature profile of the PCR. After the last cycle, a terminal elongation step ensures extension of all remaining ssDNA strands.

Amplification of *ERAP1*

The AccuScript High Fidelity 1st Strand cDNA Synthesis Kit was used for samples that were later sent for sequencing. In this thesis, cDNA from cell lines was synthetized in order to amplify *ERAP1* by a

subsequent PCR using the KOD enzyme (*Thermococcus kodakaraenis*). For this purpose, a high fidelity enzyme was absolutely necessary to ensure that the sequence was correct after reverse transcription.

The reaction was set up as indicated in Table 2.1. First, the RNA and the primers had to be denatured at 65°C. The reaction was chilled to room temperature, DTT and the AccuScript enzyme were added to the reaction. Subsequently, cDNA synthesis was performed at 42°C. A final heat inactivation of the enzyme was done because the AccuScript enzyme could inhibit subsequent PCR reactions. For a shorter time period cDNA was stored at -20°C or at -80°C for long-term storage.

Table 2.1: Reverse transcription reaction using the AccuScript High Fidelity 1st Strand cDNA Synthesis Kit.

RNA	0.5µg, max. 12µl	**RNA and primer denaturation**
Oligo dT Primer	1µl	
AccuScript RT buffer	2µl	
dNTP mix	0.8µl	
Distilled DNase/RNase free water	ad 17µl	
	Total volume 17µl	
	5min, 65°C	
DTT	2µl	**cDNA synthesis**
AccuScript RT	1µl	
	Total volume 20µl	
	90min, 42°C	
	15min, 70°C	**Enzyme inactivation**

The human *ERAP1* gene from cell lines was then amplified by PCR to determine single nucleotide polymorphisms (SNPs). As a positive control for cDNA quality, primers targeting *hypoxanthine-guanine phosphoribosyltransferase* (*HPRT1*) were used (data not shown). Table 2.2 displays the pipetting scheme of the PCR reaction and Table 2.3 summarizes the temperature profile used for this PCR.

Table 2.2: PCR reaction using the KOD polymerase.

	Stock concentration	**Volume**	**Final concentration**
Template DNA		2µl	
5' Primer	10µM	1.5µl	0.3µM
3' Primer	10µM	1.5µl	0.3µM
KOD Hot Start Master Mix	0.04U/µl	25µl	0.02U/µl
Distilled DNase/RNase free water		20µl	
			Total volume 50µl

Table 2.3: Temperature profile of the PCR reaction using the KOD polymerase.

Number of cycles	**Temperature**	**Time**	**Step**
1	95°C	2min	Polymerase activation
35	95°C	20sec	Denaturation
	60°C	10sec	Annealing
	70°C	2min (20sec/kb)	Extension
1	70°C	10min	Terminal elongation
	4°C	∞	

PCR using AmpliTaq Gold® DNA polymerase

For any analytic PCR, the AmpliTaq Gold® DNA polymerase was used. The PCR reaction was set up as described in Table 2.4 and the reaction was run in a thermocycler as described in Table 2.5.

Table 2.4: PCR reaction using the AmpliTaq Gold® polymerase.

	Stock concentration	Volume	Final concentration
Template DNA		1-2ng, max. 16µl	1-2ng
Primer F	10µM	0.75µl	0.3µM
Primer R	10µM	0.75µl	0.3µM
10x buffer	10x	2.5µl	1x
dNTPs	10mM	2µl	0.2mM
$MgCl_2$	25mM	2µl	2.5mM
AmpliTaq Gold®	5U/µl	0.125µl	0.625U
Distilled DNase/RNase free water		ad 25µl	
			Total volume 25µl

Table 2.5: Temperature profile of the PCR reaction using the AmpliTaq Gold® polymerase.

Number of cycles	Temperature	Time	Step
1	95°C	5min	Polymerase activation
34	95°C	40sec	Denaturation
	60°C	30sec	Annealing
	72°C	1min	Elongation
1	72°C	10min	Terminal elongation
	4°C	∞	

2.2.1.7 PCR product purification

The PCR-amplified product was purified directly after the PCR reaction using the QIAquick PCR Purification Kit to remove enzymes chemicals included in the buffer used for the PCR. Enzyme contamination of DNA samples could interfere with subsequent applications. First, 5 volumes of PBI buffer were added to 1 volume of the PCR reaction mix (250µl PBI buffer + 50µl PCR reaction mix). Then, the color of the mix had to be checked and, if deviating from the yellow color of the PBI buffer, 10µl of 3M sodium acetate (pH 5) had to be added. The sample was transferred onto the membrane of the spin column and DNA bound to the column by centrifugation (1min, full speed). The flow through was discarded. 750µl of PE washing buffer was added and the column was again centrifuged (1min, full speed). Then, the flow through was discarded and the column spun dry (1min, full speed). 30µl of distilled DNase/RNase free water was added to the column and incubated for 1min. For the elution step, the column was put into a new reaction tube and centrifuged (1min, full speed). Purified PCR products were stored at -20°C or at -80°C for long-term storage.

2.2.1.8 Sequencing of human *ERAP1*

DNA was diluted in distilled DNase/RNase free water to a final concentration of 50ng/µl and a total volume of 20µl and then sent for sequencing. Sanger sequencing was conducted by GATC Biotech, Konstanz. Primers had a concentration of 10µM in a total volume of 20µl. DNA and primers were prepared in 1.5ml reaction tubes.

2.2.1.9 Analysis of the human *ERAP1* sequences

In order to analyze *ERAP1* variants present in our cell lines the most common haplotype of *ERAP1* (203) was used as a reference sequence (NM 001198541.1). Sequence alignments were conducted using SnapGene® 3.1 and GENtle. Human genes have two alleles within the genome of cells. Therefore, the sequences were checked in parallel with the Chromas 2.1.1 software in order to detect SNPs as ambiguities in the sequence traces. By this means, sequence differences within *ERAP1* were identified. If nucleotide exchanges were detected, the respective codon was checked for silent or missense mutations using SnapGene® 3.1.

2.2.1.10 Quantitative Real-Time PCR (qRT-PCR)

QuantiTect Reverse Transcription Kit

This kit was used for samples that were subsequently analyzed by qRT-PCR. All steps were performed on ice unless otherwise indicated. For each reverse transcription reaction 0.5-1µg of RNA was used. The reaction was pipetted following the pipetting scheme in Table 2.6. First, the RNA was diluted in distilled DNase/RNase free water in a maximal volume of 12µl. Next, gDNA wipeout buffer was added to remove genomic DNA contaminants. The total volume of this first reaction was 14µl and was incubated for 2min at 42°C. Afterwards, the sample was directly put back on ice and a mixture of RT buffer, RT primer and reverse transcriptase was added so that the total volume of the reaction was 20µl. The reverse transcription reaction was incubated for 15min at 42°C and the enzyme was inactivated for 3min at 95°C. The cDNA was stored at -20°C or at -80°C for long-term storage.

Table 2.6: Reverse transcription reaction using the QuantiTect Reverse Transcription Kit.

RNA	0.5-1µg, max. 12µl	**DNase treatment**
gDNA wipeout buffer	2µl	
Distilled DNase/RNase free water	ad 14µl	
	Total volume 14µl	
	2min, 42°C	
RT primer	1µl	**cDNA synthesis**
RT buffer	4µl	
RT enzyme	1µl	
	Total volume 20µl	
	15min, 42°C	
	3min, 95°C	**Enzyme inactivation**

Quantitative Real-Time PCR (qRT-PCR) is a quantitative technique which monitors the relative amplification of a specific cDNA sequence during a PCR reaction, in real-time. In this study, the TaqMan® system was used. Applied TaqMan® Gene Expression Assays consist of a pair of unlabeled PCR primers and a TaqMan® probe with a FAM™ (fluorescein amidite) dye label. The TaqMan® Gene Expression Master Mix reagent contains general PCR reagents: AmpliTaq Gold® DNA polymerase, desoxiribonucleotide triphosphates, ROX™ (6-carboxyl-X-rhodamine) dye and buffer. A maximum of four reference genes was used (*GAPDH*, *PGK1*, *PPIA*, *IPO8*) that have been validated previously (204). The qPCR was performed in semi-skirted 96-well qPCR plates based on

the sample maximization approach (205) in a reaction volume of 20µl. The cDNA was diluted 1:90 in distilled DNase/RNase free water and the reaction was set up as described in the pipetting scheme in Table 2.7. Each sample was run in triplicates. In addition, each run included a no template control (NTC) for the respective target gene.

Table 2.7: Pipetting scheme of the qRT-PCR reaction.

1:90 diluted cDNA (cDNA input 0.1µl)	9µl
Gene-specific TaqMan® Gene Expression Assay TaqMan® Gene Expression Master Mix	1µl 10µl
	Total volume 20µl

The thermal profile of the qPCR is shown in Table 2.8 and was composed of two plateau phases and two segments. The relative quantification of gene expression was conducted by the relative quantification strategy (206) and was corrected for differences in PCR efficiency by LinRegPCR.

Table 2.8: qRT-PCR temperature profile.

Number of cycles	Temperature	Time	Step
1	50°C	2min	**Preincubation**
1	95°C	10min	**AmpliTaq enzyme activation**
45	95°C	15sec	**Denaturation**
	60°C	1min	**Annealing/Elongation**

2.2.1.11 qRT-PCR data analysis and quantification

Analysis of quantitative real-time PCR data was done using Notepad++, MxPro Software, LinRegPCR and qBase Plus. After passive normalization, raw data was exported from MxPro software and imported to LinRegPCR. Within LinRegPCR, the baseline was estimated, both PCR efficiencies and the Cq value were calculated and the qPCR quality of each single well was checked. Data was stored as an RDML file (207) and finally analyzed using the qBase Plus software.

2.2.2 Biochemical Methods

2.2.2.1 Sodium dodecyl sulfate polyacrylamide gel electrophoresis (SDS-PAGE)

Sodium dodecyl sulfate polyacrylamide gel electrophoresis (SDS-PAGE) is widely used to separate proteins in an electric field according to their molecular weight. In this work, the most commonly used Laemmli system with Tris-glycine buffers was employed (208). Mini-PROTEAN®TGX™ gels, any kD™, were used to separate protein samples. β-mercaptoethanol was added to the 4x loading buffer and then the buffer was stored at 4°C and was used within 4 weeks. Prior to sample loading, samples were mixed with 4x protein loading buffer and boiled for 5min at 95°C. If not indicated otherwise, 50µg of whole protein extract was pipetted into the gel slots. As a marker for molecular weight, 4µl of the Precision Plus Protein™ Standards Kaleidoscope™ 10-250kDa was loaded for Western blot. The gel was run at 90V until the samples had completely entered the gel. Then, the gel was run at 150V. Afterwards, the gel was used for Western blot analysis (see 2.2.2.4).

SDS-PAGE from CaSki cells treated with siRNAs knocking down HPV16 *E6* and *E7* (see 2.2.3.5) was performed using NuPAGE Novex 4-12% Bis-Tris Mini Gels as described in (209) and used for semidry Western blot (see 2.2.2.4).

2.2.2.2 Protein extraction

In order to analyze the expression of a particular protein from cell lines by Western blot, protein extraction was performed. All steps of this isolation were strictly performed on ice. PMSF and complete mini protease inhibitor cocktail were always added freshly to the RIPA buffer prior to use. Cells were washed twice with ice-cold 1xPBS and all residual liquid was removed. For 10cm ø cell culture dishes (2-6x10^6 cells), 0.5ml of RIPA buffer was added, cells were scraped from the dishes and transferred to a reaction tube. For protein extracts that were isolated from cells grown in one well of a 12-well plate (1-5x10^5 cells per well), cells were harvested by trypsinization (see 2.2.3.2), washed twice with ice-cold 1xPBS and resuspended in 50µl of RIPA buffer. Then, cells were incubated for 10min on ice with vortexing every 30 seconds. Samples were centrifuged (15min, 12,000xg, 4°C) and supernatants were transferred to a new reaction tube. A second centrifugation step was performed (5min, 12,000xg, 4°C), the supernatants were again transferred to a new reaction tube and protein concentration was determined (see 2.2.2.3). Protein samples were stored at -80°C.

Protein extraction from CaSki cells treated with siRNAs for knocking down HPV16 *E6* and *E7* (see 2.2.3.5) was performed by lysing cells in RIPA buffer II as described in (209).

2.2.2.3 DC™ Protein Assay

The DC™ Protein Assay is a detergent compatible colorimetric assay to determine protein concentration. First, 1ml of solution A was mixed with 20µl of solution S. A bovine serum albumin (BSA) standard curve was prepared every time the assay was performed in concentrations ranging from 1.5mg/ml to 0.02mg/ml. 2µl of protein sample or BSA standard was pipetted into a 96-well plate to be tested in triplicates. Then, 20µl of the A/S mix was added to each well. Finally, 200µl solution B was added to each well and incubated for 15min at room temperature. Absorbance was measured with the Multiskan™ FC microplate photometer at 750nm within 1h. The concentration was calculated according to the BSA standard curve using MS Excel.

2.2.2.4 Western blot

Proteins that were first separated by SDS-PAGE (see 2.2.2.1), were transferred to a PVDF membrane and were detected by using specific antibodies. The gel and the membrane were put in direct contact to each other in a transfer chamber (tank blot chamber or semidry blot chamber) and an electric field was applied. Due to SDS, all proteins are negatively charged and migrate from the gel towards the anode and are fixed onto the PVDF membrane via hydrophobic interactions. By this means, the electrophoretic patterns are conserved on the membrane.

Tank blot

The PVDF Transfer Membrane was activated in 100% methanol for 1min. Afterwards, the membrane, the gel, 2 filter papers and a sponge on each side were incubated shortly in tank transfer buffer and assembled in the WB transfer chamber (tank blot) to a Western blot "sandwich" with removal of occurring bubbles. Proteins were transferred for 90min, at 30V and 4°C. A magnetic stir was placed into the transfer chamber to ensure a constant temperature within the entire chamber.

Semidry blot

First, the PVDF Transfer Membrane was activated in 100% methanol for 1min. Afterwards, the membrane, 2 filter papers on each side and the gel were incubated shortly in semidry transfer buffer and assembled in the WB transfer chamber (semidry) to a Western blot "sandwich" with removal of occurring bubbles. Proteins were transferred at 150mA for 1h.

This methodology was used for HPV16 *E6* and *E7* knockdown CaSki samples with the Trans-blot Semidry Transfer Cell and the Immobilon®-P PVDF Transfer Membrane as described in (209).

2.2.2.5 Immunodetection of proteins

All incubation steps were performed on a platform shaker. After Western blot transfer (see 2.2.2.4), the membrane was blocked for 45min in 5% of low-fat milk powder diluted in 1xPBS at room temperature. Then, the blot was incubated for 1h with the desired primary antibody diluted in 1.5% low-fat milk powder in 1xPBS at room temperature for 1h or at 4°C overnight. The antibody solution was poured off and the membrane washed three times for 5min with Western blot washing buffer. After washing, the blot was incubated with goat-anti-mouse (Dianova) or goat-anti-rabbit (Rockland) secondary antibody coupled to horseradish peroxidase (HRP) diluted 1:5,000 in 1.5% milk powder in 1xPBS for 1h at room temperature. Subsequently, the blot was washed three times for 5min with Western blot washing buffer. Residual buffer was removed and 500µl of ECL Western Blotting Substrate was applied to each blot and incubated for 3min at room temperature. Chemiluminescent signals were detected using the Fusion-SL chemiluminescence camera.

Immunodetection of HPV16 E7 from CaSki cells treated with siRNAs in order to knockdown HPV16 *E6* and *E7* (see 2.2.3.5) was performed using the secondary anti-mouse HRP coupled antibody from Promega and the ECL Prime Western Blotting Detection Reagent as described in (209).

2.2.2.6 Immunoprecipitation

In this thesis, immunoprecipitation (IP) of HLA-A2 molecules was performed in order to analyze via mass spectrometry (MS) which HPV16 epitopes were bound to this MHC molecule. Prior to IP, cells were treated with an *ERAP1*-targeting siRNA pool or a control siRNA pool (see 2.2.3.5) and cultured in 10cm ø dishes (see 2.2.3.2) for 72h. 1ml of GammaBind™ Plus Sepharose™ beads were washed in one volume of 10% acetic acid (pH 3.0), vortexed and centrifuged in a swinging-bucket rotor (3min,

2,500xg). The supernatant was removed and beads were washed five times with 1xPBS until they were finally resuspended in 1ml 1xPBS supplemented with 0.02% sodium azide for storage at 4°C.

50µl of the bead suspension was washed three times using 1.5ml 0.5% IGE-PAL-630 buffer and coupled with 20µg of HLA-A2 antibody and filled up with 0.5% IGE-PAL-630 buffer to 1ml. Antibody coupling was done in 15ml falcons on a rotator for 2-3h at room temperature. Meanwhile, the cells plated in 10cm ø dishes were put on ice, washed two times with 1xPBS and covered with 1ml of ice cold IP lysis buffer. Subsequently, cells were scraped from the dish and the lysate was transferred to the next dish. This procedure was repeated for a total of four dishes (4 dishes = 1 IP sample) and approximately 1.2-2.4x10^7 cells in 1ml of lysis buffer. The lysates were incubated for 10min on ice, vortexed every 3min and then centrifuged (30min, 20,000xg, 4°C). Supernatants were pooled in 15ml falcons (4-5 IP samples in one falcon) to achieve homogeneity and to be equally distributed to the coupled beads. After coupling of antibodies to beads, the beads were centrifuged (3min, 4,700xg) and washed twice with 5ml of 0.5% IGE-PAL-630 buffer. The cleared lysate of 4-5 IP samples was incubated with 20µg/ml coupled antibody-beads for 3-4h at 4°C on a rotator platform.

After incubation, samples were centrifuged (3min, 4,700xg, 4°C), the supernatant was removed and beads containing the immunoprecipitated HLA-A2 molecules were washed nine times with ice cold 1xPBS. The beads were transferred to protein low binding tubes and the supernatant was removed completely by using thin gel-loading tips. Finally, the IP samples were stored at -80°C until liquid chromatography-mass spectrometry (LC-MS) analysis or quality analysis by Western blot (see 2.2.2.4).

2.2.2.7 Liquid chromatography-mass spectrometry (LC-MS) analysis of cell surface epitopes

The preparation of samples and LC-MS analysis were performed by Dr. Renata Blatnik in the group. Synthetic versions of the peptides to be detected were analyzed by MS first. Three of the four most intense fragments were assigned per peptide during injection of synthetic peptides. Mass spectrometer parameters were manually optimized to yield the highest signal for selected fragments. Epitopes dissociate from HLA class I molecules at a low pH (< 2.9), therefore IP samples were subjected to acetic elution with 0.3% TFA in LC/MS grade water. This results in a complex eluate out of which peptides were extracted with a Seppak reverse phase C18 material cartridge for LC-MS analysis.

For Seppak reverse phase C18 material cartridge sample processing, IP eluates were resuspended in 800µl of 0.1% TFA in LC/MS grade water. The cartridge was prewetted with 1ml 100% ACN twice, then once with 1ml 70% ACN/0.1% TFA in LC/MS grade water and finally three times with 1ml 40% ACN/0.1% in LC/MS grade water. The cartridge was equilibrated by washing three times with 1ml 0.1% TFA in LC/MS grade water before sample loading. After the sample was loaded, the cartridge was washed three times with 1ml 0.1% TFA in LC/MS grade water. Elution of the sample from the cartridge was conducted with 1ml 35% ACN/0.1% TFA in LC/MS grade water.

The eluate was subjected to drying in a vacuum centrifuge.

Samples were resuspended in 3% ACN/0.1% TFA in LC/MS grade water and sonicated in an ultrasonic water bath before nano ultra-performance liquid chromatography mass spectrometry (nano-UPLC-MS) analysis. The analysis was performed using a NanoAcquity UPLC system coupled to a Qtrap6500 mass spectrometer, which was equipped with a nano-ESI (electron spray ionization) source. Chromatographic separation was performed using a nanoAquity CSH130 C18 material column and the solutions for mobile phase A and B indicated in section 2.1.15. Solvent A of the mobile phase was composed of 0.1% FA and 0.01% TFA in ACN. The linear gradient started with 37% eluent B to 10% eluent B by 1min and then to 40% eluent B by 50min with a linear gradient at a flow rate of 300nl/min. The content of the eluate from the LC column was on-line analyzed with the Qtrap6500 mass spectrometer during separation. The instrument was operated in the targeted MS^3 measuring mode. Targeted MS^3 analysis measures only pre-defined and optimized peptides achieving optimal sensitivity for low abundant (HLA-A2 HPV16 E6 and E7-derived) peptides. The MS^3 data analysis was evaluated by manual comparison of MS^3 reference spectra of synthetic peptides with MS^3 spectra of IP samples using the Analyst 1.6.2 software. Identity of the targeted peptides was confirmed by their retention times, chromatographic profiles and MS^3 spectra of each fragment.

2.2.3 General cell culture methods

Working with cells was always performed in a laminar flow hood under sterile conditions. Equipment, material and solutions were sterilized and equipment and material was additionally disinfected by wiping with 80% ethanol prior to usage under the laminar flow hood. Mycoplasma testing and cell authentication was conducted for every newly acquired cell line. Additionally, mycoplasma and cell authenticity testing were conducted regularly. For this purpose, either an analytical PCR to detect Mycoplasma specific genes was performed using the AmpliTaq Gold® DNA polymerase (see 2.2.1.6) or a cell pellet was sent to Multiplexion (Multiplexion, Immenstaad) for a comprehensive cell contamination test or cell authentication test.

2.2.3.1 Freezing and thawing of cells

DMSO was used as a cryoprotective agent hindering crystallization of the cells. For the freezing procedure, cells were grown to a confluency of 90% in a T75 cell culture flask. First, cells were trypsinized for approximately 2min, harvested by centrifugation (3min, 400xg) and the supernatant was discarded. Cells were counted and $1x10^6$-$1x10^7$ cells were resuspended in 1ml of the corresponding culture medium. Then, 1ml of freezing medium was added to reach a final DMSO concentration of 10%, mixed gently and the suspension was transferred to a 2ml cryogenic vial. This step had to be performed quickly, because of the cytotoxicity of DMSO. The tubes were immediately placed into a pre-cooled (4°C) Cryo-Safe cryogenic vial cooler allowing a gradual temperature drop of

1°C/min, and kept in a -80°C freezer. On the next day, the tubes could be placed into the liquid nitrogen tank for permanent storage.

Also the thawing procedure had to be performed quickly, because of the cytotoxicity of DMSO. 20ml of pre-warmed culture medium was filled into 50ml falcons. Cells were rapidly thawed in a 37°C water bath and then transferred to the prepared falcon and distributed properly. Subsequently, they were centrifuged (3min, 400xg) and the supernatant was decanted. Cells were washed once in their respective cell culture media and then they were put into in a suitable cell culture flask or cell culture plate depending on the cell number and the particular cell type. The following day, the culture medium was exchanged to remove any residual DMSO.

2.2.3.2 Culturing and passaging of cells

In this study, all cell lines were cultured in an incubator at 37°C, 95% relative humidity and 5% CO_2 in either cell culture flasks or cell culture plates. While adherent cells were grown in horizontally lying flasks, suspension cells were grown in flasks standing upright. The flasks or well plates were always replaced after each second cell passage. Cells were split when they reached a confluency of 80-100%.

Adherent cells were passaged by removing the medium and gentle washing with 1xPBS to remove residual medium which could interfere with the subsequent trypsinization. Then, cells were detached by incubation with a suitable volume of trypsin-EDTA solution completely covering the cell layer at 37°C (e.g. 2ml for a T75 cell culture flask). Cell detachment was checked by microscopy. When cells were detached, the reaction was stopped by the addition of serum-containing medium (at least five times the volume of the trypsin solution) and pipetting up and down. Cells were transferred to a 50ml falcon and centrifuged (3min, 400xg). After removal of the supernatant, cells were resuspended in an appropriate amount of fresh culture medium (e.g. 10ml medium in a T75 cell culture flask) and either split at ratios depending on the particular cell type or used for experiments.

Suspension cells were harvested from the flask or plate, centrifuged (3min, 400xg) and the supernatant was discarded. Then, they were resuspended in fresh culture medium and for splitting a desired amount of cells was added to a fresh culture plate or flask. Approximately, 0.5-1x10^6cells/ml were seeded depending on the growth characteristics of the particular cell type.

2.2.3.3 Counting of cells

Cells were harvested via trypsinization (see 2.2.3.2), diluted in 1xPBS and then mixed 1:1 with Trypan blue stain for life-dead discrimination. Cells were either counted employing a Neubauer counting chamber or automatically using the Countess® Automated Cell Counter. For counting with the Countess® Automated Cell Counter, the cell suspension has to be of a concentration ranging from 1x10^4 up to 1x10^7cells/ml, because the cell counter only counts accurately in this range. For manual counting with the Neubauer counting chamber the cell number was calculated according to this formula:

$$\text{cell number/ml} = \frac{\text{counted cells in large squares}}{\text{number of counted large squares}} \text{ x dilution factor x chamber factor (10000)}$$

2.2.3.4 Treatment of cells with IFNγ

In this study, cells were treated with recombinant human IFNγ to analyze the expression of APM components under these conditions either by qRT-PCR, Western blot or flow cytometry. Cells were grown until they reached a confluency of 70-80%. Then, medium was removed and exchanged for fresh medium. IFNγ was diluted in 1xPBS and added with a final concentration of 50ng/ml. Cells were cultured for another 48h.

The IFNγ used within this study had a specific activity of $5x10^7$IU/mg protein and reached an antiviral bioassay titer of $5.5x10^7$IU determined in the lab of Prof. Rainer Zawatzky (Prof. Frank Rösl, Viral Transformation Mechanisms, DKFZ, Heidelberg).

2.2.3.5 Transfection of eukaryotic cells with siRNA

Knockdown of *ERAP1*

ERAP1 (NCBI ID: 51752) was knocked down with a siPOOL from siTOOLs BIOTECH. As a negative control a non-targeting siPOOL was used. The experiments were either conducted in 12-well plates or in 10cm ø dishes for subsequent IPs (see 2.2.2.6). First, cells were trypsinized (see 2.2.3.2), counted (see 2.2.3.3) and diluted in 900µl (for one well of a 12-well plate) of the respective culture medium. Depending on the cell size and growth properties different amounts of cells were needed for the knockdown experiments:

Table 2.9: Cell numbers and siRNA concentration needed to efficiently knockdown *ERAP1*.

Cell line	Cell number per well	siRNA concentration
CaSki	$1x10^5$	10nM
866	$5x10^4$	5nM
SNU17	$4x10^5$	5nM
SNU703	$3x10^5$	8nM
SiHa	$1x10^5$	10nM
FK16A	$1x10^5$	10nM

The siRNA dilution was prepared in RNase-free water provided by the company. The siRNA pool was in a volume of 10µl and 40µl of Opti-MEM® was added. For one reaction 2µl of the transfection reagent RNAiMAX was diluted in 48µl of Opti-MEM®. The siRNA mix and the transfection reagent mix were combined (1:1) and incubated for 5min at room temperature. Afterwards, 100µl of the mix was transferred per well of a 12-well plate and the cell suspension was added. For 10cm ø dishes, cell number, medium and siRNA/RNAiMAX were scaled up proportionally. Cells were incubated for 72h if not indicated otherwise.

Knockdown of HPV16 *E6* and *E7*

Knockdown of the HPV16 oncogenes *E6* and *E7* was performed in cooperation with Prof. Karin Hoppe-Seyler (Prof. Felix Hoppe-Seyler, Molecular Therapy of Virus-Associated Cancers, DKFZ, Heidelberg). HPV16 *E6* and *E7* were knocked down using three specific siRNAs (see 2.1.12) that target all three HPV16 *E6* and *E7* transcript classes. As a negative control a non-targeting siRNA was used that had at least 4 mismatches to all known human genes. CaSki cells were transfected using DharmaFECT I based on the manufacturer's instructions. All three siRNAs were pooled at equimolar concentrations to reach a final siRNA concentration of 10nM. Cells were incubated with siRNAs for 72h. Afterwards, cells were lysed (see 2.2.2.2) and used for semidry Western blot analysis (see 2.2.2.4).

2.2.4 *In vitro* assessment of T cell function

2.2.4.1 Peripheral blood mononuclear cell (PBMC) isolation

Peripheral blood mononuclear cells (PBMCs) were isolated from fresh blood donations of healthy donors by density gradient centrifugation. Ficoll-Paque™ Plus and ACK lysis buffer were used at room temperature.

First, 15ml of Ficoll-Paque™ Plus was pipetted into Leucosep™ tubes and centrifuged, passaging the porous layer (1min, 300xg). After blood donation, 10ml of heparinized blood was poured carefully into Leucosep™ tubes onto the porous barrier. In order to dilute the blood, 15ml of 1xPBS was added carefully and the blood was centrifuged (10min, 300xg, centrifuge break turned off). Tubes were removed cautiously from the centrifuge in order to preserve the layering. The Ficoll-Paque™ Plus and most of the erythrocytes and granulocytes were located on the bottom of the tube. Above the porous barrier, the desired PBMC layer was found. The blood plasma located above the PBMCs was taken off down to 1cm above the PBMC layer and discarded. Then, the PBMC layer was carefully taken up with a 10ml pipette and transferred into a fresh 50ml tube which was then filled up with 1xPBS in order to wash the cells. Cells were centrifuged (10min, 300xg) and erythrocyte lysis was performed to get rid of residual erythrocytes. In general, 3-5ml of ACK lysis buffer was used for cell pellet resuspension. The tubes were shaken gently for 3-5min depending on the amount of residual erythrocytes. Lysis was stopped by filling up the tubes with 1xPBS. Cells were washed twice with 1xPBS, counted (see 2.2.3.3) and stored on ice for subsequent experiments.

2.2.4.2 Magnetic-activated cell sorting (MACS)

Magnetic-activated cell sorting (MACS) was used for separating different cell types according to their surface molecules. Separation was achieved by incubation with magnetic microbeads coated with antibodies specific for a particular surface molecule. The antibody binds to the cell surface marker of

the corresponding cell type and this complex can be subjected to a magnetic field, thereby separating the desired cell population from a mixed cell population. In this study, MACS was used to isolate CD14 monocytes from PBMCs (see 2.2.4.1) using CD14 microbeads and to isolate CD8 T cells via the "untouched CD8 T Cell Isolation Kit" from T cell cultures (see 2.2.4.3). The whole procedure was conducted with ice-cold buffers and under sterile conditions. Prior to isolation, the cell number was determined (see 2.2.3.3), cells were resuspended in ice-cold MACS buffer and a maximum of $1x10^8$ cells per column were used. MACS isolations were performed strictly following the manual of the company. Afterwards, cells were counted and used for the experiments described in the following paragraphs.

2.2.4.3 Generation of peptide-specific T cell lines

In this study, HPV16-specific T cells were expanded in order to investigate immunogenicity of certain peptides in the donors and as a read-out tool to observe changes in the presented HPV16 epitopes on tumor cell lines. HPV16-specific T cell memory was analyzed using short-term T cell lines whereas long-term T cell lines were used as a read-out tool. For long-term T cell lines, autologuous DCs and B cells were matured and activated, and used as antigen-presenting cells (APCs) for T cell stimulations.

Generation of monocyte-derived dendritic cells (Mo-DCs)

CD14-positive monocytes were either purified by MACS (see 2.2.4.2) or using the monocyte adherence strategy described in detail below. MACS purified cells were resuspended at a concentration of $1x10^6$cells/ml in DC medium, supplemented with 500U/ml IL-4 and 1000U/ml GM-CSF and 2ml of this cell suspension was added to one well of a 6-well plate. For the monocyte adherence strategy, $1x10^7$ PBMCs were cultured in one well of a 6-well plate with DC medium for 2-3h at 37°C. During this time, monocytes adhered to the plastic surface. Floating cells containing other lymphocytes were harvested, transferred to tubes and further used to generate T cell lines or CD40-activated B cells. Adherent monocytes were washed twice using DC medium. Then, 2ml DC medium containing 500U/ml IL-4 and 1000U/ml GM-CSF was added to each well. On day 3, DC medium supplemented with IL-4 and GM-CSF reaching a final concentration of 500U/ml and 1000U/ml, respectively, was added in a volume of 500µl to each well. On day 6 or 7, the maturation cocktail containing 1000U/ml TNFα, 10ng/ml IL-1β, 10ng/ml IL-6, 1µM PGE2 (1mg/ml) and 1µl/ml LPS (5mg/ml, $5x10^4$ EU/ml) was added to the cells and incubated for at least 36h up to 48h before cells were used as APCs. After maturation, mature dendritic cells could be verified using microscopy by a unique morphology with long thread-like dendrites and were harvested by pipetting up and down thoroughly. Cells were stored on ice and were then used as APCs for T cell stimulation. Purity and expression of surface molecules (CD83, CD86 and CD80) was checked by flow cytometry analysis (see 2.2.5, data not shown).

Generation of CD40-activated B cells

The day before the B cell culture was started, the feeder cell line tCD40L NIH3T3 was harvested (see 2.2.3.2), washed with 1xPBS and irradiated at 98Gy. Then, cells were washed again with 1xPBS and were diluted in tCD40L WT medium of a concentration of $2x10^5$cells/ml. 2ml of this cell suspension was plated into one well of a 6-well plate and incubated overnight at 37°C with 5% CO_2.

The next day, the CD14-negative cell population or floating cells that did not adhere to the 6-well plate (see 2.2.4.2) were counted and diluted at a concentration of $2x10^6$cells/ml in B cell medium supplemented with 0.63µg/ml cyclosporin A, 10ng/ml or 100U/ml IL-4 and 2ng/ml IL-6 (210). Cyclosporin A was added to the cytokines in order to kill T cells contained in the mixed cell population. The medium was removed from the feeder cell line and cells were washed gently with B cell medium and 4ml of the CD14-negative cell suspension or non-adherent PBMCs was added and incubated for at least 96h.

At day 5, clustered CD40-activated B cells were harvested from 6-well plates and centrifuged (3min, 300xg). Cells were resuspended at a concentration of $2x10^6$cells/ml in B cell medium supplemented with 0.63µg/ml cyclosporin A, 10ng/ml or 100U/ml IL-4 and 2ng/ml IL-6. 4ml of the cell suspension was added to pre-plated feeder cells as described above. B cell lines were always re-cultivated every 3-4 days on feeder cells prepared one day before. After one week of culture, $4x10^6$ B cells per well of a 6-well plate were plated. At day 14, the culture consisted of more than 95% of B cells (assessed by CD19-positive expression analyzed by flow cytometry on a regular basis) and those cells were further used as APCs for T cell stimulation.

Peptide-specific short-term T cell lines

Short-term T cell lines were generated to assess the HPV16-specific T cell memory of each healthy donor. On day 0, PBMCs were prepared (see 2.2.4.1), $1\text{-}2x10^6$ cells were resuspended in 2ml of T cell medium supplemented with 10ng/ml IL-7 and in one well of a 24-well plate. Peptides were added to each well at a concentration of 10µg/ml and dispensed by pipetting. Cells were cultured at 37°C with 5% CO_2. On day 3 and 7, 1ml of the medium was carefully removed and 1ml of fresh T cell medium, supplemented with 40U/ml IL-2 with a final concentration of 20U/ml IL-2, was added. On day 12, cells were used for ELISpot analysis (see 2.2.4.4).

Peptide-specific long-term T cell lines

Long-term T cell lines were generated by expanding HPV16-reactive T cells. First, autologous mature DCs were pulsed with selected HPV16-derived peptides. To this end, mature Mo-DCs (see above) were harvested and washed with serum-free DC medium, resuspended at a concentration of $1x10^6$cells/ml in serum-free DC medium in 50ml tubes and selected peptides were added (10µg/ml final concentration). Cells were incubated for 3-4h at 37°C with 5% CO_2 with gently tapping of the tube each hour. Afterwards, cells were washed with serum-free DC medium, counted and resuspended

in 1ml of T cell medium. In between, PBMCs from the same healthy donor were prepared (2.2.4.1) and $1x10^7$ were diluted in 1ml T cell medium supplemented with 20ng/ml IL-7 to reach a final concentration of 10ng/ml. The DCs were added to the PBMCs in a volume of 1ml. Peptide pulsed DCs and PBMCs were plated at a ratio of 1:10-1:200 in 24-well plates. On day 5 after stimulation, 1ml of the supernatant was carefully removed and 1ml of fresh T cell medium containing 40U/ml IL-2 was added to each well with a final concentration of 20U/ml IL-2. One week after the first stimulation, PBMCs were restimulated with matured peptide-pulsed DCs and IL-7 supplemented T cell medium. 5 days after this stimulation, IL-2 was added as described before. The third stimulation was performed one week after the second one using peptide-pulsed CD40-activated B cells. For the HLA-A24 positive donor the autologous EBV-immortalized B cell line, RiSh, could be used. B cells were pulsed with peptides as described above, but afterwards they were irradiated at 32Gy (RiSh cells were irradiated at 70Gy), washed twice with T cell medium and were added to the T cell lines at a ratio of 1:5 (B to T cells). 5 days after stimulation, IL-2 was added as described before. One week after the third stimulation, T cell lines were harvested and used for subsequent experiments.

2.2.4.4 Interferon (IFN)γ enzyme-linked immunospot (IFNγ ELISpot)

The ELISpot assay was used to quantify peptide-specific T cell responses. Short-term T cell lines (see 2.2.4.3) were tested for peptide-specificity in an ELISpot assay via restimulation with the corresponding peptide within the ELISpot plate.

On day 1, 96-well MultiScreen®-HA plates were coated using 100µL/well of anti-human IFNγ capture antibody diluted 1:500 in 1xPBS. Plates were incubated at 4°C overnight. On the following day, the capture antibody was removed by inverting the plate shortly. Then, plates were washed three times with 1xPBS. For blocking, 200µl of ELISpot medium was added to each well and plates were incubated for 1-2h at 37°C with 5% CO_2. Meanwhile, T cells were harvested and diluted to the desired concentration. Blocking medium was removed and 100µl of ELISpot medium containing a control peptide or a HPV16-derived peptide diluted to a final concentration of 10µg/ml was added to each well. As positive controls, 2µg/ml ConA or 1µg/ml of a CEF or a CE peptide pool was used; whereas a HIV-derived peptide for the respective HLA type of the donor and the peptide diluent DMSO served as negative controls. 1 or $2x10^5$cells resuspended in 100µl ELISpot medium were added per well. The total volume of each well was 200µl and if possible at least triplicates were prepared for each sample if not indicated otherwise. The ELISpot was incubated for 18-24h at 37°C with 5% CO_2 without any movement of the plate. After incubation, the plates were quickly inverted and washed twice with 1xPBS and twice with ELISpot washing buffer. 100µl of biotinylated anti-human IFNγ antibody, diluted 1:1,000 in 1xPBS, was added per well and incubated for 2h at room temperature. Plates were washed four times with ELISpot washing buffer. Then, 100µl of Streptavidin-alkaline phosphatase, diluted 1:2,000 in 1xPBS, was added per well and incubated for 90min at room temperature. Then, plates were washed four times with ELISpot washing buffer and 100µl of BCIP/NBT-Plus substrate was added to each well and incubated for 20-25min. The reaction

was stopped by rinsing the plates on both sides of the membrane with tap water. The plates were air dried in a flow hood. ELISpot plates were scanned and spot forming units (SFU) were counted with the CTL ImmunoSpot 5.1.36 Professional DC software using the Smart Count™-ImmunoSpot "wizard" counting mode with automated parameter set up. Finally, SFU were calculated to $1x10^6$ input cells.

2.2.4.5 VITAL-FR cytotoxicity assay

The VITAL-FR cytotoxicity assay is a flow cytometry based assay to assess small frequencies of CTLs by their cytolytic function. This assay was established in the group of Dr. Andreas Kaufmann (211, 212). On the first day, $1x10^6$/ml target cells were incubated with 5µM CFSE (carboxyfluorescein) or 0.25µM FarRed (dimethyldodecylamine oxide-succinimidyl ester) in a 50ml falcon for 10min, at 37°C, in a waterbath. The reaction was stopped by adjusting the volume to 50ml with pre-warmed RPMI supplemented with 10% FCS. Labeled cells were centrifuged (5min, 300xg) and either directly plated into 12-well plates or first used for siRNA-mediated knockdown (see 2.2.3.5), then plated and incubated at 37°C with 5% CO_2. Cells treated with control siRNA were labeled with FarRed, whereas those treated with the *ERAP1*-specific siRNA pool were stained with CFSE.

On the second day, purified CD8 T cells from long-term T cell lines (see 2.2.4.2 and 2.2.4.3) and target cells were harvested and counted. Triplicates or duplicates of effector T cells were titrated in 48-well plates (effector:target ratios ranging from 1.25:1 to 20:1) and $3x10^3$ CFSE-labeled as well as $3x10^3$ FarRed-labeled target cells were added to each well. Wells containing only target cells were plated, serving as negative control. Cells were plated in T cell medium supplemented with 10U/ml IL-2, reaching a final volume of 200µl. The mixes were incubated for 48h at 37°C and carefully resuspended after 24h. After 48h, cells were collected and either directly used for flow cytometry analysis (see 2.2.5) or fixed in fixation buffer for 10min, washed in FACS buffer and stored for max. 3 days at 4°C until analysis. For analysis of specific killing, the entire target cell population was defined in a life gate with the forward/sideward scatter. CFSE- and FarRed-labeled target cells were detected and calculated as the percentage from the life gate. Specific lysis was calculated using this formula:

$$\text{specific lysis (\%)} = 100 - \left[\frac{\text{frequency of target cells with T cells}}{\text{frequency of target cells only}} \text{x } 100\right]$$

2.2.5 Flow cytometry

The FACS Canto II™ flow cytometer provided by the DKFZ FACS Core Facility was used. All reagents were ice-cold throughout the experiments and incubation was either performed on ice or at 4°C. Stainings were either performed in 96-well plates or in reaction tubes depending on the amount of samples. In general, $1x10^6$ cells were used for flow cytometry staining and out of these $1x10^4$-$1x10^5$

cells were recorded. After harvesting, cells were washed with FACS buffer, centrifuged (3min, 400xg, 4°C) and blocked for 15min in 1xPBS supplemented with 10% FCS on ice. Then, the cells were resuspended in 100µl FACS buffer containing the appropriate dilution of antibody. After 30min of incubation, covered from light, at 4°C, cells were washed twice with FACS buffer. When the primary antibody was unlabeled and a secondary antibody staining was necessary, the secondary antibody was diluted in FACS buffer, applied to the cells and incubated for 30min, covered from light and at 4°C. Then, cells were washed twice with FACS buffer, resuspended in an appropriate volume of FACS buffer and analyzed on the FACS Canto II™. For later analysis, cells were fixed in fixation buffer for 10min in the dark. Cells were washed once with FACS buffer, resuspended in an appropriate volume of FACS buffer, stored at 4°C and flow cytometry analysis was performed within 3 days.

Throughout flow cytometry analysis, cells were kept on ice and protected from light. Acquisition of unstained cells was used to determine background autofluorescence. If staining with a labeled secondary antibody was necessary, cells stained with the secondary antibody only served as background control. Voltages and compensation were adjusted using single color stainings. For this, cells and compensation beads were stained with only one antibody. OneComp eBeads were stained with the corresponding antibodies used for cell stainings. The single-color stained cells and beads were then acquired with the FACS Canto II™ to perform manual compensation. Data processing was performed with the FlowJo 6.5 software.

2.2.6 Immunohistochemistry

In this study, immunohistochemistry (IHC) for ERAP1 in human tissue sections was performed in cooperation with Dr. Miriam Reuschenbach (Prof. Magnus von Knebel Döberitz, Department of Applied Tumor Biology, Institute of Pathology, University of Heidelberg). Human tissue sections were anonymized in accordance with the regional ethical regulations and exclusion of personal data of the subjects.

For validating the ERAP1 antibody, CaSki cells were plated and either transfected with a siPOOL specific for *ERAP1*, a non-targeting siRNA pool (see 2.2.3.5) or left untreated. Cells were trypsinized 72h after transfection, washed twice with 1xPBS and pelleted (3min, 400xg). Cell pellets were resuspended in 10ml of the methanol-based preservation solution, PreservCyt, and stored at 4°C. Cells were prepared on thin-layer ThinPrep® cytology slides using a cytology processor.

For immunohistochemistry stainings, human tissue sections of formalin-fixed, paraffin-embedded cervical cancer biopsy specimens were deparaffinized and rehydrated using xylol and a series of graded alcohols as shown in Table 2.10.

Table 2.10: Deparaffinization and rehydration of tissue sections.

Alcohol type	Incubation time
100% xylol I	5min
100% xylol II	5min
100% xylol III	5min
100% ethanol I	5min
100% ethanol II	5min
96% ethanol	5min
70% ethanol	5min
deionized H_2O	5min

Afterwards, sections were placed into a black cuvette and filled with deionized H_2O (dH_2O). dH_2O was replaced with fresh dH_2O four times. Sections were placed in antigen retrieval buffer and microwaved three times for 5min at 550W. Sections were chilled for 20min. Sections were washed two to three times with dH_2O and incubated for 15min in 3.5M HCl solution at room temperature. Subsequently, sections were washed for 5min in dH_2O and then incubated in dH_2O containing 3% H_2O_2. Sections were washed several times with dH_2O. Then, they were placed in permeabilization buffer for 2-3min. Blocking (horse serum) and development (secondary biotinylated antibody and avidin/biotin complex) of the sections was done using the VECTASTAIN Elite ABC Kit. Immunostainings were encircled with a Pap Pen and put into a humidity chamber. Sections were blocked with blocking buffer for 20-30min. The blocking solution was removed by tapping. Sections were incubated with antibodies for ERAP1 and p16 diluted 1:2,000 in 1xPBS supplemented with 1% horse serum overnight at 4°C. The following day, sections were washed twice for 5min with immunohistochemistry washing buffer. Then, the secondary biotinylated antibody was diluted 1:50 in 1% horse serum diluted in 1xPBS and incubated for 1h at room temperature. The sections were washed twice for 5min with immunohistochemistry washing buffer. Afterwards, sections were incubated with component A and B of the avidin/biotin complex mixed 1:50 in 1xPBS for 30min at 4°C. Sections were washed three times for 5min with immunohistochemistry washing buffer. For color development, one drop of the DAB chromogen was added to 1ml of substrate, applied to the section and incubated for several minutes. Sections were washed with dH_2O and placed in Mayer's Hematoxylin solution for 1-3min. Subsequently, sections were washed by rinsing them with tap water for 5min. Finally, sections were embedded in Aquatex® aqueous mounting agent and stored in darkness until microscopical analysis.

2.2.6.1 Analysis of IHC data

To evaluate ERAP1 expression an immunohistochemical score was calculated as the product of the staining frequency and maximal intensity based on the following system: the staining frequency ranged from 0 (no ERAP1 expressing cells) to 5 (< 10%), 30 (10-50%), 70 (50-90%) or 95 (> 90%) reflecting the percentage of ERAP1 expressing cells and the maximal intensity was set to 0 = no, 1 = low, 2 = intermediate and 3 = high expression. The staining frequency (0, 5, 30, 70 or 95) and the maximal intensity (0, 1, 2 or 3) were multiplied to determine the immunohistological score. The

immunohistochemical score of ERAP1 expression was determined for the cytoplasmic and perinuclear regions of the cells within a section. Finally, the average of the immunohistochemical score for the cytoplasmic and perinuclear region was calculated. All sections were analyzed independently, randomly and by two different researchers (Dr. Miriam Reuschenbach and Alina Steinbach). An average score was determined for the rare occasion of differing histological scores.

2.2.7 Statistics

For statistical analyses the PRISM® 5 software was used. The employed statistical test is indicated in the figure legend of the respective experiment.

3 Results

Diseases caused by human papillomavirus (HPV) are a global health burden. Despite the success of prophylactic anti-HPV vaccines there is a need for a therapeutic vaccine that can cure already established infections. In order to develop a clinically successful vaccine it is crucial to elucidate molecular evasion strategies that HPV-mediated cancers use to evade the immune system. The present study aimed at the systematic identification of components of the antigen processing machinery (APM) that are altered in HPV-mediated cancers and to investigate whether these changes have an impact on the HLA class I epitope presentation of HPV16, the most common HPV high-risk type.

The first part of the results section describes the assessment of the APM on the mRNA and protein level in HPV16-positive compared to HPV-negative cell lines. Furthermore, the impact of the cytokine interferon (IFN)γ on APM component expression was analyzed. These experiments revealed that the endoplasmic reticulum aminopeptidase 1 (ERAP1) was consistently overexpressed in HPV16-positive tumor cell lines. Thus, ERAP1 was further analyzed by immunohistochemistry in cervical tissue. Immunohistochemical analysis showed that ERAP1 levels increased with disease state and were significantly higher than in histologically normal cervical epithelium. Further, possible mechanisms were studied that could account for ERAP1 overexpression and imply functional consequences. Single nucleotide polymorphisms (SNPs) of *ERAP1* were analyzed in several HPV16-positive cell lines and one HPV-negative cell line. Additionally, the influence of the HPV16 oncogenes *E6* and *E7* on ERAP1 expression was investigated.

In the final part of this thesis, a small interference RNA (siRNA) approach to knockdown *ERAP1* was established. This tool was used to analyze whether overexpression of ERAP1 affects the presentation of HLA class I of HPV16 E6 and E7-derived peptides. For the direct detection of naturally processed and presented epitopes on HPV16-transformed cells a highly sensitive mass spectrometry approach was used. HPV16 E6 and E7-specific CD8 T cells were used in cytotoxicity assays to study the impact of ERAP1 expression on defined epitopes.

3.1 Analysis of the antigen processing machinery (APM)

HPV is able to perturb antigen processing (see 1.2.2) which is the intracellular pathway for the generation of T cell epitopes. Thereby, anti-tumor responses mediated by CD8 T cells could be hampered. However, so far no comprehensive screen of the APM is available in HPV-induced cancers. Thus, the expression of the whole APM was analyzed in a comprehensive collection of cell lines in the first part of this study. This collection included HPV-negative cell lines, HPV16-positive cervical cancer cell lines, HPV16-positive head and neck squamous carcinoma (HNSCC) cell lines, and cell lines that have been transfected with the HPV16 genome. The collection included long-standing as

well as newly-established cell lines. First, APM component expression on the mRNA level was investigated in all cell lines using quantitative Real-Time PCR (qRT-PCR). Constitutive expression as well as expression upon IFNγ stimulation was investigated. Secondly, the protein expression of selected APM components in selected cell lines was analyzed to confirm the observations of the qRT-PCR approach. Thirdly, immunohistochemistry of cervical tissue sections was performed to compare ERAP1 expression in histologically normal and HPV-transformed tissue.

3.1.1 Expression of APM components on the mRNA level

In the initial part of the APM component expression analysis, a qRT-PCR screen was used to assess the expression of 20 APM components in 29 cell lines. The qRT-PCR approach used in this study was thoroughly established in our laboratory by Jan Winter (213). Quality control parameters applied by the data processing software LinRegPCR and qBase plus for qRT-PCR are summarized in Table 7.1 in the appendix. For data analysis, passive normalization was done by the MxPro software of the qPCR machine. The LinRegPCR software (214, 215) was used for baseline subtraction, Cq and PCR efficiency determination. LinRegPCR has many advantages over simple qPCR analysis using only the supplied software of the qPCR machine. LinRegPCR finds the linear log-phase for each qPCR reaction, the background is subtracted individually and only then the Cq values are calculated. In addition, LinRegPCR includes single well kinetics for baseline subtraction and PCR efficiency calculation, thereby further minimizing variations. Mean PCR efficiencies calculated by LinRegPCR of all used genes are illustrated in Figure 7.1 A and B in the appendix. A second software, qBase plus, was employed for reference gene normalization, calibration and data management. Since reference genes can be regulated (216), multiple experimentally validated reference genes (*GAPDH*, *PGK1*, *PPIA*, *IPO8*) for keratinocyte-derived cell lines were used in our approach (204).

The HPV-negative control group included human primary keratinocytes from three different donors (pHKI-III) and primary human foreskin keratinocytes (pHFK) pooled from multiple neonatal foreskins. In addition, the HPV-negative normal oral keratinocytes (NOK), which were immortalized by human telomerase reverse transcriptase (hTERT), were used (193). The spontaneously immortalized keratinocyte cell line HaCat also served as a HPV-negative control (192). HPV16-positive cell lines consisted of 12 cell lines derived from cervical cancer, 6 from HNSCC and 5 keratinocyte cell lines that have been HPV16-immortalized by transfection with the whole HPV16 genome (for names and origin of the cell lines see Figure 3.1).

3.1.1.1 Constitutive expression of APM components

The first qRT-PCR screen was done to analyze constitutive expression of APM components in HPV16-positive cell lines compared to HPV-negative cell lines. Total RNA was isolated, genomic DNA was removed, and RNA reverse transcribed into cDNA. FAM (fluorescein amidite)-labeled

TaqMan® hydrolysis probes were used for qRT-PCR (see 2.1.11). In order to minimize variation of the results, the sample maximization approach introduced by Hellemans *et al.* (205) was followed. To this end, all cell lines were analyzed for one particular gene on one qPCR plate. The determined expression levels were calibrated to the HPV-negative cell line NOK.

Figure 3.1 shows the obtained data of constitutive APM component expression as a heatmap generated by R. Genes that are overexpressed compared to NOK are shown in green, while downregulated genes are shown in red. A similar expression level to the NOK cell line is shown in black. The first observation was that the HPV-negative cell lines had a strikingly uniform behavior. Cell lines transfected with the whole HPV16 genome (except for HPK1A and 2A3) behaved similarly to the HPV-negative group. However, gene expression levels of tumor-derived cell lines either from cervical cancer or from HNSCC were different for many APM components. Gene expression of *HLA-A* and *-B* was elevated in the majority of tumor cell lines, as were *β2m* (*β2-microglobulin*) levels. Many peptide loading complex associated genes, *tapasin*, *calnexin*, *calreticulin*, *ERAP1* and *ERAP2*, also showed a trend to upregulation when compared to the HPV-negative group. Furthermore, all tested components of the immunoproteasome, *PSMB8*, *PSMB9*, *PSMB10*, *PSME1* and *PSME2*, had higher expression levels in the cervical cancer and HNSCC group. Detailed bar diagrams of each tested gene for all cell lines of this screen are given in Figure 7.2 to 7.5 in the appendix.

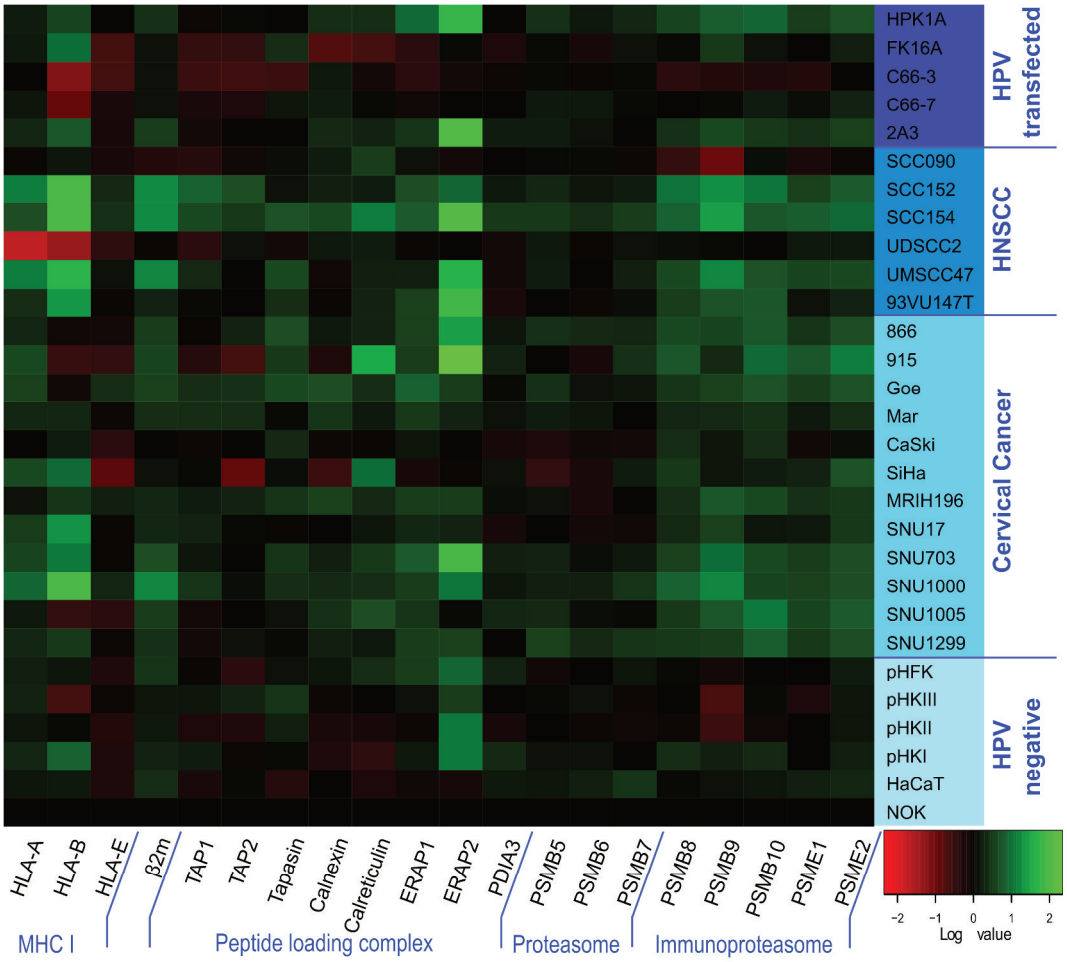

Figure 3.1: Constitutive expression of the APM on the mRNA level. Total RNA was purified from cells, reverse transcribed to cDNA and analyzed for APM component expression by qRT-PCR using TaqMan® probes. PCR reactions were run in triplicates. At least three of the following genes were used as internal reference genes: *GAPDH*, *PGK1*, *PPIA* and *IPO8*. Gene expression was calibrated to the NOK cell line. All quantitative qRT-PCR data were processed by LinRegPCR and data management was done by qbasePLUS 2. Log_{10} data were plotted as a heatmap using R. Expression of 20 APM components is shown. Each column represents a single gene and each row represents one cell line. Increased expression is shown in green and decreased expression is shown in red (see scale bar in the bottom right corner). HNSCC = head and neck squamous cell carcinoma

Since in the heatmap representation a trend was observed that many APM associated genes were upregulated in tumor-derived cell lines, the next step was to statistically validate these observations. To this end, the different cell lines were grouped into HPV-negative cell lines and HPV16-positive tumor cell lines, including cervical and HNSCC. Statistical significance for gene expression was tested between the two groups. Of note, the HPV16-transfected group was omitted from this analysis because this group behaved similarly to HPV-negative cells as described above. Figure 3.2 A shows all genes that were found to be significantly upregulated in tumor-derived cell lines. These genes were the chaperone *calreticulin*, the aminopeptidase *ERAP1* and all tested components of the immunoproteasome (*PSMB8*, *PSMB9*, *PSMB10*, *PSME1* and *PSME2*). All other genes did not show a significantly different expression from the HPV-negative group (Figure 3.2 B). These results complement observations made by the heatmap representation. This provides a first indication that APM components are indeed constitutively altered in HPV16-positive cell lines.

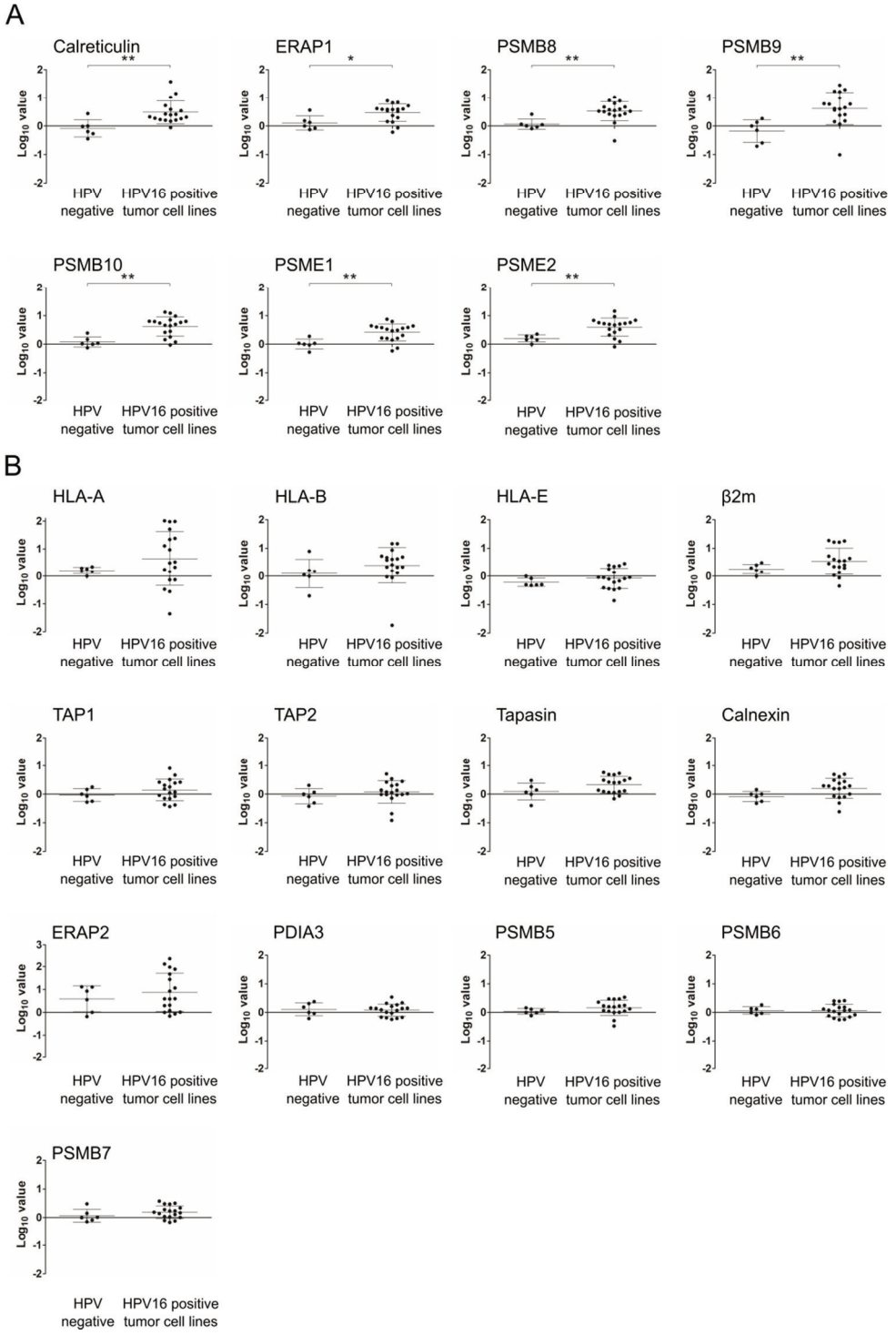

Figure 3.2: Constitutive expression of the APM on the mRNA level. Total RNA was purified from cells, reverse transcribed to cDNA and analyzed for APM component expression by qRT-PCR using TaqMan® probes. PCR reactions were run in triplicates. At least three of the following genes were used as internal reference genes: *GAPDH*, *PGK1*, *PPIA* and *IPO8*. Gene expression was calibrated to the NOK cell line. All quantitative qRT-PCR data were processed by LinRegPCR and data management was done by qbasePLUS 2. Log_{10} expression data were plotted for each cell line, additionally mean ± SD of each group are shown. **A.** APM components that showed a significantly elevated expression in cervical cancer and head and neck squamous cell carcinoma (HNSCC) compared to HPV-negative cells. * $p \leq 0.05$, ** $p \leq 0.01$ (unpaired t-test) **B.** APM components that showed no significantly different expression in HPV16-positive tumor cell lines compared to HPV-negative cells.

3.1.1.2 The influence of interferon (IFN)γ on APM component expression

The second qRT-PCR screen was performed to analyze expression of APM components in HPV16-positive cell lines compared to HPV-negative cell lines after IFNγ stimulation. There are many genes of the APM known to be inducible by IFNγ, namely *HLA-A*, *HLA-B*, *HLA-E*, *β2m*, *TAP1*, *TAP2*, *tapasin*, *ERAP1*, *ERAP2*, *PSMB8*, *PSMB9*, *PSMB10*, *PSME1* and *PSME2* (67, 217, 218), which is crucial during anti-viral immune responses. These genes are written in red below the heatmap in Figure 3.3. Total RNA was isolated, genomic DNA was removed, and RNA reverse transcribed into cDNA. FAM-labeled TaqMan® hydrolysis probes were used for qRT-PCR (see 2.1.11). In order to minimize variation of the results, untreated and treated samples of the same cell line were analyzed for gene expression on one qPCR plate. The IFNγ-induced determined expression levels were calibrated to the respective untreated expression levels.

Figure 3.3 shows the obtained data of IFNγ stimulated APM component expression as a heatmap like in Figure 3.1. In general, the results revealed that all APM components that should be IFNγ-inducible were upregulated upon stimulation, but to a variable extent. HPV-negative as well as HPV16-positive cell lines all reacted to the cytokine, suggesting that IFNγ signaling is intact in the cell lines.

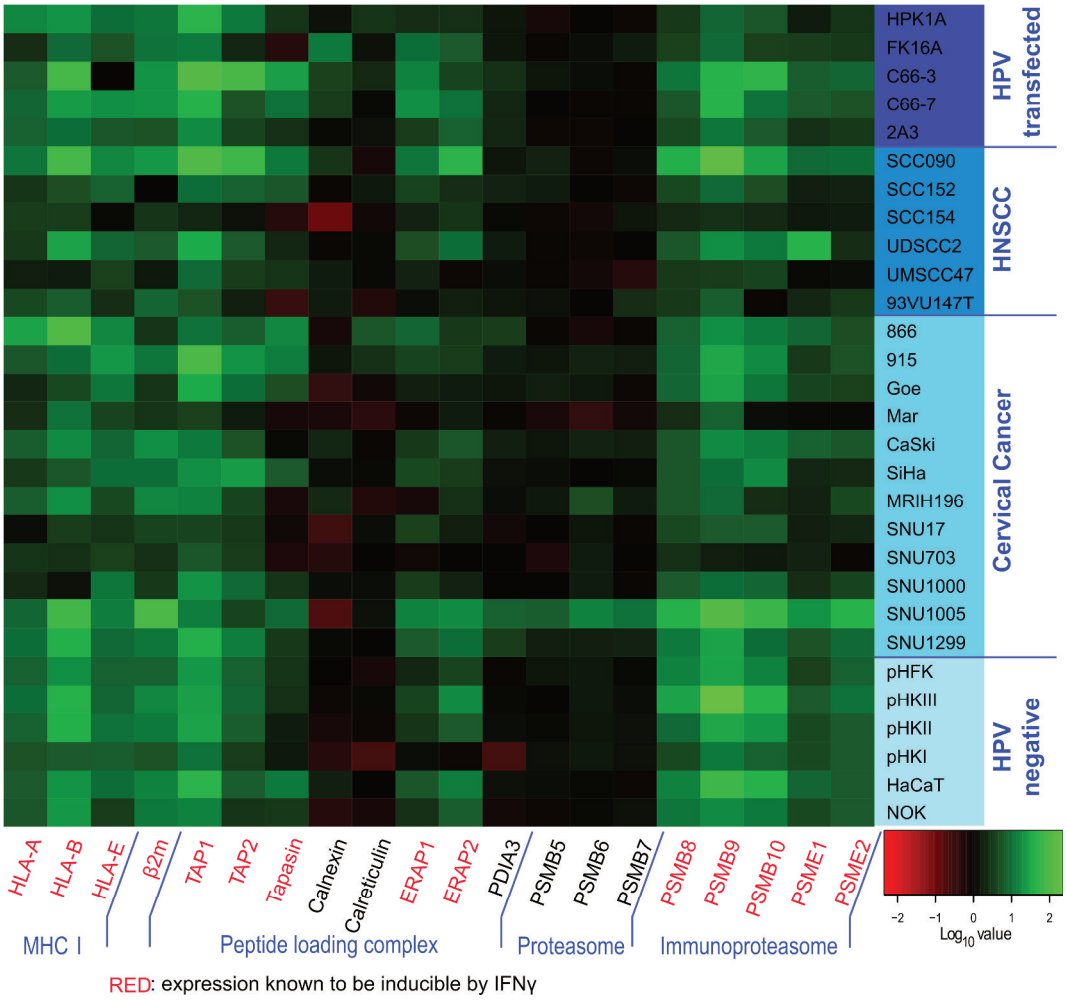

Figure 3.3: Relative expression level change per cell line of indicated APM components after IFNγ treatment. Cells were either treated with IFNγ for 48h or left untreated. Total RNA was purified from cells, reverse transcribed to cDNA and analyzed for APM component expression by qRT-PCR using TaqMan® probes. PCR reactions were run in triplicates. At least two of the following genes were used as internal reference genes: *GAPDH*, *PGK1*, *PPIA* and *IPO8*. Gene expression was calibrated to the respective untreated expression levels. All quantitative qRT-PCR data were processed by LinRegPCR and data management was done by qbasePLUS 2. Log_{10} data were plotted as a heatmap using R. Expression of 20 APM components is shown. Known IFNγ-inducible genes are labeled in red. Each column represents a single gene and each row represents one cell line. Increased expression is shown in green and decreased expression is shown in red (see scale bar in the bottom right corner). HNSCC = head and neck squamous cell carcinoma

Figure 3.4 shows the data obtained from the IFNγ stimulated APM screening in a dot plot diagram. Data was calibrated to the respective untreated level of each cell line. Thus, values below zero indicate a downregulation of a particular gene in a cell line upon IFNγ exposure. Conversely, values above zero indicate an IFNγ-mediated upregulation of a particular gene. Blue dots represent data from HPV-negative cell lines. The mean value of all IFNγ inducible genes, *HLA-A*, *HLA-B*, *HLA-E*, *β2m*, *TAP1*, *TAP2*, *tapasin*, *ERAP1*, *ERAP2*, *PSMB8*, *PSMB9*, *PSMB10*, *PSME1* and *PSME2*, was highly elevated (marked by asterisks in Figure 3.4). This indicated that IFNγ signaling was intact in all our cell lines, supporting observations from the heatmap representation. All cell lines upregulated *HLA-A*, *HLA-B*, *TAP1*, *TAP2*, *PSME8*, *PSME9* and *PSME1* and almost all cell lines upregulated

HLA-E, *β2m*, *tapasin*, *ERAP1*, *ERAP2*, *PSMB10* and *PSME2*. As expected, the mean expression values for the genes *calnexin*, *calreticulin*, *PDIA3*, *PSMB5*, *PSMB6* and *PSMB7* were close to zero.

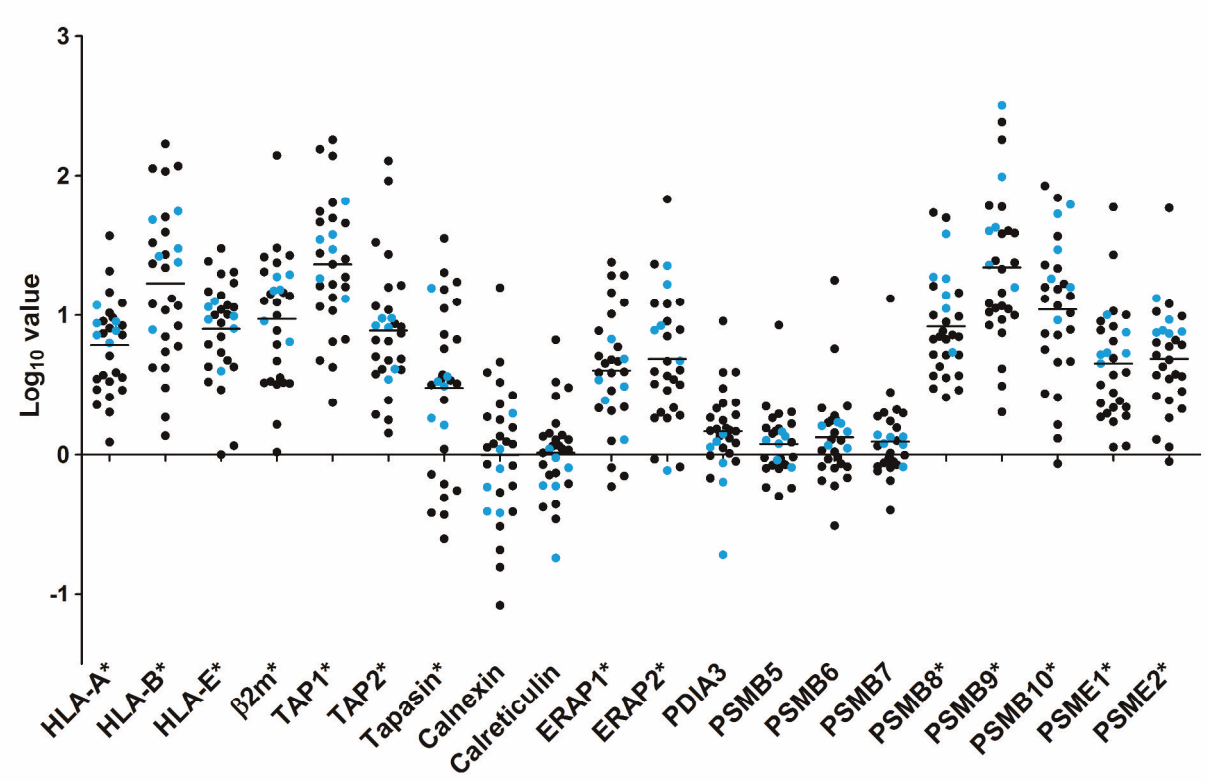

Figure 3.4: Relative expression level change per cell line of indicated APM components after IFNγ treatment. Cells were either treated with IFNγ for 48h or left untreated. Total RNA was purified from cells, reverse transcribed to cDNA and analyzed for APM component expression by qRT-PCR using TaqMan® probes. PCR reactions were run in triplicates. At least two of the following genes were used as internal reference genes: *GAPDH*, *PGK1*, *PPIA* and *IPO8*. Gene expression was calibrated to the respective untreated expression levels. All quantitative qRT-PCR data were processed by LinRegPCR and data management was done by qbasePLUS 2. Log_{10} expression data were plotted for each cell line, additionally mean ± SD of each group are shown. Blue symbols stand for HPV-negative cell lines. Genes marked with an asterisk (*) are known to be inducible by IFNγ.

It seemed that most HPV-negative cell lines reacted with a higher expression of IFNγ-inducible APM components than the mean expression level (Figure 3.3 and blue dots in Figure 3.4). However, these findings can be explained by a lower constitutive expression of these APM components observed in the first qRT-PCR screen (see 3.1.1.1). Constitutive expression levels from the first screen were multiplied with the fold change of IFNγ-induced levels from the second screen resulting in the calculated final levels of APM component expression after IFNγ treatment (Figure 3.5). This mathematical approach demonstrated that final expression levels upon IFNγ treatment were similar between HPV-negative and HPV16-positive cells. Only for *calreticulin* the final expression after IFNγ treatment was significantly elevated in HPV16-positive tumor cells compared to HPV-negative cells (Figure 3.5 A). Taken together, these results revealed that overall expression is not significantly different in response to IFNγ in HPV16-positive tumor cell lines and HPV-negative cell lines.

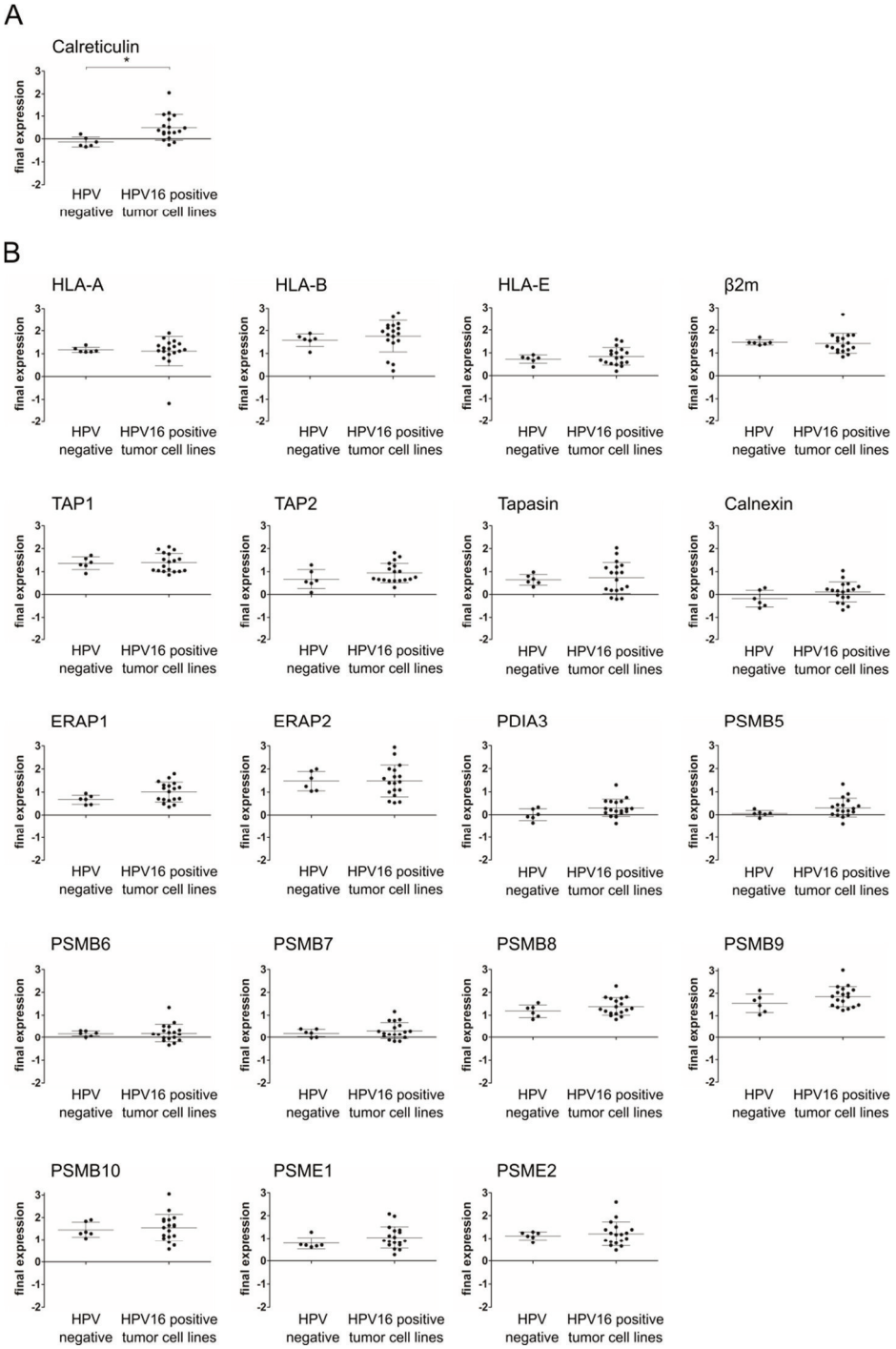

Figure 3.5: Mathematically calculated final expression levels of APM components after IFNγ treatment. Cells were either treated with IFNγ for 48h or left untreated. Total RNA was purified from cells, reverse transcribed to cDNA and analyzed for APM component expression by qRT-PCR using TaqMan® probes. PCR reactions were run in triplicates. At least two of the following genes were used as internal reference genes: *GAPDH*, *PGK1*, *PPIA* and *IPO8*. All quantitative qRT-PCR data were processed by LinRegPCR and data management was done by qbasePLUS 2. Constitutive APM expression levels were calibrated to NOK. IFNγ-induced fold change of APM expression was calculated by calibration to the respective untreated cells. Final gene expression after IFNγ treatment was calculated by multiplying constitutive APM expression with the fold change of IFNγ-induced levels of the respective APM component. Log_{10} expression data were plotted for each cell line, additionally mean ± SD of each group are shown. **A.** APM components that showed a significantly elevated expression in HPV-16 positive tumor cell lines compared to HPV-negative cells. * $p \leq 0.05$ (unpaired t-test) **B.** APM components that showed no significantly different expression in HPV16-positive tumor cell lines compared to HPV-negative cells.

3.1.2 Expression of selected APM components and surface HLA class I on the protein level

The qRT-PCR screen of the APM was conducted in all available cell lines of our collection under normal conditions and upon IFNγ exposure. Based on this broad analysis, cell lines and APM components were selected for protein expression analysis as mRNA data always needs to be confirmed on the protein level. Protein expression was either analyzed by flow cytometry or by Western blot. First, surface HLA class I levels were investigated, followed by components of the immunoproteasome, the peptide loading complex and ER-resident aminopeptidases.

3.1.2.1 Surface HLA class I expression

The qRT-PCR approach had shown that the classical HLA types, *HLA-A* and *HLA-B*, tended to have a higher expression in many HPV16-positive cell lines (see 3.1.1.1). The difference, however, was not statistically significant when HPV-negative cells were compared to cell lines derived from HPV16-positive tumor cells. Nevertheless, knowledge about HLA class I surface expression is important for later experiments with CD8 T cells and immunoprecipitation (IP) of HLA class I/peptide complexes. The qRT-PCR approach only measures mRNA levels of HLA class I, which does not reveal whether these molecules are actually presented on the cell surface. Therefore, the surface expression of HLA class I was determined in 18 HPV16-positive cell lines and compared to the HPV-negative cell lines NOK, HaCat and primary human keratinocytes (pHKs). To this end, cells were stained with an anti-HLA class I antibody and analyzed by flow cytometry (Figure 3.6). 10 out of 18 HPV16-positive cell lines had a higher mean surface HLA class I expression than the HPV16-negative cell line with the highest HLA class I expression (HaCat, Figure 3.6 A and B, dashed lines). The expression was also analyzed after IFNγ treatment (Figure 3.6 B). All cell lines responded to IFNγ by upregulating surface HLA class I. The expression was similar in the analyzed cell lines consistent with observations from the qRT-PCR screen. Only SNU1005 and SNU1299 had much higher expression levels after IFNγ stimulation. The UDSCC2 cell line showed the lowest HLA class I surface expression consistent with the qRT-PCR analysis.

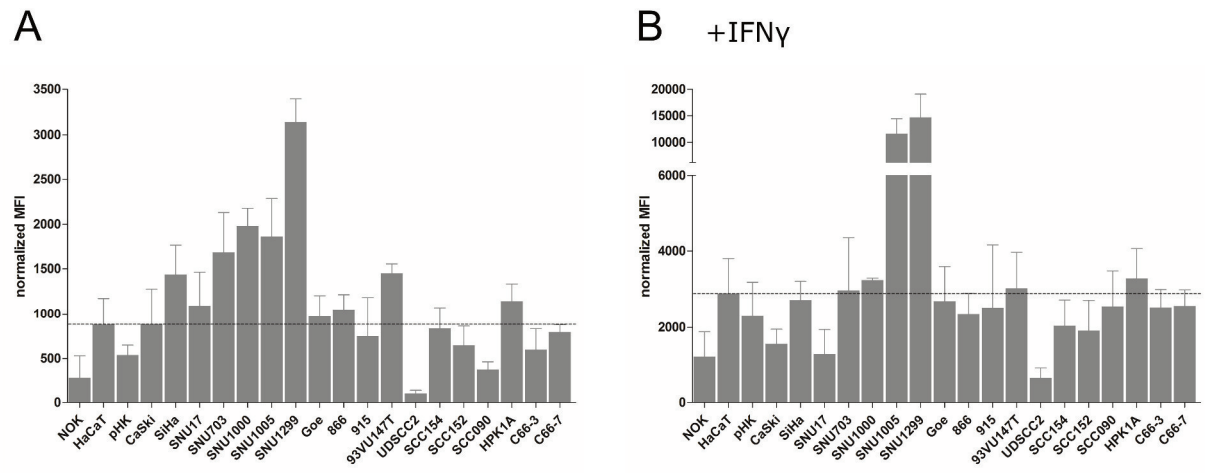

Figure 3.6: Surface HLA class I expression. Cells were left untreated (**A**) or treated with IFNγ for 48h (**B**). Afterwards, cells were harvested and stained with an anti-HLA class I antibody coupled to FITC and the mean fluorescence intensity (MFI) was analyzed by flow cytometry and calculated over the background of each cell line. Results are plotted as means ± SD of at least three independent experiments (except for data from IFNγ treated SNU1000 cells which are derived from two independent experiments). The dashed line marks the highest HLA class I surface expression of a HPV-negative cell line (HaCat).

3.1.2.2 Selected components of the immunoproteasome

The qRT-PCR approach had shown that the immunoproteasome subunits *PSMB9*, *PSMB10*, *PSME1* and *PSME2* were significantly higher expressed in cell lines derived from cervical cancer and HNSCC when compared to HPV-negative cells when no IFNγ was present (see 3.1.1.1). Therefore, their expression was analyzed on the protein level in selected cell lines by Western blot. However, on the protein level no overexpression of these components was observed in HPV16-positive cell lines.

Constitutive PSMB9 protein expression is shown in Figure 3.7 A for the HPV-negative cell lines NOK, HaCat and for pHKs from two different donors compared to 16 HPV16-positive cell lines. Below each Western blot the ratio of optical density (OD) of PSMB9 and the loading control α-tubulin is depicted. On the protein level, no higher expression of PSMB9 could be observed in the majority of HPV16-positive cell lines. Only CaSki and SNU703 expressed PBMS9 at higher levels than the control cell lines. All other cell lines had a similar or a lower PSMB9 expression than NOK, HaCat and pHKs. Figure 3.7 B shows the result of PSMB9 protein expression in an IFNγ-positive milieu. On the protein level, only the SCC152 cell line expressed more PSMB9 than the control cell lines upon IFNγ stimulation, whereas all other cell lines expressed PSMB9 at similar levels as the control cell lines.

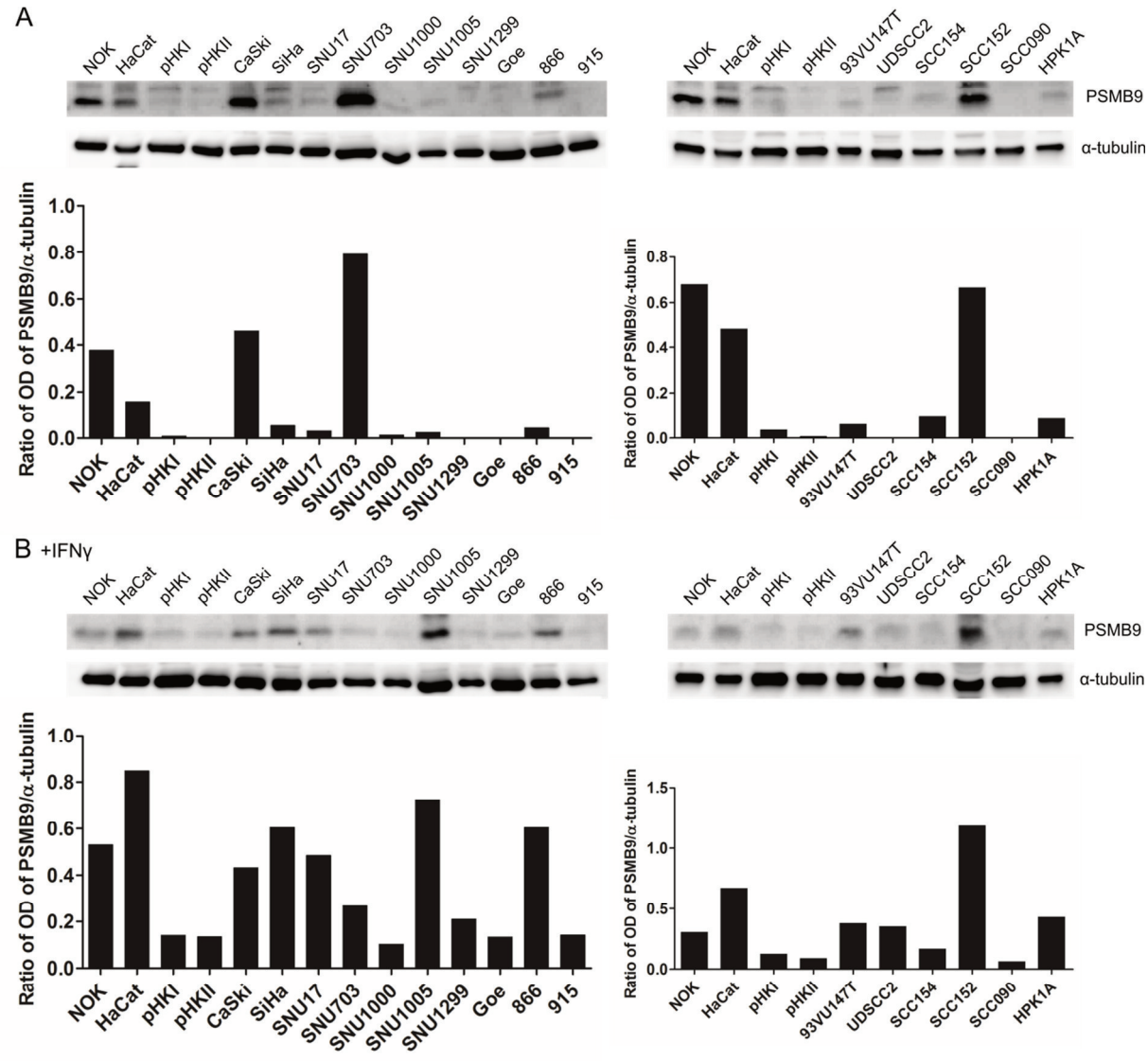

Figure 3.7: PSMB9 protein expression with and without IFNγ treatment. Cells were either left untreated (**A**) or treated with IFNγ (**B**) for 48h. 50µg of each cellular lysate was analyzed for PSMB9 expression by Western blot, with α-tubulin detection as a loading control. Optical density (OD) was quantified using the ImageJ software and PSMB9 expression was normalized to α-tubulin for each cell line, as depicted below the Western blots. Results are representative of two independent experiments.

The same analysis as for PSMB9 was done for PSMB10 (Figure 3.8). Similar to PSMB9, no higher expression of PSMB10 could be observed in the majority of HPV16-positive cell lines. Three HPV16-positive cell lines (CaSki, SNU703 and 866) expressed PBMS10 at higher levels than the control cell lines. All other cell lines had a similar or a lower PSMB10 expression. Figure 3.8 B shows the result of PSMB10 protein expression upon IFNγ treatment. On the protein level, only 93VU147T and SCC152 expressed higher levels of PSMB10 than the control cell lines upon IFNγ stimulation, whereas all other cell lines expressed similar levels as the control cell lines.

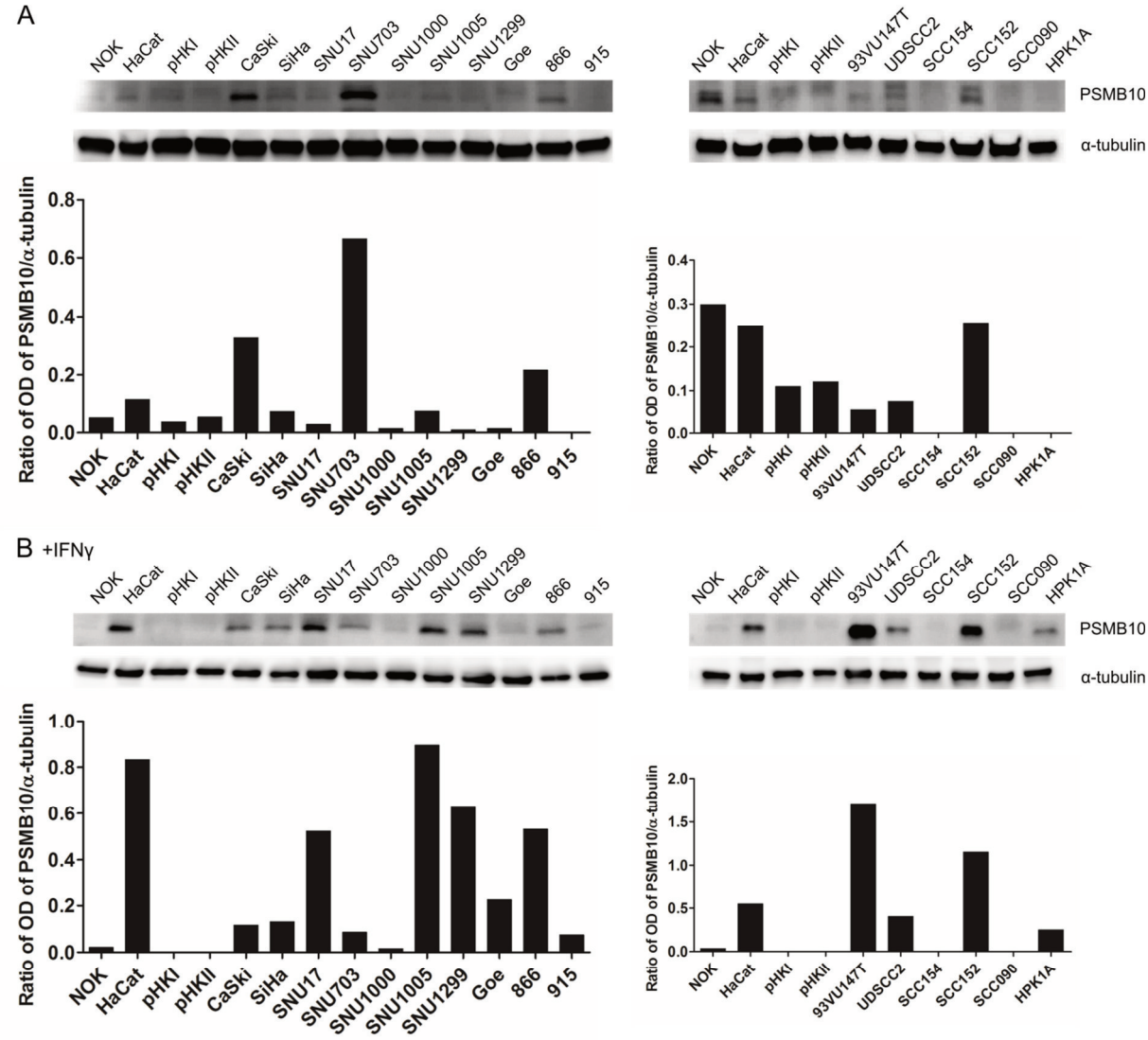

Figure 3.8: PSMB10 protein expression with and without IFNγ treatment. Cells were either left untreated (**A**) or treated with IFNγ (**B**) for 48h. 50µg of each cellular lysate was analyzed for PSMB10 expression by Western blot as in Figure 3.7. Optical density (OD) was quantified using the ImageJ software and PSMB10 expression was normalized to α-tubulin for each cell line, as depicted below the Western blots. Results are representative of two independent experiments.

Figure 3.9 illustrates constitutive PSME1 protein expression in HPV-negative cell lines (NOK, HaCat and pHKs from two different donors) compared to 16 HPV16-positive cell lines. On the protein level, no higher expression of PSME1 could be observed in the majority of HPV16-positive cell lines. Three HPV16-positive cell lines (SNU703, SNU1005 and SCC152) expressed PSME1 at slightly higher levels and SiHa at higher levels than control cell lines. All other cell lines had a similar or a lower PSME1 expression.

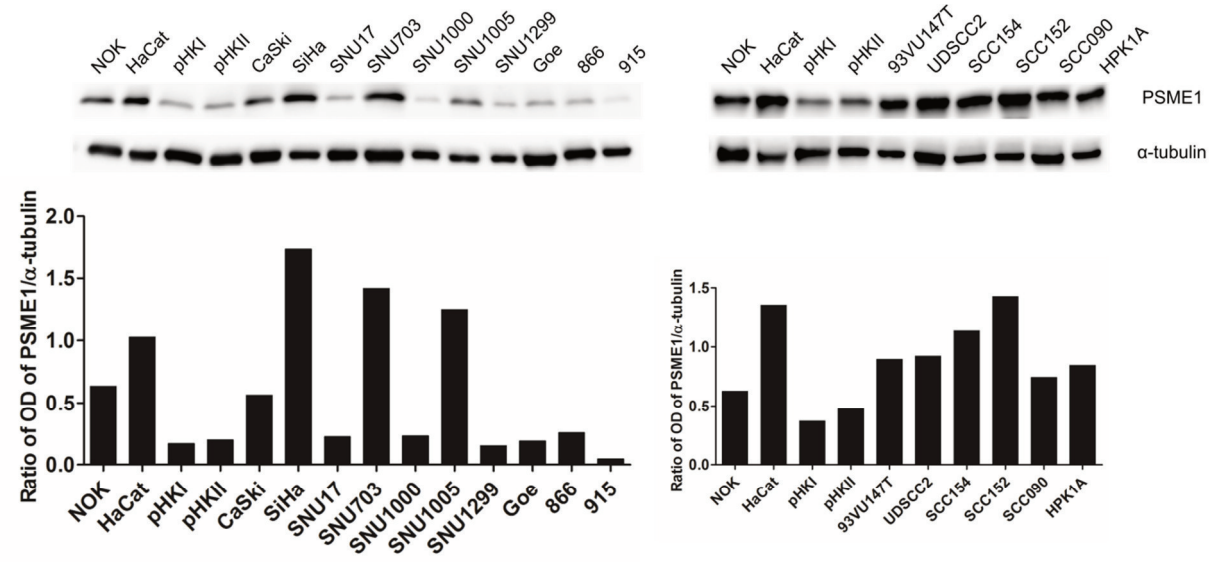

Figure 3.9: PSME1 protein expression. 50µg of each cellular lysate was analyzed for PSME1 expression by Western blot as in Figure 3.7. Optical density (OD) was quantified using the ImageJ software and PSME1 expression was normalized to α-tubulin for each cell line, as depicted below the Western blots. Results are representative of two independent experiments.

Constitutive PSME2 protein expression was analyzed as it was done for PSME1 (Figure 3.10). Again no higher expression of PSME2 could be observed in the majority of HPV16-positive cell lines. 6 out of 16 tested HPV16-positive cell lines (SiHa, SNU703, SNU1005, 93VU147T, SCC152 and HPK1A) expressed PSME2 at higher levels and SCC154 expressed slightly higher levels than the control cell lines. All other cell lines had a similar or a lower PSME2 expression.

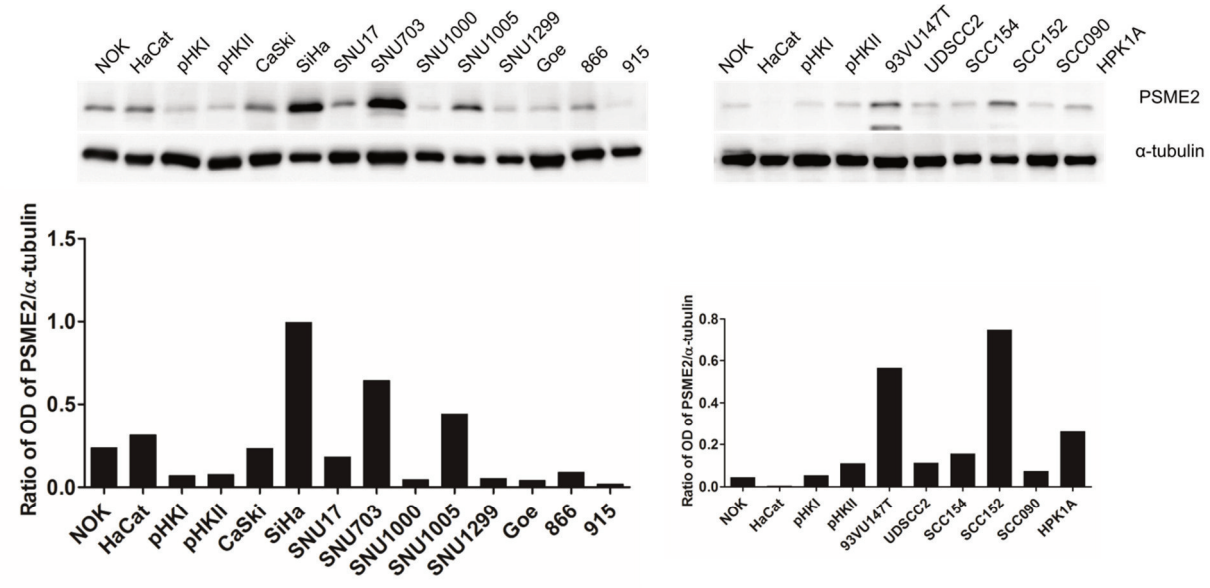

Figure 3.10: PSME2 protein expression. 50µg of each cellular lysate was analyzed for PSME2 expression by Western blot as in Figure 3.7. Optical density (OD) was quantified using the ImageJ software and PSME2 expression was normalized to α-tubulin for each cell line, as depicted below the Western blots. Results are representative of two independent experiments.

3.1.2.3 Selected components of the peptide loading complex (PLC)

A set of HPV16-positive cell lines expressed the PLC component tapasin at higher mRNA levels than control cell lines without IFNγ treatment, but the difference was not significant (see 3.1.1.1). Nevertheless, tapasin expression was investigated on the protein level because it was shown by Kanaseki and colleagues (219) that tapasin is directly involved in editing the peptide repertoire. Of note, the qRT-PCR approach had shown that the PLC component calreticulin was significantly higher expressed in cell lines derived from cervical cancer and HNSCC when compared to HPV-negative cells. For these reasons, calreticulin and tapasin were analyzed on the protein level in selected cell lines by Western blot. As for the immunoproteasome subunits, no higher expression of these PLC components was observed on the protein level (Figure 3.11 and 3.12)

Tapasin protein expression in the HPV-negative cell lines NOK, HaCat and pHKs from two different donors compared to 16 HPV16-positive cell lines is shown in Figure 3.11. Only SCC152 expressed tapasin at higher levels than the control cell lines. All other cell lines had a similar or a lower tapasin expression.

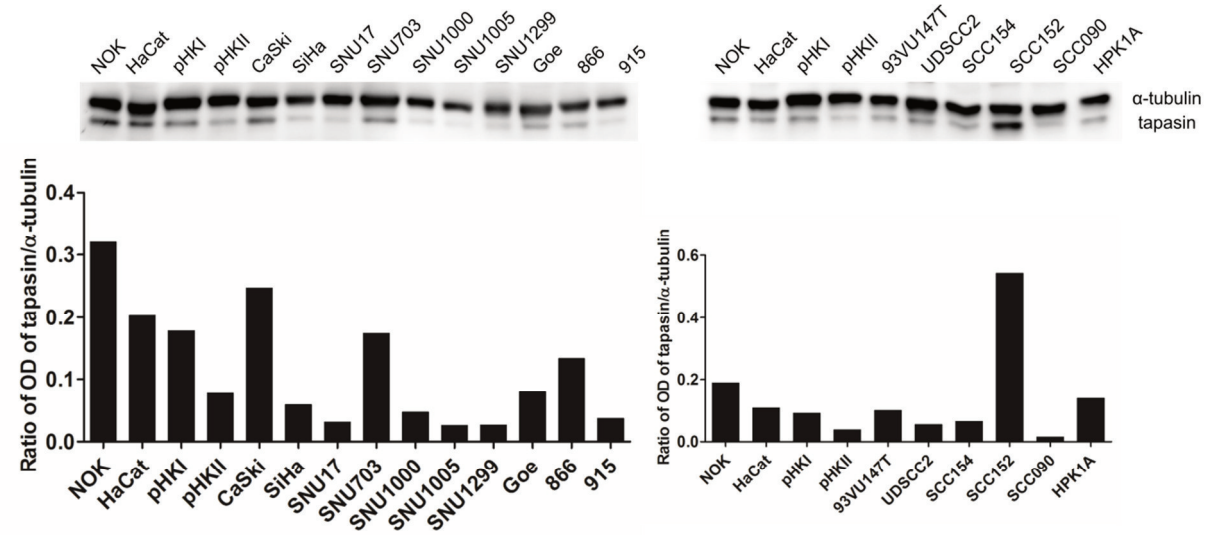

Figure 3.11: Tapasin protein expression. 50µg of each cellular lysate was analyzed for tapasin expression by Western blot as in Figure 3.7. Optical density (OD) was quantified using the ImageJ software and tapasin expression was normalized to α-tubulin for each cell line, as depicted below the Western blots. Results are representative of two independent experiments.

Figure 3.12 shows the result of constitutive calreticulin protein expression in the same cell lines as before. Below each Western blot the ratio of OD from calreticulin and the loading control α-tubulin is depicted. One HPV16-positive cell line (SCC152) expressed calreticulin at higher levels than the control cell lines. All other cell lines had a similar or a lower calreticulin expression.

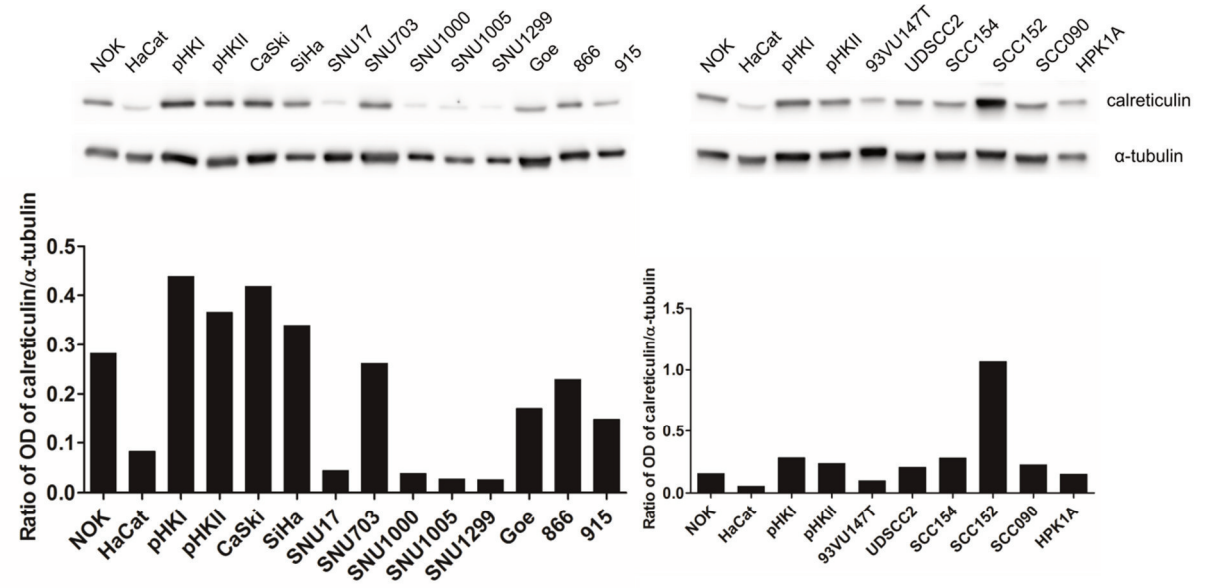

Figure 3.12: Calreticulin protein expression. 50µg of each cellular lysate was analyzed for calreticulin expression by Western blot as in Figure 3.7. Optical density (OD) was quantified using the ImageJ software and calreticulin expression was normalized to α-tubulin for each cell line, as depicted below the Western blots. Results are representative of two independent experiments.

3.1.2.4 Endoplasmic reticulum aminopeptidase 1 (ERAP1) and 2 (ERAP2)

The qRT-PCR approach had also shown that ERAP1 was significantly higher expressed in HPV16-positive tumor cell lines than in HPV-negative cells (see 3.1.1.1). In humans, a second aminopeptidase, ERAP2, is expressed, which most probably developed from a gene duplication event (59). Furthermore, it was suggested that ERAP1 and ERAP2 could work in concert (60). Thus, the expression of both aminopeptidases was analyzed by Western blot in selected cell lines.

The result of constitutive ERAP1 protein expression in the same cell lines as before is depicted in Figure 3.13 A. The experiments revealed that ERAP1 was higher expressed in the majority (13/16) of HPV16-positive cell lines in comparison to the HPV-negative cell lines (Figure 3. A). In Figure 3.13 C, pooled data of three independent experiments is shown. Here, all tested HPV16-positive cell lines had a higher mean ERAP1 expression than HPV16-negative cells. After IFNγ-treatment, only 6 out of 16 HPV16-positive cell lines had a higher ERAP1 expression than the HPV-negative cells (Figure 3.13 B). Lower ERAP1 levels were observed in 4 out of 16 HPV16-positive cell lines and the others had similar levels as the control cells. In pooled data of three independent experiments, mean ERAP1 expression upon IFNγ treatment was still elevated (Figure 3.13 D) in all HPV16-positive cell lines except for SCC152.

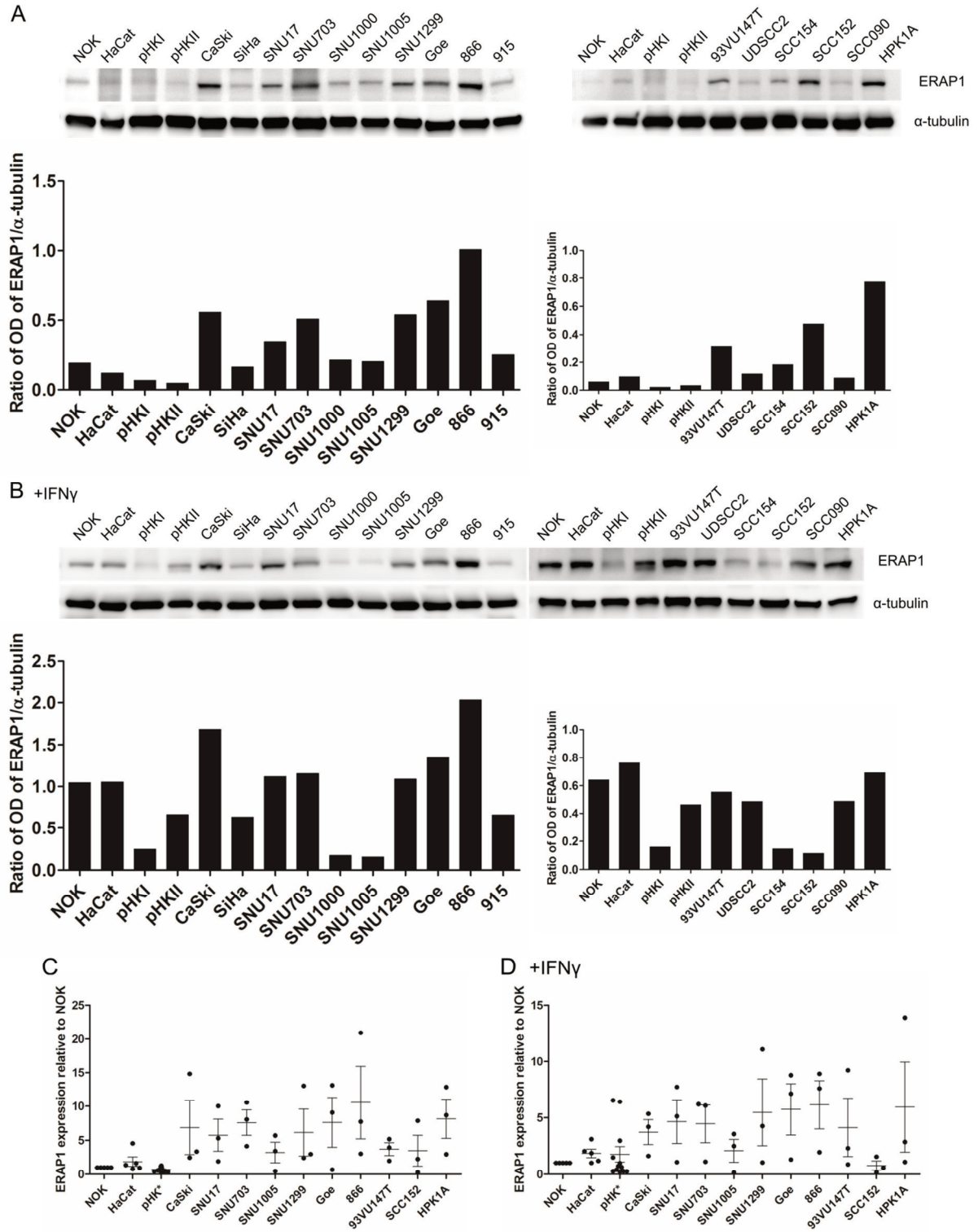

Figure 3.13: ERAP1 protein expression with and without IFNγ treatment. Cells were either left untreated (**A**) or treated with IFNγ (**B**) for 48h. 50µg of each cellular lysate was analyzed for ERAP1 expression by Western blot as in Figure 3.7. Optical density (OD) was quantified using the ImageJ software and ERAP1 expression was normalized to α-tubulin for each cell line, as depicted below the Western blots. Results are representative of three independent experiments. **C.** and **D.** represent pooled data from these three independent experiments. ERAP1 expression of untreated (**C**) and IFNγ treated cells (**D**) was calculated relative to NOK. Results are plotted as means ± SEM. pHK* = pooled data from primary human keratinocytes derived from three donors and pooled primary human foreskin keratinocytes from multiple donors.

Constitutive ERAP2 protein expression in the selected HPV-negative and HPV16-positive cell lines is shown in Figure 3.14 A. The experiments revealed that ERAP2 was very variable with either a low or a high expression, which is also shown in pooled data from three independent experiments (Figure 3.14 B). A higher mean ERAP2 expression than the HPV-negative cells was seen in 5 out of 16 HPV16-positive cell lines (SNU703, SNU1005, 866, 93VU147T and HPK1A). Interestingly, these cell lines also overexpressed ERAP1 as described above. However, it has to be noted that also some pHKs expressed ERAP2 at high levels.

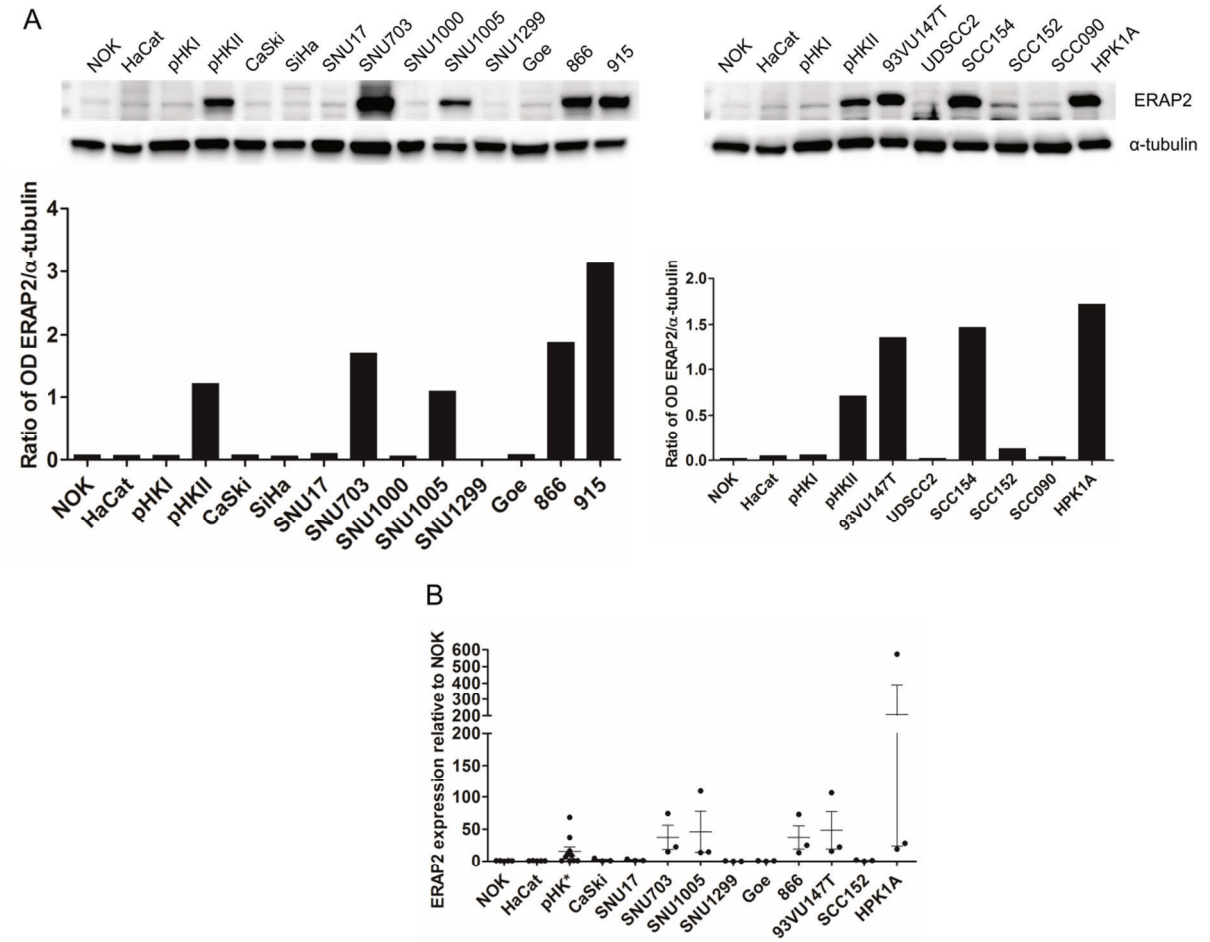

Figure 3.14: ERAP2 protein expression. A. 50µg of each cellular lysate was analyzed for ERAP2 expression by Western blot as in Figure 3.7. Optical density (OD) was quantified using the ImageJ software and ERAP2 expression was normalized to α-tubulin for each cell line, as depicted below the Western blots. Results are representative of three independent experiments. **B.** Pooled data from these three independent experiments. ERAP2 expression was calculated relative to NOK. Results are plotted as means ± SEM. pHK* = pooled data from primary human keratinocytes derived from three donors and pooled primary human foreskin keratinocytes from multiple donors.

In conclusion, protein expression analysis of the analyzed APM components revealed that only ERAP1 was expressed at higher levels in the majority of tested HPV16-positive cell lines compared to HPV-negative cell lines. ERAP1 has the ability to directly edit the MHC I epitope repertoire (86). Therefore, we decided to focus all subsequent experiments on ERAP1.

3.1.3 Immunohistochemistry of ERAP1 in cervical tissue

ERAP1 was shown to be overexpressed *in vitro* in HPV16-positive cell lines on the mRNA as well as on the protein level (see 3.1.1.1 and 3.1.2.4). Thus, we next investigated whether this also holds true in human dysplastic cervical tissue sections. The anti-ERAP1 antibody was first validated for immunohistochemistry. Afterwards, immunohistochemistry of ERAP1 in all three grades of cervical intraepithelial neoplasia (CIN) and cervical cancer was performed. ERAP1 expression in dysplastic tissue was compared to its expression in histologically normal cervical epithelium.

3.1.3.1 Validation of the anti-ERAP1 antibody

In order to perform immunohistochemistry of ERAP1 in cervical tissue sections, the anti-ERAP1 antibody used in this study had to be validated for this application first. CaSki cells were either left untreated or were transfected with a non-targeting siRNA control pool or an *ERAP1*-targeting siRNA pool. The siRNA-mediated knockdown of *ERAP1* is described in detail in chapter 3.3.1. After 72h of transfection, CaSki cells were harvested, fixed and a thin layer of the cells was prepared on cytology slides. The cells were analyzed for ERAP1 expression following the immunohistochemistry staining protocol described in section 2.2.6. Figure 3.15 shows the validation results of the anti-ERAP1 antibody in CaSki cells. ERAP1 was readily detectable in cells that were not transfected and cells that were transfected with the siRNA control pool. In contrast, ERAP1 signals in cells with siRNA-mediated *ERAP1* knockdown were clearly lower. The results confirm that the antibody is specific for ERAP1 and is suitable to evaluate different ERAP1 expression levels in immunohistochemistry.

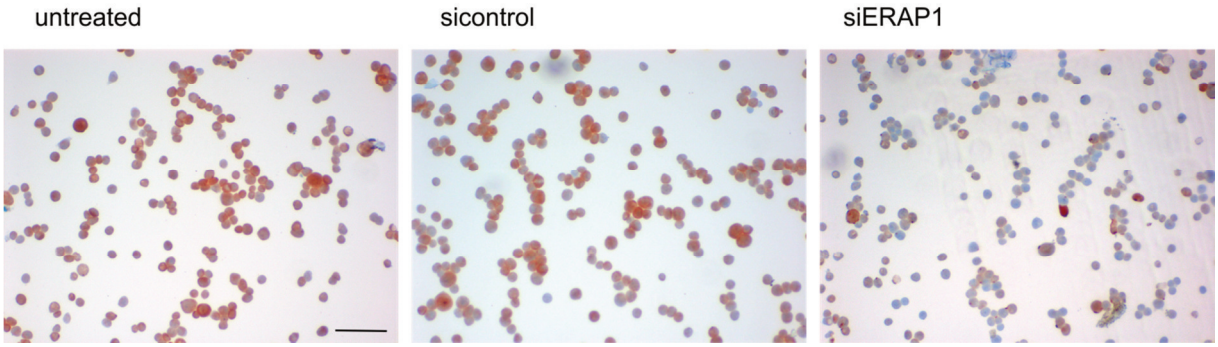

Figure 3.15: Validation of the anti-ERAP1 antibody for immunohistochemistry. CaSki cells were left untreated or were transfected with either a non-targeting RNA (sicontrol) or an *ERAP1*-targeting siRNA (siERAP1). After 72h, cells were harvested and fixed. A thin layer of cells was prepared on cytology slides and cells were stained for ERAP1. Scale bar corresponds to 100µm.

3.1.3.2 Expression of ERAP1 in cervical tissue

Immunohistochemical analysis of ERAP1 was performed in human cervical tissue sections and expression in dysplastic tissue was compared to histologically normal cervical epithelium. Different degrees of cervical intraepithelial neoplasias (CIN): CIN I (n = 9), CIN II (n = 6), CIN III (n = 9), and squamous cell carcinomas (SCC, n = 6) were analyzed and compared to normal cervical epithelium (n = 23). As a surrogate marker for HPV oncogene expression p16 was used (118). p16-negative normal

cervical epithelium showed very weak ERAP1 protein expression (Figure 3.16). On the contrary, epithelial ERAP1 expression was clearly increased in dysplastic CIN I to III lesions and in established cervical cancers. Notably, ERAP1 expression increased with disease progression since the expression in CIN I was much lower than in advanced degrees of CIN and in SCC.

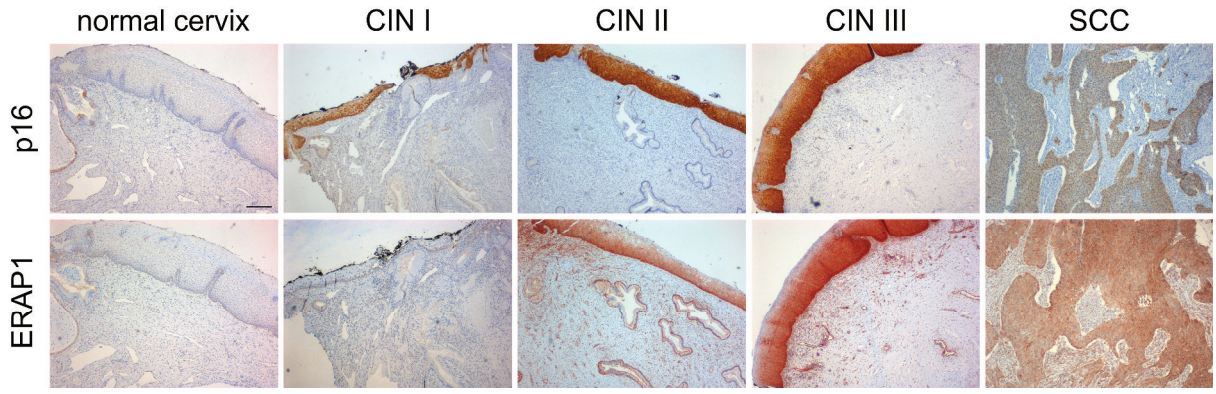

Figure 3.16: Immunohistochemical analysis of ERAP1 expression in cervical tissue. Human tissue sections were stained for ERAP1 and p16, a surrogate marker for HPV oncogene expression. The protein expression was analyzed in histologically normal cervical epithelium (normal cervix), in HPV16-positive dysplastic CIN (cervical intraepithelial neoplasia) I to CIN III lesions and in SCC (cervical squamous cell carcinoma). Scale bar corresponds to 200µm.

A CIN III lesion directly adjacent to p16-negative normal cervical epithelium is shown in Figure 3.17. The drastic difference in ERAP1 expression between CIN III (highly elevated expression) and histologically normal tissue (weak expression) can be directly compared.

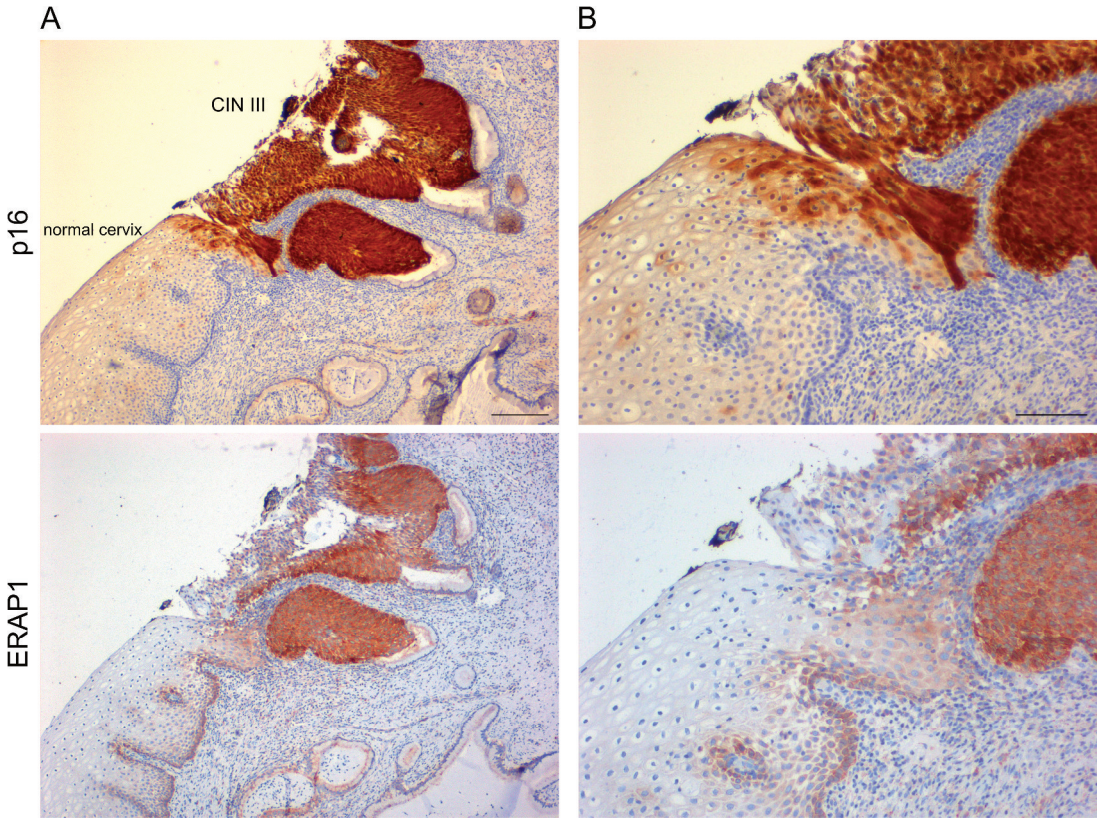

Figure 3.17: Immunohistochemical analysis of ERAP1 expression in normal cervical epithelium and CIN III. Human tissue sections were stained for ERAP1 and p16, a surrogate marker for HPV oncogene expression. The expression was analyzed in histologically normal cervical epithelium adjacent to a HPV16-positive CIN (cervical intraepithelial neoplasia) III lesion. **A.** Scale bar corresponds to 200µm. **B.** Higher magnification of the sections shown in **A**. Scale bar corresponds to 100µm.

In order to quantitatively assess ERAP1 expression, a score was applied that considered both the percentage of ERAP1 expressing cells and the intensity of ERAP1 staining. Analysis of this histological score showed that epithelial ERAP1 levels were significantly increased in CIN and SCC when compared to normal epithelium (Figure 3.18 A and B). In addition, ERAP1 expression significantly increased with disease progression, being highest in SCC and lowest in CIN I. Three CIN I tissue sections showed similar ERAP1 expression levels as normal tissue. However, all analyzed CIN II, CIN III and SCC tissue sections had elevated ERAP1 expression levels. For most of the sections, HPV genotyping information was available. HPV16-positive tissue sections are highlighted in blue in Figure 3.18 A. Notably, HPV16-positive sections did not behave differently than other high-risk HPV-positive sections regarding ERAP1 expression. In Figure 3.18 B, an alternative way of representing ERAP1 expression is shown. Histological scores were equally categorized into low (0-95), intermediate (96-190) and high expression (191-285). This analysis nicely demonstrated that ERAP1 expression increased with disease progression, consistent with the other representation of this data set. Furthermore, this way of presentation revealed that histologically normal tissue expressed ERAP1 only at low levels as well as 67% of CIN I lesions. The percentage of tissue sections that expressed ERAP1 at high levels was rising from CIN II to SCC. In Figure 3.18 C, the HPV type information is summarized. All detected HPV types (HPV16, 18, 31, 33, 52, 56, 59 and 73) are high-risk types (220). HPV16 was the most prevalent high-risk type in the analyzed tissue sections, which is consistent with the general worldwide type distribution (101). One tissue section of CIN I was typed positive for both HPV31 and HPV56, and one cervical cancer section was positive for both HPV16 and HPV52.

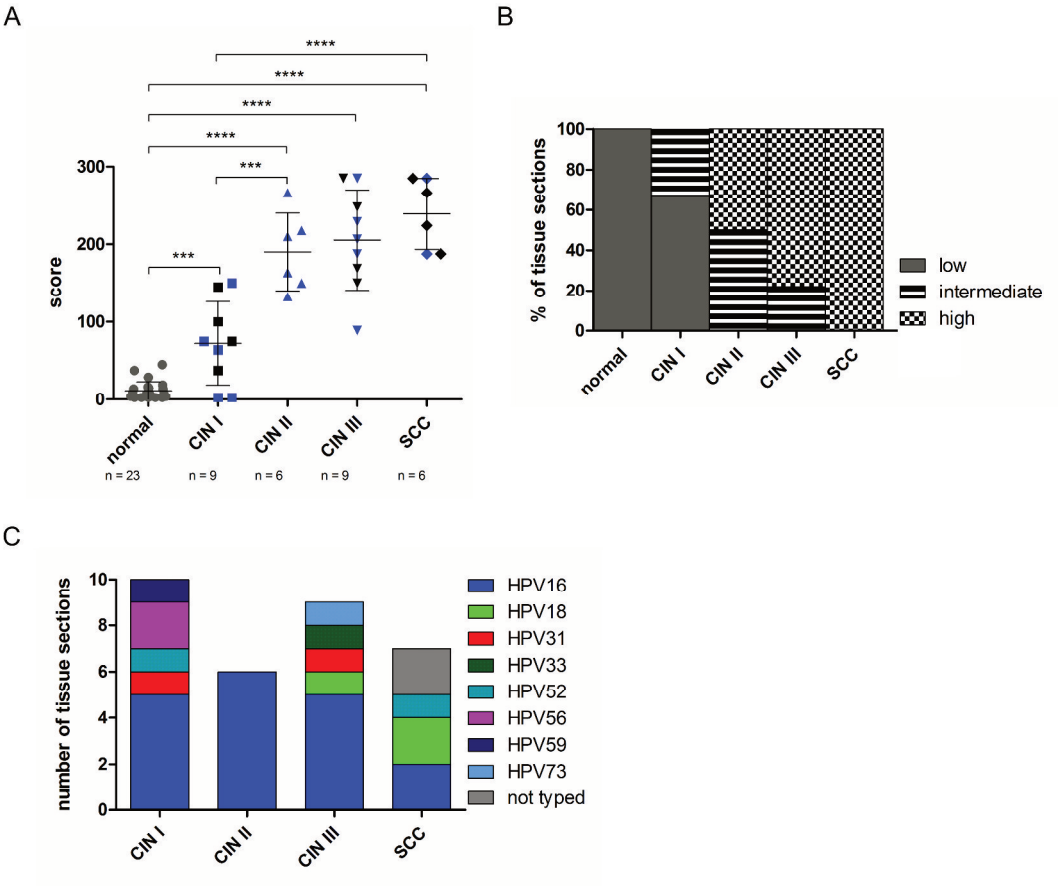

Figure 3.18: ERAP1 protein expression in cervical tissue. Human tissue sections were analyzed for ERAP1 expression by immunohistochemistry. The expression was analyzed in histologically normal cervical epithelium, in dysplastic cervical intraepithelial neoplasia (CIN) I to CIN III and in cervical squamous cell carcinoma (SCC). Normal tissue n = 23, CIN I n = 9, CIN II n = 6, CIN III n = 9 and SCC n = 6. **A.** Immunohistochemical scores were determined by multiplying the frequency of ERAP1 expressing cells with the maximum intensity of ERAP1 expression. Each symbol represents one sample, symbols in blue represent HPV16-transformed tissue. Means ± SD are also given. *** $p \leq 0.001$, **** $p \leq 0.0001$ (unpaired t test). **B.** Immunohistological scores were equally categorized into low (0-95), intermediate (96-190) and high expression (191-285). **C.** HPV type information of the analyzed human tissue sections. Note that one section within the CIN I and one section within the SCC group were transformed with two HPV types.

In conclusion, immunohistochemical analysis of ERAP1 protein expression showed that ERAP1 is clearly overexpressed in HPV-positive CIN II-III and SCC compared to p16-negative normal cervical tissue. These results are consistent with the data from cell lines described in the previous chapters (see 3.1.1.1 and 3.1.2.4).

3.2 Exploration of possible mechanisms leading to ERAP1 upregulation

3.2.1 Analysis of single nucleotide polymorphisms (SNPs) of *ERAP1* in selected cell lines

In recent years, it has become clear that *ERAP1* is a polymorphic gene with many naturally occurring haplotypes in the human population (203). Single nucleotide polymorphisms (SNPs) are under extensive research because some are associated with human diseases (73, 74, 82), can affect enzymatic properties (73) and also the expression level of ERAP1 (221). For all these reasons, we investigated the haplotypes present in our cell lines. The approach was the following: isolation of total RNA, reverse transcription into cDNA, amplification of *ERAP1* by PCR and SNP analysis by sequencing at GATC Biotech. As a reference sequence, the commonly accepted most frequent haplotype of *ERAP1* in the human population (NM 001198541.1) according to Reeves and colleagues (203) was used. At least 5 primers were used for sequencing, so that sequencing results overlapped, thus ensuring the reliability of the sequences. The positions of the employed primers in *ERAP1* are depicted in Figure 7.6 in the appendix. For sequence alignments and SNP identification, SnapGene®, GENtle and Chromas were used. SNPs were determined in the HPV-negative cell line NOK and in 6 HPV16-positive cell lines. CaSki, 866, SNU17 and SNU703 were analyzed because they showed elevated ERAP1 levels compared to HPV-negative cell lines (see 3.1.2.4). SiHa and FK16A were included in this analysis because they were later used as target cells in cytotoxicity assays (see 3.5.2.2). Table 3.1 shows the identified SNPs of *ERAP1* in all tested cell lines compared to the reference sequence. The SNPs within *ERAP1* that were found in the tested cell lines were already described as naturally occurring SNPs indicated by the respective NCBI (National Center for Biotechnology Information) SNP ID in the table. CaSki, SNU17 and SiHa were homozygous for the most common haplotype of *ERAP1*, whereas NOK, 866, SNU703 and FK16A harbored differing *ERAP1* haplotypes. The analysis revealed that the SNPs detected in our cell lines did not cause ERAP1 overexpression.

Table 3.1: Single nucleotide polymorphisms (SNPs) determined in one HPV-negative cell line (NOK) and HPV16-positive cell lines (CaSki, 866, SNU17, SNU703, SiHa and FK16A). Total RNA was purified from cell lines and reverse transcribed into cDNA. *ERAP1* was amplified from cDNA by PCR and analyzed by sequencing. The reference sequence (NM 001198541.1) is the most common haplotype of *ERAP1* in the human population (203). Bases are given for the sense strand. Cell lines highlighted in blue are homozygous for the reference haplotype of *ERAP1*. Deviations from the reference haplotype are highlighted in red. AA = amino acid

		NOK		CaSki		866		SNU17		SNU703		SiHa		FK16A	
SNP ID	**Polymorphism**	**Base**	**AA**	**Base**	**AA**	**Base**	**AA**	**Base**	**AA**	**Base**	**AA**	**Base**	**AA**	**Base**	**AA**
rs72773968	T12I	C	T	C	T	C	T	C	T	C	T	C	T	T	I
rs26653	R127P	G/C	R/P	G	R	G	R	G	R	G/C	R/P	G	R	G/C	R/P
rs26618	I276M	A	I	A	I	A/G	I/M	A	I	A/G	I/M	A	I	A	I
rs2287987	M349V	A/G	M/V	A	M	A	M	A	M	A	M	A	M	A	M
rs30187	K528R	A/G	K/R	A	K	A/G	K/R	A	K	A/G	K/R	A	K	A	K
rs17482078	R725Q	G/A	R/Q	G	R	G	R	G	R	G	R	G	R	G	R
rs27044	Q730E	C/G	Q/E	C	Q	G	E	C	Q	C/G	Q/E	C	Q	C	Q

3.2.2 The effect of HPV16 *E6* and *E7* knockdown on ERAP1 expression

The HPV oncogenes E6 and E7 have multiple targets within the host cell and can manipulate growth behavior and promote immune evasion (see 1.2.2). E6 and E7 have also been reported to perturb expression of the APM components PSMB8, PSMB9, TAP1 and MHC I. Thus, we next addressed the question whether E6 and E7 also have an impact on ERAP1 expression. To answer this question, *E6* and *E7* were silenced using a siRNA pool targeting all three HPV16 *E6/E7* transcript classes and a non-targeting control siRNA (209). CaSki cells were transfected for 72h and subsequently cell lysates were analyzed using Western blot. Figure 3.18 A shows the Western blot that confirms the knockdown of HPV16 *E7*. Knockdown of *E7* ensures that *E6* is silenced too because the transcript of *E7* is generated from the *E6* transcript by alternative splicing (222). Figure 3.19 B shows the expression of ERAP1 after HPV16 *E6* and *E7* knockdown and in C the quantification these experiments. The experiments revealed that silencing the HPV16 oncogenes *E6* and *E7* had no impact on ERAP1 expression. Thus, the observed ERAP1 overexpression is likely caused either by other viral proteins or by other mechanisms.

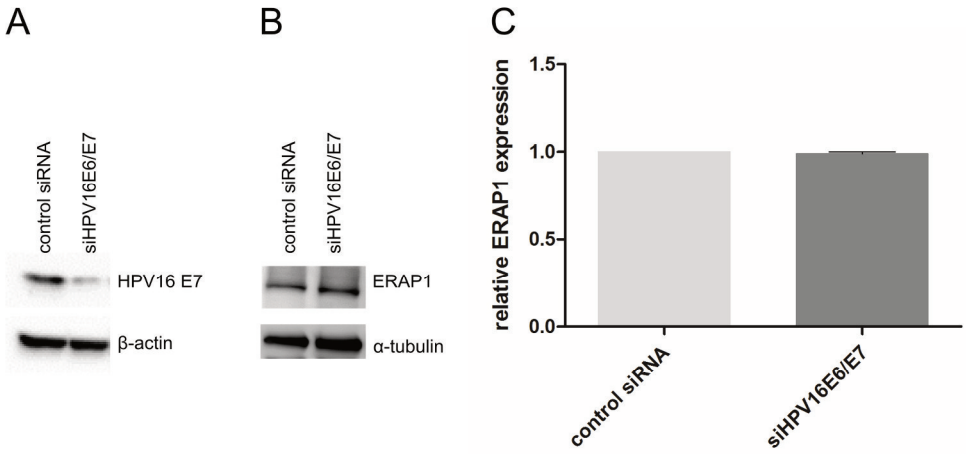

Figure 3.19: ERAP1 expression after HPV16 *E6*/*E7* knockdown. CaSki cells were treated either with a HPV16 *E6/E7*-targeting (siHPV16E6/E7) or a non-targeting control siRNA for 72h. 50µg of each cellular lysate was loaded and analyzed for E7 or ERAP1 expression by Western blot. **A.** Western blot analysis of HPV16 E7 and β-actin detection as a loading control. The result is representative of two independent experiments. **B.** Western blot analysis of ERAP1 and α-tubulin antibody as a loading control. The result is representative of two independent experiments. **C.** Quantification using the ImageJ software. ERAP1 protein expression was normalized to α-tubulin expression and then calculated relative to CaSki cells treated with control siRNA. The results are plotted as means ± SD from two independent experiments.

3.3 Analysis of ERAP1 upregulation on HPV16 epitope presentation

ERAP1 is of high interest in immunotherapeutic approaches since it can directly shape the epitope repertoire (64, 67). Interestingly, ERAP1 generates or destroys epitopes (64) depending on the cell type, HLA type, the particular antigen and on *ERAP1* alleles. Of note, attenuation of *ERAP1* expression has been shown to improve CD8 T cell-mediated anti-tumor immunity in different models (83, 84). The expression of ERAP1 is elevated in many different human tumors (77, 78) and there have been approaches to inhibit ERAP1 function by specific synthetic inhibitors (86). This study revealed that ERAP1 is overexpressed in HPV-induced malignancies (see 3.1.1.1, 3.1.2.4 and 3.1.3). Thus, we decided to focus the subsequent experiments on the investigation whether ERAP1 expression levels influence HPV16 epitope presentation. We addressed this question by using direct detection of HPV16-derived epitopes by mass spectrometry and cytotoxicity mediated by HPV16-specific CD8 T cells. To elucidate ERAP1 attenuation, a siRNA-mediated approach to knockdown *ERAP1* expression was established. First, this tool was used in context with immunoprecipitations of HLA-A2:peptide complexes to compare the presentation of selected HPV16-derived HLA-A2-restricted epitopes with and without *ERAP1* knockdown. Second, the influence of *ERAP1* knockdown in HPV16-positive target cells on cytotoxicity mediated by CD8 T cells specific for HPV16 E6 and E7 peptides was investigated.

3.3.1 Normalization of ERAP1 expression

A siRNA-mediated knockdown of *ERAP1* was established to normalize overexpressed ERAP1 levels back to a level expressed in HPV-negative keratinocytes. The influence of ERAP1 attenuation on surface HLA class I expression was investigated as well. CaSki, 866, SNU17 and SNU703 were chosen for these experiments. These cell lines were selected because on the one hand they overexpressed ERAP1 and on the other hand they are HLA-A2-positive which is one of the most frequent HLA types (223). This consideration was important for later experiments with T cells and immunoprecipitations. In addition, the HLA-A24-positive cell lines FK16A and SiHa were used, because a HLA-A24-positive donor was available whose PBMCs were used for HPV16-specific long-term T cell generation in our lab (194).

3.3.1.1 Establishment of *ERAP1* knockdown using siRNA pools

In order to normalize ERAP1 expression, a siRNA pool from siTOOLs Biotech was used. The siRNA pool consisted of 30 specific siRNAs. This allowed using very low concentrations of siRNA compared to single siRNA approaches leading to lower off-target effects. The optimal concentration of the *ERAP1*-specific siRNA pool was established in the four HLA-A2-positive cell lines and in the two HLA-A24-positive cell lines mentioned above. The knockdown was set up with the intention to be

stable for at least 72h, providing a time window broad enough for subsequent read-out assays.

Figure 3.20 A illustrates the knockdown of *ERAP1* after 72h in CaSki, 866, SNU17 and SNU703 using qRT-PCR. The residual *ERAP1* transcript expression was below 15% in all cell lines compared to cells treated with the non-targeting siRNA control pool. Figure 3.20 B shows ERAP1 expression after 72h of *ERAP1* knockdown assessed by Western blot. Residual ERAP1 expression was below 20% in all cell lines when compared to the cells treated with the siRNA control pool (quantification data not shown).

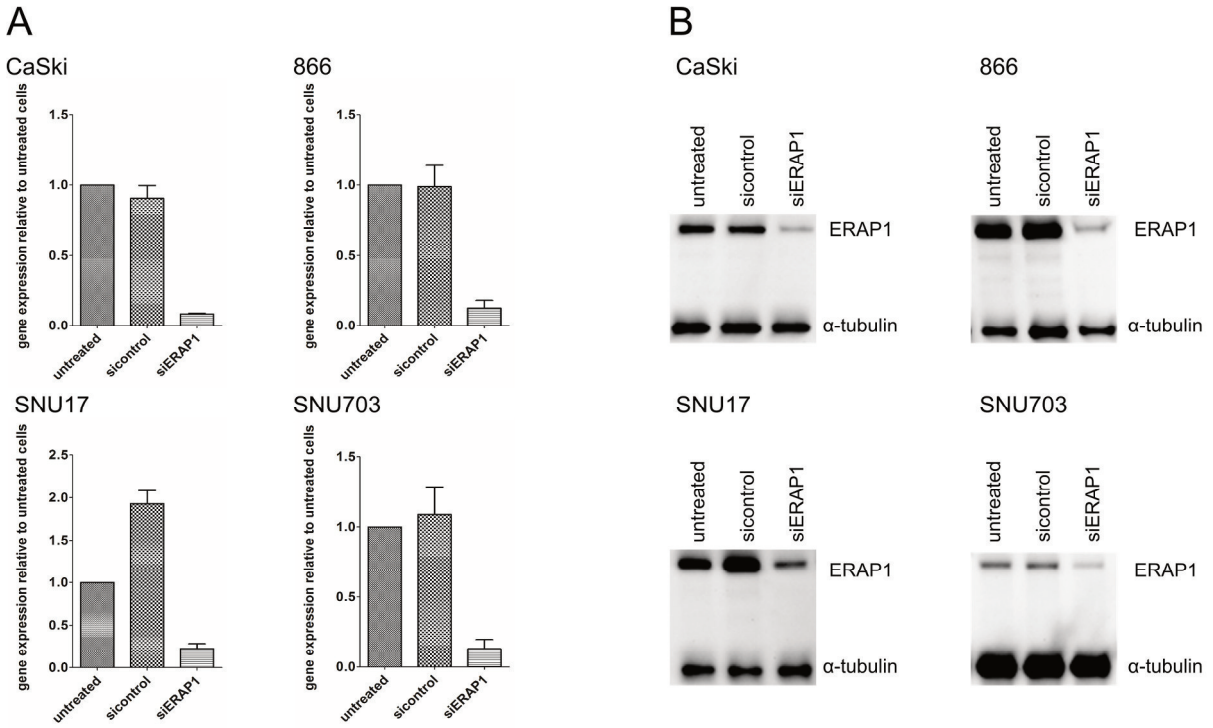

Figure 3.20: Knockdown of *ERAP1* using siRNAs in HPV16-positive and HLA-A2-positive cells. Cells were left untreated or were treated either with an *ERAP1*-targeting (siERAP1) or a non-targeting control siRNA pool (sicontrol) for 72h. **A.** Total RNA was purified from cells, reverse transcribed to cDNA and analyzed for *ERAP1* expression by qRT-PCR using TaqMan® probes. PCR reactions were performed in triplicates. *GAPDH* and *PGK1* were used as internal reference genes and *ERAP1* expression was calculated relative to untreated cells. The results are plotted as means ± SD from at least three independent experiments. **B.** 50µg of each cellular lysate was loaded and ERAP1 expression analyzed by Western blot with α-tubulin detection as a loading control. The results are representative of at least three independent experiments.

Figure 3.21 A illustrates the knockdown of *ERAP1* after 72h in SiHa and FK16A using qRT-PCR. The residual *ERAP1* transcript expression was in all cell lines below 21.5% compared to cells treated with the siRNA control pool. Figure 3.21 B shows successful attenuation of ERAP1 expression after 72h assessed by Western blot.

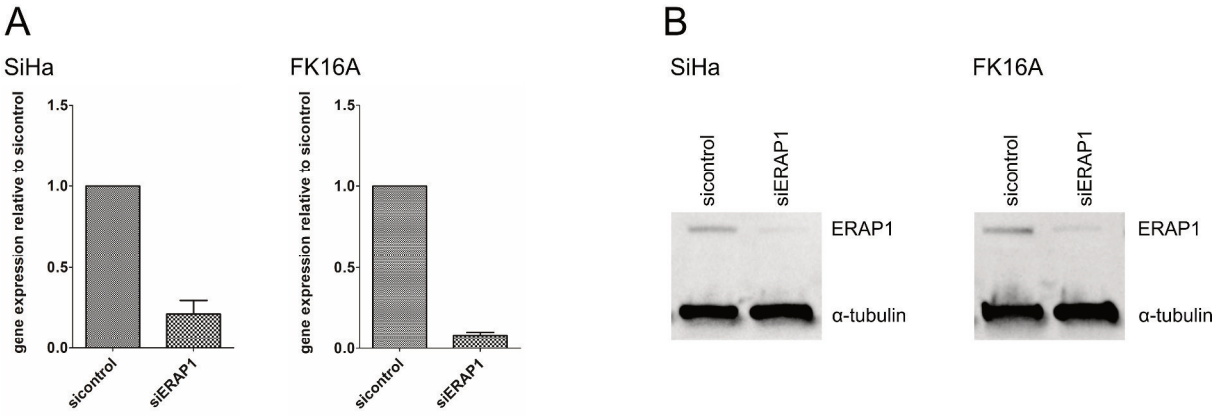

Figure 3.21: Knockdown of *ERAP1* using siRNAs in HPV16-positve and HLA-A24-positive cells. Cells were left untreated or were treated either with an *ERAP1*-targeting (siERAP1) or a non-targeting control siRNA pool (sicontrol) for 72h. **A.** Total RNA was purified from cells, reverse transcribed to cDNA and analyzed for *ERAP1* expression by qRT-PCR using TaqMan® probes. PCR reactions were performed in triplicates. *PGK1* was used as internal reference gene and *ERAP1* expression was calculated relative to sicontrol treated cells. The results are plotted as means ± SD from at least two independent experiments. **B.** 50µg of each cellular lysate was loaded and ERAP1 expression analyzed by Western blot with anti-α-tubulin detection as a loading control. The results are representative of at least two independent experiments.

3.3.1.2 Surface expression of HLA-A2 and HLA-A24 after *ERAP1* knockdown

The impact of *ERAP1* knockdown on HLA class I expression is not clearly defined and differs with cell type, but most studies reported a moderate downregulation (63, 64, 84, 224). In this study, the expression of HLA-A2 and HLA-A24 was studied after 72h of *ERAP1* knockdown using flow cytometry analysis.

In Figure 3.22 A, changes in surface expression of HLA-A2 in CaSki, 866, SNU17 and SNU703 cells treated with a siRNA control pool or an ERAP1-targeting siRNA pool are shown in representative histograms. Figure 3.22 B shows the pooled data of these experiments. CaSki cells had a significantly lower expression of HLA-A2 (on average reduced by 34%) after *ERAP1* knockdown. In contrast, all other cell lines had no significant change in HLA surface expression although a slight trend towards a lowered expression was observed.

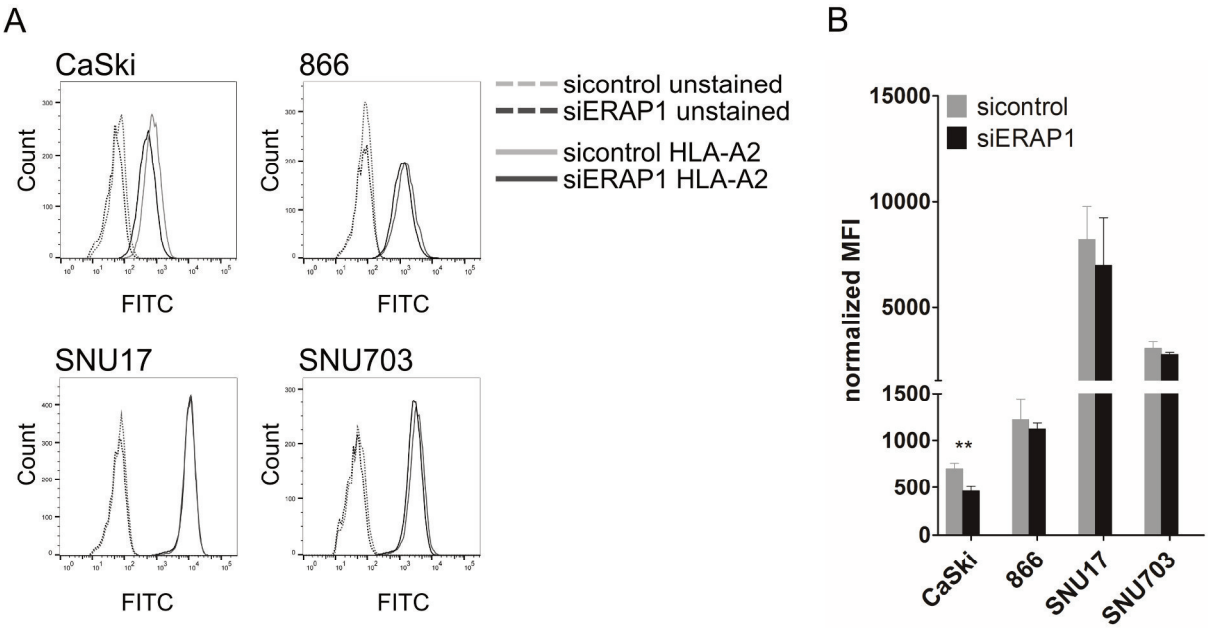

Figure 3.22: HLA-A2 expression after *ERAP1* knockdown. Cells were treated either with an *ERAP1*-targeting (siERAP1) or a non-targeting control siRNA pool (sicontrol) for 72h. Afterwards, cells were harvested, stained with an anti-HLA-A2 antibody coupled to FITC and mean fluorescence intensity (MFI) was analyzed by flow cytometry and calculated over the background of each cell line. **A.** Histogram representation of HLA-A2 stainings. The histograms are representative of three independent experiments. **B.** Results are plotted as means ± SD of three independent experiments. ** $p \leq 0.01$ (paired t-test)

Figure 3.23 A shows the HLA-A24 surface expression of SiHa and FK16A cells treated with a siRNA control or an *ERAP1*-targeting siRNA pool. In Figure 3.23 B, representative histograms show whether the surface expression of HLA-A24 differed after *ERAP1* knockdown. Similar to most HLA-A2-positive cell lines the change in surface HLA-A24 was not significant, although the expression tended to be slightly lower in cells with attenuated ERAP1 expression.

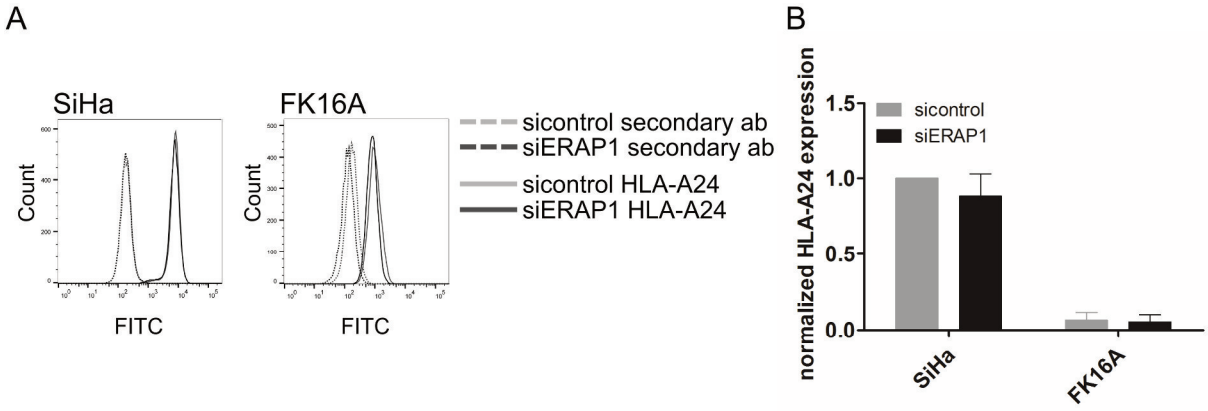

Figure 3.23: HLA-A24 expression after *ERAP1* knockdown. Cells were treated either with an *ERAP1*-targeting (siERAP1) or a non-targeting control siRNA pool (sicontrol) for 72h. Afterwards, cells were harvested, first stained with an anti-HLA-A24 antibody and then with a secondary antibody coupled to FITC. Mean fluorescence intensity (MFI) was analyzed by flow cytometry. **A.** Histogram representation of HLA-A24 stainings. The histograms are representative of at least two independent experiments. **B.** Data was calculated relative to SiHa sicontrol. Results are plotted as means ± SD of at least two independent experiments.

3.3.2 Direct detection of HLA-A2 HPV16-derived epitopes by liquid chromatography-mass spectrometry (LC-MS)

To assess whether ERAP1 levels have an influence on the presentation of HPV16 E6 and E7-derived epitopes, a targeted and highly sensitive liquid chromatography-mass spectrometry (LC-MS) approach was used. This method allows direct detection of low abundant epitopes bound to HLA class I on the surface of cells. In the present study, HLA-A2 molecules were immunoprecipitated from CaSki cells that were either treated with a siRNA pool specific for *ERAP1* or a siRNA control pool. Peptides were eluted from HLA-A2-peptide complexes and purified before targeted LC-MS^3 analysis.

3.3.2.1 Immunoprecipitation of HLA-A2 molecules from HPV16-transformed cells

Before immunoprecipitation (IP), CaSki cells were transfected for 72h with either an *ERAP1*-targeting siRNA pool or a siRNA control pool (see 3.3.1.1). HLA-A2 molecules were immunoprecipitated from CaSki cells using protein G coated sepharose beads coupled with an anti-HLA-A2 antibody. The successful enrichment of HLA-A2 molecules is shown in Figure 3.24. Detection with a pan-anti-MHC I antibody revealed a band at approximately 44kDa, which corresponds to the molecular weight of the HLA class I heavy chain. The most intense band in the IP sample indicates successful enrichment of HLA-A2. Weaker bands were detected in the cell lysate before and after IP. As detection was performed with a pan-anti-MHC class I antibody, which binds to all MHC class I types, the band of 44kDa is still detected in the lysate after the IP. It contains the remaining heavy chains from other HLA class I molecules (HLA-A3, -B7, -B37 and C7; see Table 7.2 in the appendix). As expected, the HLA-A2 band was not detected in the negative control, only containing sepharose beads coupled to the HLA-A2 antibody. IPs from CaSki cells treated with the siRNA control pool (Figure 3.24 A) and the *ERAP1*-specific siRNA pool (Figure 3.24 B) show similar results.

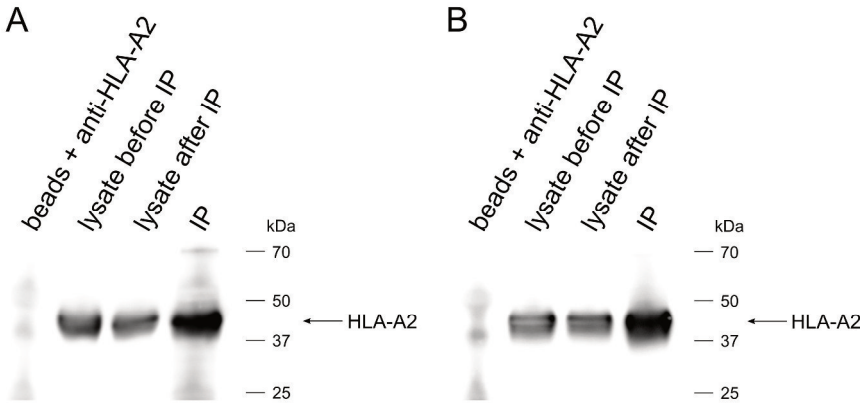

Figure 3.24: Immunoprecipitation of HLA-A2 molecules from CaSki cells. Cells were treated either with a non-targeting control siRNA pool (**A**) or an *ERAP1*-targeting siRNA pool (**B**) for 72h. Afterwards, immunoprecipitation (IP) of HLA-A2 was performed. Western blot detection was done using a pan-anti-MHC I antibody. Arrows mark the HLA-A2 heavy chain.

3.3.2.2 Direct detection of HLA-A2 HPV16-derived epitopes by LC-MS^3

The HPV16 E6-derived epitope $E6_{29-38}$ and the E7-derived epitope $E7_{11-19}$ are the only HPV16-derived epitopes that have been directly detected on the surface of tumor cells by mass spectrometry analysis to date (173, 225). Recently, other epitopes from HPV16 have been detected on CaSki and other HPV16-positive tumor cells by Dr. Renata Blatnik in our group (unpublished data). The immunological importance of other HPV16 epitopes was mostly shown by *in vitro* T cell assays or *in vivo* vaccinations (132, 155, 226). The second aim of the present thesis was to analyze the effect of high and low ERAP1 expression levels on the presentation of HPV16 E6 and E7-derived peptides. To this end, CaSki cells were either transfected with a control siRNA pool or an *ERAP1*-targeting siRNA pool for 72h. HLA-A2 molecules were immunoprecipitated from the cells as described in the previous chapter. HPV16-derived peptides are presented at very low levels that were estimated to be 25 copies of $E7_{11-19}$ per cell (173). Thus, $1x10^8$ to $3x10^8$ cells were used for one IP experiment per treatment group to ensure the reliable detection of these peptides by LC-MS^3 analysis. The same number of cells for each treatment group was used in one experiment. Peptides were eluted from HLA-A2:peptide complexes by acetic treatment and isolated for LC-MS^3 analysis by Dr. Renata Blatnik. In total, 16 peptides derived from HPV16 E7, one peptide derived from HPV16 E6 and endogenous control peptides were monitored by LC-MS^3. To identify the target peptides in IP samples, synthetic peptides were manually optimized for the best MS^3 reference spectra. MS spectra of three to four fragments per peptide were monitored. The IP MS^3 spectra were manually compared to reference MS^3 spectra. Only when the fingerprint of the reference spectra matched the fingerprint of the IP sample spectra, peptide presence in the IP sample was confirmed. In addition, retention times of the detected fragments in synthetic peptide and IP analysis had to match each time. Chromatographic profiles of peptide fragments showing retention times and MS^3 spectra of peptide fragments are shown in Figure 7.7 in the appendix. Positive control peptides derived from endogenous constitutively expressed proteins (indicated in material section 2.1.16.1) were detected in all IP samples (data not shown). In one experiment, the presence of 13 of the 17 HPV16 peptides was confirmed of which 6 detected peptides and 4 not detected peptides are shown in Table 3.2. MS analysis of the other 7 HPV16 peptides which were detected showed similar results (data not shown). LC-MS^3 identification of HLA-A2 HPV16 E6 and E7-derived epitopes revealed that there were no major changes in peptide presentation between CaSki cells with high levels of ERAP1 expression and CaSki cells with attenuated ERAP1 expression. The peptide quantities seem to be similar, too, given that all peptides were detected in low amounts and taking sample preparation and/or LC-MS^3 measurement variance into consideration. However, only an absolute quantification would give exact results about peptide amounts. Table 3.2 indicates 6 out of the 13 detected peptides and 4 peptides that were not detected. This data is from one representative experiment of three independent experiments. In repetition experiments, fewer peptides were reliably detected due to lower cell number input and low presentation of these peptides on the cell surface in general. However, the trend observed in the repetition experiments matched the

observations made in the presented experiment. Taken together, direct detection of HPV16-derived peptides showed that ERAP1 overexpression did not result in a loss of HPV16 epitopes. In addition, quantities of detected peptides seem to be in the same range in both CaSki control cells and cells knocked down for *ERAP1*.

Table 3.2: HLA-A2 HPV16 E7-derived peptides detected in CaSki cells. CaSki cells were treated with either a non-targeting siRNA pool (sicontrol) or an *ERAP1*-targeting siRNA pool (siERAP1) for 72h. HLA-A2 molecules were immunoprecipitated, peptides were eluted, isolated and analyzed by LC-MS^3. Results are representative of three independent experiments. n.d. = not detected

Peptide	CaSki sicontrol	CaSki siERAP1
$E7_{7-15}$	n.d.	n.d.
$E7_{7-17}$	n.d.	n.d.
$E7_{10-19}$	n.d.	n.d.
$E7_{11-19}$	detected	detected
$E7_{11-20}$	detected	detected
$E7_{12-20}$	n.d.	n.d.
$E7_{77-86}$	detected	detected
$E7_{78-86}$	detected	detected
$E7_{81-90}$	detected	detected
$E7_{82-90}$	detected	detected

3.3.3 T cell responses

To elucidate whether high or low expression levels of ERAP1 have an impact on HPV16 HLA class I epitope presentation, T cell lines against peptides derived from HPV16 E6 and E7 were generated. First, blood donors were screened with the intention to find E6 and E7-specific memory T cell responses. Peptides positive in this initial screen were used to expand peptide-specific T cells in long-term T cell lines. These long-term T cell lines were subsequently used in cytotoxicity assays.

In the scope of this thesis, blood from two female donors was used. One blood donor was HLA-A2-positive and one was HLA-A24-positive. The HLA-A24-positive donor was 39 years old while the HLA-A2 donor was 34 years old during the time of the experiments. No history of persistent infection with HPV was known for the donors. HLA typing and donor characteristics can be found in Table 7.3 in the appendix.

3.3.3.1 T cell memory screening against HPV16-derived epitopes by IFNγ ELISpot assay using short-term T cell lines

Prior to long-term T cell line generation, it was necessary to define T cell memory responses against epitopes derived from HPV16 E6 and E7 in our donors. Almost every sexually active individual has contact with an HPV-high risk type once in his or her life time (102). Among these, HPV16 is the most common high-risk type. Even though we assume that the donors have had contact with the virus,

immune responses are highly complex and it is not possible to predict to which peptide an individual reacts. Thus, HLA-A2 and HLA-A24 binding peptides derived from HPV16 E6 and E7 (194, 227), including binding peptides of HPV16 variants, were used in a T cell memory screening using IFNγ ELISpot. Peripheral blood mononuclear cells (PBMCs) were isolated and peptide-specific short-term T cell lines were generated *ex vivo* by peptide stimulation. Additionally, short-term T cell lines were regularly supplemented with cytokines. By these means, it is possible that existing T cell memory responses of the respective individual are triggered. Responses were only considered to be positive if the following criteria were fulfilled: a minimum of 200 SFU (spot forming units) per $1x10^6$ cells, and a stimulation index (SI = fold change of SFU compared to background) of at least 2.

Figure 3.25 shows the results of the two T cell memory screening experiments of HLA-A2 binding HPV16 E6 and E7 epitopes. For the ELISpot assay, every individually cultured short-term T cell line was seeded in medium with the peptide diluent DMSO serving as a background control, with ConA as a positive control and with the addition of the peptide that was initially used for stimulation. A negative control T cell line was generated with a HLA-A2 binding peptide derived from HIV. The CEF peptide pool, containing epitopes for the most frequent HLA types from CMV, EBV and influenza virus, was used to generate a positive control short-term T cell line. In Figure 3.25 A, SFU of each T cell line are plotted and in B stimulation indices are shown. Black bars represent responses that were positive for both criteria mentioned above. Peptide-specific T cell responses against $E6_{18\text{-}26variant}$ and $E7_{81\text{-}91}$ were detected. In a second independent experiment, very strong peptide-specific responses were again detected for $E7_{81\text{-}91}$. One plausible explanation for absence of $E6_{18\text{-}26variant}$-specific responses in the second experiment is that only low numbers of PBMCs could be seeded per short-term T cell line in this screening setup. Thus, it is possible to miss T cell memory responses especially for low abundant memory T cells. $E7_{81\text{-}91}$ was chosen for long-term T cell line generation.

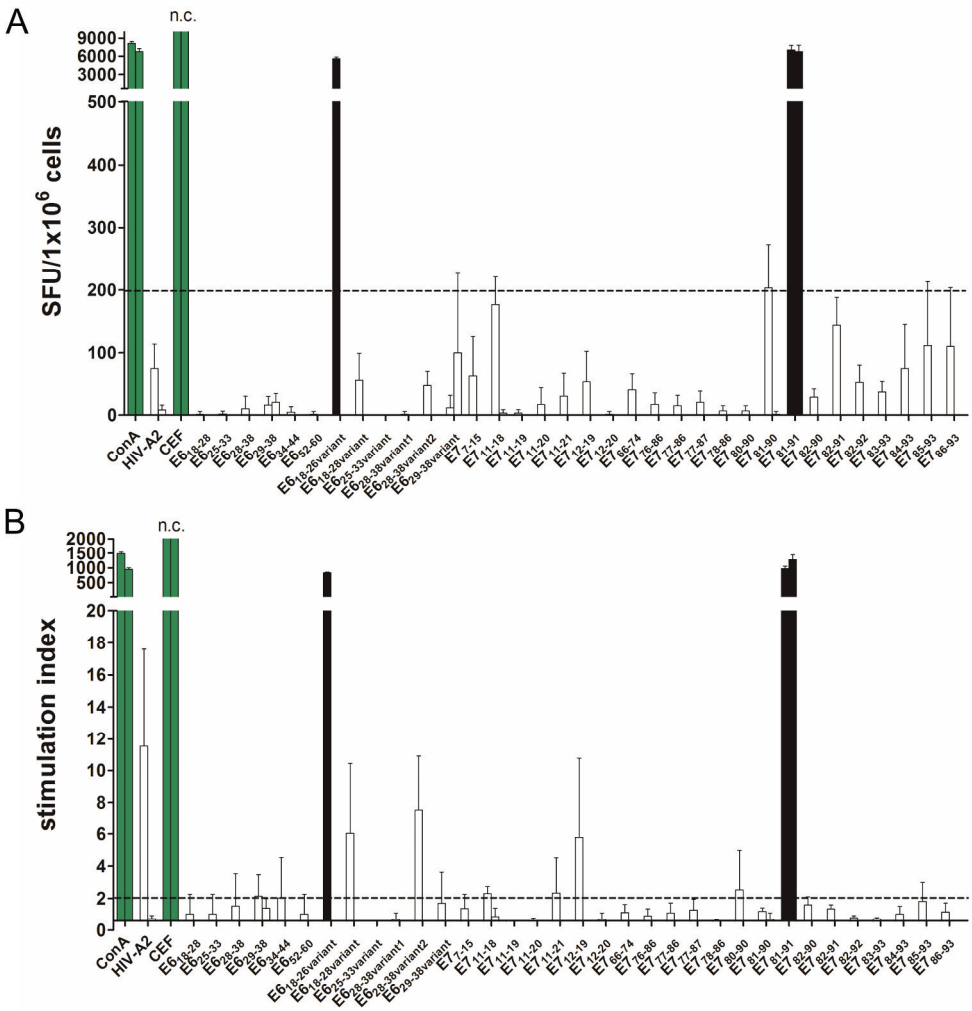

Figure 3.25. T cell memory screening of HPV16 E6 and E7 epitopes by IFNγ ELISpot in a HLA-A2-positive donor. Short-term T cell lines were cultured in medium with either the peptide diluent DMSO serving as a background control, with ConA as a positive control and with the respective cognate peptide used for initial stimulation. A negative control short-term T cell line was generated using a HLA-A2-restricted HIV-derived epitope (HIV-A2) and a positive control short-term line with the CEF peptide pool. Data is plotted as mean ± SD from at least triplicates. Whenever there are two bars they represent data from two independent experiments. **A.** A peptide-specific T cell response was considered positive when the mean spot forming units (SFU) for a given peptide were ≥ 200/10^6 PBMCs (dashed line). **B.** The stimulation index (SI) was determined by calculating the ratio between specific SFU and background SFU. A peptide-specific T cell response was considered positive when the SI was at least 2 (dashed line). Positive responses by both criteria are indicated by green (positive controls) and black bars.

Figure 3.26 shows the result of the T cell memory screening of HLA-A24 binding HPV16 E6 and E7 epitopes. The ELISpot assay was set up as described above. We could detect peptide-specific T cell responses against 8 peptides ($E6_{26\text{-}34}$, $E6_{49\text{-}59}$, $E6_{66\text{-}75}$, $E6_{85\text{-}95}$, $E6_{90\text{-}99}$, $E6_{131\text{-}139}$, $E6_{26\text{-}34variant}$ and $E7_{69\text{-}76}$). Peptide-specific responses were also detected in a second independent experiment for $E6_{26\text{-}34variant}$ and $E7_{69\text{-}76}$. As described above, due to the low number of cells seeded in the experiment it was possible to miss T cell memory responses especially for extremely low frequent T cells. The peptides $E7_{69\text{-}76}$ and $E6_{90\text{-}99}$ had highly positive responses regarding both criteria, SFU and SI. Therefore, these two peptides were chosen for the generation of peptide-specific long-term T cell lines. The strong response against $E6_{90\text{-}99}$ was not observed in the repetition of the screening. Nevertheless, we decided to generate peptide-specific long-term T cell lines against this peptide based on the very strong response in the first screening. For our experiments, we omitted the $E6_{26\text{-}34}$ variant

peptide, which also showed positive results, because only one HPV16-positive cell line in our collection carried the HPV16 variant harboring this mutation. Moreover, this cell line had poor growth properties, thus precluding its use in subsequent cytotoxicity assays.

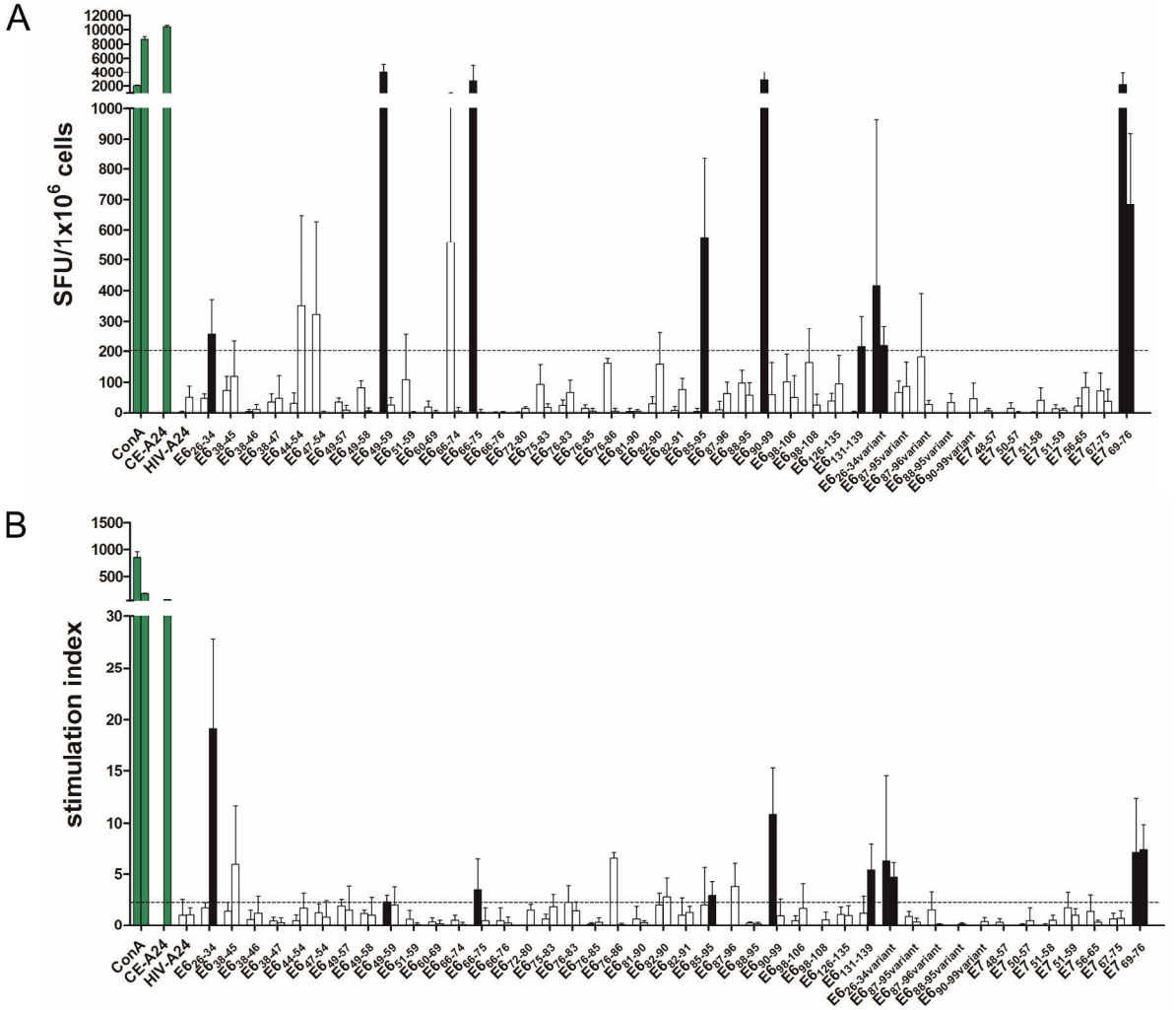

Figure 3.26. T cell memory screening of HPV16 E6 and E7 epitopes by IFNγ ELISpot using a HLA-A24-positive donor. Short-term T cell lines were cultured in medium either with the peptide diluent DMSO serving as a background control, with ConA as a positive control and with the respective cognate peptide used for initial stimulation. A negative control short-term T cell line was generated using a HLA-A2-restricted HIV-derived epitope (HIV-A24) and a positive control short-term line with the CE-A24 peptide pool. Data is plotted as mean ± SD from at least triplicates. Whenever there are two bars, they represent data from two independent experiments. **A.** A peptide-specific T cell response was considered positive when the mean spot forming units (SFU) for a given peptide were ≥ 200/10^6 PBMCs (dashed line). **B.** The stimulation index (SI) was determined by calculating by calculating the ratio between specific SFU and background SFU. A peptide-specific T cell response was considered positive when the SI was at least 2 (dashed line). Positive responses by both criteria are indicated by green (positive controls) and black bars.

3.3.3.2 The effect of ERAP1 attenuation in target cells on cytotoxicity measured by HPV16-specific CD8 T cells

Based on the results from the T cell memory screening, long-term T cell lines were generated by three weekly stimulations of PBMCs with antigen-presenting cells (APCs) of the respective donor pulsed with one of the peptides described in the previous section. One week after the last stimulation, CD8 T cells were purified by negative selection. These CD8 T cells were co-cultured with HLA-matched

tumor cells in a cytotoxicity assay. We employed the recently established VITAL-FR cytotoxicity assay (211, 212). This assay is a flow cytometry-based assay allowing the simultaneous co-culture of effector CD8 T cells with two target cell populations, due to different labeling of target cells either with CFSE or FarRed. Target cells were first labeled and then treated with an *ERAP1*-targeting siRNA pool or a control siRNA pool for 24h. Afterwards, target cells and CD8 T cells were co-cultured in different ratios (effector:target ratio) for 48h. As a background control, a HPV16-negative, HLA-matched cell line was used. Detailed information of HLA types and HPV16 variants contained in the cell lines used in this study is summarized in Table 7.2 in the appendix.

Figure 3.27 shows the result of the cytotoxicity assays using the $E7_{81-91}$-specific T cell line generated from PBMCs of the HLA-A2-positive donor. As target cell lines, 866 and CaSki were used. The HLA-matched, HPV16-negative control cell line was C33A. The experiments revealed that CaSki transfected with the *ERAP1*-specific siRNA pool were killed better by $E6_{81-91}$-specific T cells than target cells treated with the siRNA control pool (Figure 3.27 A). In a repetition experiment, the same trend was observed, but the difference in killing was less pronounced, possibly due to the use of a different T cell line (data not shown). In contrast, no difference in killing was observed with 866 target cells (Figure 3.27 B). A much lower cytotoxicity was detected for the HPV16-negative control cell line (Figure 3.27 A and B).

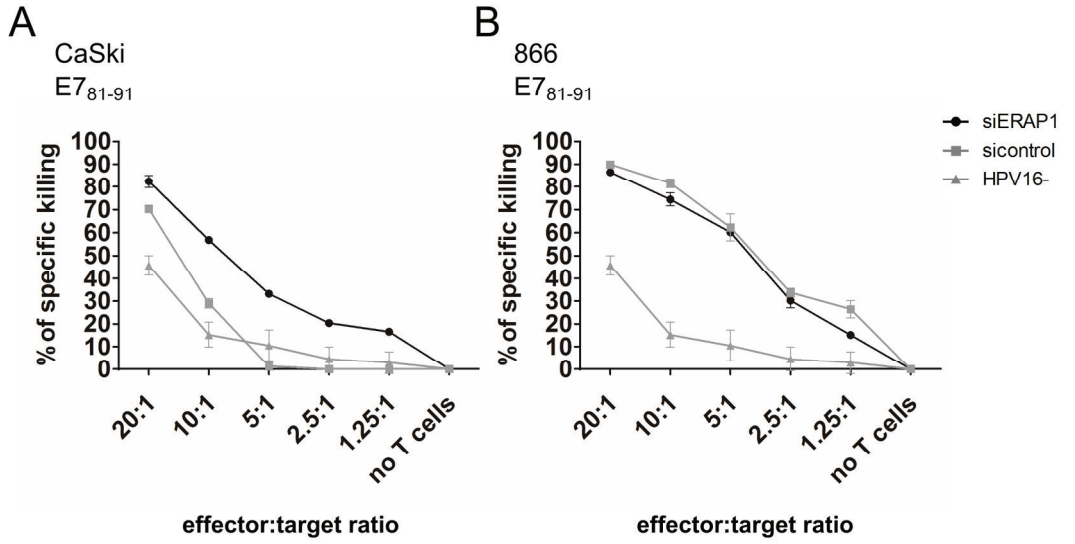

Figure 3.27: The effect of *ERAP1* attenuation in target cells on cytotoxicity mediated by HPV16 $E7_{81-91}$-specific CD8 T cells. Vital-FR assay using HPV16 $E7_{81-91}$-specific CD8 effector T cells from a HLA-A2-positive donor. The HLA-A2-positive and HPV16-positive cell lines CaSki (**A**) and 866 (**B**) were used as target cells, whereas the HLA-A2-positive and HPV16-negative cell line C33A (HPV16-) served as background control. 24h after siRNA transfection, target cells and titrated numbers of effector cells were incubated for another 48h and were then analyzed by flow cytometry. One representative experiment of two independent experiments is shown. The results are plotted as mean ± SD from at least duplicates.

Figure 3.28 illustrates the results from cytotoxicity assays using long-term T cell lines from the HLA-A24-positive donor generated with the peptides $E7_{69-76}$ and $E6_{90-99}$. As a target cell line, the HLA-A24-positive and HPV16-positive cell line FK16A was used. The HLA-matched HPV16-negative control cell line was SNU1160. The experiments surprisingly revealed that FK16A cells treated with a control siRNA pool were killed better by $E7_{69-76}$-specific T cells than those treated with the *ERAP1*-targeting siRNA pool (Figure 3.28 A). In addition, $E7_{69-76}$-specific T cells were also cultured with SiHa target cells (HLA-A24-positive and HPV16-positive), which resulted in similar effects as with FK16A (data not shown). The same effect was obtained for $E6_{90-99}$-specific T cells (Figure 3.28 B). $E6_{90-99}$-specific T cells could not be used on SiHa, as the HPV16variant present in this cell line contains a mutation in the $E6_{90-99}$ epitope. In comparison, a much lower cytotoxicity was detected for the HPV16-negative control cell line (Figure 3.28 A and B).

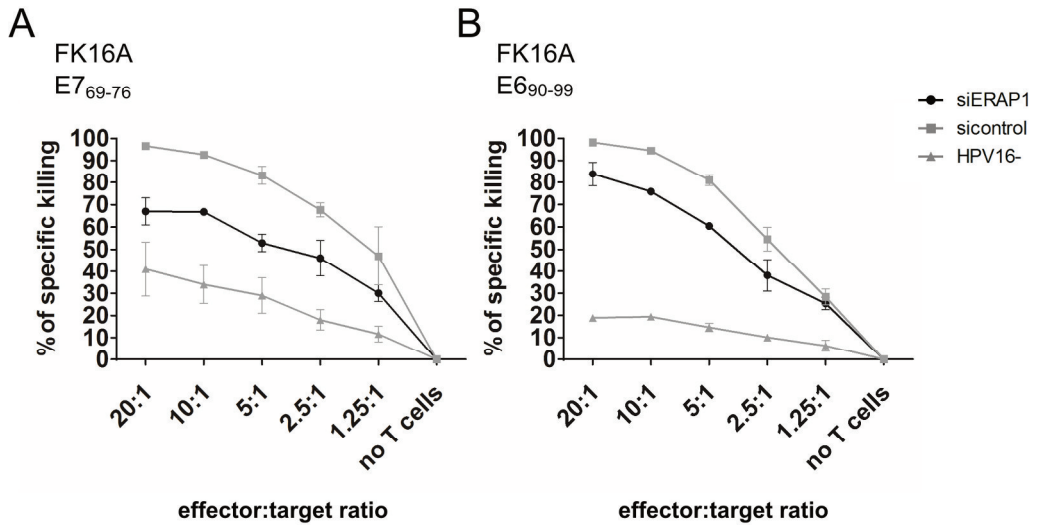

Figure 3.28: The effect of *ERAP1* attenuation in target cells on cytotoxicity mediated by HPV16 $E7_{69-76}$-specific and $E6_{90-99}$-specific CD8 T cells. Vital-FR assay with HPV16 $E7_{69-76}$-specific (**A**) and $E6_{90-99}$-specific (**B**) CD8 effector T cells from a HLA-A24-positive donor. The HLA-matched and HPV16-positive cell line FK16A was used as target cells, whereas the HLA-matched and HPV16-negative cell line SNU1160 (HPV16-) served as background control. 24h after siRNA transfection, target cells and titrated numbers of effector cells were incubated for another 48h and were then analyzed by flow cytometry. One representative experiment of two independent experiments is shown. The results are plotted as mean ± SD from at least duplicates.

In conclusion, these results revealed that killing of FK16A by $E6_{90-99}$- and $E7_{69-76}$-specifc T cell lines was inhibited by ERAP1 normalization. Cytotoxicity of an $E7_{81-91}$-specific T cell line towards 866 was not affected by ERAP1 attenuation. However, killing of CaSki cells by $E7_{81-91}$-specific T cells was improved when ERAP1 was normalized to levels observed in HPV-negative keratinocytes.

4 Discussion

HPV-induced malignancies are a major health problem worldwide. The development of therapeutic vaccination strategies is important to cure people already infected with high-risk types of HPV. However, the overall clinical success of therapeutic vaccines is so far limited. One reason may be immune evasion mechanisms employed by HPV. In this thesis, HPV16-mediated changes in antigen processing machinery (APM) component expression were systematically analyzed, since these may directly interfere with anti-tumor CTL immune responses. ERAP1 was found to be consistently overexpressed in HPV16-positive tumor cells, CIN lesions and cervical cancer. The immunological consequences of ERAP1 overexpression were investigated by mass spectrometry (MS) and in functional T cell assays.

4.1 Expression of APM components in HPV-induced malignancies

Correct processing and presentation of tumor-specific antigens by the APM is crucial for effective cytotoxic T lymphocyte (CTL) responses against malignant cells, and HPV-induced malignancies are no exception. Several changes in the APM have been observed in HPV-induced malignancies. For instance, Evans and colleagues reported that presentation of the HPV16-derived epitope $E6_{29-38}$ is dependent on TAP and TAP was expressed at low levels in a cervical carcinoma cell line (132). This study demonstrated for the first time in the context of HPV-induced malignancies that changes in the APM are correlated with functional consequences in anti-HPV CTL responses. Many studies presented further data on APM defects in cervical and head and neck cancer (81, 133, 134, 226, 228), but one has to bear in mind that only 20-30% of head and neck cancers are HPV positive (229, 230). Furthermore, these studies do not present a complete picture of the APM situation since the APM is a tightly regulated process that needs a coordinated interplay of its many components (see 1.1.4). For instance, the presentation of HLA class I strongly depends on TAP, which channels peptides from the cytosol into the ER, thereby providing the peptide supply for HLA class I. In the light of these issues, a systematic analysis of all APM components in many different HPV16-positive tumor cells, compared to a group of HPV-negative cells, was conducted in this thesis (see 3.1.1.1). 23 HPV16-positive cell lines, including cervical cancer cell lines, head and neck squamous cell carcinoma (HNSCC) lines and cell lines transformed with the whole HPV16 genome were compared to 6 HPV-negative cell lines for the expression of 20 APM-associated genes. Furthermore, the influence of IFNγ on APM component expression was analyzed (see 3.1.1.2). The presence of IFNγ is known to increase the expression of several APM components (67, 217, 218), thereby augmenting and altering antigen presentation.

The qRT-PCR screen of constitutive APM component expression showed that the HPV-negative group had a strikingly uniform gene expression and cell lines transfected (but not naturally transformed) with the HPV16 genome were similar to the HPV-negative group. In contrast, this screen revealed that *calreticulin*, *ERAP1* and the immunoproteasome subunits *PSMB8*, *PSMB9*, *PSMB10*, *PSME1* and *PSME2* were significantly overexpressed in HPV16-positive tumor cells. Expression of APM components upon IFNγ treatment showed that all cell lines upregulated *HLA-A*, *HLA-B*, *TAP1*, *TAP2*, *PSME8*, *PSME9* and *PSME1* and almost all cell lines upregulated *HLA-E*, *β2m*, *tapasin*, *ERAP1*, *ERAP2*, *PSMB10* and *PSME2*. As expected, gene expression of non-IFNγ-inducible genes, namely *calreticulin*, *calnexin*, *PDIA3*, *PSMB5*, *PSMB6* and *PSMB7*, was not upregulated. Further, a mathematical approach to determine final expression levels after IFNγ treatment demonstrated that expression of APM components after IFNγ treatment was comparable between HPV-negative and HPV16-positive tumor cells. Taken together, these results suggest that the cell lines tested in this screen have no defect in IFNγ signaling. In previous studies, an overall responsiveness to IFNγ reflected by upregulation of IFNγ-inducible genes was typically observed in HPV-induced malignancies, but these studies only analyzed few APM components (132, 178, 226). In contrast, especially melanomas have often been found to be insensitive to IFNγ in order to avoid immune recognition (231, 232). Viruses target IFNγ signaling in order to evade the host's immune system. Poxviruses, for instance, produce a protein that is secreted and binds to IFNγ in the extracellular matrix, thereby neutralizing its effects on host cells (233, 234). So far, HPV is known to perturb IFN type I signaling (IFNα, IFNβ and IFNκ). HPV16 E6 is able to inhibit IRF3 transactivation which hampers IFNβ induction (235). Further, HPB16 E7 blocks the translocation of the p48/IRF9 complex necessary for IFN translation in the nucleus (236). Recently, it was reported that IFNκ, which is mainly expressed in keratinocytes, is silenced by *de novo* methylation mediated by HPV16 E6 (129). However, IFNγ signaling as shown by us and former studies is functional in HPV-induced malignancies.

After the broad qRT-PCR screen, protein expression of selected APM components and cell lines was analyzed (see 3.1.2). The analysis of HLA class I surface expression showed that 56% of HPV16-positve cell lines had higher surface HLA class I expression than HPV-negative cells. The other HPV16-positive cell lines had similar levels to the control group. Only one cell line, UDSCC2, had very low HLA class I surface expression consistent with low mRNA levels observed during the qRT-PCR screen. HLA class I was upregulated upon IFNγ stimulation confirming observations from the qRT-PCR screen. In a previous study, a tissue microarray in cervical cancer was conducted and described a downregulation of total HLA class I in 24% and even a total loss of expression in 21% of cases (81). On the contrary, in this thesis a strong downregulation of HLA class I was only observed in the UDSCC2 cell line on the mRNA and on the protein level. Other studies also report a downregulation of HLA class I in cervical cancer or HNSCC (132, 134, 226, 228, 237). A difference of two of these studies compared to the approach in this thesis is the use of tumor stroma cells as an

internal control (228, 237). Also Evans and colleagues (132) used a different control, since they compared protein expression in cervical carcinoma cell lines to an immortalized B cell line. Conversely, we used HPV-negative keratinocytes as negative controls for screening our cell line collection.

Besides HLA class I expression levels, the protein expression levels of other APM components in HPV-induced malignancies were investigated. In contrast to the qRT-PCR approach, the proteins PSMB9, PSMB10, PSME1 and PSME2 were not upregulated in the majority of tested HPV16-positive cell lines. Protein expression of PSMB9 and PSMB10 after IFNγ treatment was similar between HPV-negative and HPV16-positive cell lines, which is consistent with the qRT-PCR results. Similarly, no overexpression on the protein level was observed for tapasin and calreticulin. These data suggest that the regulation of APM component expression is complex and includes posttranscriptional mechanisms. Indeed, several microRNAs have recently been identified that target APM genes confirming the presence of posttranscriptional regulation. For instance, *PSMB8*, *PSMB10*, *TAP1* and *HLA-B* are proposed to be targeted by microRNA9 but the direct association of this microRNA with the mRNA of these components still needs experimental evidence (238). TAP1 is a direct target of microRNA346, which is induced during ER stress (239). Furthermore, a discordant mRNA/protein expression was often observed in human tumors for the non-classical HLA molecule, HLA-G. The reason for this phenomenon was again the involvement of several microRNAs (240, 241). Recently, HPV-encoded microRNAs have been identified (242). No association of these with APM components has been found to date, but as HPV-encoded microRNAs are a novel discovery it is possible that more HPV-encoded microRNAs and more target genes will be identified in the future.

In a study from 2008, HLA class I downregulation was significantly associated with the downregulation of other APM components: TAP1, TAP2, tapasin, PDIA3, PSMB8 and PSMB9 (81). Conversely, PSMB10, calnexin and calreticulin were reported to be normally expressed, which is consistent with the data of this study. Hasim and colleagues, however, provide experimental evidence for a downregulation of calnexin and calreticulin in cervical cancer (134). As we do not observe defects in HLA class I surface expression in this study it is not surprising that we do not find downregulation of the mentioned APM components.

In contrast, ERAP1 was found to be overexpressed in the majority of HPV16-positive cell lines on the protein and on the mRNA level. ERAP1 expression after IFNγ treatment was still elevated in HPV16-positive cell lines. Five of these cell lines (SNU703, SNU1005, 866 and 93VU147T) also had elevated levels of ERAP2. Other studies report that ERAP1 and ERAP2 expression is often discordant, and also the correlation of one or the other enzyme with surface HLA class I expression is controversially discussed (77-79). Overall, studies working with ERAP2 expression or function have to be regarded with caution, because it has recently been reported that there is an ERAP2 allele leading to nonsense-mediated mRNA decay, resulting in absence of ERAP2 protein expression in 25% of the population (59). In general, it appears that ERAP1 expression is more coordinated with HLA class I

expression, highlighting the pivotal role of this enzyme on the overall ligand supply of HLA class I (77, 243).

To further confirm the obtained results in cell lines, ERAP1 expression was analyzed in immunohistochemical stainings (see 3.1.3). The obtained data strengthened the data from the cell line screen and showed overexpression of ERAP1 in all three grades of CIN and in cervical cancer. In addition, immunohistochemistry complemented our data by showing that the expression of ERAP1 was increasing with disease progression, being lowest in CIN I and highest in established cervical cancer. Histologically normal cervical epithelium was used as a control for these experiments. In contrast to our results, Mehta and colleagues reported a downregulation of ERAP1 in cervical cancer, but only in 15% of cases (81). They also found that downregulation of ERAP1 is an independent bad prognostic factor. As described above, the use of tumor stroma as internal control may in part explain these different observations. The Human Protein Atlas available from *www.proteinatlas.org* observed both overexpression and downregulation of ERAP1 in cervical carcinoma, indicating that both scenarios are possible (80). Studies from other tumor entities revealed that ERAP1 expression is considerably variable, ranging from low to high expression. Ovarian, breast and lung cancers tend to downregulate ERAP1, whereas colorectal adenocarcinoma, renal cell carcinoma, skin cancer and melanoma tend to have high ERAP1 expression levels (77, 78, 244). Discordance between mRNA expression and protein expression was also observed (244), again suggesting a complex regulation of ERAP1 expression controlled by transcriptional and posttranscriptional mechanisms.

Taken together, APM expression analyses revealed that the APM is often dysregulated in HPV-induced malignancies. However, findings differ between studies. This may be explained by the use of different protocols and techniques, ranging from immunohistochemistry of tissue to molecular analysis of cell lines. Furthermore, it is important to point out that the use of controls varies, although the APM is differentially expressed in different tissues and cell types (78). The strength of the screen conducted in this thesis is the use of multiple HPV-negative controls that all originate from keratinocytes, as well as the use of histologically normal epithelium in immunohistochemistry. The variable expression of ERAP1 in human tumors – either upregulated as observed in this study or downregulated as observed in some other studies – leads to the hypothesis of ERAP1 dysregulation being a possible tumor immune evasion mechanism. Since ERAP1 is a critical determinant of the HLA class I peptide repertoire, tumors could evade CTL detection by altered ERAP1 expression. In the case of ERAP1 upregulation, it is reasonable to presume that the presentation of one or many dominant tumor-associated antigens is reduced due to overtrimming. In fact, this phenomenon has already been observed in melanoma and colorectal carcinoma (83, 84).

4.2 Possible mechanisms leading to ERAP1 overexpression

After the identification of ERAP1 overexpression in HPV-induced malignancies, we decided to investigate possible mechanisms that could cause this overexpression. In recent years, nonsynonymous single nucleotide polymorphisms (SNPs) within *ERAP1* have gained attention. In the inflammatory diseases ankylosing spondylitis (AS), Behçet's disease and psoriasis, a strong association of MHC I alleles (HLA-B27, HLA-B51 and HLA-C6:02, respectively) and *ERAP1* SNPs was found (75, 245, 246). Interestingly, SNPs within *ERAP1* do not only predispose for certain diseases but can influence enzymatic activity and expression levels. Therefore, a genomic sequencing analysis was performed to identify SNPs in *ERAP1* of one HPV-negative (NOK), 4 HPV16-positive ERAP1 high expressing cell lines (CaSki, 866, SNU17 and SNU703) and two HPV16-positive cell lines with similar ERAP1 expression to HPV-negative cells (SiHa and FK16A). The nonsynonymous SNPs (residue positions: 12, 127, 276, 349, 528, 725 and 730) found in the tested cell lines were all already described as naturally occurring SNPs of *ERAP1*.

Concerning ERAP1 expression, ERAP1 variants harboring 528K were reported to be higher expressed than variants harboring 528R. Similarly, ERAP1 with 730Q was expressed at higher levels than with 730E (74, 221, 246). In our cell lines, both 528K and 730Q were present in low and high ERAP1 expressing cell lines, indicating that ERAP1 overexpression in our cell lines is not due to these SNPs. In cervical cancer, Mehta and colleagues show that a homozygosity of 56E/127P or the 56K/127R haplotype combined with any other haplotype reduces survival to 50% (82). Furthermore, heterozygosity at position 127 or heterozygosity of the 56E/127P haplotype was significantly associated with normal protein expression. Haplotype combinations that were reported to be associated with reduced overall survival were found in none of the analyzed cell lines in this study. Heterozygosity of ERAP1 at position 127 was found in NOK and SNU703, but SNU703 was associated with a high ERAP1 expression whereas NOK had a normal ERAP1 expression level. E56/127P in combination with another haplotype that was linked to normal expression according to Mehta *et al.* (82) was found in NOK, SNU703 and FK16A, among which only NOK and FK16A have normal expression levels. In summary, ERAP1 expression – especially overexpression – in our cell lines cannot be explained by SNPs.

Besides an association of SNPs and ERAP1 expression, several but not all SNPs have an influence on its enzymatic activity. From a structural point of view, it was reported that residue 127 is located near domain junctions in the peptidase M1 domain, residues 276 and 528 both near domain junctions in domain III, residue 349 in the active site and residues 725 and 730 in the substrate binding cavity (82, 247, 248). It has been shown that SNPs distal from the active site can also affect function of ERAP1 (249). The enzymatic cycle of ERAP1 is strongly dependent on conformational changes between its domains. ERAP1 has an "open" and a "closed" state (see 1.1.4.1) mediating substrate binding and product release. Residue 528 affects conformational changes of ERAP1 since it is located at the beginning of domain III near to the hinge region. On the other hand, residue 730, located in the

substrate binding cavity, has an impact on substrate length selection. Given these facts, it is likely that amino acid variations at these positions change enzymatic functions of ERAP1. The influence of *ERAP1* SNPs on the enzymatic activity has been investigated in numerous studies. In general, 127P, 276M, 575N and 730E had a small or no effect on the trimming activity *in vitro* (71, 248, 250). On the contrary, Evnouchidou and colleagues provided experimental evidence that 730E leads to highly decreased presentation of an HLA-B27 epitope *in vivo* (72). Higher trimming activities were attributed to 528K, 528K/575N, 725R and 725Q/730E (203, 251, 252) whereas poor trimming activities were reported for 349V, 528R and 725Q (251, 253). Conversely, 349V was reported to have higher trimming activities in the Seliger laboratory (244). Garcia-Medel and colleagues (251) describe that variants containing the 575N SNP have a poorer trimming activity, which is in conflict with the observation that a combination of 528K /575N renders ERAP1 very active. According to the body of research on the impact of *ERAP1* SNPs, there is clear evidence for the association of ERAP1 variants with functional consequences. However, the exact impact of SNPs on ERAP1 is very complex, which is reflected by discrepancies between the studies. These differences are likely due to different methodological approaches. For instance, earlier studies analyzed functions of single SNPs whereas later studies used naturally occurring alleles of ERAP1. Also different assays and protein purification techniques were employed in the studies and may have resulted in the different observed outcomes. In our cell lines, SNPs that were reported to confer high trimming activities to ERAP1 and SNPs associated with low trimming activities were found in both ERAP1-overexpressing cell lines and cell lines with normal expression. The cell lines CaSki, SNU17, SiHa and FK16A contain only variants reported to have a higher trimming activity.

The dysregulated expression of ERAP1 in HPV-mediated lesions could also be caused by effects of the HPV oncogenes. HPV E6 and E7 are constitutively expressed in HPV-positive malignant cells and maintain their malignant phenotype. Besides manipulating the cell cycle, E6 and E7 also have intracellular targets associated with immune escape (125). E6 and E7 can hamper the IFN signaling cascade at multiple steps (129, 235, 236, 254) as described in section 4.1. Interestingly, the E7 oncoprotein also has multiple targets within the APM. On the one hand, there is evidence that E7 inhibits both *PSMB9* and *TAP1* expression on the transcriptional level and on the other hand E7 also represses the promoter of the MHC I heavy chain (133). Therefore, we investigated whether E6 and E7 play a role in ERAP1 expression. To test this, HPV16 *E6* and *E7* were knocked down in CaSki cells using a siRNA approach (209). ERAP1 expression was assessed after 72h. However, the level of ERAP1 expression remained unchanged, suggesting that neither E6 nor E7 affect ERAP1 expression. It cannot be ruled out that other viral proteins play a role in this context.

Analysis of *ERAP1* SNPs and knockdown of HPV16 *E6* and *E7* did not elucidate the reason why ERAP1 is overexpressed in HPV-induced malignancies. Other mechanisms on the transcriptional level, such as mutations or DNA modifications in the promoter region, may play a role. For instance, two ERAP1-deficient melanoma cell lines share a mutation in the promoter of *ERAP1* and it has been

demonstrated that this mutation leads to reduced transcriptional activity. This study showed that mutations in the *ERAP1* promoter exist in a disease associated context (244). Another study analyzed the mechanism underlying ERAP1 downregulation observed in 15% of cervical cancer (255). The authors found a complete or partial loss of heterozygosity in 50% of cases with ERAP1 downregulation. Epigenetic changes, namely the DNA methylation status of ERAP1 was analyzed as well, but this did not contribute to dysregulated expression (134, 244). Unfortunately, the molecular background of ERAP1 upregulation in tumors has not been studied so far, but is reasonable to assume that mechanisms for overexpression may take place on similar molecular levels as those for downregulation.

Additionally, there are hints that ERAP1 expression can be regulated on multiple levels, since discordance between mRNA and protein levels was detected already in a previous study (244), as well as in this thesis. Thus, not only transcriptional but also posttranscriptional processes could account for ERAP1 overexpression. Recently, a novel immune evasion mechanism of human cytomegalovirus (HCMV) has been unraveled (69). The authors identified a viral microRNA (miR-US4-1) which inhibited ERAP1 expression during viral infection, thereby hampering HCMV-specific CTL recognition of infected cells. MicroRNAs are involved in almost all developmental and pathological processes since they are critical regulators of gene expression and have the potential to induce or inhibit expression of a particular gene. In cancer, overexpression of oncogenic microRNAs or loss of tumor suppressor microRNAs has gained much interest, because it was demonstrated that these changes are sufficient to promote cancer development *in vivo* (256). Cellular or HPV-encoded microRNAs that influence ERAP1 expression have not yet been discovered, but it is possible that microRNAs with either a cellular or a viral origin might play a role in ERAP1 expression. In the context of HPV-induced malignancies, there are studies on dysregulation of cellular microRNA expression as well on HPV-encoded microRNAs (242, 257, 258). Cellular microRNAs have been identified that are altered in HPV-induced malignancies and these are mostly involved in cell cycle control (257, 258). The first papillomavirus encoded microRNAs were described in 2013 (242) and predicted targets are involved in cell cycle, cell adhesion and oncogenesis. It remains to be investigated if posttranscriptional processes, such as microRNAs, play an important role in ERAP1 upregulation.

4.3 Possible consequences of altered ERAP1 expression

4.3.1 ERAP1 functions besides antigen processing

After the discovery of ERAP1 in 1999 (57), multiple cellular functions have been ascribed to this aminopeptidase (61, 243). In Figure 4.1, the roles of ERAPs in peptide trimming, cytokine receptor shedding, post-natal angiogenesis and blood pressure are illustrated. In this chapter, the functions of ERAP1 not related to antigen processing will be discussed.

ERAP1 mediates **cytokine receptor shedding** (259-261), including shedding of tumor necrosis factor receptor 1 (TNFR1), IL-6 receptor alpha subunit (IL-6Rα) and type II IL-1 decoy receptor (IL-1RII). For this function, ERAP1 is associated with the plasma membrane as a type II integral membrane protein. The enzymatic activity of ERAP1 is not necessary for TNFR shedding but it rather supports the activity of the TNFR1 sheddase. On the contrary, IL-1RII and IL-6Rα shedding is dependent on the catalytic activity of ERAP1. Shedding of these receptors is important in the regulation of innate and inflammatory responses. IL-1RII shedding attenuates the bioactivity of IL-1 by binding the cytokine and preventing binding to its membrane-bound receptor and subsequent intracellular signaling. Similarly, TNFR1 shedding decreases TNF signaling. Shedded IL-6Rα, however, prolongs the half-like of bound IL-6, thereby augmenting its effects (262). Thus, ERAP1 has the ability to orchestrate immune responses by influencing cytokine signaling. In this thesis, ERAP1 expression was studied in cell lysates and immunohistochemistry. In immunohistochemical stainings, ERAP1 expression was strongly cytoplasmic and in some cases also perinuclear in normal and malignant cervical tissue and CaSki cells. Thus, a predominant role in cytokine receptor shedding in HPV-mediated malignancies can be excluded in the light of the results presented herein.

ERAP1 also plays a role in **post-natal angiogenesis** (263, 264). During the process of neo-angiogenesis, new blood vessels are formed from already existing vessels. This process is achieved by proliferation and migration of endothelial cells (ECs). ERAP1 is expressed in ECs after stimulation with vascular endothelial growth factor (VEGF) and mediates G1/S transition during EC proliferation and also spreading of ECs during vessel formation. As this function of ERAP1 is limited to ECs (265), ERAP1 overexpression in the HPV16-positive cancer cells is unlikely to have an effect on angiogenesis.

Furthermore, ERAP1 is involved in **blood pressure regulation** through the renin-angiotensin system. For this purpose, ERAP1 is secreted from cells and cleaves angiotensin II to angiotensin III and IV (57, 266), thereby preventing an increase in blood pressure. Secreted ERAP1 has the same enzymatic functions as ER-resident ERAP1, but it has a different glycosylation pattern, which is formed during secretion (267). However, it is improbable that ERAP1-mediated regulation of blood pressure poses an advantage for cancer cells. Thus, we did not investigate mechanisms associated with this ERAP function.

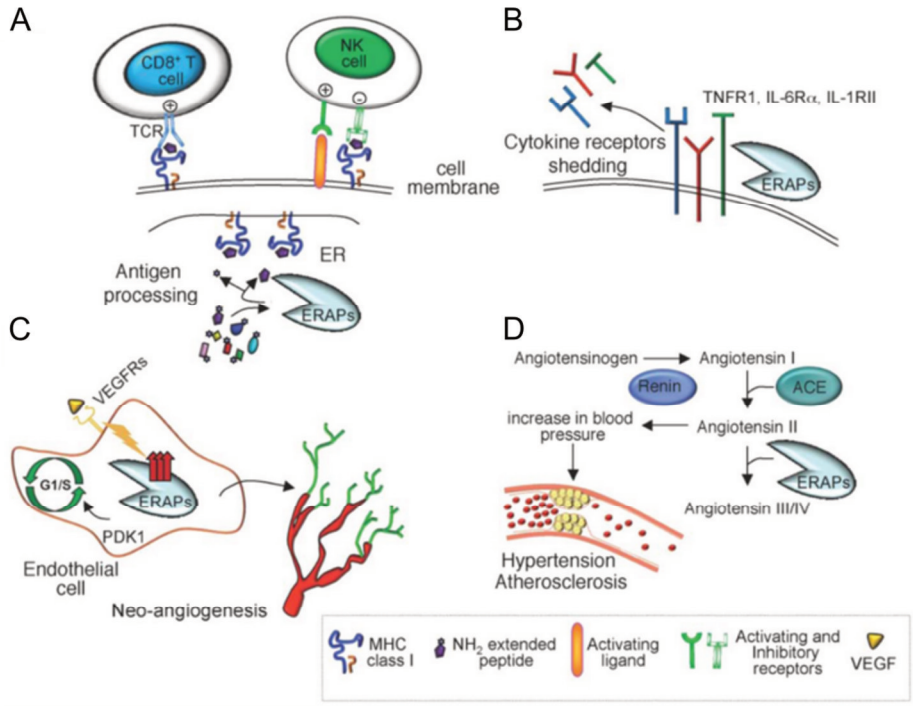

Figure 4.1: ERAPs have multiple functions. ERAP1 and ERAP2 exert functions in many physiological processes. **A.** ERAPs perform the final trimming of peptides in the ER so that they perfectly fit into the MHC I binding groove. **B.** Cell membrane-associated ERAPs are involved in the shedding of cytokine receptors. **C.** ERAPs regulate post-natal angiogenesis in endothelial cells. **D.** Secreted ERAPs play a role in blood pressure regulation. Taken from (61).

4.3.2 ERAP1 functions related to antigen processing

4.3.2.1 Effects of ERAP1 on levels of HLA class I surface expression

It is known that aberrant expression or activity of ERAP1 can lead to suboptimal peptide supply for HLA class I and thereby leads to altered stability and surface expression of HLA class I complexes (73, 268, 269). A siRNA-mediated knockdown of *ERAP1* was established (see 3.3.1) to elucidate the effect of ERAP1 expression at similar levels as in HPV-negative cells. Former studies following similar research questions in the context of other epitopes also chose siRNA- or shRNA-mediated knockdown approaches (48, 63, 83, 84, 270-272). A complete knockout of *ERAP1* was not desirable, since *ERAP1* knockout changes the whole nature of the epitope repertoire on the cell surface (273) and also does not reflect the situation in normal epithelial cells. In the absence of *ERAP1*, surface MHC I:peptide complexes are unstable, because they are mostly loaded with N-terminally extended, poorly binding peptides. This also leads to a reduced MHC I surface expression by 15% up to 80%, depending on the respective MHC I:peptide complex. However, in this study the aim was to mimic the physiologic situation in nonmalignant cells, which is given by a lower ERAP1 expression but not ERAP1 absence. Normalization of ERAP1 expression to a protein expression similar to normal levels was successfully established in several HPV16-positive cell lines (see 3.3.1.1).

The impact of *ERAP1* attenuation on surface HLA-A2 and HLA-A24 surface expression was investigated (see 3.3.1.2). HLA-A2 is one of the most common HLA class I types in the Caucasian population (223) whereas HLA-A24 is most abundant in the Asian population (274). Previous

assessments of surface MHC I presentation upon *ERAP1* knockdown led to contradictory results. One study reported decreased surface expression of murine MHC I K^k by 23% and L^d levels by 44% (270). On the contrary, another study describes an increase of overall HLA class I surface expression in HeLa cells upon ERAP1 attenuation (63). In a more recent study, the effect in 5 human tumor cell lines was tested (272). The authors demonstrated that inhibition of *ERAP1* expression affects human tumor cell lines differently with either a decreased, unchanged or increased HLA class I surface expression. This is possibly due to the differing levels of ERAP1, i.e. if they were reduced, normally or overexpressed in the respective cancer cell. Moreover, it has been recently observed that *ERAP1* knockdown improves rejection of RMA cells in mice mediated by NK cells indicating that ERAP1 affects innate immune responses as well (275). In a follow up study, it was shown, as expected, that cells with reduced MHC I expression (approximately 50%) are more susceptible to NK killing (272). In the present thesis, *ERAP1* knockdown affected HLA class I (HLA-A2 and HLA-A24) surface expression differently in 6 human HPV16-positive cell lines, which is in accordance with previous studies. HLA-A2 surface expression was significantly reduced by 34% in CaSki cells while the change in the other cell lines was not significant. Interestingly, a lowered HLA class I expression does not necessarily lower CTL responses as shown by James *et al.* (84). Presentation of the immunodominant colon carcinoma epitope GSW11 was enhanced in spite of an overall decreased MHC I expression upon ERAP1 attenuation. Different effects of *ERAP1* knockdown on MHC I surface expression are certainly also dependent on MHC I and ERAP1 alleles. Indeed, the interplay of ERAP1 and MHC I molecules seems to be very complex, because it was recently reported for the first time that ERAP1 polymorphisms can influence the surface expression of HLA class I depending on the HLA subtype (271). Haroon and colleagues further complemented previous findings by demonstrating that *ERAP1* suppression by siRNA only led to an increase in HLA class I surface expression in cells expressing certain HLA-B27 subtypes, which are associated with AS.

4.3.2.2 Effects of ERAP1 on the epitope repertoire

To fully understand the influence of ERAP1 on the peptide repertoire, it is important to know its enzymatic properties. The trimming preferences of ERAP1 have been analyzed in multiple studies. It was not possible to find a chemical determinant that renders a substrate good or bad, because ERAP1 is able to hydrolyze many residues from the N-terminus of peptides and bind peptides with different C-terminal residues. However, a preference profile of ERAP1 for its substrates could be defined. First, ERAP1 is known to have a preference for longer peptides (10 up to 16 amino acids) whereas short peptides with 8 to 9 residues, which have optimal length for MHC I, remain mostly untouched (63, 66). *In vitro* trimming assays showed that ERAP1 spared 8-mers or had strongly reduced trimming activities compared to longer peptides (63, 66, 67). In addition to *in vitro* trimming assays, there is experimental evidence in cells demonstrating that 8-mers are protected from ERAP1. For this reason, the aminopeptidase is often described to have the unique property to act as a "molecular ruler" (66). Further, ERAP1 prefers to bind peptides with a hydrophobic C-terminal residue such as isoleucine,

leucine or valine (66). At the N-terminus, ERAP1 shows highest catalytic activities towards hydrophobic amino acids such as leucine, methionine, phenylalanine, isoleucine and tyrosine (66, 276). With this in mind, it is not surprising that altered ERAP1 expression and function has most profound immunological effects with certain HLA molecules, whose peptide binding motifs are particularly sensitive to ERAP1 trimming.

Examples of autoimmune diseases

The three autoimmune diseases ankylosing spondylitis (AS), Birdshot Chorioretinopathy and Behçet's disease are associated with certain ERAP1 variants and HLA class I types. In an effort to unravel the pathogenesis mechanism of AS, a model of altered ERAP1 trimming activity was proposed. ERAP1 variants in patients were shown to mostly have either lower or higher trimming activities compared to variants isolated from healthy people (73). This imbalanced ERAP1 activity results in both cases in aberrant HLA-B27:peptide complexes and presentation. It has been proposed that aberrant forms of HLA-B27 at the cellular surface may induce inflammatory immune responses mediated by Th17 cells and innate immune cells (268), ultimately resulting in the symptoms of AS.

Birdshot Chorioretinopathy is strongly associated with HLA-A29 and genetic studies revealed that ERAP1 and ERAP2 may be genetic risk factors. In fact, it has been demonstrated that the HLA-A29 peptidome is influenced by ERAP1 variants, suggesting that certain ERAP1 SNPs predispose for the disease by altering the peptidome (74). Follow up studies will have to elucidate the consequences of this altered expression and maybe also other pathogenic mechanisms that drive disease progression.

In addition, the *ERAP1* locus has been identified in combination with HLA-B51 as a risk factor for Behçet's disease, a systemic vasculitis (245). Recently, the peptidome of HLA-B51 was studied (277) revealing that ERAP1 shapes the peptidome of HLA-B51. Taken together, the involvement of ERAP1 in inflammatory diseases stresses its pivotal role in editing immune responses by antigen processing and influencing folding and stability of HLA class I:peptide complexes. One or both of these issues may have a strong impact on the pathogenesis of these inflammatory diseases (269).

Examples of viral diseases

There is experimental evidence that ERAP1 affects immune responses to viruses such as HIV and CMV. A striking example for this phenomenon comes from the HIV research field. HIV has a high mutation rate in order to be able to evade from the host's immune system. The N-terminal region of a dominant epitope from the Gag protein is often mutated at one residue from alanine to proline. This residue change inhibits ERAP1 from trimming the precursor peptide and eventually suppresses the presentation of the dominant epitope, leading to CTL escape (68). This mechanism demonstrates how a virus-associated mutation exploits the specificity of ERAP1, because peptides with a proline (P) at position 2 (consensus motif: X-P-X_n) are poor substrates for ERAP1. These peptides are not

transported into the ER by TAP (278, 279) suggesting that they enter the ER as longer precursor peptides (motif: X_n-P-X_n) and are dependent on further trimming by ERAP1. For example, the murine MHC I molecule L^d harbors this motif. Indeed, the effect of *ERAP1* deficiency on L^d expression is very strong, with a loss of surface expression of up to 80% (273). There also is experimental evidence that ERAP1 has an impact on CTL responses towards one peptide from LCMV ($NP_{396-404}$) but not to another one (GP_{33-41}) originating from the same virus (224). CTL responses against $NP_{396-404}$ were strongly inhibited in *ERAP1* knockout mice, whereas CTL responses against GP_{33-41} were not impaired. The authors from an elegant study analyzing the impact of different peptidases on the generation of the CMV epitope $pp65_{495-503}$ reported that downregulation of *ERAP1* strongly impairs presentation of this immunodominant epitope (48). As already mentioned in chapter 4.2, human CMV encodes for a microRNA that is targeting *ERAP1* (69). Strikingly, CTL responses against 5 of 6 CMV epitopes (restricted to different HLA class I types) were inhibited by microRNA-mediated *ERAP1* attenuation.

Examples in cancer

Studies from recent years demonstrate the importance of a thorough analysis of epitope processing/presentation, which is indispensable for antigen-specific cancer immunotherapy. ERAP1 has been shown to play a role in the presentation of different clinically important tumor-associated epitopes. A study on the melanoma epitope $MART_{126-35}$ supports the hypothesis that ERAP1 can destroy tumor-associated epitopes. ERAP1 downregulation rescues $MART_{126-35}$ presentation reflected by enhanced anti-tumor CTL responses (83). Similarly, the presentation of the potent colon carcinoma epitope GSW11 is strongly enhanced when ERAP1 is attenuated (84, 86). These findings fit to studies showing that melanoma and colorectal adenocarcinoma show elevated ERAP1 expression when compared to nonmalignant counterparts (see 4.1). It is, thus, not surprising that the development of an ERAP1-specific inhibitor is an attractive tool for enhancing immunotherapies and is currently ongoing (85, 86, 280, 281). However, the efficacy and of course toxicity of newly found inhibitors remains to be studied *in vitro* and *in vivo*.

ERAP1 and HPV16-derived epitopes

In the light of the concept of epitope destruction by ERAP1 overexpression in melanoma and colon cancer cells, we investigated the role of ERAP1 overexpression in the generation of HPV16 E6 and E7-derived epitopes. Our first approach was targeted mass spectrometry (MS) analysis of 17 HLA-A2-restricted HPV16 E6 and E7 peptides in CaSki cells. These peptides were chosen because their MS detection was already established in the laboratory. The targeted MS approach was primarily designed to investigate absolute differences in presentation, i.e. to see whether there was a loss of peptides in ERAP1 overexpressing cells. With this approach we did not observe a loss of any of the 17 selected HLA-A2 HPV16 E6 and E7-derived peptides. As explained above, ERAP1 is strict in its length dependence. In this context, it has to be noted that half of the selected peptides were short 8- or 9-

mers, which are expected to be protected from ERAP1-trimming due to its "molecular ruler" function. Thus, it is not surprising to see no effects on this group of peptides. Moreover, a recent study showed that there is a considerable proportion of the peptide repertoire that is not ERAP1-dependent (282). This may explain why we did not observe a difference in the presentation of the other half of the selected peptides in cells with attenuated ERAP1 expression compared to ERAP1-overexpressing cells.

Another approach to assess HPV16 epitope presentation is the generation of peptide-specific T cell lines and cytotoxicity assays. Peptide-specific functional T cells can sense even a small variance in peptide presentation. For T cell line experiments, our choice of peptides was limited, because we had to choose peptides that were shown to have strong memory responses in our donors. We were able to generate T cell lines against the HLA-A2-restricted 11-mer $E7_{81-91}$, the HLA-A24-restircted 8-mer $E7_{69-76}$ and the HLA-A24-restricted 10-mer $E6_{90-99}$. These peptides were not contained in the MS analysis. Given the length preferences of ERAP1 we expected to observe differences in epitope presentation only in experiments with the 10-mer and 11-mer. The HLA-A24-restricted 8-mer $E7_{69-76}$ is likely too short to be prone to ERAP1 trimming. Furthermore, for HLA-A24 we had to use a target cell line that does not endogenously overexpress ERAP1 (FK16A) due to limited choice of HLA-A24-positive HPV16-positive cell lines. ERAP1 expression levels in FK16A are comparable to HPV-negative cell lines. Indeed, no enhanced killing of these cells after *ERAP1* knockdown was observed. On the contrary, we observed reduced killing of FK16A cells in cytotoxicity assays using $E7_{69-76}$-specific and $E6_{90-99}$-specific T cell lines when ERAP1 expression was attenuated (see 3.3.3.2). It is likely that the levels of ERAP1, when further knocked down in FK16A cells that express ERAP1 at low levels anyway, are no longer sufficient for proper epitope presentation.

In contrast, in the last experiment, employing a T cell line against the 11-mer $E7_{81-91}$ with naturally ERAP1-overexpressing CaSki as target cells, differences in killing were more likely to occur. Indeed, CaSki cells were killed better by this T cell line when ERAP1 expression was attenuated. Conversely, killing of 866 target cells (which also overexpress ERAP1) by the same $E7_{81-91}$-specific T cell line was not affected by ERAP1 attenuation. The difference in killing of these two target cell lines by the same T cell line may at least be partly explained by different ERAP1 alleles within these cells. As described in chapter 4.2, the enzymatic function of ERAP1 can be determined by SNPs. Thus, it is possible that ERAP1 variants in the CaSki cell line have, for instance, a higher binding affinity or trimming activity for $E7_{81-91}$, so that overexpression of the peptidase results in destruction of the peptide. Indeed, the *ERAP1* alleles in CaSki cells only harbor SNPs that are associated with a higher trimming activity in the majority of studies. In addition, *ERAP1* knockdown in CaSki cells had the strongest effect on HLA-A2 surface expression levels in comparison to other cell lines. Thus, there is a fundamental difference in CaSki cells compared to the 866 cell line considering ERAP1 alleles and the interplay with HLA-A2. The exact catalytic mechanism of ERAP1 is not known, but a "bind-trim-release" mechanism model is suggested, involving high substrate on and off rates (83, 84). Based on

this model, ERAP1 hydrolyzes one amino acid at a time and releases its substrate. The released peptide has either the chance to bind to MHC I or it will bind to ERAP1 again and the next amino acid will be cleaved. Thus, MHC I and ERAP1 compete for the available peptide pool and this competition decides about the fate of a peptide. In case of a high affinity peptide, the peptide would bind stably to MHC I and is protected from further trimming. On the contrary, low affinity peptides briefly bind to MHC I and are released again, rendering them susceptible to another round of trimming by ERAP1 before they are efficiently bound to the MHC I binding groove. Indeed, GSW11 and $MART1_{26-35}$, the peptides mentioned earlier to be strongly influenced by ERAP1, have poor binding affinities for MHC I, supporting the "bind-trim-release" mechanism (83, 84). Interestingly, the $E7_{81-91}$ epitope also has a weak binding affinity to HLA-A2 (227). It is thus very likely that this peptide is destroyed in ERAP1 overexpressing cells. As we worked with T cell lines from healthy donors, this indicates that the memory response was formed during an early stage of infection, which was subsequently cleared. In immunohistochemical stainings, we observed that ERAP1 expression increased with the disease stage. Thus, presentation of $E7_{81-91}$ may decrease with the disease stage while ERAP1 expression increases, leading to removal of a target of an existing memory response.

In conclusion, ERAP1 overexpression can hamper some HPV16-specific CD8 T cell responses and hence possibly represents a novel immune evasion mechanism of HPV-induced malignancies.

4.4 Summary and outlook

Induction of potent antitumor-specific CTL responses is crucial to develop therapeutic anti-HPV vaccines. The efficacy of these CTLs against HPV-induced lesions or tumors is significantly determined by antigen presentation of the malignant cells. In the scope of this thesis, it was demonstrated that ERAP1 is upregulated in HPV16-positive tumor cells, CIN lesions and established cervical cancer. ERAP1 plays a key role in editing the HLA class I peptidome by generating but also destroying HLA-binding peptides. It was shown by targeted MS detection that ERAP1 overexpression has no major influence on the presentation of a panel of 17 HLA-A2 HPV16 E6 and E7 epitopes. However, T cell assays using other target peptides revealed that presentation of some HPV16-derived epitopes is influenced by ERAP1 expression levels. Remarkably, a T cell line against an 11-mer E7 peptide showed increased killing upon ERAP1 attenuation in one HPV16-positive tumor cell line, indicating that destruction of this epitope may happen when ERAP1 is expressed at high levels. This implies that the overexpression of ERAP1 in advanced HPV disease stages can alter the presentation of HPV16-derived antigens. In conclusion, the results of this thesis highlight the importance of thoroughly studying the APM and the functional consequences of changes on the epitope repertoire and distinct epitopes. This analysis should always precede antigen choice of peptide-based anti-tumor immunotherapies, since the success of these therapies is strongly dependent on the presence of the exact peptide on target cells. The inhibition of ERAP1 might enhance the efficiency of immunotherapies in cases where clinically relevant epitopes are destroyed by the peptidase.

5. References

1. Murphy, K., Travers, P., Walport, M., and Janeway, C. (2012) *Janeway's immunobiology*, 8th ed., Garland Science, New York
2. Collin, M., McGovern, N., and Haniffa, M. (2013) Human dendritic cell subsets. *Immunology* **140**, 22-30
3. Steinman, R. M., and Cohn, Z. A. (1973) Pillars Article: Identification of a novel cell type in peripheral lymphoid organs of mice. I. Morphology, quantitation, tissue distribution. *J. Exp. Med.* **178**, 5-25
4. Mayer, C. T., Berod, L., and Sparwasser, T. (2012) Layers of dendritic cell-mediated T cell tolerance, their regulation and the prevention of autoimmunity. *Front Immunol* **3**, 183
5. Steinman, R. M., and Nussenzweig, M. C. (2002) Avoiding horror autotoxicus: the importance of dendritic cells in peripheral T cell tolerance. *Proc Natl Acad Sci U S A* **99**, 351-358
6. Rock, K. L. (2003) The ins and outs of cross-presentation. *Nat Immunol* **4**, 941-943
7. Paludan, C., Schmid, D., Landthaler, M., Vockerodt, M., Kube, D., Tuschl, T., and Munz, C. (2005) Endogenous MHC class II processing of a viral nuclear antigen after autophagy. *Science* **307**, 593-596
8. Joffre, O. P., Segura, E., Savina, A., and Amigorena, S. (2012) Cross-presentation by dendritic cells. *Nat Rev Immunol* **12**, 557-569
9. Alloatti, A., Kotsias, F., Pauwels, A. M., Carpier, J. M., Jouve, M., Timmerman, E., Pace, L., Vargas, P., Maurin, M., Gehrmann, U., Joannas, L., Vivar, O. I., Lennon-Dumenil, A. M., Savina, A., Gevaert, K., Beyaert, R., Hoffmann, E., and Amigorena, S. (2015) Toll-like Receptor 4 Engagement on Dendritic Cells Restrains Phago-Lysosome Fusion and Promotes Cross-Presentation of Antigens. *Immunity* **43**, 1087-1100
10. Elgueta, R., Benson, M. J., de Vries, V. C., Wasiuk, A., Guo, Y., and Noelle, R. J. (2009) Molecular mechanism and function of CD40/CD40L engagement in the immune system. *Immunol Rev* **229**, 152-172
11. Geisler, C., Larsen, J. K., and Plesner, T. (1988) Identification of alpha beta and gamma delta T cell receptor-positive cells. *Scand J Immunol* **28**, 741-745
12. Parnham, F. P. N. a. M. J. (2011) *Principles of Immunopharmacology: 3rd revised and extended edition*, Springer Basel AG
13. Takada, K., and Jameson, S. C. (2009) I T cell homeostasis: from awareness of space to a sense of place. *Nat Rev Immunol* **9**, 823-832
14. Grakoui, A., Bromley, S. K., Sumen, C., Davis, M. M., Shaw, A. S., Allen, P. M., and Dustin, M. L. (2015) Pillars article: The immunological synapse: a molecular machine controlling T cell activation. Science. 1999. 285: 221-227. *J Immunol* **194**, 4066-4072
15. Dong, C., Juedes, A. E., Temann, U. A., Shresta, S., Allison, J. P., Ruddle, N. H., and Flavell, R. A. (2001) ICOS co-stimulatory receptor is essential for T-cell activation and function. *Nature* **409**, 97-101
16. Tafuri, A., Shahinian, A., Bladt, F., Yoshinaga, S. K., Jordana, M., Wakeham, A., Boucher, L. M., Bouchard, D., Chan, V. S., Duncan, G., Odermatt, B., Ho, A., Itie, A., Horan, T., Whoriskey, J. S., Pawson, T., Penninger, J. M., Ohashi, P. S., and Mak, T. W. (2001) ICOS is essential for effective T-helper-cell responses. *Nature* **409**, 105-109
17. Walunas, T. L., Lenschow, D. J., Bakker, C. Y., Linsley, P. S., Freeman, G. J., Green, J. M., Thompson, C. B., and Bluestone, J. A. (1994) CTLA-4 can function as a negative regulator of T cell activation. *Immunity* **1**, 405-413
18. Kaplan, M. H., Hufford, M. M., and Olson, M. R. (2015) The development and in vivo function of T helper 9 cells. *Nat Rev Immunol* **15**, 295-307
19. Ma, C. S., Deenick, E. K., Batten, M., and Tangye, S. G. (2012) The origins, function, and regulation of T follicular helper cells. *J Exp Med* **209**, 1241-1253
20. Luckheeram, R. V., Zhou, R., Verma, A. D., and Xia, B. (2012) CD4(+)T cells: differentiation and functions. *Clin Dev Immunol* **2012**, 925135
21. Curotto de Lafaille, M. A., and Lafaille, J. J. (2009) Natural and adaptive foxp3+ regulatory T cells: more of the same or a division of labor? *Immunity* **30**, 626-635

22. Wang, F., Chi, J., Peng, G., Zhou, F., Wang, J., Li, L., Feng, D., Xie, F., Gu, B., Qin, J., Chen, Y., and Yao, K. (2014) Development of virus-specific CD4+ and CD8+ regulatory T cells induced by human herpesvirus 6 infection. *J Virol* **88**, 1011-1024
23. Zheng, J., Liu, Y., Liu, Y., Liu, M., Xiang, Z., Lam, K. T., Lewis, D. B., Lau, Y. L., and Tu, W. (2013) Human CD8+ regulatory T cells inhibit GVHD and preserve general immunity in humanized mice. *Sci Transl Med* **5**, 168ra169
24. Heusel, J. W., Wesselschmidt, R. L., Shresta, S., Russell, J. H., and Ley, T. J. (1994) Cytotoxic lymphocytes require granzyme B for the rapid induction of DNA fragmentation and apoptosis in allogeneic target cells. *Cell* **76**, 977-987
25. Peter, M. E., Hadji, A., Murmann, A. E., Brockway, S., Putzbach, W., Pattanayak, A., and Ceppi, P. (2015) The role of CD95 and CD95 ligand in cancer. *Cell Death Differ* **22**, 549-559
26. Li-Weber, M., and Krammer, P. H. (2002) The death of a T-cell: expression of the CD95 ligand. *Cell Death Differ* **9**, 101-103
27. Sallusto, F., Geginat, J., and Lanzavecchia, A. (2004) Central memory and effector memory T cell subsets: function, generation, and maintenance. *Annu Rev Immunol* **22**, 745-763
28. Leone, P., Shin, E. C., Perosa, F., Vacca, A., Dammacco, F., and Racanelli, V. (2013) MHC class I antigen processing and presenting machinery: organization, function, and defects in tumor cells. *J Natl Cancer Inst* **105**, 1172-1187
29. Vyas, J. M., Van der Veen, A. G., and Ploegh, H. L. (2008) The known unknowns of antigen processing and presentation. *Nat Rev Immunol* **8**, 607-618
30. Rammensee, H. G. (1995) Chemistry of peptides associated with MHC class I and class II molecules. *Curr Opin Immunol* **7**, 85-96
31. Goldberg, A. L. (2003) Protein degradation and protection against misfolded or damaged proteins. *Nature* **426**, 895-899
32. Schubert, U., Anton, L. C., Gibbs, J., Norbury, C. C., Yewdell, J. W., and Bennink, J. R. (2000) Rapid degradation of a large fraction of newly synthesized proteins by proteasomes. *Nature* **404**, 770-774
33. Yewdell, J. W., Schubert, U., and Bennink, J. R. (2001) At the crossroads of cell biology and immunology: DRiPs and other sources of peptide ligands for MHC class I molecules. *J Cell Sci* **114**, 845-851
34. Seufert, W., and Jentsch, S. (1990) Ubiquitin-conjugating enzymes UBC4 and UBC5 mediate selective degradation of short-lived and abnormal proteins. *EMBO J* **9**, 543-550
35. Tanaka, K. (2009) The proteasome: overview of structure and functions. *Proc Jpn Acad Ser B Phys Biol Sci* **85**, 12-36
36. Dick, T. P., Nussbaum, A. K., Deeg, M., Heinemeyer, W., Groll, M., Schirle, M., Keilholz, W., Stevanovic, S., Wolf, D. H., Huber, R., Rammensee, H. G., and Schild, H. (1998) Contribution of proteasomal beta-subunits to the cleavage of peptide substrates analyzed with yeast mutants. *J Biol Chem* **273**, 25637-25646
37. Heinemeyer, W., Fischer, M., Krimmer, T., Stachon, U., and Wolf, D. H. (1997) The active sites of the eukaryotic 20 S proteasome and their involvement in subunit precursor processing. *J Biol Chem* **272**, 25200-25209
38. Braun, B. C., Glickman, M., Kraft, R., Dahlmann, B., Kloetzel, P. M., Finley, D., and Schmidt, M. (1999) The base of the proteasome regulatory particle exhibits chaperone-like activity. *Nat Cell Biol* **1**, 221-226
39. Shin, E. C., Seifert, U., Kato, T., Rice, C. M., Feinstone, S. M., Kloetzel, P. M., and Rehermann, B. (2006) Virus-induced type I IFN stimulates generation of immunoproteasomes at the site of infection. *J Clin Invest* **116**, 3006-3014
40. Sorokin, A. V., Kim, E. R., and Ovchinnikov, L. P. (2009) Proteasome system of protein degradation and processing. *Biochemistry (Mosc)* **74**, 1411-1442
41. Stohwasser, R., Standera, S., Peters, I., Kloetzel, P. M., and Groettrup, M. (1997) Molecular cloning of the mouse proteasome subunits MC14 and MECL-1: reciprocally regulated tissue expression of interferon-gamma-modulated proteasome subunits. *Eur J Immunol* **27**, 1182-1187
42. Macagno, A., Gilliet, M., Sallusto, F., Lanzavecchia, A., Nestle, F. O., and Groettrup, M. (1999) Dendritic cells up-regulate immunoproteasomes and the proteasome regulator PA28 during maturation. *Eur J Immunol* **29**, 4037-4042

43. Strehl, B., Seifert, U., Kruger, E., Heink, S., Kuckelkorn, U., and Kloetzel, P. M. (2005) Interferon-gamma, the functional plasticity of the ubiquitin-proteasome system, and MHC class I antigen processing. *Immunol Rev* **207**, 19-30
44. Raule, M., Cerruti, F., Benaroudj, N., Migotti, R., Kikuchi, J., Bachi, A., Navon, A., Dittmar, G., and Cascio, P. (2014) PA28alphabeta reduces size and increases hydrophilicity of 20S immunoproteasome peptide products. *Chem Biol* **21**, 470-480
45. Kessler, J. H., Khan, S., Seifert, U., Le Gall, S., Chow, K. M., Paschen, A., Bres-Vloemans, S. A., de Ru, A., van Montfoort, N., Franken, K. L., Benckhuijsen, W. E., Brooks, J. M., van Hall, T., Ray, K., Mulder, A., Doxiadis, II, van Swieten, P. F., Overkleeft, H. S., Prat, A., Tomkinson, B., Neefjes, J., Kloetzel, P. M., Rodgers, D. W., Hersh, L. B., Drijfhout, J. W., van Veelen, P. A., Ossendorp, F., and Melief, C. J. (2011) Antigen processing by nardilysin and thimet oligopeptidase generates cytotoxic T cell epitopes. *Nat Immunol* **12**, 45-53
46. Seifert, U., Maranon, C., Shmueli, A., Desoutter, J. F., Wesoloski, L., Janek, K., Henklein, P., Diescher, S., Andrieu, M., de la Salle, H., Weinschenk, T., Schild, H., Laderach, D., Galy, A., Haas, G., Kloetzel, P. M., Reiss, Y., and Hosmalin, A. (2003) An essential role for tripeptidyl peptidase in the generation of an MHC class I epitope. *Nat Immunol* **4**, 375-379
47. Firat, E., Huai, J., Saveanu, L., Gaedicke, S., Aichele, P., Eichmann, K., van Endert, P., and Niedermann, G. (2007) Analysis of direct and cross-presentation of antigens in TPPII knockout mice. *J Immunol* **179**, 8137-8145
48. Urban, S., Textoris-Taube, K., Reimann, B., Janek, K., Dannenberg, T., Ebstein, F., Seifert, C., Zhao, F., Kessler, J. H., Halenius, A., Henklein, P., Paschke, J., Cadel, S., Bernhard, H., Ossendorp, F., Foulon, T., Schadendorf, D., Paschen, A., and Seifert, U. (2012) The efficiency of human cytomegalovirus pp65(495-503) CD8+ T cell epitope generation is determined by the balanced activities of cytosolic and endoplasmic reticulum-resident peptidases. *J Immunol* **189**, 529-538
49. Weimershaus, M., Evnouchidou, I., Saveanu, L., and van Endert, P. (2013) Peptidases trimming MHC class I ligands. *Curr Opin Immunol* **25**, 90-96
50. Higgins, C. F., and Linton, K. J. (2004) The ATP switch model for ABC transporters. *Nat Struct Mol Biol* **11**, 918-926
51. Momburg, F., Roelse, J., Hammerling, G. J., and Neefjes, J. J. (1994) Peptide size selection by the major histocompatibility complex-encoded peptide transporter. *J Exp Med* **179**, 1613-1623
52. Saveanu, L., Carroll, O., Weimershaus, M., Guermonprez, P., Firat, E., Lindo, V., Greer, F., Davoust, J., Kratzer, R., Keller, S. R., Niedermann, G., and van Endert, P. (2009) IRAP identifies an endosomal compartment required for MHC class I cross-presentation. *Science* **325**, 213-217
53. Oliver, J. D., Roderick, H. L., Llewellyn, D. H., and High, S. (1999) ERp57 functions as a subunit of specific complexes formed with the ER lectins calreticulin and calnexin. *Mol Biol Cell* **10**, 2573-2582
54. Sadasivan, B., Lehner, P. J., Ortmann, B., Spies, T., and Cresswell, P. (1996) Roles for calreticulin and a novel glycoprotein, tapasin, in the interaction of MHC class I molecules with TAP. *Immunity* **5**, 103-114
55. Seliger, B., Maeurer, M. J., and Ferrone, S. (2000) Antigen-processing machinery breakdown and tumor growth. *Immunol Today* **21**, 455-464
56. Seliger, B. (2008) Different regulation of MHC class I antigen processing components in human tumors. *J Immunotoxicol* **5**, 361-367
57. Hattori, A., Matsumoto, H., Mizutani, S., and Tsujimoto, M. (1999) Molecular cloning of adipocyte-derived leucine aminopeptidase highly related to placental leucine aminopeptidase/oxytocinase. *J Biochem* **125**, 931-938
58. Tsujimoto, M., and Hattori, A. (2005) The oxytocinase subfamily of M1 aminopeptidases. *Biochim Biophys Acta* **1751**, 9-18
59. Andres, A. M., Dennis, M. Y., Kretzschmar, W. W., Cannons, J. L., Lee-Lin, S. Q., Hurle, B., Program, N. C. S., Schwartzberg, P. L., Williamson, S. H., Bustamante, C. D., Nielsen, R., Clark, A. G., and Green, E. D. (2010) Balancing selection maintains a form of ERAP2 that undergoes nonsense-mediated decay and affects antigen presentation. *PLoS Genet* **6**, e1001157

60. Saveanu, L., Carroll, O., Lindo, V., Del Val, M., Lopez, D., Lepelletier, Y., Greer, F., Schomburg, L., Fruci, D., Niedermann, G., and van Endert, P. M. (2005) Concerted peptide trimming by human ERAP1 and ERAP2 aminopeptidase complexes in the endoplasmic reticulum. *Nat Immunol* **6**, 689-697
61. Cifaldi, L., Romania, P., Lorenzi, S., Locatelli, F., and Fruci, D. (2012) Role of endoplasmic reticulum aminopeptidases in health and disease: from infection to cancer. *Int J Mol Sci* **13**, 8338-8352
62. Stratikos, E., and Stern, L. J. (2013) Antigenic peptide trimming by ER aminopeptidases--insights from structural studies. *Mol Immunol* **55**, 212-219
63. York, I. A., Chang, S. C., Saric, T., Keys, J. A., Favreau, J. M., Goldberg, A. L., and Rock, K. L. (2002) The ER aminopeptidase ERAP1 enhances or limits antigen presentation by trimming epitopes to 8-9 residues. *Nat Immunol* **3**, 1177-1184
64. York, I. A., Brehm, M. A., Zendzian, S., Towne, C. F., and Rock, K. L. (2006) Endoplasmic reticulum aminopeptidase 1 (ERAP1) trims MHC class I-presented peptides in vivo and plays an important role in immunodominance. *Proc Natl Acad Sci U S A* **103**, 9202-9207
65. Hammer, G. E., Gonzalez, F., James, E., Nolla, H., and Shastri, N. (2007) In the absence of aminopeptidase ERAAP, MHC class I molecules present many unstable and highly immunogenic peptides. *Nat Immunol* **8**, 101-108
66. Chang, S. C., Momburg, F., Bhutani, N., and Goldberg, A. L. (2005) The ER aminopeptidase, ERAP1, trims precursors to lengths of MHC class I peptides by a "molecular ruler" mechanism. *Proc Natl Acad Sci U S A* **102**, 17107-17112
67. Saric, T., Chang, S. C., Hattori, A., York, I. A., Markant, S., Rock, K. L., Tsujimoto, M., and Goldberg, A. L. (2002) An IFN-gamma-induced aminopeptidase in the ER, ERAP1, trims precursors to MHC class I-presented peptides. *Nat Immunol* **3**, 1169-1176
68. Draenert, R., Le Gall, S., Pfafferott, K. J., Leslie, A. J., Chetty, P., Brander, C., Holmes, E. C., Chang, S. C., Feeney, M. E., Addo, M. M., Ruiz, L., Ramduth, D., Jeena, P., Altfeld, M., Thomas, S., Tang, Y., Verrill, C. L., Dixon, C., Prado, J. G., Kiepiela, P., Martinez-Picado, J., Walker, B. D., and Goulder, P. J. (2004) Immune selection for altered antigen processing leads to cytotoxic T lymphocyte escape in chronic HIV-1 infection. *J Exp Med* **199**, 905-915
69. Kim, S., Lee, S., Shin, J., Kim, Y., Evnouchidou, I., Kim, D., Kim, Y. K., Kim, Y. E., Ahn, J. H., Riddell, S. R., Stratikos, E., Kim, V. N., and Ahn, K. (2011) Human cytomegalovirus microRNA miR-US4-1 inhibits CD8(+) T cell responses by targeting the aminopeptidase ERAP1. *Nat Immunol* **12**, 984-991
70. Fierabracci, A., Milillo, A., Locatelli, F., and Fruci, D. (2012) The putative role of endoplasmic reticulum aminopeptidases in autoimmunity: insights from genomic-wide association studies. *Autoimmun Rev* **12**, 281-288
71. Evans, D. M., Spencer, C. C., Pointon, J. J., Su, Z., Harvey, D., Kochan, G., Oppermann, U., Dilthey, A., Pirinen, M., Stone, M. A., Appleton, L., Moutsianas, L., Leslie, S., Wordsworth, T., Kenna, T. J., Karaderi, T., Thomas, G. P., Ward, M. M., Weisman, M. H., Farrar, C., Bradbury, L. A., Danoy, P., Inman, R. D., Maksymowych, W., Gladman, D., Rahman, P., Spondyloarthritis Research Consortium of, C., Morgan, A., Marzo-Ortega, H., Bowness, P., Gaffney, K., Gaston, J. S., Smith, M., Bruges-Armas, J., Couto, A. R., Sorrentino, R., Paladini, F., Ferreira, M. A., Xu, H., Liu, Y., Jiang, L., Lopez-Larrea, C., Diaz-Pena, R., Lopez-Vazquez, A., Zayats, T., Band, G., Bellenguez, C., Blackburn, H., Blackwell, J. M., Bramon, E., Bumpstead, S. J., Casas, J. P., Corvin, A., Craddock, N., Deloukas, P., Dronov, S., Duncanson, A., Edkins, S., Freeman, C., Gillman, M., Gray, E., Gwilliam, R., Hammond, N., Hunt, S. E., Jankowski, J., Jayakumar, A., Langford, C., Liddle, J., Markus, H. S., Mathew, C. G., McCann, O. T., McCarthy, M. I., Palmer, C. N., Peltonen, L., Plomin, R., Potter, S. C., Rautanen, A., Ravindrarajah, R., Ricketts, M., Samani, N., Sawcer, S. J., Strange, A., Trembath, R. C., Viswanathan, A. C., Waller, M., Weston, P., Whittaker, P., Widaa, S., Wood, N. W., McVean, G., Reveille, J. D., Wordsworth, B. P., Brown, M. A., Donnelly, P., Australo-Anglo-American Spondyloarthritis, C., and Wellcome Trust Case Control, C. (2011) Interaction between ERAP1 and HLA-B27 in ankylosing spondylitis implicates peptide handling in the mechanism for HLA-B27 in disease susceptibility. *Nat Genet* **43**, 761-767

72. Evnouchidou, I., Kamal, R. P., Seregin, S. S., Goto, Y., Tsujimoto, M., Hattori, A., Voulgari, P. V., Drosos, A. A., Amalfitano, A., York, I. A., and Stratikos, E. (2011) Cutting Edge: Coding single nucleotide polymorphisms of endoplasmic reticulum aminopeptidase 1 can affect antigenic peptide generation in vitro by influencing basic enzymatic properties of the enzyme. *J Immunol* **186**, 1909-1913
73. Reeves, E., Colebatch-Bourn, A., Elliott, T., Edwards, C. J., and James, E. (2014) Functionally distinct ERAP1 allotype combinations distinguish individuals with Ankylosing Spondylitis. *Proc Natl Acad Sci U S A* **111**, 17594-17599
74. Alvarez-Navarro, C., Martin-Esteban, A., Barnea, E., Admon, A., and Lopez de Castro, J. A. (2015) Endoplasmic Reticulum Aminopeptidase 1 (ERAP1) Polymorphism Relevant to Inflammatory Disease Shapes the Peptidome of the Birdshot Chorioretinopathy-Associated HLA-A*29:02 Antigen. *Mol Cell Proteomics* **14**, 1770-1780
75. GeneticAnalysisofPsoriasisConsortium&theWellcomeTrustCaseControlConsortium2, Strange, A., Capon, F., Spencer, C. C., Knight, J., Weale, M. E., Allen, M. H., Barton, A., Band, G., Bellenguez, C., Bergboer, J. G., Blackwell, J. M., Bramon, E., Bumpstead, S. J., Casas, J. P., Cork, M. J., Corvin, A., Deloukas, P., Dilthey, A., Duncanson, A., Edkins, S., Estivill, X., Fitzgerald, O., Freeman, C., Giardina, E., Gray, E., Hofer, A., Huffmeier, U., Hunt, S. E., Irvine, A. D., Jankowski, J., Kirby, B., Langford, C., Lascorz, J., Leman, J., Leslie, S., Mallbris, L., Markus, H. S., Mathew, C. G., McLean, W. H., McManus, R., Mossner, R., Moutsianas, L., Naluai, A. T., Nestle, F. O., Novelli, G., Onoufriadis, A., Palmer, C. N., Perricone, C., Pirinen, M., Plomin, R., Potter, S. C., Pujol, R. M., Rautanen, A., Riveira-Munoz, E., Ryan, A. W., Salmhofer, W., Samuelsson, L., Sawcer, S. J., Schalkwijk, J., Smith, C. H., Stahle, M., Su, Z., Tazi-Ahnini, R., Traupe, H., Viswanathan, A. C., Warren, R. B., Weger, W., Wolk, K., Wood, N., Worthington, J., Young, H. S., Zeeuwen, P. L., Hayday, A., Burden, A. D., Griffiths, C. E., Kere, J., Reis, A., McVean, G., Evans, D. M., Brown, M. A., Barker, J. N., Peltonen, L., Donnelly, P., and Trembath, R. C. (2010) A genome-wide association study identifies new psoriasis susceptibility loci and an interaction between HLA-C and ERAP1. *Nat Genet* **42**, 985-990
76. Kirino, Y., Zhou, Q., Ishigatsubo, Y., Mizuki, N., Tugal-Tutkun, I., Seyahi, E., Ozyazgan, Y., Ugurlu, S., Erer, B., Abaci, N., Ustek, D., Meguro, A., Ueda, A., Takeno, M., Inoko, H., Ombrello, M. J., Satorius, C. L., Maskeri, B., Mullikin, J. C., Sun, H. W., Gutierrez-Cruz, G., Kim, Y., Wilson, A. F., Kastner, D. L., Gul, A., and Remmers, E. F. (2013) Targeted resequencing implicates the familial Mediterranean fever gene MEFV and the toll-like receptor 4 gene TLR4 in Behcet disease. *Proc Natl Acad Sci U S A* **110**, 8134-8139
77. Fruci, D., Ferracuti, S., Limongi, M. Z., Cunsolo, V., Giorda, E., Fraioli, R., Sibilio, L., Carroll, O., Hattori, A., van Endert, P. M., and Giacomini, P. (2006) Expression of endoplasmic reticulum aminopeptidases in EBV-B cell lines from healthy donors and in leukemia/lymphoma, carcinoma, and melanoma cell lines. *J Immunol* **176**, 4869-4879
78. Fruci, D., Giacomini, P., Nicotra, M. R., Forloni, M., Fraioli, R., Saveanu, L., van Endert, P., and Natali, P. G. (2008) Altered expression of endoplasmic reticulum aminopeptidases ERAP1 and ERAP2 in transformed non-lymphoid human tissues. *J Cell Physiol* **216**, 742-749
79. Stoehr, C. G., Buettner-Herold, M., Kamphausen, E., Bertz, S., Hartmann, A., and Seliger, B. (2013) Comparative expression profiling for human endoplasmic reticulum-resident aminopeptidases 1 and 2 in normal kidney versus distinct renal cell carcinoma subtypes. *Int J Clin Exp Pathol* **6**, 998-1008
80. Uhlen, M., Fagerberg, L., Hallstrom, B. M., Lindskog, C., Oksvold, P., Mardinoglu, A., Sivertsson, A., Kampf, C., Sjostedt, E., Asplund, A., Olsson, I., Edlund, K., Lundberg, E., Navani, S., Szigyarto, C. A., Odeberg, J., Djureinovic, D., Takanen, J. O., Hober, S., Alm, T., Edqvist, P. H., Berling, H., Tegel, H., Mulder, J., Rockberg, J., Nilsson, P., Schwenk, J. M., Hamsten, M., von Feilitzen, K., Forsberg, M., Persson, L., Johansson, F., Zwahlen, M., von Heijne, G., Nielsen, J., and Ponten, F. (2015) Proteomics. Tissue-based map of the human proteome. *Science* **347**, 1260419
81. Mehta, A. M., Jordanova, E. S., Kenter, G. G., Ferrone, S., and Fleuren, G. J. (2008) Association of antigen processing machinery and HLA class I defects with clinicopathological outcome in cervical carcinoma. *Cancer Immunol Immunother* **57**, 197-206

82. Mehta, A. M., Jordanova, E. S., Corver, W. E., van Wezel, T., Uh, H. W., Kenter, G. G., and Jan Fleuren, G. (2009) Single nucleotide polymorphisms in antigen processing machinery component ERAP1 significantly associate with clinical outcome in cervical carcinoma. *Genes Chromosomes Cancer* **48**, 410-418
83. Keller, M., Ebstein, F., Burger, E., Textoris-Taube, K., Gorny, X., Urban, S., Zhao, F., Dannenberg, T., Sucker, A., Keller, C., Saveanu, L., Kruger, E., Rothkotter, H. J., Dahlmann, B., Henklein, P., Voigt, A., Kuckelkorn, U., Paschen, A., Kloetzel, P. M., and Seifert, U. (2015) The proteasome immunosubunits, PA28 and ER-aminopeptidase 1 protect melanoma cells from efficient MART-126-35 -specific T-cell recognition. *Eur J Immunol* **45**, 3257-3268
84. James, E., Bailey, I., Sugiyarto, G., and Elliott, T. (2013) Induction of protective antitumor immunity through attenuation of ERAAP function. *J Immunol* **190**, 5839-5846
85. Papakyriakou, A., Zervoudi, E., Theodorakis, E. A., Saveanu, L., Stratikos, E., and Vourloumis, D. (2013) Novel selective inhibitors of aminopeptidases that generate antigenic peptides. *Bioorg Med Chem Lett* **23**, 4832-4836
86. Zervoudi, E., Saridakis, E., Birtley, J. R., Seregin, S. S., Reeves, E., Kokkala, P., Aldhamen, Y. A., Amalfitano, A., Mavridis, I. M., James, E., Georgiadis, D., and Stratikos, E. (2013) Rationally designed inhibitor targeting antigen-trimming aminopeptidases enhances antigen presentation and cytotoxic T-cell responses. *Proc Natl Acad Sci U S A* **110**, 19890-19895
87. Van Doorslaer, K., Tan, Q., Xirasagar, S., Bandaru, S., Gopalan, V., Mohamoud, Y., Huyen, Y., and McBride, A. A. (2013) The Papillomavirus Episteme: a central resource for papillomavirus sequence data and analysis. *Nucleic Acids Res* **41**, D571-578
88. zur Hausen, H., Gissmann, L., Steiner, W., Dippold, W., and Dreger, I. (1975) Human papilloma viruses and cancer. *Bibl Haematol*, 569-571
89. zur Hausen, H. (1977) Human papillomaviruses and their possible role in squamous cell carcinomas. *Curr Top Microbiol Immunol* **78**, 1-30
90. Durst, M., Gissmann, L., Ikenberg, H., and zur Hausen, H. (1983) A papillomavirus DNA from a cervical carcinoma and its prevalence in cancer biopsy samples from different geographic regions. *Proc Natl Acad Sci U S A* **80**, 3812-3815
91. Boshart, M., Gissmann, L., Ikenberg, H., Kleinheinz, A., Scheurlen, W., and zur Hausen, H. (1984) A new type of papillomavirus DNA, its presence in genital cancer biopsies and in cell lines derived from cervical cancer. *EMBO J* **3**, 1151-1157
92. Gissmann, L., Boshart, M., Durst, M., Ikenberg, H., Wagner, D., and zur Hausen, H. (1984) Presence of human papillomavirus in genital tumors. *J Invest Dermatol* **83**, 26s-28s
93. zur Hausen, H. (2009) Papillomaviruses in the causation of human cancers - a brief historical account. *Virology* **384**, 260-265
94. Forman, D., de Martel, C., Lacey, C. J., Soerjomataram, I., Lortet-Tieulent, J., Bruni, L., Vignat, J., Ferlay, J., Bray, F., Plummer, M., and Franceschi, S. (2012) Global burden of human papillomavirus and related diseases. *Vaccine* **30 Suppl 5**, F12-23
95. Moscicki, A. B., Schiffman, M., Burchell, A., Albero, G., Giuliano, A. R., Goodman, M. T., Kjaer, S. K., and Palefsky, J. (2012) Updating the natural history of human papillomavirus and anogenital cancers. *Vaccine* **30 Suppl 5**, F24-33
96. Gillison, M. L., Alemany, L., Snijders, P. J., Chaturvedi, A., Steinberg, B. M., Schwartz, S., and Castellsague, X. (2012) Human papillomavirus and diseases of the upper airway: head and neck cancer and respiratory papillomatosis. *Vaccine* **30 Suppl 5**, F34-54
97. WHO. (2015) Human papillomavirus (HPV) and cervical cancer; Fact sheet Nr. 380.
98. Goon, P., Sonnex, C., Jani, P., Stanley, M., and Sudhoff, H. (2008) Recurrent respiratory papillomatosis: an overview of current thinking and treatment. *Eur Arch Otorhinolaryngol* **265**, 147-151
99. Egawa, N., Egawa, K., Griffin, H., and Doorbar, J. (2015) Human Papillomaviruses; Epithelial Tropisms, and the Development of Neoplasia. *Viruses* **7**, 3863-3890
100. Ottinger, M., Smith, J. A., Schweiger, M. R., Robbins, D., Powell, M. L., You, J., and Howley, P. M. (2009) Cell-type specific transcriptional activities among different papillomavirus long control regions and their regulation by E2. *Virology* **395**, 161-171
101. Munoz, N., Castellsague, X., de Gonzalez, A. B., and Gissmann, L. (2006) Chapter 1: HPV in the etiology of human cancer. *Vaccine* **24 Suppl 3**, S3/1-10

102. Woodman, C. B., Collins, S. I., and Young, L. S. (2007) The natural history of cervical HPV infection: unresolved issues. *Nat Rev Cancer* **7**, 11-22
103. Crosbie, E. J., Einstein, M. H., Franceschi, S., and Kitchener, H. C. (2013) Human papillomavirus and cervical cancer. *Lancet* **382**, 889-899
104. Stanley, M. (2008) Immunobiology of HPV and HPV vaccines. *Gynecol Oncol* **109**, S15-21
105. Doorbar, J., Egawa, N., Griffin, H., Kranjec, C., and Murakami, I. (2015) Human papillomavirus molecular biology and disease association. *Rev Med Virol* **25 Suppl 1**, 2-23
106. Zheng, Z. M., and Baker, C. C. (2006) Papillomavirus genome structure, expression, and post-transcriptional regulation. *Front Biosci* **11**, 2286-2302
107. Johansson, C., and Schwartz, S. (2013) Regulation of human papillomavirus gene expression by splicing and polyadenylation. *Nat Rev Microbiol* **11**, 239-251
108. Stanley, M. A. (2012) Epithelial cell responses to infection with human papillomavirus. *Clin Microbiol Rev* **25**, 215-222
109. Doorbar, J., Quint, W., Banks, L., Bravo, I. G., Stoler, M., Broker, T. R., and Stanley, M. A. (2012) The biology and life-cycle of human papillomaviruses. *Vaccine* **30 Suppl 5**, F55-70
110. Pyeon, D., Pearce, S. M., Lank, S. M., Ahlquist, P., and Lambert, P. F. (2009) Establishment of human papillomavirus infection requires cell cycle progression. *PLoS Pathog* **5**, e1000318
111. Herfs, M., Yamamoto, Y., Laury, A., Wang, X., Nucci, M. R., McLaughlin-Drubin, M. E., Munger, K., Feldman, S., McKeon, F. D., Xian, W., and Crum, C. P. (2012) A discrete population of squamocolumnar junction cells implicated in the pathogenesis of cervical cancer. *Proc Natl Acad Sci U S A* **109**, 10516-10521
112. Gravitt, P. E., Lacey, J. V., Jr., Brinton, L. A., Barnes, W. A., Kornegay, J. R., Greenberg, M. D., Greene, S. M., Hadjimichael, O. C., McGowan, L., Mortel, R., Schwartz, P. E., Zaino, R., and Hildesheim, A. (2001) Evaluation of self-collected cervicovaginal cell samples for human papillomavirus testing by polymerase chain reaction. *Cancer Epidemiol Biomarkers Prev* **10**, 95-100
113. Bosch, F. X., and de Sanjose, S. (2003) Chapter 1: Human papillomavirus and cervical cancer--burden and assessment of causality. *J Natl Cancer Inst Monogr*, 3-13
114. Maglennon, G. A., McIntosh, P., and Doorbar, J. (2011) Persistence of viral DNA in the epithelial basal layer suggests a model for papillomavirus latency following immune regression. *Virology* **414**, 153-163
115. Doorbar, J. (2006) Molecular biology of human papillomavirus infection and cervical cancer. *Clin Sci (Lond)* **110**, 525-541
116. Klingelhutz, A. J., and Roman, A. (2012) Cellular transformation by human papillomaviruses: lessons learned by comparing high- and low-risk viruses. *Virology* **424**, 77-98
117. Felsani, A., Mileo, A. M., and Paggi, M. G. (2006) Retinoblastoma family proteins as key targets of the small DNA virus oncoproteins. *Oncogene* **25**, 5277-5285
118. Klaes, R., Friedrich, T., Spitkovsky, D., Ridder, R., Rudy, W., Petry, U., Dallenbach-Hellweg, G., Schmidt, D., and von Knebel Doeberitz, M. (2001) Overexpression of p16(INK4A) as a specific marker for dysplastic and neoplastic epithelial cells of the cervix uteri. *Int J Cancer* **92**, 276-284
119. Elsum, I., Yates, L., Humbert, P. O., and Richardson, H. E. (2012) The Scribble-Dlg-Lgl polarity module in development and cancer: from flies to man. *Essays Biochem* **53**, 141-168
120. Modis, Y., Trus, B. L., and Harrison, S. C. (2002) Atomic model of the papillomavirus capsid. *EMBO J* **21**, 4754-4762
121. Frazer, I. H., Leggatt, G. R., and Mattarollo, S. R. (2011) Prevention and treatment of papillomavirus-related cancers through immunization. *Annu Rev Immunol* **29**, 111-138
122. Isaacson Wechsler, E., Wang, Q., Roberts, I., Pagliarulo, E., Jackson, D., Untersperger, C., Coleman, N., Griffin, H., and Doorbar, J. (2012) Reconstruction of human papillomavirus type 16-mediated early-stage neoplasia implicates E6/E7 deregulation and the loss of contact inhibition in neoplastic progression. *J Virol* **86**, 6358-6364
123. Stanley, M. (2006) Immune responses to human papillomavirus. *Vaccine* **24 Suppl 1**, S16-22
124. Stern, P. L., and Einstein, M. H. (2012) *HPV and Cervical Cancer: Achievements in Prevention and Future Prospects*, Springer Science+Business Media

125. Grabowska, A. K., and Riemer, A. B. (2012) The invisible enemy - how human papillomaviruses avoid recognition and clearance by the host immune system. *Open Virol J* **6**, 249-256
126. Matthews, K., Leong, C. M., Baxter, L., Inglis, E., Yun, K., Backstrom, B. T., Doorbar, J., and Hibma, M. (2003) Depletion of Langerhans cells in human papillomavirus type 16-infected skin is associated with E6-mediated down regulation of E-cadherin. *J Virol* **77**, 8378-8385
127. Guess, J. C., and McCance, D. J. (2005) Decreased migration of Langerhans precursor-like cells in response to human keratinocytes expressing human papillomavirus type 16 E6/E7 is related to reduced macrophage inflammatory protein-3alpha production. *J Virol* **79**, 14852-14862
128. Hasan, U. A., Bates, E., Takeshita, F., Biliato, A., Accardi, R., Bouvard, V., Mansour, M., Vincent, I., Gissmann, L., Iftner, T., Sideri, M., Stubenrauch, F., and Tommasino, M. (2007) TLR9 expression and function is abolished by the cervical cancer-associated human papillomavirus type 16. *J Immunol* **178**, 3186-3197
129. Rincon-Orozco, B., Halec, G., Rosenberger, S., Muschik, D., Nindl, I., Bachmann, A., Ritter, T. M., Dondog, B., Ly, R., Bosch, F. X., Zawatzky, R., and Rosl, F. (2009) Epigenetic silencing of interferon-kappa in human papillomavirus type 16-positive cells. *Cancer Res* **69**, 8718-8725
130. Karim, R., Meyers, C., Backendorf, C., Ludigs, K., Offringa, R., van Ommen, G. J., Melief, C. J., van der Burg, S. H., and Boer, J. M. (2011) Human papillomavirus deregulates the response of a cellular network comprising of chemotactic and proinflammatory genes. *PLoS One* **6**, e17848
131. Niebler, M., Qian, X., Hofler, D., Kogosov, V., Kaewprag, J., Kaufmann, A. M., Ly, R., Bohmer, G., Zawatzky, R., Rosl, F., and Rincon-Orozco, B. (2013) Post-translational control of IL-1beta via the human papillomavirus type 16 E6 oncoprotein: a novel mechanism of innate immune escape mediated by the E3-ubiquitin ligase E6-AP and p53. *PLoS Pathog* **9**, e1003536
132. Evans, M., Borysiewicz, L. K., Evans, A. S., Rowe, M., Jones, M., Gileadi, U., Cerundolo, V., and Man, S. (2001) Antigen processing defects in cervical carcinomas limit the presentation of a CTL epitope from human papillomavirus 16 E6. *J Immunol* **167**, 5420-5428
133. Georgopoulos, N. T., Proffitt, J. L., and Blair, G. E. (2000) Transcriptional regulation of the major histocompatibility complex (MHC) class I heavy chain, TAP1 and LMP2 genes by the human papillomavirus (HPV) type 6b, 16 and 18 E7 oncoproteins. *Oncogene* **19**, 4930-4935
134. Hasim, A., Abudula, M., Aimiduo, R., Ma, J. Q., Jiao, Z., Akula, G., Wang, T., and Abudula, A. (2012) Post-transcriptional and epigenetic regulation of antigen processing machinery (APM) components and HLA-I in cervical cancers from Uighur women. *PLoS One* **7**, e44952
135. Ashrafi, G. H., Haghshenas, M. R., Marchetti, B., O'Brien, P. M., and Campo, M. S. (2005) E5 protein of human papillomavirus type 16 selectively downregulates surface HLA class I. *Int J Cancer* **113**, 276-283
136. Schapiro, F., Sparkowski, J., Adduci, A., Suprynowicz, F., Schlegel, R., and Grinstein, S. (2000) Golgi alkalinization by the papillomavirus E5 oncoprotein. *J Cell Biol* **148**, 305-315
137. Azar, K. K., Tani, M., Yasuda, H., Sakai, A., Inoue, M., and Sasagawa, T. (2004) Increased secretion patterns of interleukin-10 and tumor necrosis factor-alpha in cervical squamous intraepithelial lesions. *Hum Pathol* **35**, 1376-1384
138. Moerman-Herzog, A., and Nakagawa, M. (2015) Early Defensive Mechanisms against Human Papillomavirus Infection. *Clin Vaccine Immunol* **22**, 850-857
139. Mantovani, A., Sica, A., Allavena, P., Garlanda, C., and Locati, M. (2009) Tumor-associated macrophages and the related myeloid-derived suppressor cells as a paradigm of the diversity of macrophage activation. *Hum Immunol* **70**, 325-330
140. Otsuji, M., Kimura, Y., Aoe, T., Okamoto, Y., and Saito, T. (1996) Oxidative stress by tumor-derived macrophages suppresses the expression of CD3 zeta chain of T-cell receptor complex and antigen-specific T-cell responses. *Proc Natl Acad Sci U S A* **93**, 13119-13124
141. Kreider, J. W., and Bartlett, G. L. (1981) The Shope papilloma-carcinoma complex of rabbits: a model system of neoplastic progression and spontaneous regression. *Adv Cancer Res* **35**, 81-110

142. Kirnbauer, R., Booy, F., Cheng, N., Lowy, D. R., and Schiller, J. T. (1992) Papillomavirus L1 major capsid protein self-assembles into virus-like particles that are highly immunogenic. *Proc Natl Acad Sci U S A* **89**, 12180-12184
143. Christensen, N. D., Reed, C. A., Cladel, N. M., Hall, K., and Leiserowitz, G. S. (1996) Monoclonal antibodies to HPV-6 L1 virus-like particles identify conformational and linear neutralizing epitopes on HPV-11 in addition to type-specific epitopes on HPV-6. *Virology* **224**, 477-486
144. Poljak, M. (2012) Prophylactic human papillomavirus vaccination and primary prevention of cervical cancer: issues and challenges. *Clin Microbiol Infect* **18 Suppl 5**, 64-69
145. Harper, D. M., Franco, E. L., Wheeler, C., Ferris, D. G., Jenkins, D., Schuind, A., Zahaf, T., Innis, B., Naud, P., De Carvalho, N. S., Roteli-Martins, C. M., Teixeira, J., Blatter, M. M., Korn, A. P., Quint, W., Dubin, G., and GlaxoSmithKline, H. P. V. V. S. G. (2004) Efficacy of a bivalent L1 virus-like particle vaccine in prevention of infection with human papillomavirus types 16 and 18 in young women: a randomised controlled trial. *Lancet* **364**, 1757-1765
146. Villa, L. L., Costa, R. L., Petta, C. A., Andrade, R. P., Ault, K. A., Giuliano, A. R., Wheeler, C. M., Koutsky, L. A., Malm, C., Lehtinen, M., Skjeldestad, F. E., Olsson, S. E., Steinwall, M., Brown, D. R., Kurman, R. J., Ronnett, B. M., Stoler, M. H., Ferenczy, A., Harper, D. M., Tamms, G. M., Yu, J., Lupinacci, L., Railkar, R., Taddeo, F. J., Jansen, K. U., Esser, M. T., Sings, H. L., Saah, A. J., and Barr, E. (2005) Prophylactic quadrivalent human papillomavirus (types 6, 11, 16, and 18) L1 virus-like particle vaccine in young women: a randomised double-blind placebo-controlled multicentre phase II efficacy trial. *Lancet Oncol* **6**, 271-278
147. Joura, E. A., Giuliano, A. R., Iversen, O. E., Bouchard, C., Mao, C., Mehlsen, J., Moreira, E. D., Jr., Ngan, Y., Petersen, L. K., Lazcano-Ponce, E., Pitisuttithum, P., Restrepo, J. A., Stuart, G., Woelber, L., Yang, Y. C., Cuzick, J., Garland, S. M., Huh, W., Kjaer, S. K., Bautista, O. M., Chan, I. S., Chen, J., Gesser, R., Moeller, E., Ritter, M., Vuocolo, S., Luxembourg, A., and Broad Spectrum, H. P. V. V. S. (2015) A 9-valent HPV vaccine against infection and intraepithelial neoplasia in women. *N Engl J Med* **372**, 711-723
148. Naud, P. S., Roteli-Martins, C. M., De Carvalho, N. S., Teixeira, J. C., de Borba, P. C., Sanchez, N., Zahaf, T., Catteau, G., Geeraerts, B., and Descamps, D. (2014) Sustained efficacy, immunogenicity, and safety of the HPV-16/18 AS04-adjuvanted vaccine: final analysis of a long-term follow-up study up to 9.4 years post-vaccination. *Hum Vaccin Immunother* **10**, 2147-2162
149. Apter, D., Wheeler, C. M., Paavonen, J., Castellsague, X., Garland, S. M., Skinner, S. R., Naud, P., Salmeron, J., Chow, S. N., Kitchener, H. C., Teixeira, J. C., Jaisamrarn, U., Limson, G., Szarewski, A., Romanowski, B., Aoki, F. Y., Schwarz, T. F., Poppe, W. A., Bosch, F. X., Mindel, A., de Sutter, P., Hardt, K., Zahaf, T., Descamps, D., Struyf, F., Lehtinen, M., Dubin, G., and Group, H. P. S. (2015) Efficacy of human papillomavirus 16 and 18 (HPV-16/18) AS04-adjuvanted vaccine against cervical infection and precancer in young women: final event-driven analysis of the randomized, double-blind PATRICIA trial. *Clin Vaccine Immunol* **22**, 361-373
150. FutureI/IIStudyGroup., Dillner, J., Kjaer, S. K., Wheeler, C. M., Sigurdsson, K., Iversen, O. E., Hernandez-Avila, M., Perez, G., Brown, D. R., Koutsky, L. A., Tay, E. H., Garcia, P., Ault, K. A., Garland, S. M., Leodolter, S., Olsson, S. E., Tang, G. W., Ferris, D. G., Paavonen, J., Lehtinen, M., Steben, M., Bosch, F. X., Joura, E. A., Majewski, S., Munoz, N., Myers, E. R., Villa, L. L., Taddeo, F. J., Roberts, C., Tadesse, A., Bryan, J. T., Maansson, R., Lu, S., Vuocolo, S., Hesley, T. M., Barr, E., and Haupt, R. (2010) Four year efficacy of prophylactic human papillomavirus quadrivalent vaccine against low grade cervical, vulvar, and vaginal intraepithelial neoplasia and anogenital warts: randomised controlled trial. *BMJ* **341**, c3493
151. van Bogaert, L. (2013) Are the currently existing anti-human papillomavirus vaccines appropriate for the developing world? *Ann Med Health Sci Res* **3**, 306-312
152. Bonanni, P., Bechini, A., Donato, R., Capei, R., Sacco, C., Levi, M., and Boccalini, S. (2015) Human papilloma virus vaccination: impact and recommendations across the world. *Ther Adv Vaccines* **3**, 3-12
153. Garland, S. M. (2014) The Australian experience with the human papillomavirus vaccine. *Clin Ther* **36**, 17-23

154. Hildesheim, A., Gonzalez, P., Kreimer, A. R., Wacholder, S., Schussler, J., Rodriguez, A. C., Porras, C., Schiffman, M., Sidawy, M., Schiller, J. T., Lowy, D. R., Herrero, R., and CostaRica-HPV-VaccineTrialGroup. (2016) Impact of human papillomavirus (HPV) 16 and 18 vaccination on prevalent infections and rates of cervical lesions after excisional treatment. *Am J Obstet Gynecol* **215**, 212 e211-212 e215
155. Khallouf, H., Grabowska, A. K., and Riemer, A. B. (2014) Therapeutic Vaccine Strategies against Human Papillomavirus. *Vaccines (Basel)* **2**, 422-462
156. Skeate, J. G., Woodham, A. W., Einstein, M. H., Da Silva, D. M., and Kast, W. M. (2016) Current therapeutic vaccination and immunotherapy strategies for HPV-related diseases. *Hum Vaccin Immunother*, 1-12
157. Sheets, E. E., Urban, R. G., Crum, C. P., Hedley, M. L., Politch, J. A., Gold, M. A., Muderspach, L. I., Cole, G. A., and Crowley-Nowick, P. A. (2003) Immunotherapy of human cervical high-grade cervical intraepithelial neoplasia with microparticle-delivered human papillomavirus 16 E7 plasmid DNA. *Am J Obstet Gynecol* **188**, 916-926
158. Garcia, F., Petry, K. U., Muderspach, L., Gold, M. A., Braly, P., Crum, C. P., Magill, M., Silverman, M., Urban, R. G., Hedley, M. L., and Beach, K. J. (2004) ZYC101a for treatment of high-grade cervical intraepithelial neoplasia: a randomized controlled trial. *Obstet Gynecol* **103**, 317-326
159. Trimble, C. L., Morrow, M. P., Kraynyak, K. A., Shen, X., Dallas, M., Yan, J., Edwards, L., Parker, R. L., Denny, L., Giffear, M., Brown, A. S., Marcozzi-Pierce, K., Shah, D., Slager, A. M., Sylvester, A. J., Khan, A., Broderick, K. E., Juba, R. J., Herring, T. A., Boyer, J., Lee, J., Sardesai, N. Y., Weiner, D. B., and Bagarazzi, M. L. (2015) Safety, efficacy, and immunogenicity of VGX-3100, a therapeutic synthetic DNA vaccine targeting human papillomavirus 16 and 18 E6 and E7 proteins for cervical intraepithelial neoplasia 2/3: a randomised, double-blind, placebo-controlled phase 2b trial. *Lancet* **386**, 2078-2088
160. Borysiewicz, L. K., Fiander, A., Nimako, M., Man, S., Wilkinson, G. W., Westmoreland, D., Evans, A. S., Adams, M., Stacey, S. N., Boursnell, M. E., Rutherford, E., Hickling, J. K., and Inglis, S. C. (1996) A recombinant vaccinia virus encoding human papillomavirus types 16 and 18, E6 and E7 proteins as immunotherapy for cervical cancer. *Lancet* **347**, 1523-1527
161. Kaufmann, A. M., Stern, P. L., Rankin, E. M., Sommer, H., Nuessler, V., Schneider, A., Adams, M., Onon, T. S., Bauknecht, T., Wagner, U., Kroon, K., Hickling, J., Boswell, C. M., Stacey, S. N., Kitchener, H. C., Gillard, J., Wanders, J., Roberts, J. S., and Zwierzina, H. (2002) Safety and immunogenicity of TA-HPV, a recombinant vaccinia virus expressing modified human papillomavirus (HPV)-16 and HPV-18 E6 and E7 genes, in women with progressive cervical cancer. *Clin Cancer Res* **8**, 3676-3685
162. Baldwin, P. J., van der Burg, S. H., Boswell, C. M., Offringa, R., Hickling, J. K., Dobson, J., Roberts, J. S., Latimer, J. A., Moseley, R. P., Coleman, N., Stanley, M. A., and Sterling, J. C. (2003) Vaccinia-expressed human papillomavirus 16 and 18 e6 and e7 as a therapeutic vaccination for vulval and vaginal intraepithelial neoplasia. *Clin Cancer Res* **9**, 5205-5213
163. Davidson, E. J., Boswell, C. M., Sehr, P., Pawlita, M., Tomlinson, A. E., McVey, R. J., Dobson, J., Roberts, J. S., Hickling, J., Kitchener, H. C., and Stern, P. L. (2003) Immunological and clinical responses in women with vulval intraepithelial neoplasia vaccinated with a vaccinia virus encoding human papillomavirus 16/18 oncoproteins. *Cancer Res* **63**, 6032-6041
164. Brun, J. L., Dalstein, V., Leveque, J., Mathevet, P., Raulic, P., Baldauf, J. J., Scholl, S., Huynh, B., Douvier, S., Riethmuller, D., Clavel, C., Birembaut, P., Calenda, V., Baudin, M., and Bory, J. P. (2011) Regression of high-grade cervical intraepithelial neoplasia with TG4001 targeted immunotherapy. *Am J Obstet Gynecol* **204**, 169 e161-168
165. Maciag, P. C., Radulovic, S., and Rothman, J. (2009) The first clinical use of a live-attenuated Listeria monocytogenes vaccine: a Phase I safety study of Lm-LLO-E7 in patients with advanced carcinoma of the cervix. *Vaccine* **27**, 3975-3983
166. Van Damme, P., Bouillette-Marussig, M., Hens, A., De Coster, I., Depuydt, C., Goubier, A., Van Tendeloo, V., Cools, N., Goossens, H., Hercend, T., Timmerman, B., and Bissery, M. C. (2016) GTL001, A Therapeutic Vaccine for Women Infected with Human Papillomavirus 16 or 18 and Normal Cervical Cytology: Results of a Phase I Clinical Trial. *Clin Cancer Res* **22**, 3238-3248

167. Rosalia, R. A., Quakkelaar, E. D., Redeker, A., Khan, S., Camps, M., Drijfhout, J. W., Silva, A. L., Jiskoot, W., van Hall, T., van Veelen, P. A., Janssen, G., Franken, K., Cruz, L. J., Tromp, A., Oostendorp, J., van der Burg, S. H., Ossendorp, F., and Melief, C. J. (2013) Dendritic cells process synthetic long peptides better than whole protein, improving antigen presentation and T-cell activation. *Eur J Immunol* **43**, 2554-2565
168. Kenter, G. G., Welters, M. J., Valentijn, A. R., Lowik, M. J., Berends-van der Meer, D. M., Vloon, A. P., Essahsah, F., Fathers, L. M., Offringa, R., Drijfhout, J. W., Wafelman, A. R., Oostendorp, J., Fleuren, G. J., van der Burg, S. H., and Melief, C. J. (2009) Vaccination against HPV-16 oncoproteins for vulvar intraepithelial neoplasia. *N Engl J Med* **361**, 1838-1847
169. de Vos van Steenwijk, P. J., van Poelgeest, M. I., Ramwadhdoebe, T. H., Lowik, M. J., Berends-van der Meer, D. M., van der Minne, C. E., Loof, N. M., Stynenbosch, L. F., Fathers, L. M., Valentijn, A. R., Oostendorp, J., Osse, E. M., Fleuren, G. J., Nooij, L., Kagie, M. J., Hellebrekers, B. W., Melief, C. J., Welters, M. J., van der Burg, S. H., and Kenter, G. G. (2014) The long-term immune response after HPV16 peptide vaccination in women with low-grade pre-malignant disorders of the uterine cervix: a placebo-controlled phase II study. *Cancer Immunol Immunother* **63**, 147-160
170. van Poelgeest, M. I., Welters, M. J., Vermeij, R., Stynenbosch, L. F., Loof, N. M., Berends-van der Meer, D. M., Lowik, M. J., Hamming, I. L., van Esch, E. M., Hellebrekers, B. W., van Beurden, M., Schreuder, H. W., Kagie, M. J., Trimbos, J. B., Fathers, L., Daemen, T., Hollema, H., Valentijn, R., Oostendorp, J., Oude Elberink, J. H., Fleuren, G. J., Bosse, T., Kenter, G. G., Stijnen, T., Nijman, H. W., Melief, C. J., and van der Burg, S. H. (2016) Vaccination against oncoproteins of HPV16 for non-invasive vulvar/vaginal lesions: lesion clearance is related to the strength of the T-cell response. *Clin Cancer Res*
171. Welters, M. J., van der Sluis, T. C., van Meir, H., Loof, N. M., van Ham, V. J., van Duikeren, S., Santegoets, S. J., Arens, R., de Kam, M. L., Cohen, A. F., van Poelgeest, M. I., Kenter, G. G., Kroep, J. R., Burggraaf, J., Melief, C. J., and van der Burg, S. H. (2016) Vaccination during myeloid cell depletion by cancer chemotherapy fosters robust T cell responses. *Sci Transl Med* **8**, 334ra352
172. Haen, S. P., and Rammensee, H. G. (2013) The repertoire of human tumor-associated epitopes--identification and selection of antigens and their application in clinical trials. *Curr Opin Immunol* **25**, 277-283
173. Riemer, A. B., Keskin, D. B., Zhang, G., Handley, M., Anderson, K. S., Brusic, V., Reinhold, B., and Reinherz, E. L. (2010) A conserved E7-derived cytotoxic T lymphocyte epitope expressed on human papillomavirus 16-transformed HLA-A2+ epithelial cancers. *J Biol Chem* **285**, 29608-29622
174. Wiesel, M., and Oxenius, A. (2012) From crucial to negligible: functional CD8(+) T-cell responses and their dependence on CD4(+) T-cell help. *Eur J Immunol* **42**, 1080-1088
175. Grabowska, A. K., Kaufmann, A. M., and Riemer, A. B. (2015) Identification of promiscuous HPV16-derived T helper cell epitopes for therapeutic HPV vaccine design. *Int J Cancer* **136**, 212-224
176. Muderspach, L., Wilczynski, S., Roman, L., Bade, L., Felix, J., Small, L. A., Kast, W. M., Fascio, G., Marty, V., and Weber, J. (2000) A phase I trial of a human papillomavirus (HPV) peptide vaccine for women with high-grade cervical and vulvar intraepithelial neoplasia who are HPV 16 positive. *Clin Cancer Res* **6**, 3406-3416
177. Greenfield, W. W., Stratton, S. L., Myrick, R. S., Vaughn, R., Donnalley, L. M., Coleman, H. N., Mercado, M., Moerman-Herzog, A. M., Spencer, H. J., Andrews-Collins, N. R., Hitt, W. C., Low, G. M., Manning, N. A., McKelvey, S. S., Smith, D., Smith, M. V., Phillips, A. M., Quick, C. M., Jeffus, S. K., Hutchins, L. F., and Nakagawa, M. (2015) A phase I dose-escalation clinical trial of a peptide-based human papillomavirus therapeutic vaccine with skin test reagent as a novel vaccine adjuvant for treating women with biopsy-proven cervical intraepithelial neoplasia 2/3. *Oncoimmunology* **4**, e1031439
178. Brady, C. S., Bartholomew, J. S., Burt, D. J., Duggan-Keen, M. F., Glenville, S., Telford, N., Little, A. M., Davidson, J. A., Jimenez, P., Ruiz-Cabello, F., Garrido, F., and Stern, P. L. (2000) Multiple mechanisms underlie HLA dysregulation in cervical cancer. *Tissue Antigens* **55**, 401-411

179. Lee, J. H., Yi, S. M., Anderson, M. E., Berger, K. L., Welsh, M. J., Klingelhutz, A. J., and Ozbun, M. A. (2004) Propagation of infectious human papillomavirus type 16 by using an adenovirus and Cre/LoxP mechanism. *Proc Natl Acad Sci U S A* **101**, 2094-2099
180. Pattillo, R. A., Hussa, R. O., Story, M. T., Ruckert, A. C., Shalaby, M. R., and Mattingly, R. F. (1977) Tumor antigen and human chorionic gonadotropin in CaSki cells: a new epidermoid cervical cancer cell line. *Science* **196**, 1456-1458
181. de Wilde, J., Wilting, S. M., Meijer, C. J., van de Wiel, M. A., Ylstra, B., Snijders, P. J., and Steenbergen, R. D. (2008) Gene expression profiling to identify markers associated with deregulated hTERT in HPV-transformed keratinocytes and cervical cancer. *Int J Cancer* **122**, 877-888
182. Henderson, J., Sebag, M., Rhim, J., Goltzman, D., and Kremer, R. (1991) Dysregulation of parathyroid hormone-like peptide expression and secretion in a keratinocyte model of tumor progression. *Cancer Res* **51**, 6521-6528
183. Schmitt, M., and Pawlita, M. (2011) The HPV transcriptome in HPV16 positive cell lines. *Mol Cell Probes* **25**, 108-113
184. Friedl, F., Kimura, I., Osato, T., and Ito, Y. (1970) Studies on a new human cell line (SiHa) derived from carcinoma of uterus. I. Its establishment and morphology. *Proc Soc Exp Biol Med* **135**, 543-545
185. Ku, J. L., Kim, W. H., Park, H. S., Kang, S. B., and Park, J. G. (1997) Establishment and characterization of 12 uterine cervical-carcinoma cell lines: common sequence variation in the E7 gene of HPV-16-positive cell lines. *Int J Cancer* **72**, 313-320
186. Harris, M., Wang, X. G., Jiang, Z., Goldberg, G. L., Casadevall, A., and Dadachova, E. (2011) Radioimmunotherapy of experimental head and neck squamous cell carcinoma (HNSCC) with E6-specific antibody using a novel HPV-16 positive HNSCC cell line. *Head Neck Oncol* **3**, 9
187. Steenbergen, R. D., Hermsen, M. A., Walboomers, J. M., Joenje, H., Arwert, F., Meijer, C. J., and Snijders, P. J. (1995) Integrated human papillomavirus type 16 and loss of heterozygosity at 11q22 and 18q21 in an oral carcinoma and its derivative cell line. *Cancer Res* **55**, 5465-5471
188. Ragin, C. C., Reshmi, S. C., and Gollin, S. M. (2004) Mapping and analysis of HPV16 integration sites in a head and neck cancer cell line. *Int J Cancer* **110**, 701-709
189. White, J. S., Weissfeld, J. L., Ragin, C. C., Rossie, K. M., Martin, C. L., Shuster, M., Ishwad, C. S., Law, J. C., Myers, E. N., Johnson, J. T., and Gollin, S. M. (2007) The influence of clinical and demographic risk factors on the establishment of head and neck squamous cell carcinoma cell lines. *Oral Oncol* **43**, 701-712
190. Hoffmann, T. K., Sonkoly, E., Hauser, U., van Lierop, A., Whiteside, T. L., Klussmann, J. P., Hafner, D., Schuler, P., Friebe-Hoffmann, U., Scheckenbach, K., Erjala, K., Grenman, R., Schipper, J., Bier, H., and Balz, V. (2008) Alterations in the p53 pathway and their association with radio- and chemosensitivity in head and neck squamous cell carcinoma. *Oral Oncol* **44**, 1100-1109
191. Virolainen, E., Vanharanta, R., and Carey, T. E. (1984) Steroid hormone receptors in human squamous carcinoma cell lines. *Int J Cancer* **33**, 19-25
192. Boukamp, P., Petrussevska, R. T., Breitkreutz, D., Hornung, J., Markham, A., and Fusenig, N. E. (1988) Normal keratinization in a spontaneously immortalized aneuploid human keratinocyte cell line. *J Cell Biol* **106**, 761-771
193. Piboonniyom, S. O., Duensing, S., Swilling, N. W., Hasskarl, J., Hinds, P. W., and Munger, K. (2003) Abrogation of the retinoblastoma tumor suppressor checkpoint during keratinocyte immortalization is not sufficient for induction of centrosome-mediated genomic instability. *Cancer Res* **63**, 476-483
194. Hoppe, S. (2015) *Identification of target T cell epitopes for a therapeutic HPV16 vaccine.* Doctor of Natural Sciences, Ruperto-Carola University of Heidelberg
195. Schultze, J. L., Cardoso, A. A., Freeman, G. J., Seamon, M. J., Daley, J., Pinkus, G. S., Gribben, J. G., and Nadler, L. M. (1995) Follicular lymphomas can be induced to present alloantigen efficiently: a conceptual model to improve their tumor immunogenicity. *Proc Natl Acad Sci U S A* **92**, 8200-8204
196. Merrifield, R. B. (1963) Solid Phase Peptide Synthesis. I. The Synthesis of a Tetrapeptide. *J Am Chem Soc* **85**, 2149-2154

197. Carpino, A., and Han, G. Y. (1972) 9-Fluorenylmethoxycarbonyl amino-protecting group. *J Org Chem* **37**, 3404-3409
198. Vaslin, B., Claverie, J. M., Benveniste, O., Barre-Sinoussi, F. C., and Dormont, D. (1994) Nef and Gag synthetic peptide priming of antibody responses to HIV type 1 antigens in mice and primates. *AIDS Res Hum Retroviruses* **10**, 1241-1250
199. Dai, L. C., West, K., Littaua, R., Takahashi, K., and Ennis, F. A. (1992) Mutation of human immunodeficiency virus type 1 at amino acid 585 on gp41 results in loss of killing by CD8+ A24-restricted cytotoxic T lymphocytes. *J Virol* **66**, 3151-3154
200. Sambrook, J., and Gething, M. J. (1989) Protein structure. Chaperones, paperones. *Nature* **342**, 224-225
201. Mullis, K., Faloona, F., Scharf, S., Saiki, R., Horn, G., and Erlich, H. (1986) Specific enzymatic amplification of DNA in vitro: the polymerase chain reaction. *Cold Spring Harb Symp Quant Biol* **51 Pt 1**, 263-273
202. Saiki, R. K., Scharf, S., Faloona, F., Mullis, K. B., Horn, G. T., Erlich, H. A., and Arnheim, N. (1985) Enzymatic amplification of beta-globin genomic sequences and restriction site analysis for diagnosis of sickle cell anemia. *Science* **230**, 1350-1354
203. Reeves, E., Edwards, C. J., Elliott, T., and James, E. (2013) Naturally occurring ERAP1 haplotypes encode functionally distinct alleles with fine substrate specificity. *J Immunol* **191**, 35-43
204. Riemer, A. B., Keskin, D. B., and Reinherz, E. L. (2012) Identification and validation of reference genes for expression studies in human keratinocyte cell lines treated with and without interferon-gamma - a method for qRT-PCR reference gene determination. *Exp Dermatol* **21**, 625-629
205. Hellemans, J., Mortier, G., De Paepe, A., Speleman, F., and Vandesompele, J. (2007) qBase relative quantification framework and software for management and automated analysis of real-time quantitative PCR data. *Genome Biol* **8**, R19
206. Logan, J., Edwards, K., and Saunders, N. (2009) *Real-Time PCR: Current Technology and Applications*, 1 ed., Caister Academic Press
207. Bustin, S. A., Benes, V., Garson, J. A., Hellemans, J., Huggett, J., Kubista, M., Mueller, R., Nolan, T., Pfaffl, M. W., Shipley, G. L., Vandesompele, J., and Wittwer, C. T. (2009) The MIQE guidelines: minimum information for publication of quantitative real-time PCR experiments. *Clin Chem* **55**, 611-622
208. Laemmli, U. K. (1970) Cleavage of structural proteins during the assembly of the head of bacteriophage T4. *Nature* **227**, 680-685
209. Honegger, A., Schilling, D., Bastian, S., Sponagel, J., Kuryshev, V., Sultmann, H., Scheffner, M., Hoppe-Seyler, K., and Hoppe-Seyler, F. (2015) Dependence of intracellular and exosomal microRNAs on viral E6/E7 oncogene expression in HPV-positive tumor cells. *PLoS Pathog* **11**, e1004712
210. Schultze, J. L., Michalak, S., Seamon, M. J., Dranoff, G., Jung, K., Daley, J., Delgado, J. C., Gribben, J. G., and Nadler, L. M. (1997) CD40-activated human B cells: an alternative source of highly efficient antigen presenting cells to generate autologous antigen-specific T cells for adoptive immunotherapy. *J Clin Invest* **100**, 2757-2765
211. Stanke, J., Hoffmann, C., Erben, U., von Keyserling, H., Stevanovic, S., Cichon, G., Schneider, A., and Kaufmann, A. M. (2010) A flow cytometry-based assay to assess minute frequencies of CD8+ T cells by their cytolytic function. *J Immunol Methods* **360**, 56-65
212. Liao, T., Kaufmann, A. M., Qian, X., Sangvatanakul, V., Chen, C., Kube, T., Zhang, G., and Albers, A. E. (2013) Susceptibility to cytotoxic T cell lysis of cancer stem cells derived from cervical and head and neck tumor cell lines. *J Cancer Res Clin Oncol* **139**, 159-170
213. Winter, J. (2013) *Systematic Analysis of the Antigen Processing Machinery in HPV-positive Cell Lines.* Master of Science, Ruperto-Carola University of Heidelberg
214. Ruijter, J. M., Pfaffl, M. W., Zhao, S., Spiess, A. N., Boggy, G., Blom, J., Rutledge, R. G., Sisti, D., Lievens, A., De Preter, K., Derveaux, S., Hellemans, J., and Vandesompele, J. (2013) Evaluation of qPCR curve analysis methods for reliable biomarker discovery: bias, resolution, precision, and implications. *Methods* **59**, 32-46

215. Ruijter, J. M., Ramakers, C., Hoogaars, W. M., Karlen, Y., Bakker, O., van den Hoff, M. J., and Moorman, A. F. (2009) Amplification efficiency: linking baseline and bias in the analysis of quantitative PCR data. *Nucleic Acids Res* **37**, e45
216. Zhu, G., Chang, Y., Zuo, J., Dong, X., Zhang, M., Hu, G., and Fang, F. (2001) Fudenine, a C-terminal truncated rat homologue of mouse prominin, is blood glucose-regulated and can up-regulate the expression of GAPDH. *Biochem Biophys Res Commun* **281**, 951-956
217. Ma, W., Lehner, P. J., Cresswell, P., Pober, J. S., and Johnson, D. R. (1997) Interferon-gamma rapidly increases peptide transporter (TAP) subunit expression and peptide transport capacity in endothelial cells. *J Biol Chem* **272**, 16585-16590
218. Mellman, I., and Cresswell, P. (2010) Antigen processing and presentation. *Curr Opin Immunol* **22**, 78-80
219. Kanaseki, T., Lind, K. C., Escobar, H., Nagarajan, N., Reyes-Vargas, E., Rudd, B., Rockwood, A. L., Van Kaer, L., Sato, N., Delgado, J. C., and Shastri, N. (2013) ERAAP and tapasin independently edit the amino and carboxyl termini of MHC class I peptides. *J Immunol* **191**, 1547-1555
220. de Villiers, E. M. (2013) Cross-roads in the classification of papillomaviruses. *Virology* **445**, 2-10
221. Costantino, F., Talpin, A., Evnouchidou, I., Kadi, A., Leboime, A., Said-Nahal, R., Bonilla, N., Letourneur, F., Leturcq, T., Ka, Z., van Endert, P., Garchon, H. J., Chiocchia, G., and Breban, M. (2015) ERAP1 Gene Expression Is Influenced by Nonsynonymous Polymorphisms Associated With Predisposition to Spondyloarthritis. *Arthritis Rheumatol* **67**, 1525-1534
222. Ajiro, M., and Zheng, Z. M. (2014) Oncogenes and RNA splicing of human tumor viruses. *Emerg Microbes Infect* **3**, e63
223. Gonzalez-Galarza, F. F., Takeshita, L. Y., Santos, E. J., Kempson, F., Maia, M. H., da Silva, A. L., Teles e Silva, A. L., Ghattaoraya, G. S., Alfirevic, A., Jones, A. R., and Middleton, D. (2015) Allele frequency net 2015 update: new features for HLA epitopes, KIR and disease and HLA adverse drug reaction associations. *Nucleic Acids Res* **43**, D784-788
224. Firat, E., Saveanu, L., Aichele, P., Staeheli, P., Huai, J., Gaedicke, S., Nil, A., Besin, G., Kanzler, B., van Endert, P., and Niedermann, G. (2007) The role of endoplasmic reticulum-associated aminopeptidase 1 in immunity to infection and in cross-presentation. *J Immunol* **178**, 2241-2248
225. Keskin, D. B., Reinhold, B., Lee, S. Y., Zhang, G., Lank, S., O'Connor, D. H., Berkowitz, R. S., Brusic, V., Kim, S. J., and Reinherz, E. L. (2011) Direct identification of an HPV-16 tumor antigen from cervical cancer biopsy specimens. *Front Immunol* **2**, 75
226. Albers, A., Abe, K., Hunt, J., Wang, J., Lopez-Albaitero, A., Schaefer, C., Gooding, W., Whiteside, T. L., Ferrone, S., DeLeo, A., and Ferris, R. L. (2005) Antitumor activity of human papillomavirus type 16 E7-specific T cells against virally infected squamous cell carcinoma of the head and neck. *Cancer Res* **65**, 11146-11155
227. Küpper, M. (2014) *Analysis of the potential HLA-A2 E6 and E7 epitome derived from prototype HPV16 or its variants.* Master of Science, Ruperto-Carola University of Heidelberg
228. de Boer, M. A., Jordanova, E. S., van Poelgeest, M. I., van den Akker, B. E., van der Burg, S. H., Kenter, G. G., and Fleuren, G. J. (2007) Circulating human papillomavirus type 16 specific T-cells are associated with HLA Class I expression on tumor cells, but not related to the amount of viral oncogene transcripts. *Int J Cancer* **121**, 2711-2715
229. Gillison, M. L., and Shah, K. V. (2001) Human papillomavirus-associated head and neck squamous cell carcinoma: mounting evidence for an etiologic role for human papillomavirus in a subset of head and neck cancers. *Curr Opin Oncol* **13**, 183-188
230. Gillison, M. L., Koch, W. M., Capone, R. B., Spafford, M., Westra, W. H., Wu, L., Zahurak, M. L., Daniel, R. W., Viglione, M., Symer, D. E., Shah, K. V., and Sidransky, D. (2000) Evidence for a causal association between human papillomavirus and a subset of head and neck cancers. *J Natl Cancer Inst* **92**, 709-720
231. Rodriguez, T., Mendez, R., Del Campo, A., Jimenez, P., Aptsiauri, N., Garrido, F., and Ruiz-Cabello, F. (2007) Distinct mechanisms of loss of IFN-gamma mediated HLA class I inducibility in two melanoma cell lines. *BMC Cancer* **7**, 34

232. Respa, A., Bukur, J., Ferrone, S., Pawelec, G., Zhao, Y., Wang, E., Marincola, F. M., and Seliger, B. (2011) Association of IFN-gamma signal transduction defects with impaired HLA class I antigen processing in melanoma cell lines. *Clin Cancer Res* **17**, 2668-2678
233. Upton, C., Mossman, K., and McFadden, G. (1992) Encoding of a homolog of the IFN-gamma receptor by myxoma virus. *Science* **258**, 1369-1372
234. Devasthanam, A. S. (2014) Mechanisms underlying the inhibition of interferon signaling by viruses. *Virulence* **5**, 270-277
235. Ronco, L. V., Karpova, A. Y., Vidal, M., and Howley, P. M. (1998) Human papillomavirus 16 E6 oncoprotein binds to interferon regulatory factor-3 and inhibits its transcriptional activity. *Genes Dev* **12**, 2061-2072
236. Barnard, P., Payne, E., and McMillan, N. A. (2000) The human papillomavirus E7 protein is able to inhibit the antiviral and anti-growth functions of interferon-alpha. *Virology* **277**, 411-419
237. Keating, P. J., Cromme, F. V., Duggan-Keen, M., Snijders, P. J., Walboomers, J. M., Hunter, R. D., Dyer, P. A., and Stern, P. L. (1995) Frequency of down-regulation of individual HLA-A and -B alleles in cervical carcinomas in relation to TAP-1 expression. *Br J Cancer* **72**, 405-411
238. Gao, F., Zhao, Z. L., Zhao, W. T., Fan, Q. R., Wang, S. C., Li, J., Zhang, Y. Q., Shi, J. W., Lin, X. L., Yang, S., Xie, R. Y., Liu, W., Zhang, T. T., Sun, Y. L., Xu, K., Yao, K. T., and Xiao, D. (2013) miR-9 modulates the expression of interferon-regulated genes and MHC class I molecules in human nasopharyngeal carcinoma cells. *Biochem Biophys Res Commun* **431**, 610-616
239. Bartoszewski, R., Brewer, J. W., Rab, A., Crossman, D. K., Bartoszewska, S., Kapoor, N., Fuller, C., Collawn, J. F., and Bebok, Z. (2011) The unfolded protein response (UPR)-activated transcription factor X-box-binding protein 1 (XBP1) induces microRNA-346 expression that targets the human antigen peptide transporter 1 (TAP1) mRNA and governs immune regulatory genes. *J Biol Chem* **286**, 41862-41870
240. Jasinski-Bergner, S., Stoehr, C., Bukur, J., Massa, C., Braun, J., Huttelmaier, S., Spath, V., Wartenberg, R., Legal, W., Taubert, H., Wach, S., Wullich, B., Hartmann, A., and Seliger, B. (2015) Clinical relevance of miR-mediated HLA-G regulation and the associated immune cell infiltration in renal cell carcinoma. *Oncoimmunology* **4**, e1008805
241. Jasinski-Bergner, S., Reches, A., Stoehr, C., Massa, C., Gonschorek, E., Huettelmaier, S., Braun, J., Wach, S., Wullich, B., Spath, V., Wang, E., Marincola, F. M., Mandelboim, O., Hartmann, A., and Seliger, B. (2016) Identification of novel microRNAs regulating HLA-G expression and investigating their clinical relevance in renal cell carcinoma. *Oncotarget*
242. Qian, K., Pietila, T., Ronty, M., Michon, F., Frilander, M. J., Ritari, J., Tarkkanen, J., Paulin, L., Auvinen, P., and Auvinen, E. (2013) Identification and validation of human papillomavirus encoded microRNAs. *PLoS One* **8**, e70202
243. Fruci, D., Romania, P., D'Alicandro, V., and Locatelli, F. (2014) Endoplasmic reticulum aminopeptidase 1 function and its pathogenic role in regulating innate and adaptive immunity in cancer and major histocompatibility complex class I-associated autoimmune diseases. *Tissue Antigens* **84**, 177-186
244. Kamphausen, E., Kellert, C., Abbas, T., Akkad, N., Tenzer, S., Pawelec, G., Schild, H., van Endert, P., and Seliger, B. (2010) Distinct molecular mechanisms leading to deficient expression of ER-resident aminopeptidases in melanoma. *Cancer Immunol Immunother* **59**, 1273-1284
245. Kirino, Y., Bertsias, G., Ishigatsubo, Y., Mizuki, N., Tugal-Tutkun, I., Seyahi, E., Ozyazgan, Y., Sacli, F. S., Erer, B., Inoko, H., Emrence, Z., Cakar, A., Abaci, N., Ustek, D., Satorius, C., Ueda, A., Takeno, M., Kim, Y., Wood, G. M., Ombrello, M. J., Meguro, A., Gul, A., Remmers, E. F., and Kastner, D. L. (2013) Genome-wide association analysis identifies new susceptibility loci for Behcet's disease and epistasis between HLA-B*51 and ERAP1. *Nat Genet* **45**, 202-207
246. Harvey, D., Pointon, J. J., Evans, D. M., Karaderi, T., Farrar, C., Appleton, L. H., Sturrock, R. D., Stone, M. A., Oppermann, U., Brown, M. A., and Wordsworth, B. P. (2009) Investigating the genetic association between ERAP1 and ankylosing spondylitis. *Hum Mol Genet* **18**, 4204-4212

247. Nguyen, T. T., Chang, S. C., Evnouchidou, I., York, I. A., Zikos, C., Rock, K. L., Goldberg, A. L., Stratikos, E., and Stern, L. J. (2011) Structural basis for antigenic peptide precursor processing by the endoplasmic reticulum aminopeptidase ERAP1. *Nat Struct Mol Biol* **18**, 604-613
248. Kochan, G., Krojer, T., Harvey, D., Fischer, R., Chen, L., Vollmar, M., von Delft, F., Kavanagh, K. L., Brown, M. A., Bowness, P., Wordsworth, P., Kessler, B. M., and Oppermann, U. (2011) Crystal structures of the endoplasmic reticulum aminopeptidase-1 (ERAP1) reveal the molecular basis for N-terminal peptide trimming. *Proc Natl Acad Sci U S A* **108**, 7745-7750
249. Stamogiannos, A., Koumantou, D., Papakyriakou, A., and Stratikos, E. (2015) Effects of polymorphic variation on the mechanism of Endoplasmic Reticulum Aminopeptidase 1. *Mol Immunol* **67**, 426-435
250. Goto, Y., Hattori, A., Ishii, Y., and Tsujimoto, M. (2006) Reduced activity of the hypertension-associated Lys528Arg mutant of human adipocyte-derived leucine aminopeptidase (A-LAP)/ER-aminopeptidase-1. *FEBS Lett* **580**, 1833-1838
251. Garcia-Medel, N., Sanz-Bravo, A., Van Nguyen, D., Galocha, B., Gomez-Molina, P., Martin-Esteban, A., Alvarez-Navarro, C., and de Castro, J. A. (2012) Functional interaction of the ankylosing spondylitis-associated endoplasmic reticulum aminopeptidase 1 polymorphism and HLA-B27 in vivo. *Mol Cell Proteomics* **11**, 1416-1429
252. Martin-Esteban, A., Gomez-Molina, P., Sanz-Bravo, A., and Lopez de Castro, J. A. (2014) Combined effects of ankylosing spondylitis-associated ERAP1 polymorphisms outside the catalytic and peptide-binding sites on the processing of natural HLA-B27 ligands. *J Biol Chem* **289**, 3978-3990
253. Kadi, A., Izac, B., Said-Nahal, R., Leboime, A., Van Praet, L., de Vlam, K., Elewaut, D., Chiocchia, G., and Breban, M. (2013) Investigating the genetic association between ERAP1 and spondyloarthritis. *Ann Rheum Dis* **72**, 608-613
254. Li, S., Labrecque, S., Gauzzi, M. C., Cuddihy, A. R., Wong, A. H., Pellegrini, S., Matlashewski, G. J., and Koromilas, A. E. (1999) The human papilloma virus (HPV)-18 E6 oncoprotein physically associates with Tyk2 and impairs Jak-STAT activation by interferon-alpha. *Oncogene* **18**, 5727-5737
255. Mehta, A. M., Osse, M., Kolkman-Uljee, S., Fleuren, G. J., and Jordanova, E. S. (2015) Molecular backgrounds of ERAP1 downregulation in cervical carcinoma. *Anal Cell Pathol (Amst)* **2015**, 367837
256. Lin, S., and Gregory, R. I. (2015) MicroRNA biogenesis pathways in cancer. *Nat Rev Cancer* **15**, 321-333
257. Gocze, K., Gombos, K., Kovacs, K., Juhasz, K., Gocze, P., and Kiss, I. (2015) MicroRNA expressions in HPV-induced cervical dysplasia and cancer. *Anticancer Res* **35**, 523-530
258. Gunasekharan, V., and Laimins, L. A. (2013) Human papillomaviruses modulate microRNA 145 expression to directly control genome amplification. *J Virol* **87**, 6037-6043
259. Cui, X., Hawari, F., Alsaaty, S., Lawrence, M., Combs, C. A., Geng, W., Rouhani, F. N., Miskinis, D., and Levine, S. J. (2002) Identification of ARTS-1 as a novel TNFR1-binding protein that promotes TNFR1 ectodomain shedding. *J Clin Invest* **110**, 515-526
260. Cui, X., Rouhani, F. N., Hawari, F., and Levine, S. J. (2003) Shedding of the type II IL-1 decoy receptor requires a multifunctional aminopeptidase, aminopeptidase regulator of TNF receptor type 1 shedding. *J Immunol* **171**, 6814-6819
261. Cui, X., Rouhani, F. N., Hawari, F., and Levine, S. J. (2003) An aminopeptidase, ARTS-1, is required for interleukin-6 receptor shedding. *J Biol Chem* **278**, 28677-28685
262. Peters, M., Jacobs, S., Ehlers, M., Vollmer, P., Mullberg, J., Wolf, E., Brem, G., Meyer zum Buschenfelde, K. H., and Rose-John, S. (1996) The function of the soluble interleukin 6 (IL-6) receptor in vivo: sensitization of human soluble IL-6 receptor transgenic mice towards IL-6 and prolongation of the plasma half-life of IL-6. *J Exp Med* **183**, 1399-1406
263. Miyashita, H., Yamazaki, T., Akada, T., Niizeki, O., Ogawa, M., Nishikawa, S., and Sato, Y. (2002) A mouse orthologue of puromycin-insensitive leucyl-specific aminopeptidase is expressed in endothelial cells and plays an important role in angiogenesis. *Blood* **99**, 3241-3249

264. Yamazaki, T., Akada, T., Niizeki, O., Suzuki, T., Miyashita, H., and Sato, Y. (2004) Puromycin-insensitive leucyl-specific aminopeptidase (PILSAP) binds and catalyzes PDK1, allowing VEGF-stimulated activation of S6K for endothelial cell proliferation and angiogenesis. *Blood* **104**, 2345-2352
265. Brock, T. A., Dvorak, H. F., and Senger, D. R. (1991) Tumor-secreted vascular permeability factor increases cytosolic Ca2+ and von Willebrand factor release in human endothelial cells. *Am J Pathol* **138**, 213-221
266. Hattori, A., Kitatani, K., Matsumoto, H., Miyazawa, S., Rogi, T., Tsuruoka, N., Mizutani, S., Natori, Y., and Tsujimoto, M. (2000) Characterization of recombinant human adipocyte-derived leucine aminopeptidase expressed in Chinese hamster ovary cells. *J Biochem* **128**, 755-762
267. Goto, Y., Ogawa, K., Hattori, A., and Tsujimoto, M. (2011) Secretion of endoplasmic reticulum aminopeptidase 1 is involved in the activation of macrophages induced by lipopolysaccharide and interferon-gamma. *J Biol Chem* **286**, 21906-21914
268. Chen, L., Ridley, A., Hammitzsch, A., Al-Mossawi, M. H., Bunting, H., Georgiadis, D., Chan, A., Kollnberger, S., and Bowness, P. (2016) Silencing or inhibition of endoplasmic reticulum aminopeptidase 1 (ERAP1) suppresses free heavy chain expression and Th17 responses in ankylosing spondylitis. *Ann Rheum Dis* **75**, 916-923
269. Lopez de Castro, J. A., Alvarez-Navarro, C., Brito, A., Guasp, P., Martin-Esteban, A., and Sanz-Bravo, A. (2016) Molecular and pathogenic effects of endoplasmic reticulum aminopeptidases ERAP1 and ERAP2 in MHC-I-associated inflammatory disorders: Towards a unifying view. *Mol Immunol* **77**, 193-204
270. Serwold, T., Gonzalez, F., Kim, J., Jacob, R., and Shastri, N. (2002) ERAAP customizes peptides for MHC class I molecules in the endoplasmic reticulum. *Nature* **419**, 480-483
271. Haroon, N., Tsui, F. W., Uchanska-Ziegler, B., Ziegler, A., and Inman, R. D. (2012) Endoplasmic reticulum aminopeptidase 1 (ERAP1) exhibits functionally significant interaction with HLA-B27 and relates to subtype specificity in ankylosing spondylitis. *Ann Rheum Dis* **71**, 589-595
272. Cifaldi, L., Romania, P., Falco, M., Lorenzi, S., Meazza, R., Petrini, S., Andreani, M., Pende, D., Locatelli, F., and Fruci, D. (2015) ERAP1 regulates natural killer cell function by controlling the engagement of inhibitory receptors. *Cancer Res* **75**, 824-834
273. Hammer, G. E., Gonzalez, F., Champsaur, M., Cado, D., and Shastri, N. (2006) The aminopeptidase ERAAP shapes the peptide repertoire displayed by major histocompatibility complex class I molecules. *Nat Immunol* **7**, 103-112
274. Sette, A., and Sidney, J. (1999) Nine major HLA class I supertypes account for the vast preponderance of HLA-A and -B polymorphism. *Immunogenetics* **50**, 201-212
275. Cifaldi, L., Lo Monaco, E., Forloni, M., Giorda, E., Lorenzi, S., Petrini, S., Tremante, E., Pende, D., Locatelli, F., Giacomini, P., and Fruci, D. (2011) Natural killer cells efficiently reject lymphoma silenced for the endoplasmic reticulum aminopeptidase associated with antigen processing. *Cancer Res* **71**, 1597-1606
276. Hearn, A., York, I. A., and Rock, K. L. (2009) The specificity of trimming of MHC class I-presented peptides in the endoplasmic reticulum. *J Immunol* **183**, 5526-5536
277. Guasp, P., Alvarez-Navarro, C., Gomez-Molina, P., Martin-Esteban, A., Marcilla, M., Barnea, E., Admon, A., and Lopez de Castro, J. A. (2016) The Peptidome of Behcet's Disease-Associated HLA-B*51:01 Includes Two Subpeptidomes Differentially Shaped by Endoplasmic Reticulum Aminopeptidase 1. *Arthritis Rheumatol* **68**, 505-515
278. Neisig, A., Roelse, J., Sijts, A. J., Ossendorp, F., Feltkamp, M. C., Kast, W. M., Melief, C. J., and Neefjes, J. J. (1995) Major differences in transporter associated with antigen presentation (TAP)-dependent translocation of MHC class I-presentable peptides and the effect of flanking sequences. *J Immunol* **154**, 1273-1279
279. van Endert, P. M., Riganelli, D., Greco, G., Fleischhauer, K., Sidney, J., Sette, A., and Bach, J. F. (1995) The peptide-binding motif for the human transporter associated with antigen processing. *J Exp Med* **182**, 1883-1895
280. Weglarz-Tomczak, E., Vassiliou, S., and Mucha, A. (2016) Discovery of potent and selective inhibitors of human aminopeptidases ERAP1 and ERAP2 by screening libraries of

phosphorus-containing amino acid and dipeptide analogues. *Bioorg Med Chem Lett* **26**, 4122-4126

281. Stamogiannos, A., Papakyriakou, A., Mauvais, F. X., van Endert, P., and Stratikos, E. (2016) Screening Identifies Thimerosal as a Selective Inhibitor of Endoplasmic Reticulum Aminopeptidase 1. *ACS Med Chem Lett* **7**, 681-685
282. Nagarajan, N. A., de Verteuil, D. A., Sriranganadane, D., Yahyaoui, W., Thibault, P., Perreault, C., and Shastri, N. (2016) ERAAP Shapes the Peptidome Associated with Classical and Nonclassical MHC Class I Molecules. *J Immunol* **197**, 1035-1043
283. Burk, R. D., Chen, Z., Harari, A., Smith, B. C., Kocjan, B. J., Maver, P. J., and Poljak, M. (2011) Classification and nomenclature system for human Alphapapillomavirus variants: general features, nucleotide landmarks and assignment of HPV6 and HPV11 isolates to variant lineages. *Acta Dermatovenerol Alp Pannonica Adriat* **20**, 113-123

6 Abbreviations

4-1BB	tumor necrosis factor receptor superfamily member 9 (TNFRSF9), CD137
A	adenine
AA	amino acid
ACN	acetonitrile
APC	antigen presenting cell
APM	antigen processing machinery
β2m	β2-microglobulin
bp	base pairs
BPV	bovine papillomavirus
BSA	bovine serum albumin
C	cytosine
C-terminus	carboxyl-terminus
°C	degree Celsius
CAD	collision gas
CALR	calreticulin
CANX	calnexin
CCR	CC chemokine receptor
CD	cluster of differentiation
cDNA	complementary desoxyribonucleic acid
CFSE	carboxyfuorescein
CIN	cervical intraepithelial neoplasia
CMV	cytomegalovirus
ConA	concanavalin A
Cq	quantification cycle
CTL	cytotoxic T lymphocyte
CTLA	cytotoxic T lymphocyte associated antigen
CXCR5	CXC motive chemokine receptor
Da	Dalton
DC	dendritic cell
ddH_2O	double distilled water
dH_2O	deionized water
DMSO	dimethylsulfoxid
dNTP	deoxynucleoside triphosphate
DNA	deoxyribonucleic acid
DRiP	defective ribosomal product
dsRNA	double stranded RNA
DTT	dithiothreithol
E6-AP	E6-associated protein
EBV	Epstein-Barr virus
EC	endothelial cell
ECL	enhanced chemiluminescence
EDTA	ethylenediaminetetraacetic acid
EGF	epidermal growth factor
ELISpot	enzyme linked immunospot
ER	endoplasmic reticulum
ERAP	endoplasmic reticulum aminopeptidase
ERAAP	endoplasmic reticulum aminopeptidase associated with antigen processing
ESI	electron spray ionization
et al.	et alii, at aliae, et alia

FA	formic acid
FACS	fluorescence-activated cell sorting
FAM	fluorescein amidite
FCS	fetal calf serum
FSC	forward scatter
FDA	Food and Drug Administration
FITC	fluorescein isothiocyanate
Foxp3	forkhead box p3
G	guanine
Gag	group-specific antigen
GAG	glycosaminoglycan
GAPDH	glyceraldehyde 3-phosphate dehydrogenase
Gy	Gray
h	hour
HEPES	4-(2-hydroxyethyl)-1-piperazineethanesulfonic acid
HIV	human immunodeficiency virus
HLA	human leukocyte antigen
HNSCC	head and neck squamous cell carcinoma
HPRT1	hypoxanthine-guanine phosphoribosyltransferase
HPV	human papillomavirus
HRP	horseradish peroxidase
HSPG	heparan sulfate proteoglycan
hTERT	human telomerase reverse transcriptase gene
ICOS	inducible T cell co-stimulator
ID	inner diameter
i.e.	id est
IFN	interferon
Ig	immunoglobulin
IL	interleukin
IL-1RII	type II IL-1 decoy receptor
IL-6Rα	IL-6 receptor alpha subunit
IP	immunoprecipitation
IPO8	importin 8
IRAP	insulin-regulated aminopeptidase
IRF3	interferon regulatory factor 3
iTreg	induced regular T cell
kb	kilobase
kDa	kilo Dalton
l	liter
LC-MS	liquid chromatography-mass spectrometry
LFA	leukocyte function antigen
LLO	listeriolysin O
LPS	lipopolysaccharide
M	molarity
MACS	magnetic-activated cell sorting
MAP	mitogen-activated protein
MDSC	myeloid-derived suppressor cells
MFI	mean fluorescence intensity
Mg	magnesium
MHC	major histocompatibility complex
min	minute
MIP-3α	macrophage inflammatory protein 3α
ml	milliliter
µl	microliter

mM	millimolar
Mo-DCs	monocyte-derived dendritic cells
MPLA	monophosphoryl lipid A
mRNA	messenger ribonucleic acid
MS	mass spectrometry
MVA	modified vaccinia virus ankara
NK	natural killer cell
N-terminus	amino terminus
nano-UPLC-MS	nano ultraperformance liquid chromatography mass spectrometry
nm	nanometer
NP-40	nonyl phenoxypolyethoxylethanol
nTreg	natural regulatory T cell
OD	optical density
ORF	open reading frame
OX40	tumor necrosis factor receptor superfamily member 4 (TNFRSF4), CD134
P	proline
PAGE	polyacrylamide gel electrophoresis
PBMC	peripheral blood mononuclear cell
PBS	phosphate buffered saline
PCR	polymerase chain reaction
PDIA3	protein disulfide isomerase A3
PFA	paraformaldehyde
PGK1	phosphoglycerate kinase 1
pH	*pondus hydrogenii*
PHA	phytohemagglutinin
pHFK	primary human foreskin keratinocytes
pHK	primary human keratinocytes
PLC	peptide loading complex
PMSF	phenylmethylsulfonylfluorid
PPIA	peptidylprolyl isomerase A
pRB	retinoblastoma protein
PRR	pattern recognition receptor
PSMA	proteasome subunit alpha
PSMB	proteasome subunit beta
PSME	proteasome activator subunit
PV	papillomavirus
qRT-PCR	quantitative real-time PCR
RNA	ribonucleic acid
ROS	reactive oxygen species
RRP	recurrent respiratory papillomatosis
rpm	rounds per minute
RT	room temperature
RT-PCR	real-time polymerase chain reaction
SCC	squamous cell carcinoma
SCX	strong cation exchange chromatography
SD	standard deviation
SDS	sodium dodecyl sulfate
sec	seconds
SFU	spot forming units
siRNA	small interference RNA
SLP	synthetic long peptides
SNP	single nucleotide polymorphism
SSC	side scatter

T	thymine
T_{CM}	central memory T cell
T_{EM}	effector memory T cell
T_{FH}	follicular helper T cell
TAM	tumor-associated macrophages
TAP	transporter associated with antigen processing
Taq	*Thermus aquaticus*
TCR	T cell receptor
TFA	trifluoroacetic acid
TGF	transforming growth factor
Th	helper T cell
TNF	tumor necrosis factor
TNFR	tumor necrosis factor receptor
TOP	thimet oligopeptidase
TPP	tripeptidyl peptidase
Tris	Tris(hydroxylmethyl)-aminoethane
Treg	regulatory T cell
TYK2	tyrosine kinase 2
U	unit
UPLC	ultra performance liquid chromatography
URR	upstream regulatory region
UV	ultraviolet
V	Volt
VEGF	vascular endothelial growth factor
VIN	vulvar intraepithelial neoplasia
VLA-4	very late antigen 4
VLP	virus-like particle
W	Watt
WHO	World Health Organization
x	times, -fold

7 Appendix

Table 7.1: Quality control parameters for qRT-PCR. The quality control parameters employed by LinRegPCR and qBase plus are summarized below.

LinRegPCR	
Correlation coefficient (R^2)	> 0.996
Point included in linear regression	≥ 4
Mean efficiency per amplicon	Exclude wells without amplicon Exclude wells without plateau Exclude wells if outside 15% of group median
qBase plus	
Replicate variability (Cq)	< 0.5
Reference target stability – geNorm M	< 0.9
Reference target stability – CV	< 0.3
Data exclusion criteria (Cq)	> 40

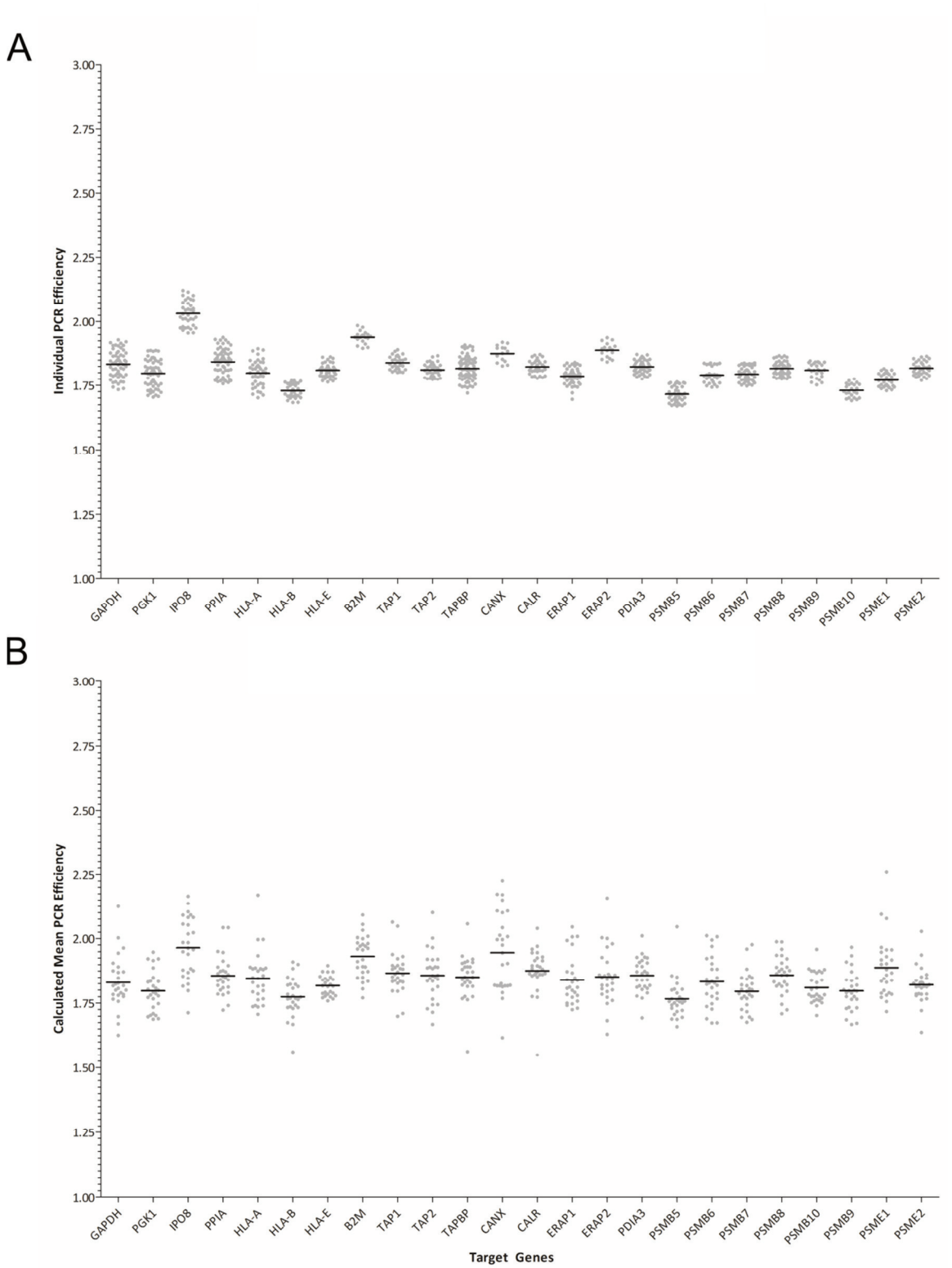

Figure 7.1: PCR efficiencies of the qRT-PCR screen calculated by LinRegPCR. Individual calculated mean PCR efficiencies in the constitutive APM expression screening (**A**) and after IFNγ treatment (**B**). **A** Individual calculated PCR efficiencies that were used for the amplicon mean efficiency calculation. Each dot represents the PCR efficiency of a single reaction well. **B** Each dot represents the calculated mean PCR efficiency of the corresponding amplicon per cell line. The amplicon mean PCR efficiencies were calculated from triplicates of both the untreated and IFN-γ treated groups for each cell line. GAPDH = glyceraldehyde 3-phosphate dehydrogenase, PGK1 = phosphoglycerate kinase 1, IPO8 = importin 8, PPIA = peptidylprolyl isomerase A, TAPBP = tapasin, CANX = calnexin, CALR = calreticulin

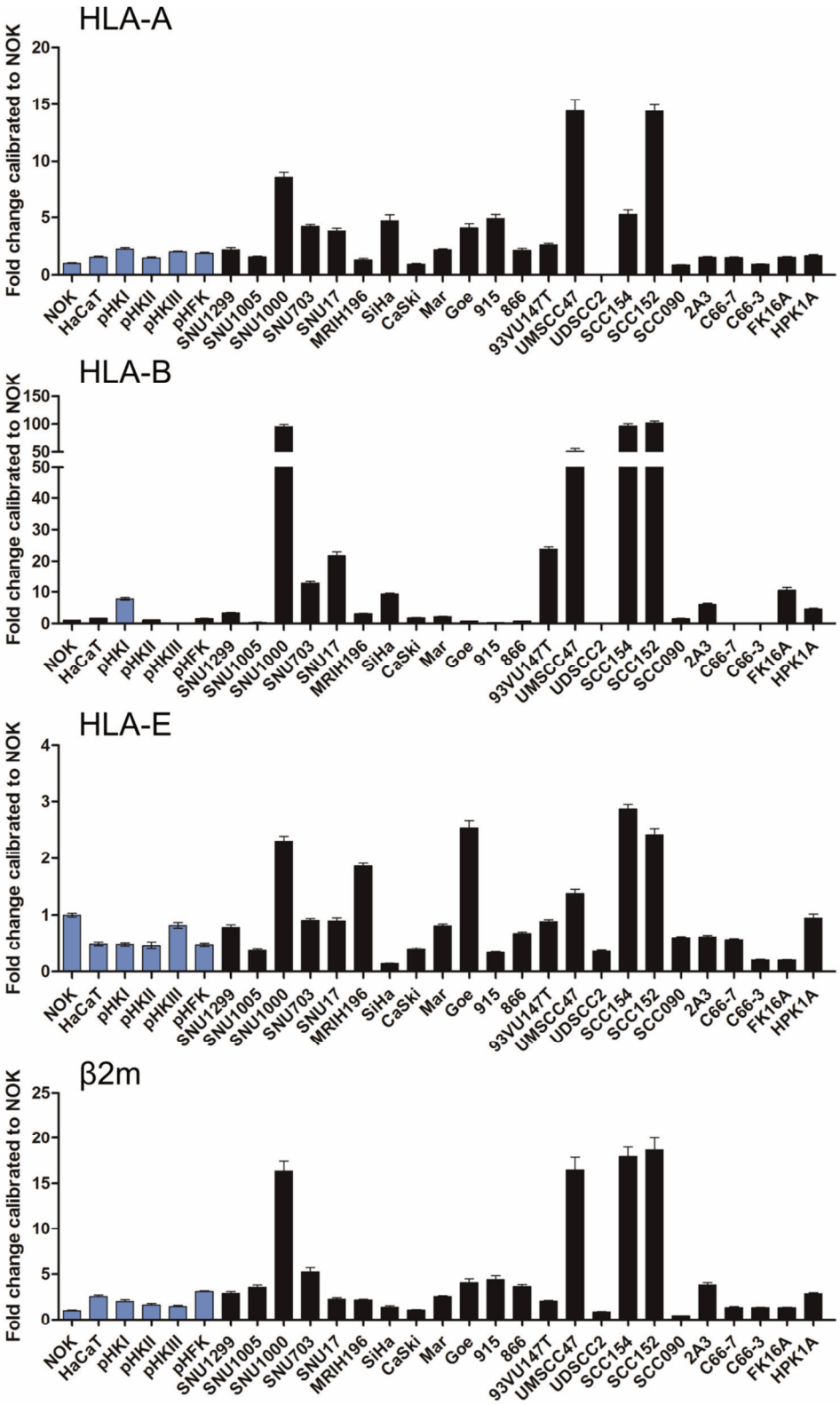

Figure 7.2: Constitutive expression of MHC I associated genes on the mRNA level. Total RNA was purified from cells, reverse transcribed to cDNA and analyzed for APM component expression by qRT-PCR using TaqMan® probes. PCR reactions were run in triplicates. At least three of the following genes were used as internal reference: *GAPDH*, *PGK1, PPIA* and *IPO8*. Gene expression was calibrated to the NOK cell line. All quantitative qRT-PCR data were processed by LinRegPCR and data management was done by qbasePLUS 2. Blue bars represent data from HPV-negative cell lines. Data is plotted as ± SD.

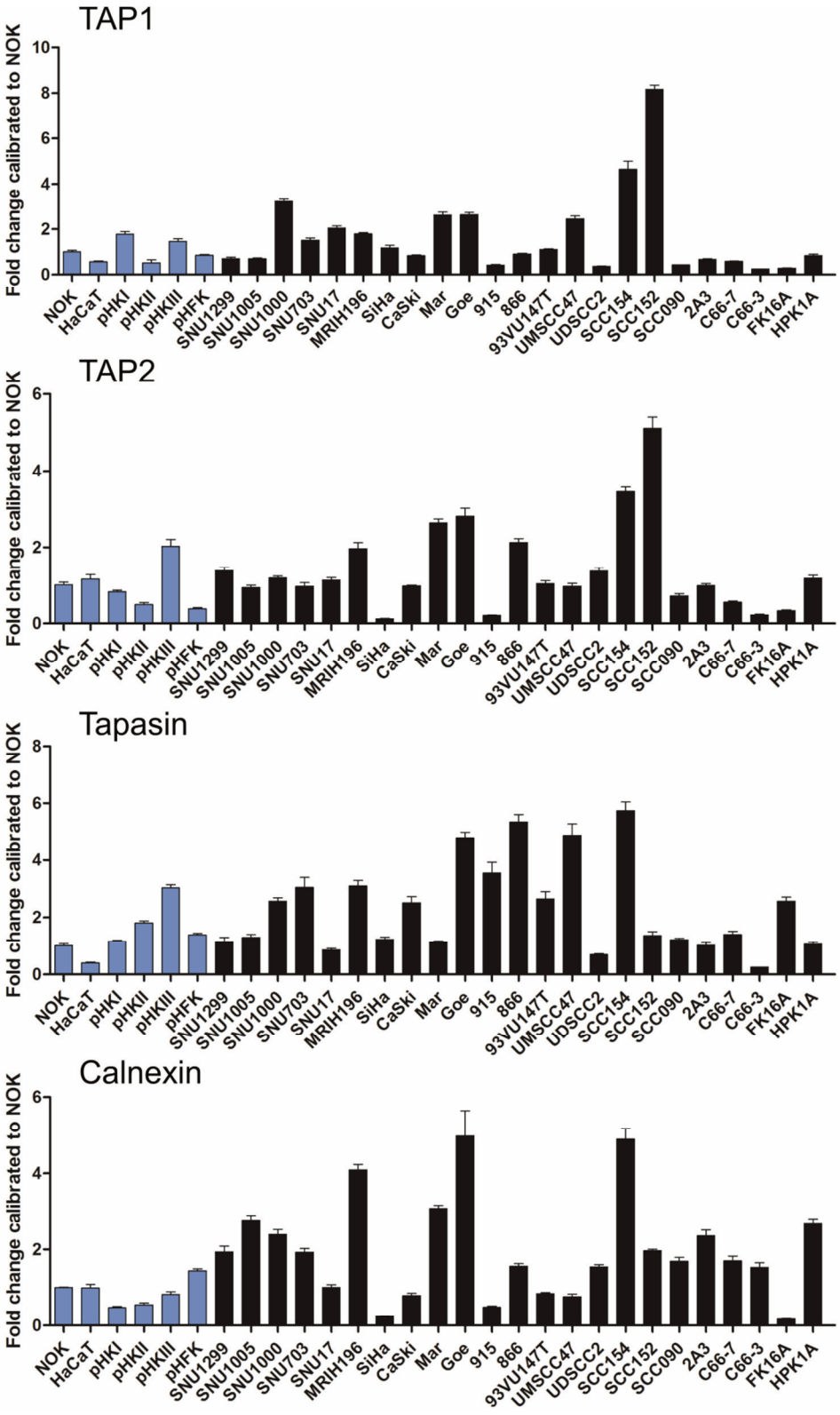

Figure is continued on the following page

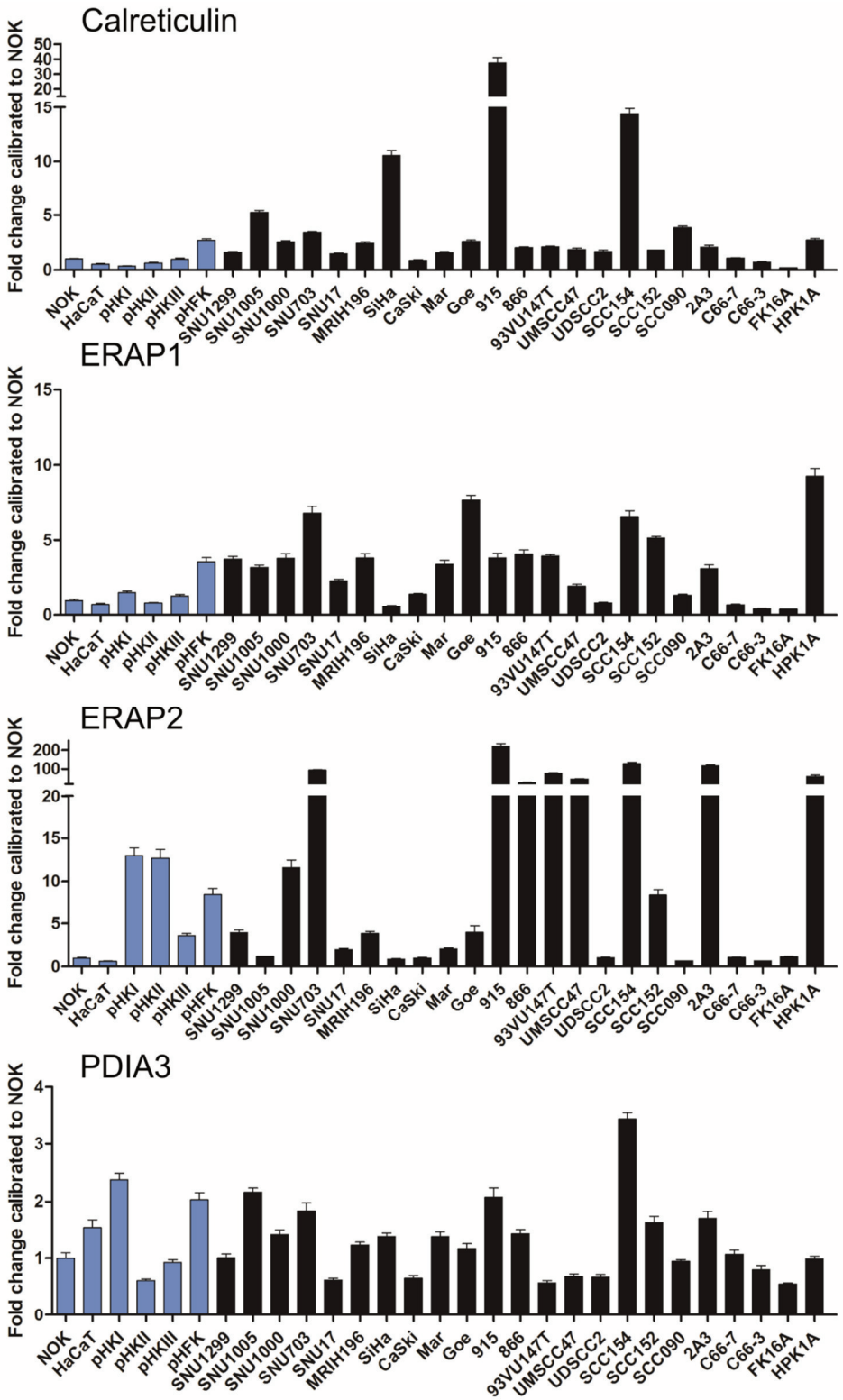

Figure 7.3: Constitutive expression of peptide loading complex associated genes on the mRNA level. Total RNA was purified from cells, reverse transcribed to cDNA and analyzed for APM component expression by qRT-PCR using TaqMan® probes. PCR reactions were run in triplicates. At least three of the following genes were used as internal reference: *GAPDH*, *PGK1, PPIA* and *IPO8*. Gene expression was calibrated to the NOK cell line. All quantitative qRT-PCR data were processed by LinRegPCR and data management was done by qbasePLUS 2. Blue bars represent data from HPV-negative cell lines. Data is plotted as ± SD.

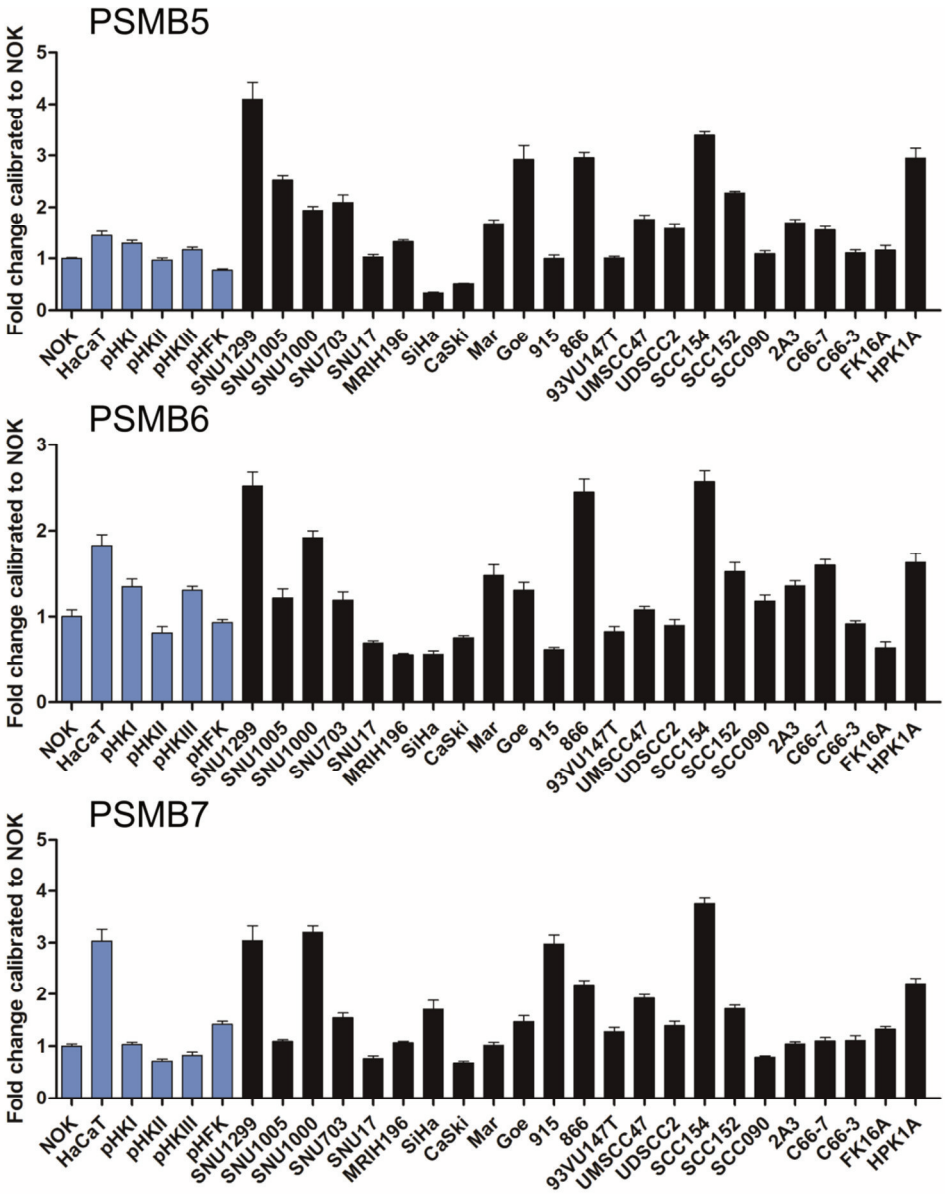

Figure 7.4: Constitutive expression of proteasome associated genes on the mRNA level. Total RNA was purified from cells, reverse transcribed to cDNA and analyzed for APM component expression by qRT-PCR using TaqMan® probes. PCR reactions were run in triplicates. At least three of the following genes were used as internal reference: *GAPDH*, *PGK1, PPIA* and *IPO8*. Gene expression was calibrated to the NOK cell line. All quantitative qRT-PCR data were processed by LinRegPCR and data management was done by qbasePLUS 2. Blue bars represent data from HPV-negative cell lines. Data is plotted as ± SD.

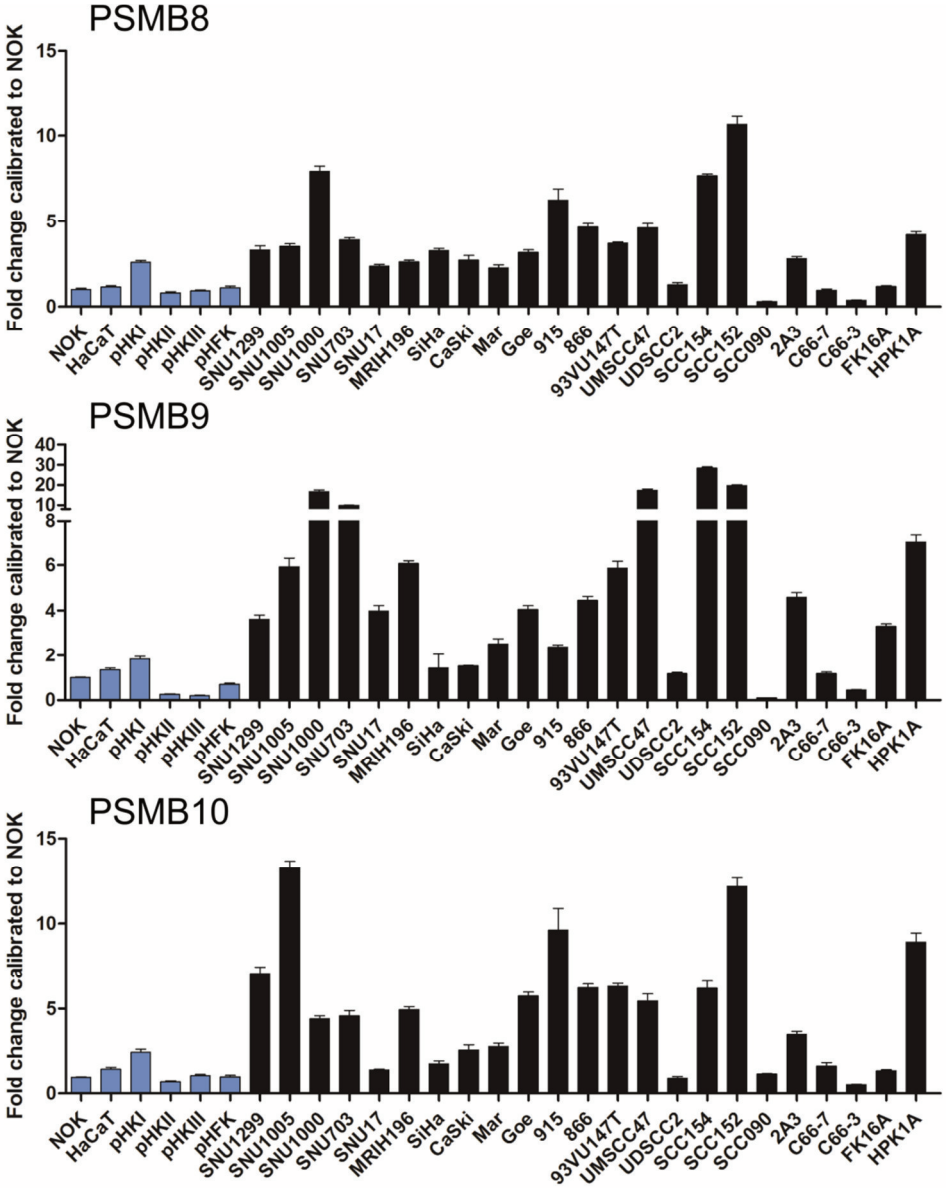

Figure is continued on the following page

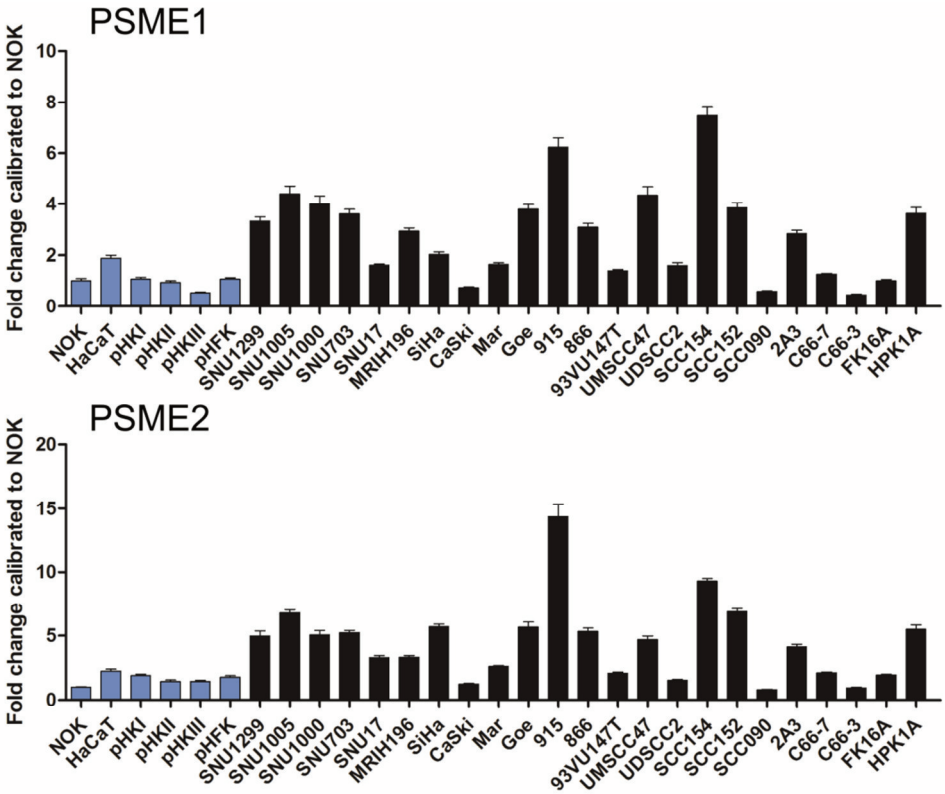

Figure 7.5: Constitutive expression of immunoproteasome associated genes on the mRNA level. Total RNA was purified from cells, reverse transcribed to cDNA and analyzed for APM component expression by qRT-PCR using TaqMan® probes. PCR reactions were run in triplicates. At least three of the following genes were used as internal reference: *GAPDH*, *PGK1, PPIA* and *IPO8*. Gene expression was calibrated to the NOK cell line. All quantitative qRT-PCR data were processed by LinRegPCR and data management was done by qbasePLUS 2. Blue bars represent data from HPV-negative cell lines. Data is plotted as ± SD.

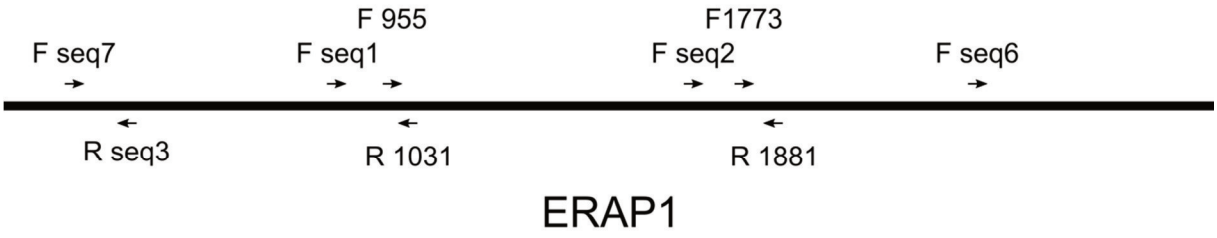

Figure 7.6: Primer positions used for *ERAP1* sequencing. The *ERAP1* gene (2826bp) was sequenced by GATC Biotech using at least five of the indicated primers. The positions of forward primers (F) are shown above and the positions of reverse primers (R) are shown below the line representing the ERAP1 gene. The primer sequences are given in the method section (2.1.10).

Table 7.2: Cell lines with their HLA type and designated HPV16 variant including nucleotide and amino acid exchanges in comparison to the HPV16 reference sequence. The first column indicates the cell line, the second its HLA class I type types, the third the identified HPV16 variant if the cell line is HPV16-positive and the last two columns nucleotide exchanges in the E6 and E7 open reading frame (ORF), respectively, that result in a missense mutation. Resulting amino acid changes are included in (). E6 and E7 mutations are taken from Dr. Stephanie Hoppe (194). HPV16 variant nomenclature is derived from Robert D. Burk (283). n.a. = not applicable

Cell line	HLA class I types	HPV16 variant	Exchanges within E6 ORF	Exchanges within E7 ORF
2A3	A*01:01, -; B*15:07, -	European Prototype 1	-	-
866	A*02:01, A*68:01; B*15:01, B*27:05	African-2	G132T (R10I), C143G (Q14D in combi), G145T (Q14D in combi), C335T (H78Y)	A647G (N29S)
915	A*03:01, - ; B*14, -	European Prototype 1	-	-
93VU147T	A*03:01, -; B*07:02, -	European Prototype 1	-	-
C33A	A*02:01, A*11:01; B*07:02, B*44:02			
C66-3	A*02:01, A*30:02; B*18:01, B*35:03	European Prototype 1	T350G (L83V)	-
C66-7	A*02:01, A*30:02; B*18:01, B*35:03	European Prototype 1	T350G (L83V)	-
CaSki	A*02:01, A*03:01; B*07:02, B*37:01; C*07, -	European Prototype 2	A131G (R10T), T350G (L83V)	-
FK16A	A*01:01, A*24:02; B*07:02, B*0801	European Prototype 1	-	-
Goe	A*01:01, - ; B*37:01, -	European Prototype 1	-	-
HaCat	A*31:01, -; B*40:01, B*51:01			
HPK1A	A*02:01, A*03:01; B*40:01,B*55:01	European Prototype 1	-	-
Mar	A*02:01, - ; B*27:02, -; C*02:02 ,-	European Prototype 1	-	n.a.
MRIH196	A*02, A*03:01; B*07:02 , B*51:01	European Prototype 1	T350G (L83V)	-
NOK	A*02:03, A*11:01; B*13:01, B*38:02			
RiSh	A*24:02, A*26:01; B*35:03, B*51:08;			
SCC090	A*02:01, A*03:01; B*44:03, B*51:01	European Prototype 2	A131G (R10T), T350G (L83V)	-
SCC152	A*02:01, A*03:01; B*44:03, B*51:01	European Prototype 2	A131G (R10T), T350G (L83V)	-
SCC154	A*25:01, -; B*44:02, B*44:03	Asian-American	G145T (Q14D), C335T (H78Y), T350G (L83V),	-
SiHa	A*24:02, - ; B*40:02, - ; C*03, -	European Prototype 1	T350G (L83V), A442C (E113D)	A645C (L28F)
SNU1000	A*02:01, A*11:01; B*40:02, -	European (Asian)	T178G (D25E), T183G (I27R)	A647G (N29S)
SNU1005	A*24:02, - ; B*52:01, -	European (Asian)	T178G (D25E)	A647G (N29S)
SNU1160	A*24:02, - ; B*13:01, -			
SNU1299	A*02:01, A*33:03; B*27:05, B*44:03	Asian-American	G145T (Q14D), C335T (H78Y), T350G (L83V),	-
SNU17	A*02:06, - , B*48:01, -	European (Asian)	T178G (D25E)	A647G (N29S)

SNU703	A*02:01, A*02:06; B*35:01, B*40:06	European (Asian)	T178G (D25E)	A647G (N29S),
UDSCC2	A*25:01, - ; B*18N	European Prototype 1	-	C712A (H51N)
UMSCC47	A*01:01, A*23:01; B*37:01, B*45:01	African-2	G132T (R10I), C143G (Q14D), G145T, G188C (E29Q), C285G (A61G), C335T (H78Y)	A647G (N29S)

Table 7.3: Blood donor characteristics and HLA types.

Donor	**Gender**	**Age**	**HLA class I**	**HLA Class II**
1	female	34	A*01:01, **A*02:01**; B*35:08, B*44:02; C*05:01, C*06:02	DRB1*01:01, DRB1*04:03; DQB1*03:02, DQB1*05:01; DPB3*04:01; DPB4*04:02
2	female	39	**A*24:02**, A*26:01; B*35:03, B*51:08	DRB1*04:08, DRB1*13:01; DQB1*03:04, DQB1*06:03; DRB3*02:02; DRB4*01; DPB1*09:02, DPB1*15:01

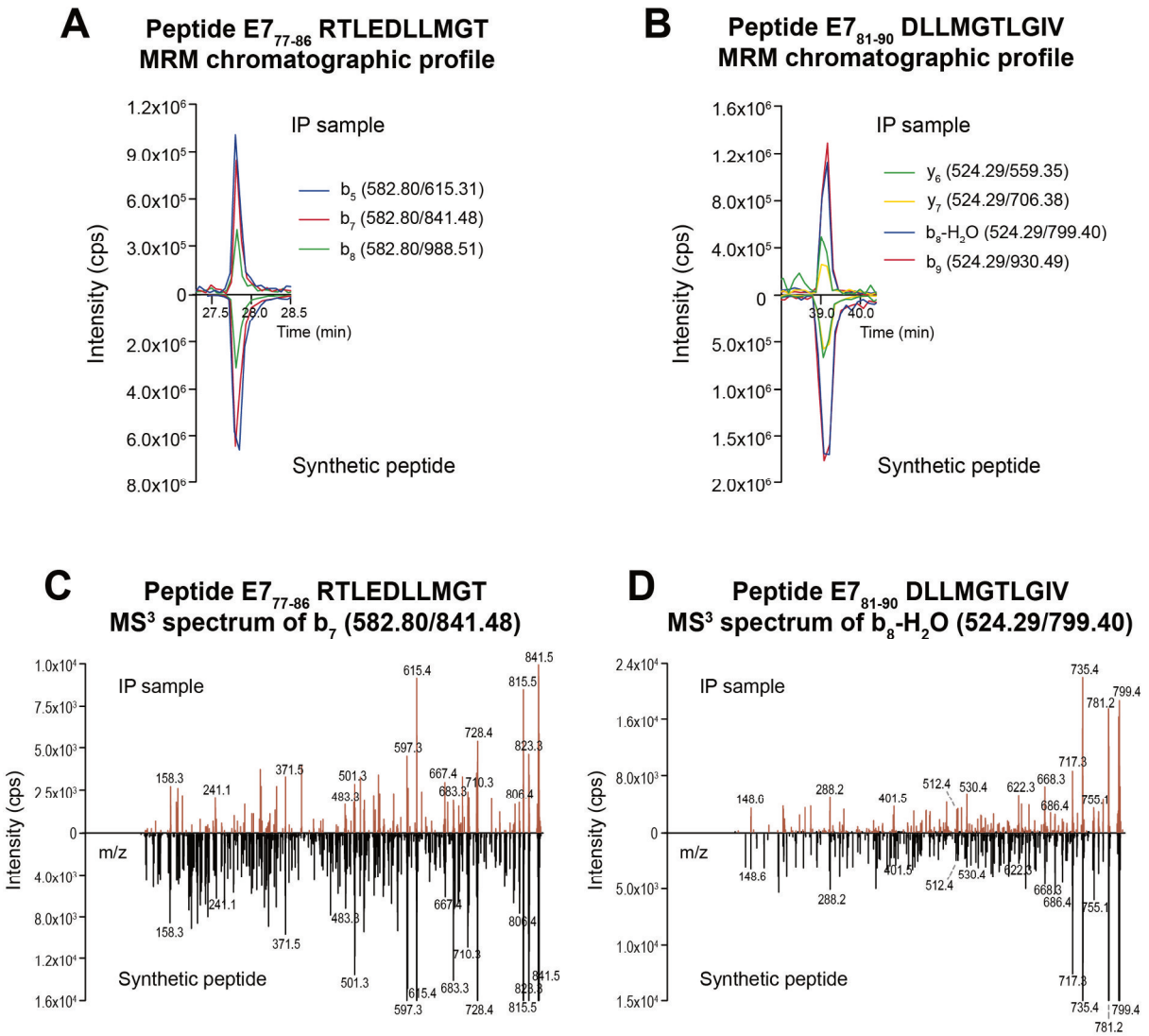

Figure 7.7: Successful detection of HPV16 peptides $E7_{77-86}$ RTLEDLLMGT and $E7_{81-90}$ DLLMGTLGIV on CaSki cells by targeted LC-MS^3 analysis in HLA-A2 IP samples. Samples were subjected to Seppak cartridge purification and subsequently to LC-MS^3 analysis on a nanoAcquity UPLC-QTrap6500 platform. **A.** Extracted ion chromatogram for fragments: b_5 (582.80/615.31), b_7 (582.80/841.48) and b_8 (582.80/988.51) for peptide $E7_{77-86}$ RTLEDLLMGT detected in the CaSki IP sample (pointing upwards) and its synthetic counterpart (pointing downwards). **B.** Extracted ion chromatogram for fragments: y_6 (524.29/559.35), y_7 (524.29/706.38), b_8-H_2O (524.29/799.40) and b_9 (524.29/930.49) for peptide $E7_{81-90}$ DLLMGTLGIV detected in the CaSki IP sample and its synthetic counterpart. **C.** MS^3 spectrum for fragment b_7 (582.80/841.48) corresponding to the detected peptide $E7_{77-86}$ in the IP sample and its synthetic counterpart. **D.** MS^3 spectrum for fragment b_8-H_2O (524.29/799.40) corresponding to the detected peptide $E7_{81-90}$ in the IP sample and its synthetic counterpart. Only one MS^3 spectrum per peptide is displayed for clarity reasons.